AD-A052 634 HONEYWELL INC MINNEAPOLIS MINN SYSTEMS AND RESEARCH --ETC F/G 22/2
NTS-2 INDEPENDENT STABILITY AND CONTROL ANALYSIS. VOLUME II. AP--ETC(U)
MAR 77 R E POPE, M D WARD, S M SCHWANTES

UNCLASSIFIED 77SRC17-VOL-2 NL

1 OF 3
AD
AD52634

F0360-24

NTS-2 INDEPENDENT STABILITY AND CONTROL ANALYSIS

by

R.E. POPE
M.D. WARD
S.M. SCHWANTES
J.G. RUPERT

Honeywell

SYSTEMS AND RESEARCH CENTER
2600 RIDGWAY PARKWAY
MINNEAPOLIS, MINNESOTA 55413

30 March 1977

FINAL REPORT

VOLUME II APPENDICES

Prepared for

SAMSO (YEES)
P.O. BOX 92960
WORLDWAY POSTAL CENTER
LOS ANGELES, CALIFORNIA 90009

Unclassified

SECURITY CLASSIFICATION OF THIS PAGE (WHEN DATA ENTERED)

REPORT DOCUMENTATION PAGE

READ INSTRUCTIONS BEFORE COMPLETING FORM

1. REPORT NUMBER: ADG Report F0360-24

2. GOV'T ACCESSION NUMBER:

RECIPIENT'S CATALOG NUMBER:

4. TITLE (AND SUBTITLE): NTS-2 Independent Stability and Control Analysis, Volume II, Appendices

5. TYPE OF REPORT/PERIOD COVERED: Final Report, Feb 76-Mar 77

6. PERFORMING ORG. REPORT NUMBER: 77SRC17-Vol-2, F0360-24-Vol-2

7. AUTHOR(S): R. E. Pope, M. D. Ward, S. M. Schwantes, J. G. Rupert

8. CONTRACT OR GRANT NUMBER(S):

9. PERFORMING ORGANIZATIONS NAME/ADDRESS: Honeywell Systems & Research Center, 2600 Ridgway Parkway, Minneapolis, Minnesota 55413

10. PROGRAM ELEMENT, PROJECT, TASK AREA & WORK UNIT NUMBERS:

11. CONTROLLING OFFICE NAME/ADDRESS: SAMSO (YEES), P. O. Box 92960, Worldway Postal Center, Los Angeles, California 90009

12. REPORT DATE: 30 Mar 77

13. NUMBER OF PAGES: 243 (260 Pp.)

14. MONITORING AGENCY NAME/ADDRESS (IF DIFFERENT FROM CONT. OFF.):

15. SECURITY CLASSIFICATION (OF THIS REPORT): Unclassified

15a. DECLASSIFICATION DOWNGRADING SCHEDULE:

16. DISTRIBUTION STATEMENT (OF THIS REPORT)

Approved for public release; distribution unlimited

17. DISTRIBUTION STATEMENT (OF THE ABSTRACT ENTERED IN BLOCK 20, IF DIFFERENT FROM REPORT)

18. SUPPLEMENTARY NOTES

This is Volume II of two volumes. Volume I contains the Introduction, Summary of Results and Recommendations, Model Development, Presentation of Results, and Conclusions (288 pages).

19. KEY WORDS (CONTINUE ON REVERSE SIDE IF NECESSARY AND IDENTIFY BY BLOCK NUMBER)

NTS-2
Stability analysis
Satellite simulation
Gravity gradient
Reaction wheels
GPS
NAVSTAR

20. ABSTRACT (CONTINUE ON REVERSE SIDE IF NECESSARY AND IDENTIFY BY BLOCK NUMBER)

Volume II presents appendices in this order:

NTS-2 Mass Properties,
One Body Mode Equations,
Three Body Model,
Nutation Damper Model,
Attitude Control Electronics System Model,
Tilted, Centered Dipole Magnetic Torque Model,

DD FORM 1 JAN 73 1473 EDITION OF 1 NOV 55 IS OBSOLETE

Unclassified

SECURITY CLASSIFICATION OF THIS PAGE (WHEN DATA ENTERED)

HD-168 REV 11/74

402 349

Solar Torque Model
NTS-2 Gravity Gradient Rod Thermal Analysis

Details of Solar Array Flexibility Modeling
Modified NTS-2 Solar Array Torsion Model
Solar Array Torsion Modes, Solution for Response to Torque Motor Angular Accelerations
Combined Earth Sensor Model

TABLE OF CONTENTS

APPENDIX A

APPENDIX A

NTS-2 MASS PROPERTIES

The mass properties for NTS-2, Tables A-1 and A-2, consist of launch and orbit conditions. DRY signifies NO hydrazine in that condition. Hydrazine usage can be obtained from Table A-3 and be added to any dry condition by

$$I \text{ Total} = I_c + WT_c \times d_c^2 + I_h + WT_h \times d_h^2$$

where

C = Condition

H = Hydrazine

d = distance CG is transferred

Individual component mass properties are shown in Tables A-1 and A-2, which along with hydrazine usage can be added to the last two conditions shown in Figure A-1.

EXAMPLE:

USING COND (DRY), AKM BURN, AKM SEP, WITHOUT SOLAR ARRAY, GRAVITY GRADIENT, NUTATION DAMPER, MAGNETOMETER, AND REACTION WHEELS, FIND MASS PROPERTIES WITH SOLAR ARRAYS STOWED AND 50 PERCENT HYDRAZINE USAGE.

$$\text{New C.G.Z.} = \frac{\Sigma WT \times CGZ}{TWT}$$

$$= \frac{(799.7)\ (25.69 + (60.6)\ (22.00) + (26)(\ 31.68)}{886.3}$$

$$= 25.61 \text{ in.}$$

$$I_{xx} = 70.02 + (799.7)\ (0)^2 + 11.82 + (60.6)\ (0)^2 + 0.1 + (26)\ (0)^2$$

$$= 81.94 \text{ Slug-Ft.}^2$$

$$I_{yy} = 56.32 + \frac{(799.7)(.08)^2}{(32.2)(144)} + 8.65 + \frac{(60.6)(3.61)^2}{(32.2)(144)} + 3.1 + \frac{(26)(6.07)^2}{(32.3)(144)}$$

$$= 68.45 \text{ Slug-Ft.}^2$$

$$I_{zz} = 102.40 + \frac{(799.7)(.08)^2}{(32.2)(144)} + 14.47 + \frac{(60.6)(3.61)^2}{(32.2)(144)} + 3.1 + \frac{(26)(6.07)^2}{(32.2)(144)}$$

$$= 120.35 \text{ Slug-Ft.}^2$$

Table A-1. Mass Properties NTS-2

NO.	EVENT	WT kg (lbs)	CENTER OF GRAVITY (in)			MOMENT OF INERTIA (slug-ft^2)			PRODUCT OF INERTIA (slug-ft^2)		
			$\bar{X}$	$\bar{Y}$	$\bar{Z}$	I_{xx}	I_{yy}	I_{zz}	I_{xy}	I_{xz}	I_{yz}
	AKM ASSY	64			47.96	1.15	1.15	2.33			
	AKM PROPELLANT	662			40.79	13.37	13.37	12.95			
	SOLAR ARRAYS										
	STOWED	60.6			22.00	11.82	8.65	14.47			
	DEPLOYED (VERT)	60.6			22.00	3.01	99.88	96.89			
	GRAVITY GRADIENT										
	STOWED	16.82		19.75	30.99	1.09	1.09	0.02			
	DEPLOYED 20 FT	16.82		19.75	30.99	216.78	216.78	0.02			
	DEPLOYED 40 FT	16.82		19.75	30.99	823.38	823.38	0.02			
	DEPLOYED 60 FT	16.82		19.75	30.99	1832.88	1832.88	0.02			
	MAGNETOMETER										
	STOWED	4.15	7.93	28.79	-10.66	0.16	0.16	0.00			
	DEPLOYED	4.15	9.06	28.79	-47.78	0.74	0.74	0.00			
	REACTION WHEELS	19.30		8.50	19.00	0.07	0.07	0.13			

Table A-2. Mass Properties NTS-2

NO.	EVENT	WT kg (lbs)	CENTER OF GRAVITY (in)			MOMENT OF INERTIA ($slug\text{-}ft^2$)			PRODUCT OF INERTIA ($slug\text{-}ft^2$)		
			$\bar{X}$	$\bar{Y}$	$\bar{Z}$	I_{xx}	I_{yy}	I_{zz}	I_{xy}	I_{xz}	I_{yz}
	LAUNCH $I_{ZZ}/I_{XX} = 1.112$ $I_{ZZ}/I_{YY} = 1.240$	1679			32.52	126.43	113.30	140.54	-2.78		
	LAUNCH (DRY)	1627			32.47	126.21	106.88	134.15	-2.78		
	AKM BURN (DRY)	965			26.76	96.15	76.81	121.19	-2.78		
	AKM SEP (DRY)	901			26.26	87.32	67.99	119.66	-2.78		
	SOLAR ARRAYS DEPOLYED (DRY)	901			25.23	78.53	159.23	202.08	-2.53		
	EVERYTHING DEPLOYED (DRY)	901			25.06	1914.51	1995.23	202.09	-2.49		
	COND (DRY) AKM BURN AKM SEP W/O SOLAR ARRAYS GRAV GRAD NUTATION DAMP NAGNETOMETER	819			25.53	70.62	56.58	102.87	-2.73		
	COND (DRY) AKM BURN AKM SEP W/O SOLAR ARRAYS GRAV GRAD NUTATION DAMP MAGNETOMETER REACTION WHLS	799.7			25.69	70.02	56.32	102.40	-2.73		

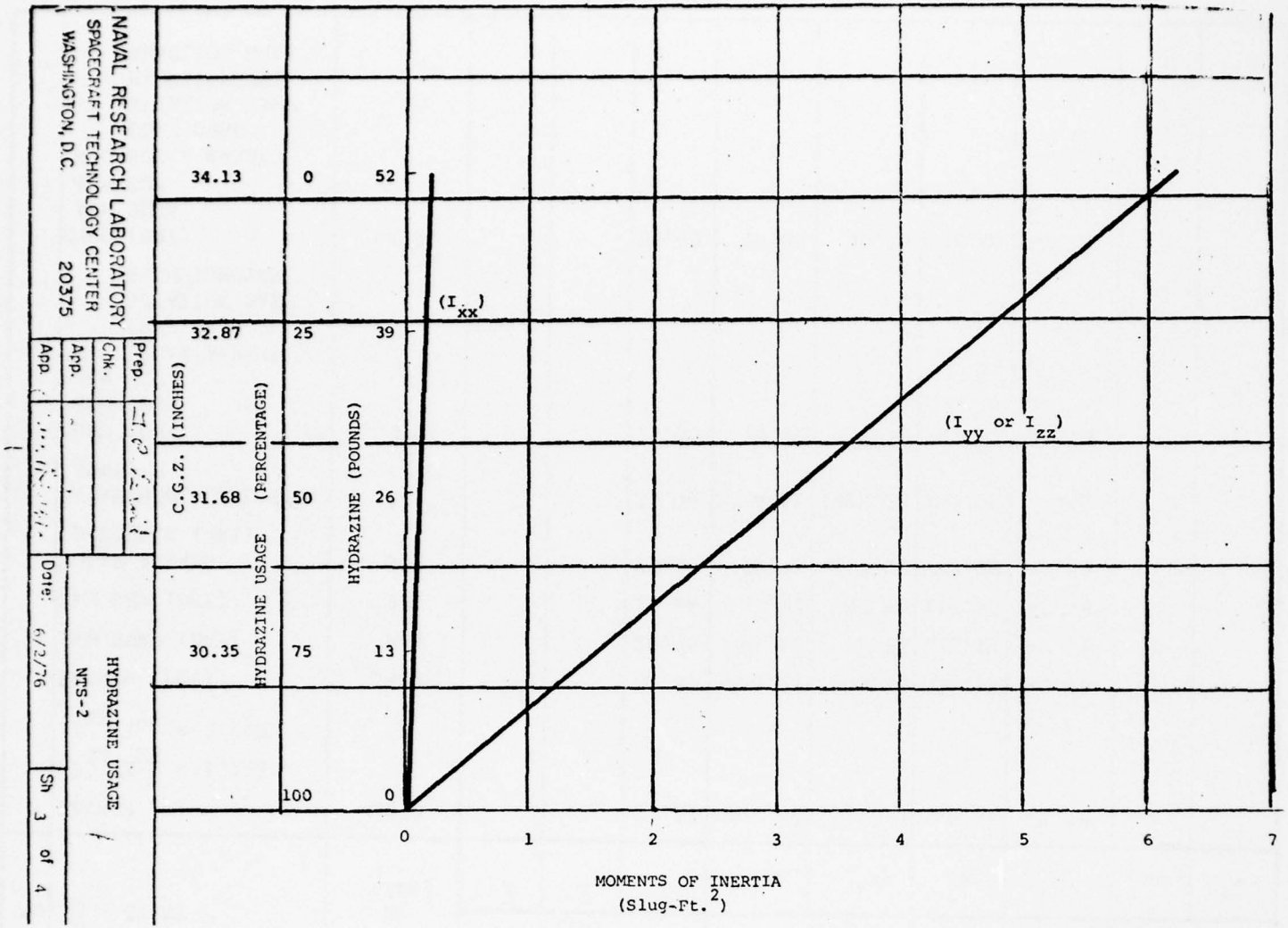

Figure A-1. Hydrazine Usage

APPENDIX B

APPENDIX B

ONE BODY MODEL EQUATIONS

This appendix presents the derivation of equations of motion used in the one body simulation. For Definition of Symbols, see Figure B-1.

Vector torque equations are given by

$$\int \bar{r} x d\bar{F} = \int \bar{r} x \frac{d^2\bar{r}}{dt^2} \, dm$$

$$= \frac{d}{dt} \int \bar{r} x \left(\frac{d\bar{r}}{dt}\right) dm \qquad \text{(B-1)}$$

$$\bar{T} = \frac{d\bar{H}}{dt}$$

where $\bar{H}$ is defined as

$$\bar{H} = \int \bar{r} x \left(\frac{d\bar{r}}{dt}\right) dm$$

$$= \left[\bar{J}_o + m_o M(\bar{r}_o, \bar{r}_o) + \sum_i \bar{J}_i + \sum_i m_i M(\bar{r}_i, \bar{r}_i)\right] \bar{\omega}_o + \sum_i \bar{J}_i \bar{\omega}_i$$

$$= \bar{I}_o \bar{\omega}_o + \sum_i \bar{I}_i \bar{\omega}_i \qquad \text{(B-2)}$$

where, in body 0 coordinates,

$$M(a,b) \triangleq a^T b I - a\, b^T$$

$$J \triangleq \begin{bmatrix} I_x & -I_{xy} & -I_{xz} \\ -I_{xy} & I_y & -I_{xy} \\ -I_{xz} & -I_{xy} & I_z \end{bmatrix}$$

$J_i = T_{oi} J_i {}^{i}T_{io}$ (T_{oi} is transformation from wheel i to body o)

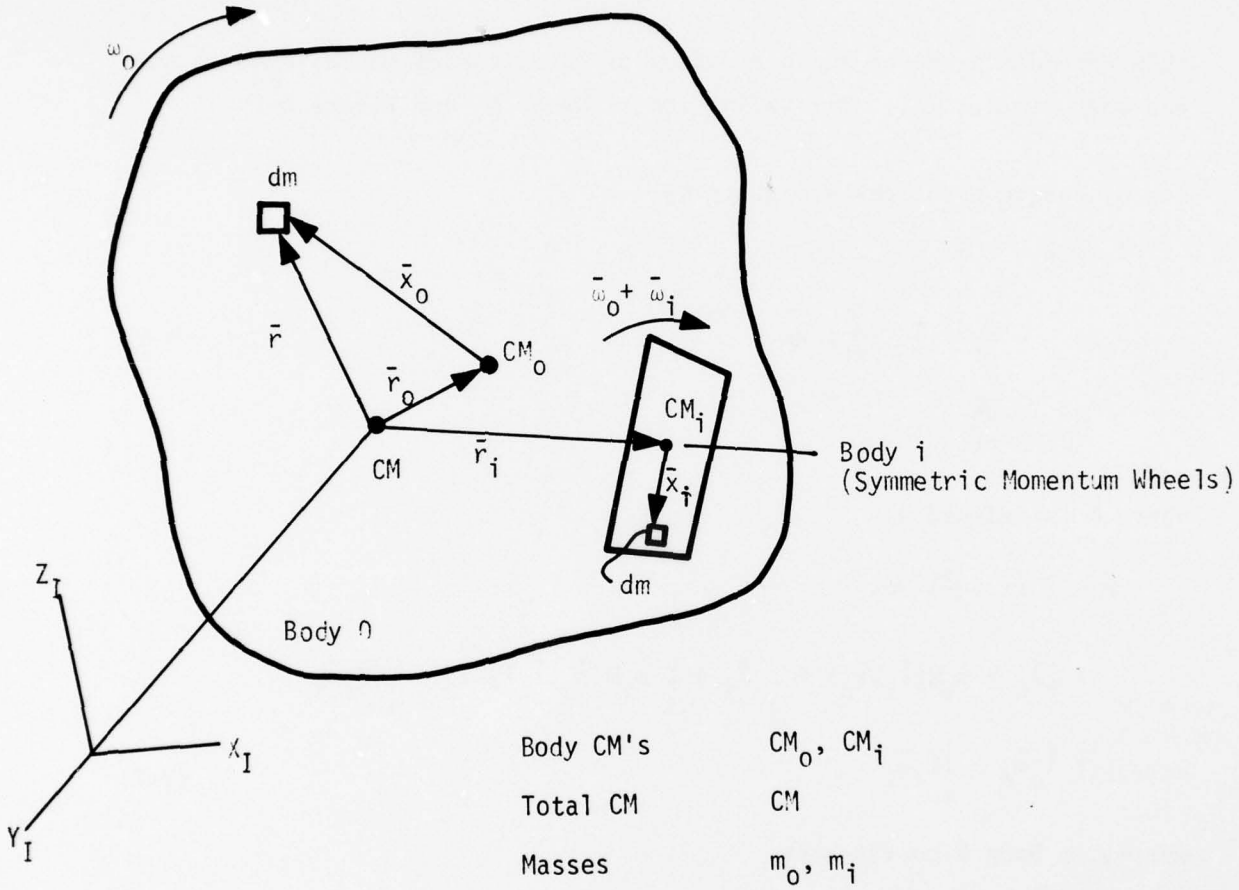

Body CM's	CM_o, CM_i
Total CM	CM
Masses	m_o, m_i
Inertia Tensors	$\bar{J}_1$, $\bar{J}_i$ (J_o, J_i are inertia tensors in reference body coordinates of inertias about CM_o and CM_i respectively)

Figure B-1. Notation

$$\omega_i = T_{oi}\omega_i^{\,i}$$

$$I_x = \int (y^2 + z^2)\,dm = I_{yy} + I_{zz} \text{ , etc.}$$

$$I_{xy} = \int xy\,dm, \text{ etc.}$$

The rotational equations of motion are then given by

$$\bar{T} = \frac{d\bar{H}}{dt}$$

$$= \frac{d}{dt}\left[\bar{I}_o\bar{\omega}_o + \sum_i \bar{I}_i\bar{\omega}_i\right]$$

$$= \frac{\delta}{\delta t}\left[\bar{I}_o\bar{\omega}_o + \sum_i \bar{I}_i\bar{\omega}_o\right] + \bar{\omega}_o x \left[\bar{I}_o\bar{\omega}_o + \sum_i \bar{I}_i\bar{\omega}_i\right]$$

$$T = I_o\dot{\omega}_o + \sum_i I_i\dot{\omega}_i + \omega_o xH \qquad \text{(B-3)}$$

Wheel Torques may be described by

$$\int \bar{x}_i x d\bar{F} = \int \bar{x}_i x \frac{d^2}{dt^2}\bar{x}_i dm$$

$$= \frac{d}{dt}\int \bar{x}_i x \frac{d\bar{x}_i}{dt}\,dm$$

$$\bar{T}_i = \frac{d\bar{H}_i}{dt}$$

Wheel momentum is given by

$$\bar{H}_i = \int \bar{x}_i x \frac{d}{dt}\bar{x}_i\,dm$$

$$= \int \bar{x}_i x \left[\frac{\delta}{\delta t}\bar{x}_i + \bar{\omega}_o x \bar{x}_i\right]\,dm$$

$$= \int \bar{x}_i x[\bar{\omega}_i \times \bar{x}_i + \bar{\omega}_o \times \bar{x}_i]\, dm$$

$$= \bar{J}_i \bar{\omega}_i + \bar{J}_i \bar{\omega}_o \qquad \text{(B-4)}$$

Differentiating

$$T_i = J_i \dot{\omega}_i + J_i \dot{\omega}_o + \omega_o \times J_i \omega_i + \omega_o \times J_i \omega_o \qquad \text{(B-5)}$$

Torques about the wheel axis are given by

$$T_i = J_i \dot{\omega}_i + J_i \dot{\omega}_o \qquad \text{(B-6)}$$

$$\sim J_i \dot{\omega}_i \qquad \text{(B-7)}$$

where T_i is the sum of motor, bearing and windage torques on wheel i. Equations B-7 and B-3 are combined to compute the body rate derivatives.

$$T = I_o \dot{\omega}_o + \sum_i T_i + \omega_o \times H \qquad \text{(B-8)}$$

Kinematics

The inertial coordinate system and the Euler sequence are consistent with the Rockwell convention presented in the AVCS splinter meeting notes at the preliminary design review. Specifically, Rockwell specified a yaw pitch roll Euler sequence with the equations:

$$\dot{\theta} = \omega \cos \psi + q \cos \phi - r \sin \phi$$

$$\dot{\psi} = (\omega \sin \psi \sin \theta + q \sin \phi + r \cos \phi)\ (1/\cos \theta)$$

$$\dot{\phi} = p + \dot{\psi} \sin \theta + \omega \sin \psi \cos \theta$$

where

ω = orbit rate
P,q,r = body rates
ϕ,θ,ψ = Euler angles
$\dot{\phi},\dot{\theta},\dot{\psi}$ = Euler rates

These equations are consistent with:

1. A local vertical system with z axis pointing toward the earth and x axis in the orbit plane and positive on the direction of motion.
2. Euler angles specifying body orientation relative to the local vertical frame.

The inertial coordinate system is the Geocentric Equatorial Frame (e.g., z axis positive North and x axis positive in the direction of the Vernal Equinox). The local vertical system is consistent with Rockwell's (e.g., z axis positive toward the earth and x axis in the orbit plane).

Two sets of Euler angles, both having a yaw pitch roll sequence, are used. The first set PSI, THETA1, PHI1 define the inertial to body transformation E. The second set, PSILV, THETA, PHI specify the orientation of the body relative to the local vertical frame and should be consistent with Rockwell's Euler angles. The inertial Euler angles are integrated in the simulation via quaternions.

Linear Motion

The simulation uses two subroutines(POSITN and RADVEC) to compute the ephemerides for the satellite and the sun. The ephemerides for the satellite and the sun are calculated using the six Kepler elements: semi major axis (a),

eccentricity (e), inclination (i), right ascension of the ascending node (Ω), argument of perigee (ω), and mean anomaly (M). The update is a simple rate term on the latter three. Table B-1 presents the six elements, their units and values for the vernal equinox condition. The rate terms are derived in the program from the fixed parameters and are given by

$$\dot{M} = \sqrt{\mu/a^3} - \frac{k\sqrt{\mu/a^3}}{[a(1-e^2)]^2}\sqrt{1-e^2}\ (1.5 \sin^2 i - 1)$$

$$\dot{\Omega} = \frac{k\sqrt{\mu/a^3}}{[a(1-e^2)]^2} \cos i$$

$$\dot{\omega} = \frac{k\sqrt{\mu/a^3}}{[a(1-e^2)]^2}\ (2.5 \sin^2 i - 2)$$

where

$\mu = Gm$ = 62630.3949

$k = R_E^2 J_2$ (first term of perturbing force due to Earth's oblateness) = -19255.96124

The rate terms for the sun are fixed and are included in Table B-1. The simulation updates M, Ω, ω by

$$M(t) = M(t_o) + \dot{M} \cdot (t-t_o) \qquad -\pi < M \leq \pi$$

$$\Omega(t) = \Omega(t_o) + \dot{\Omega} \cdot (t-t_o) \qquad -\pi < \Omega \leq \pi$$

$$\omega(t) = \omega(t_o) + \dot{\omega} \cdot (t-t_o) \qquad -\pi < \omega \leq \pi$$

A seventh term, the Greenwich Hour Angle (GHA), which relates the earth-fixed coordinate system to the inertial system, given the six elements is updated via:

$$GHA(t) = GHA(t_o) + \omega_e \cdot (t-t_o)$$

ω_e = earth rotation rate

TABLE B-1. GPS AND SOLAR EPHEMERIDES

SYMBOL	NAME	UNITS	STANDARD VALUE	
			GPS	SUN
a	Semi Major Axis	Miles	14342.	1*
e	Eccentricity	--	0.	.0167
i	Inclination	Degrees	63.	23.443
M	Mean Anomaly	Degrees	0.	88.068
Ω	Right ascension of ascending node	Degrees	0.	0.
ω	Argument of perigee	Degrees	0.	270.
$\dot{M}$		Degrees/sec	--	1.14074×10^{-5}
$\dot{\Omega}$		Degrees/sec	--	$.544773 \times 10^{-9}$
$\dot{\omega}$		Degrees/sec	--	0.0
GHA	Greenwich Hour Angle	Degrees		0.0

*Astronomical unit

APPENDIX C

APPENDIX C

THREE BODY MODEL

STRUCTURE

The overall "three" body structure is as shown in Figure C-1. It differs from that given in Reference C-1 in the addition of the gravity gradient rods and tip mass components. The vector $\bar{r}_k$ extends from the center of the space vehicle, CM_o, to the support point of rod k. The vector $\bar{\rho}_k$ extends from the support point to the center of tip mass k. The vector $\bar{x}_k$ extends from the center of tip mass k to a differential mass element. Since all torques will be referenced to the total system center of mass, CM, the vector $\bar{r}_o$ will contain the effects of center of mass variation due to rod/tip mass movement.

EQUATION DERIVATION

In modeling the dynamics associated with the gravity gradient rods and tip masses, the form, procedure, and notation developed in Reference C-1 was followed as closely as possible.

The system momentum, with respect to inertial space is given by:

$$\bar{H} = I_o\bar{\omega}_o + \Sigma_i I_i\bar{\omega}_i + \Sigma_j I_j\bar{\omega}_j + \Sigma_k\bar{H}_k + \Sigma_n\bar{H}_n \qquad \text{(C-1)}$$

where the inertia tensors

$$I_o = J_o + \Sigma_i J_i + \Sigma_j J_j + \Sigma_k J_k + \Sigma_n J_n - mM(r_o,r_o) + \Sigma_i m_i M(r_i,r_i)$$
$$+ \Sigma_j m_j M(r_j+\rho_j,r_j+\rho_j) + \Sigma_k m_k M(r_k+\rho_k,r_k+\rho_k) + \Sigma_n m_n M(r_n+\rho_n,r_n+\rho_n) \qquad \text{(C-2)}$$

$$I_i = J_i \qquad \text{(C-3)}$$

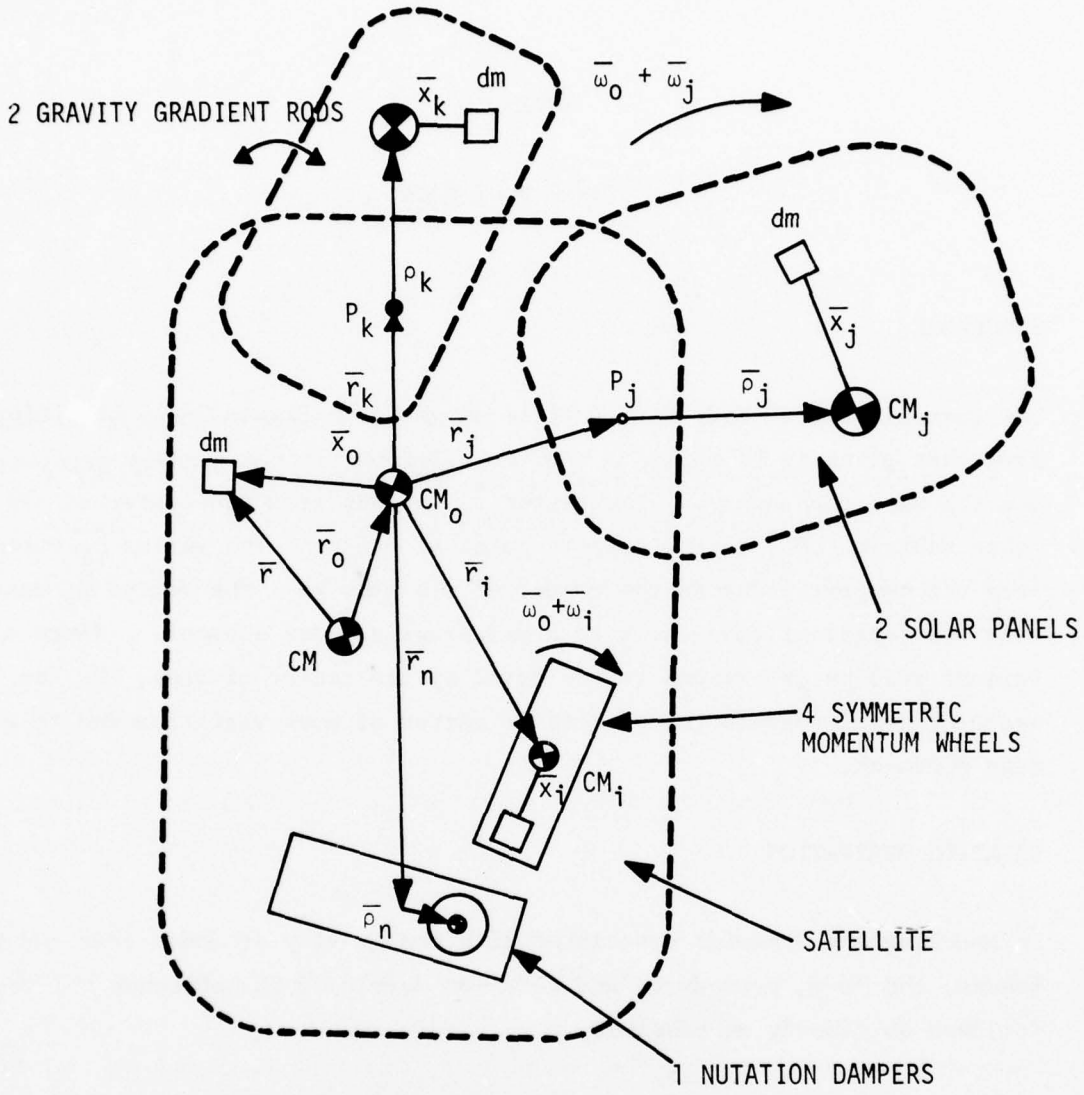

GRAVITY GRADIENT ROD SUPPORT POINT P_k

SOLAR PANEL PIVOT POINTS P_j

BODY CM's: CM_i, CM_j, CM_k; CM = TOTAL CM

MASSES: m_i, m_j, m_k, m_n; m = TOTAL MASS

INERTIA TENSORS (ABOUT CM's) J_o, J_i, J_j, J_k, J_n

Figure C-1. Three Body Structure

$$I_j = J_j + m_j M(r_o + r_j + \rho_j, \rho_j) \tag{C-4}$$

and

$$M(a,b) \triangleq b^T a I - b a^T$$

and where $\bar{r}_o$ is computed from

$$m_o \bar{r}_o + \Sigma_i m_i(\bar{r}_o + \bar{r}_i) + \Sigma_j m_j(\bar{r}_o + \bar{r}_j + \bar{\rho}_j) + \Sigma_k m_k(\bar{r}_o + \bar{r}_k + \bar{\rho}_k) + \Sigma_n m_n(\bar{r}_o + \bar{r}_n + \bar{\rho}_n) = 0 \tag{C-5}$$

If we assume a massless rod and the sphere is a point mass, then

$$J_k = 0 \tag{C-6}$$

The momentum $\bar{H}_k$ may be represented by

$$\bar{H}_k = m_k(\bar{r}_o + \bar{r}_k + \bar{\rho}_k) \times \frac{\delta \bar{\rho}_k}{\delta t} + \int_k (\bar{r}_o + \bar{r}_k + \bar{\rho}_k + x_k) \times \frac{\delta \bar{x}_k}{\delta t} \, dm \tag{C-7}$$

Since we have assumed the tip mass may be represented by a point mass, the second term in equation C-7 may be set to zero.

The torque equations which are the ultimate goal of the model are derived from

$$\bar{T} = \frac{d\bar{H}}{dt} = \frac{\delta \bar{H}}{\delta t} + \bar{\omega}_o \times \bar{H} \tag{C-8}$$

or, differentiating (1)

$$\bar{T} = I_o \dot{\bar{\omega}}_o + \dot{I}_o \bar{\omega}_o + \Sigma_i I_i \dot{\bar{\omega}}_i + \Sigma_j I_j \dot{\bar{\omega}}_j + \Sigma_k \dot{H}_k + \Sigma_n \dot{H}_n + \bar{\omega}_o \times \bar{H} \tag{C-9}$$

where the inertia tensor derivatives

$$\begin{aligned} \dot{I}_o = {} & \Sigma_j \dot{J}_j - m(M(\dot{r}_o, r_o) + M^T(\dot{r}_o, r_o)) \\ & + \Sigma_j m_j (M(r_j + \rho_j, \dot{\rho}_j) + M^T(r_j + \rho_j, \dot{\rho}_j)) \\ & + \Sigma_k m_k (M(r_k + \rho_k, \dot{\rho}_k) + M^T(r_k + \rho_k, \dot{\rho}_k)) \\ & + \Sigma_n m_n (M(r_n + \rho_n, \dot{\rho}_n) + M^T(r_n + \rho_n, \dot{\rho}_n)) \end{aligned} \tag{C-10}$$

$$\dot{I}_j = \dot{J}_j + m_j M(r_o + r_j + \rho_j, \dot{\rho}_j) + m_j M(\dot{r}_o + \dot{\rho}_j, \rho_j) \tag{C-11}$$

where

$$\dot{\rho}_j = \bar{\omega}_j \times \bar{\rho}_j \tag{C-12}$$

$$\dot{\bar{r}}_o = -\frac{1}{m}\left[\Sigma_j m_j \dot{\rho}_j + \Sigma_k m_k \dot{\rho}_k + \Sigma_n m_n \dot{\rho}_n\right] \tag{C-13}$$

The derivatives of the rod/tip mass momentum shown in equation C-9 is given by

$$\dot{H}_k = m_k \left(\frac{\overline{\delta \bar{r}_o}}{\delta t} + \frac{\overline{\delta \rho_k}}{\delta t} \right) \times \frac{\overline{\delta \rho_k}}{\delta t} + m_k (\bar{r}_o + \bar{r}_k + \bar{\rho}_k) \times \frac{\overline{\delta^2 \rho_k}}{\delta t^2} \tag{C-14}$$

$\frac{\overline{\delta^2 \rho_k}}{\delta t^2}$ is the acceleration of tip mass k with respect to the space vehicle.

At this point we introduce rod flexure considerations. Consider the location of the tip mass to be defined

$$\bar{\rho}_k = \bar{\rho}_{k_o} + \bar{\eta}_{a_k} \tag{C-15}$$

where

$\bar{\rho}_{k_o}$ = initial position of tip mass k

$\bar{\eta}_{a_k}$ = displacement of tip mass k due to flexure

Differentiating (15) with respect to body

$$\frac{\overline{\delta \rho_k}}{\delta t} = \frac{\overline{\delta \eta}_{a_k}}{\delta t} \tag{C-16}$$

and

$$\frac{\overline{\delta^2 \rho_k}}{\delta t^2} = \frac{\overline{\delta^2 \eta}_{a_k}}{\delta t^2} \tag{C-17}$$

The flexure model for the gravity gradient rods is described in Appendix I. It is a 2-node model which may be described by

$$M_k \ddot{\bar{\eta}}_k + C_k \dot{\bar{\eta}}_k + K_k \bar{\eta}_k = \bar{F}_{ext} - T_k \dot{\bar{\omega}} \qquad \text{(C-18)}$$

where η_k is a displacement vector for rod/tip mass k

$$\bar{\eta}_k = (\bar{\eta}_{k_a}, \bar{\eta}_{k_b}) \qquad \bar{\eta}_{1_a} = \begin{matrix} \eta_{1_x} \\ \eta_{1_y} \end{matrix} \quad \text{etc.}$$

$\bar{\eta}_{k_a}$ = displacement at node A (tip mass center)

η_{k_b} = displacement at node B (mid-point of rod)

M_k is the mass matrix defined by

$$m_k = \begin{bmatrix} m_{k_a} & 0 \\ 0 & m_{k_b} \end{bmatrix} \qquad \begin{aligned} m_{k_a} &= m_{k_{\text{tip mass k}}} + \tfrac{1}{4} m_{\text{rod k}} \\ m_{k_b} &= \tfrac{1}{4} m_{\text{rod k}} \end{aligned}$$

C_k is the damping matrix given by

$$C_k = C_k' \begin{bmatrix} C_{k_a} \\ C_{k_b} \end{bmatrix}$$

where C_{k_a} and C_{k_b} have been defined in Appendix I as

$$C_{k_a} = \begin{bmatrix} 201.06\text{x}10^{-6} & 0 & -.75\text{x}10^{-6} & 0 \\ 0 & 201.06\text{x}10^{-6} & 0 & -.75\text{x}10^{-6} \end{bmatrix}$$

$$C_{k_b} = \begin{bmatrix} -.75\text{x}10^{-6} & 0 & 12.17\text{x}10^{-6} & 0 \\ 0 & -.75\text{x}10^{-6} & 0 & 12.17\text{x}10^{-6} \end{bmatrix}$$

and C_k' is a scalar used for a conversion factor and for changing damping ratios. NOTE: It has been assumed that there are no deflections in the Z direction, thus there are only two degrees of freedom at each node.

K_k is the stiffness matrix

$$K_k = \left\{ K_k' \begin{bmatrix} K_{k_a} \\ K_{k_b} \end{bmatrix} \right\}^{-1}$$

where K_k' is a conversion factor and

$$K_{k_a} = \begin{bmatrix} \frac{4608\ell^3}{EI_y} + \frac{1728\ell}{JG}\left(y_{o_{a_k}} - 2y_{o_{b_k}}\right)^2 & 0 & \frac{1440\ell^3}{EI_y} & 0 \\ 0 & \frac{4608\ell^3}{EI_x} + \frac{1728\ell}{JG}\left(x_{o_{a_k}} - 2x_{o_{b_k}}\right)^2 & 0 & \frac{576\ell^3}{EI_x} \end{bmatrix}$$

$$K_{k_b} = \begin{bmatrix} \frac{1440\ell^3}{EI_y} & 0 & \frac{576\ell^3}{EI_y} & 0 \\ 0 & \frac{1440\ell^3}{EI_x} & 0 & \frac{576\ell^3}{EI_x} \end{bmatrix}$$

ℓ = rod half length = 30 ft (fully deployed)

EI_y = rod bending stiffness about y axis 3000±10 percent lb-in^2

EI_x = rod bending stiffness about x axis 3000±10 percent lb-in^2

JF = rod torsional stiffness 25 lb-in^2

x_{o_k}, y_{o_k} = initial x and y components of $\bar{r}_k$ representing unstressed position from x, y axes respectively, due to thermal and manufacturing curvatures.

$\dot{\bar{\omega}} = \begin{bmatrix} \dot{p} \\ \dot{q} \\ \dot{r} \end{bmatrix}$ is the angular acceleration of the spacecraft which is translated to the node point of rod k by transformation T_k.

$$T_k = \begin{bmatrix} & \left[r'_{k_z} + 2\ell\,\mathrm{sgn}(r'_{k_z})\right] & (y_{o_{a_k}} - \eta_{y_{a_k}}) \\ -\left[r'_{k_z} + 2\ell\,\mathrm{sgn}(r'_{k_z})\right] & 0 & (r'_{k_x} + \eta_{x_{a_k}} - x_{o_{a_k}}) \\ 0 & \left[r'_{k_z} + \ell\,\mathrm{sgn}(r'_{k_z})\right] & (y_{o_{b_k}} - \eta_{y_{b_k}}) \\ -\left[r'_{k_z} + \mathrm{sgn}(r'_{k_z})\right] & 0 & (r'_{k_x} + \eta_{x_{b_k}} - x_{o_{b_k}}) \end{bmatrix}$$

where

$$\bar{r}'_k = \bar{r}_o + \bar{r}_k$$

The external forces, F_{ext}, are composed of gravity gradient forces and solar pressure forces. The solar pressure forces acting on the tip masses are defined in Appendix G.

The gravity gradient forces are discussed below.

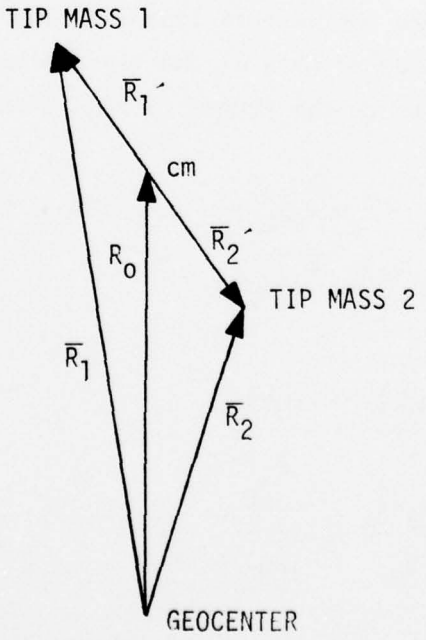

Figure C-2. Tip Mass Configuration

In a central inverse square gravitational field the force acting on a particle of mass m is given by

$$F = \frac{-mk\hat{r}}{|R|^2} = \frac{-mk\bar{R}}{|R|^3} \qquad \text{(C-19)}$$

where:

m = mass of particle

k = gravitational constant

$\bar{R}$ = vector from the particle to the mass center of the attracting body

If we assume two tip masses, the vector $\bar{R}$ would break down into $\bar{R}_1$ and $\bar{R}_2$ as shown in Figure C-2.

$$\bar{R}_1 = \bar{R}_o + \bar{R}_1' \qquad \text{(C-20)}$$

$$\bar{R}_2 = \bar{R}_o + \bar{R}_2' \qquad \text{(C-21)}$$

where $\bar{R}_1'$ and $\bar{R}_2'$ are the vectors from the center of mass of the spacecraft/rod system to the center of mass of the tip masses and $\bar{R}_o$ is a vector from the center of the earth to the center of mass ofthe space vehicle. Referring to Figure C-1

$$\bar{R}_1' = (\bar{r}_o + \bar{r}_{k_1} + \bar{\rho}_{k_1}) \qquad \text{(C-22)}$$

$$\bar{R}_2' = (\bar{r}_o + \bar{r}_{k_2} + \bar{\rho}_{k_2}) \qquad \text{(C-23)}$$

Thus

$$\bar{F}_{1_G} = \frac{-m_1 k\hat{r}_1}{|R_1|^2} = \frac{-m_1 k\bar{R}_1}{|R_1|^3} \qquad \text{(C-24)}$$

$$\bar{F}_{2_g} = \frac{-m_2 k\hat{r}_2}{|R_2|^2} = \frac{-m_2 k\bar{R}_2}{|R_2|^2} \qquad \text{(C-25)}$$

Now

$$|R_1|^2 = (\bar{R}_o + \bar{r}_o + \bar{r}_{k_1} + \bar{\rho}_{k_1}) \cdot (\bar{R}_o + \bar{r}_o + \bar{r}_{k_1} + \bar{\rho}_{k_1})$$

$$= |R_o|^2 + |\bar{r}_o + \bar{r}_{k_1} + \bar{\rho}_{k_1}|^2 + 2\bar{R}_o \cdot (\bar{r}_o + \bar{r}_{k_1} + \bar{\rho}_{k_1})$$

$$= |R_o|^2 \left[\frac{(1 + 2\bar{R}_o \cdot (\bar{r}_o + \bar{r}_{k_1} + \bar{\rho}_{k_1})}{|R_o|^2} + \frac{(\bar{r}_o + \bar{r}_{k_1} + \bar{\rho}_{k_1})^2)}{|R_o|^2} \right]$$

The last term may be neglected leaving

$$|R_1|^2 \cong |R_o|^2 \frac{(1 + 2\bar{R}_o \cdot (\bar{r}_o + \bar{r}_{k_1} + \bar{\rho}_{k_1}))}{|R_o|^2}$$

Take the -3/2 power of both sides

$$|R_1|^{-3} \cong |R_o|^{-3} \frac{(1 + 2\bar{R}_o \cdot (\bar{r}_o + \bar{r}_{k_1} + \bar{\rho}_{k_1})^{-3/2})}{|R_o|^2}$$

Using the binomial theorem

$$|R_1|^{-3} \cong \frac{1}{|R_o|^3} \frac{(1 - 3\,\bar{R}_o \cdot (\bar{r}_1 + \bar{r}_{k_1} + \bar{\rho}_{k_1}))}{|R_o|^2}$$

Therefore

$$F_{1_G} \cong \frac{m_1 k}{|R_o|^3} (\bar{R}_o + \bar{r}_o + \bar{r}_{k_1} + \bar{\rho}_{k_1}) \frac{(1 - 3\,\bar{R}_o \cdot (\bar{r}_o + \bar{r}_{k_1} + \bar{\rho}_{k_1}))}{|R_o|^2}$$

and

$$F_{2_G} \cong \frac{m_2 k}{|R_o|^3} (\bar{R}_o + \bar{r}_o + \bar{r}_{k_2} + \bar{\rho}_{k_2}) \frac{(1 - 3\,\bar{R}_o \cdot (\bar{r}_o + \bar{r}_{k_2} + \bar{\rho}_{k_2}))}{|R_o|^2}$$

The forces $\bar{F}_{1_G}$ and $\bar{F}_{2_G}$ can be separated into a gravity component and a gravity gradient component or

$$\bar{F}_{1_G} = \bar{F}_{1_{G\ \text{gravity}}} + \bar{F}_{1_{G\ \text{gravity gradient}}}$$

where

$$\bar{F}_{1_{G\ \text{gravity}}} = \frac{m_1\, k\, \bar{R}_o}{|R_o|^3}$$

and

$$\bar{F}_{1_{G\ (\text{gravity gradient})}} = \frac{m_1 k}{|R_o|^3}(\bar{r}_o + \bar{r}_{k_1} + \bar{\rho}_{k_1})\ \frac{(1-3\,\bar{R}_o \cdot (\bar{r}_o + \bar{r}_{k_1} + \bar{\rho}_{k_1})}{|R_o|^2}$$

$$- \frac{\bar{R}_o\,(3\,\bar{R}_o \cdot (\bar{r}_o + \bar{r}_{k_1} + \bar{\rho}_{k_1})}{|R_o|^2}$$

$$= \frac{m_1 k}{|R_o|^3}\ (\bar{r}_o + \bar{r}_{k_1} + \bar{\rho}_{k_1}) - \frac{-\bar{R}_o(3\bar{R}_o \cdot (\bar{r}_o + \bar{r}_{k_1} + \bar{\rho}_{k_1}))}{|R_o|^2}$$

Over the n body model the gravity forces will cancel out, leaving only the gravity gradient forces.

Summation of forces

$$m_1 \frac{\delta^2 \bar{\rho}_{k_1}}{\delta t^2} = \bar{F}_{1_G} + \bar{F}_{1_s}$$
(gravity gradient)

Where F_{1_s} = solar force

All vectors are expressed in body axis, so $R_o = T_{LV\ \text{to}\ B} \begin{bmatrix} 0 \\ 0 \\ R_o \end{bmatrix}$

Where $T_{LV/B}$ is the transformation from local vertical axes to body.

REFERENCES

C-1. Rupert, J.G., "GPS Equations of Motion," Honeywell MR 12349, May 27, 1975.

APPENDIX D

APPENDIX D

NUTATION DAMPER MODEL

This appendix summarizes the nutation damper model implemented for the digital simulation evaluation of GPS stability and control analysis.

The nutation damper is used for passive GPS spin axis stabilization during the initial mission phases by dissipating the spacecraft precession energy. The nutation damper adopted for GPS application is of the type of ball in gas filled tube. The tube is made of aluminum and the ball of tungsten carbide. The gas is a 9 : 1 ratio mixture of nitrogen and helium at 1 atm. pressure. Physical parameters of this damper is shown in Figure D-1.

A similar damper of this type was used in the Telstar satellite, Reference D-1. Discussions on the design and analysis of ball-in-tube type nutation dampers can be found in Reference D-2.

Derivation of the torque equations presented here follows the same procedure of Reference D-2 which contains numerous typographical errors. The results, in the torque form, are compatible for integration into the three body model described in Appendix C.

DAMPER MODEL DERIVATION

To facilitate the model derivation, we shall define a vehicle fixed B-frame whose origin is at the vehicle's center of mass (excluding damper ball) with the ($\underline{X}_B$ - $\underline{Y}_B$ - $\underline{Z}_B$) axes aligned with its principal axes. Also in the following consideration of vehicle rotational motions, it is assumed that the translational motion of vehicle's center of mass resulted from reactional

TYPE BALL IN GAS FILLED TUBE

TUBE CURVED TO PROVIDE CENTRIFUGAL SPRING

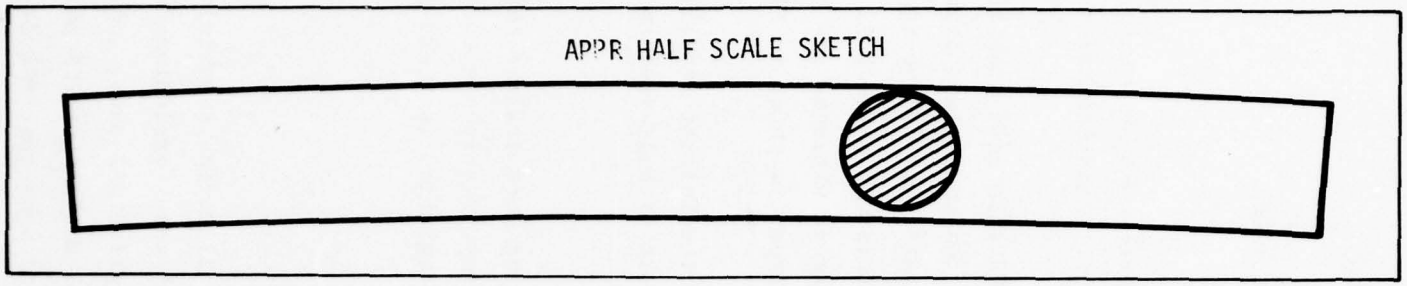

TUBE

I.D. 1.266 INCH
O.D. 1.566 INCH

LENGTH 16 INCHES

r = RADIUS OF CURVATURE 159 INCHES = 13.25 ft.

MATERIAL ~ ALUMINUM

BALL

DIAMETER 1.25 INCH r_D = 0.625 inches

MATERIAL TUNGSTEN CARBIDE

GAS

9:1 MIXTURE NITROGEN: HELIUM
1 ATMOSPHERE

WEIGHT

1.75 LBS

Figure D-1. Nutation Damper Characteristics

forces of the damper ball can be neglected. By reference to the geometrical description of damper location in B-frame, the position of center of ball, $\underline{R}_b$ can be written as, Figure D-2,

$$(\bar{\underline{P}}^B_b) = \begin{bmatrix} 0 \\ -a + \gamma \cos \alpha \\ b + \gamma \sin \alpha \end{bmatrix} \tag{D-1}$$

where

γ = 159 in. = 13.25 ft.

(a,b) = coordinates of tube center of curvature

Equation (1) implies that $\underline{Y}_B - \underline{Z}_B$ plane contains the damper tube.

Let the vehicle moment of inertia be such that

$$\begin{cases} I_{XX} = I_{YY} = A \\ I_{ZZ} = C \end{cases} \tag{D-2}$$

The rotational energy of the vehicle becomes,

$$T_V = \tfrac{1}{2} A(W_X^2 + W_Y^2) + \tfrac{1}{2} C W_Z^2 \tag{D-3}$$

The velocity of damper ball can be written through differentiation of (1) as,

$$(\bar{\underline{V}}^B_b) = T_{BI}(\bar{\underline{V}}^B_b) = T_{BI}(\dot{\bar{\underline{R}}}^I_b)$$

with $(\bar{\underline{R}}^I_b) = T_{BI}^T (\bar{\underline{R}}^B_b)$, we have

$$(\dot{\bar{\underline{R}}}^I_b) = \dot{T}_{BI}^T (\bar{\underline{R}}^B_b) + T_{BI}^T (\dot{\bar{\underline{R}}}^B_b)$$

$$= -T_{BI}^T S [(\bar{\underline{W}}^B_B)] (\bar{\underline{R}}^B_b) + T_{BI}^T (\dot{\bar{\underline{R}}}^B_b)$$

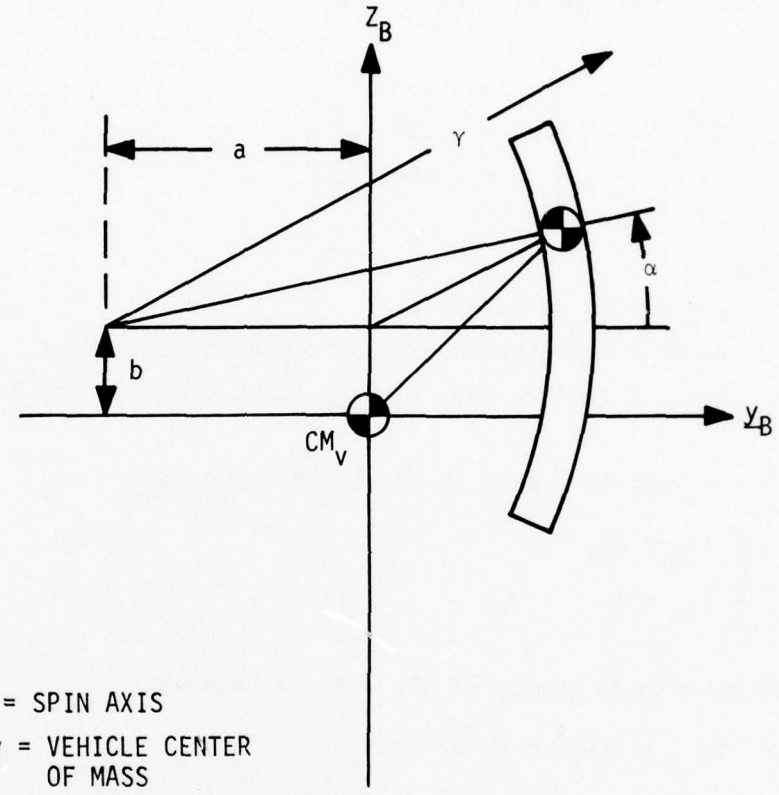

NOTE: Z_B = SPIN AXIS
cMv = VEHICLE CENTER OF MASS
DAMPER CONTAINED IN PLANE (Y_B - Z_B)

Figure D-2. Nutation Damper in Vehicle Body Fixed Frame

or

$$(\underline{\dot{V}}^B_b) = -S\,[(\underline{\omega}^B_B)]\ \ (\underline{R}^B_b) + (\underline{\dot{R}}^B_b) \qquad \text{(D-4)}$$

In component forms, (4) becomes,

$$\begin{bmatrix} V_X \\ V_Y \\ V_Z \end{bmatrix} = \begin{bmatrix} 0 & -W_Z & W_Y \\ W_Z & 0 & -W_X \\ -W_Y & W_X & 0 \end{bmatrix} \quad X \quad \begin{bmatrix} 0 \\ -a + \gamma \cos\alpha \\ b + \gamma \sin\alpha \end{bmatrix}$$

$$+ \begin{bmatrix} 0 \\ -\gamma \sin\alpha\ \dot{\alpha} \\ \gamma \cos\alpha\ \dot{\alpha} \end{bmatrix} \qquad \text{(D-5)}$$

Hence the translational kinetic energy of the damper ball is

$$\begin{aligned} T_b &= \tfrac{1}{2} M (V_X^2 + V_Y^2 + V_Z^2) \\ &= \tfrac{1}{2} M \{[-(-a + \gamma \cos\alpha) W_Z + (b + \gamma \sin\alpha) W_Y]^2 \\ &\quad + [-(b + \gamma \sin\alpha) W_X - \gamma \sin\alpha\ \dot{\alpha}]^2 \\ &\quad + [(-a + \gamma \cos\alpha) W_X + \gamma \cos\alpha\ \dot{\alpha}\}^2 \end{aligned} \qquad \text{(D-6)}$$

where M = mass of the ball

$= \frac{4}{3}\ \pi \gamma_b^3\ \rho = 263$ gm $= 0.018$ slug

ρ = density of tungsten carbide (WC) = 15.7 gm/cm^3

Assuming the ball is rolling without slipping in the tube, the magnitude of the angular velocity of the ball is related to the translational velocity of the center of the ball as

$$\begin{aligned} W_b &= \frac{1}{\gamma_b} [(\underline{\dot{R}}^B_b)^T (\underline{\dot{R}}^B_b)]^{\frac{1}{2}} \\ &= \frac{1}{\gamma_b} [\gamma^2 \sin^2\alpha\ \dot{\alpha}^2 + \gamma^2 \cos^2\alpha\ \dot{\alpha}^2]^{\frac{1}{2}} \\ &= \frac{\gamma \dot{\alpha}}{\gamma_b} \qquad \text{where } \gamma_b = \text{radius of the ball} = 0.625 \text{ in.} \end{aligned} \qquad \text{(D-7)}$$

Hence, the rotational energy of the ball is

$$T = \tfrac{1}{2} I_b W_b^2 = \tfrac{1}{2} \left(\frac{2}{5} M \gamma_b^2\right) \left(\frac{\gamma\dot{\alpha}}{\gamma_b}\right)^2$$

$$= \frac{1}{5} M \gamma^2 \dot{\alpha}^2 \qquad \text{(D-8)}$$

The drag on the ball is viscous, Reference D-3, since the tube is gas filled, the clearance between ball and tube is small and the ball moves much slower than the speed of sound. Hence, the viscous drag on the ball can be represented by Rayleigh's dissipation function as

$$F = \tfrac{1}{2} C_D \left(\dot{\underline{R}}_b\right)^T \left(\dot{\underline{R}}_b\right)$$

$$= \tfrac{1}{2} C_D \gamma^2 \dot{\alpha}^2 \qquad \text{(D-9)}$$

where C_D is a constant to be described later.

The total energy of the system then becomes

$$T = T_v + T_b + T_\gamma$$

$$= W_X^2 \{\tfrac{1}{2}A + \tfrac{1}{2}M (\gamma^2 + b^2 + a^2 + 2b\gamma \sin\alpha - 2a\gamma\cos\alpha)\}$$

$$+W_Y^2 \{\tfrac{1}{2}A + \tfrac{1}{2}M (b^2 + 2b\gamma\sin\alpha + \gamma^2 \sin^2\alpha)\}$$

$$+W_Z^2 \{\tfrac{1}{2}C + \tfrac{1}{2}M (a^2 - 2a\gamma\cos\alpha + \gamma^2\cos^2\alpha)\}$$

$$+W_Y W_Z \{-M (-ab - a\gamma\sin\alpha + b\gamma\cos\alpha + \gamma^2 \sin\alpha\cos\alpha)\}$$

$$+W_X \dot{\alpha} \{M (\gamma^2 - a\gamma\cos\alpha + b\gamma\sin\alpha)\}$$

$$+\dot{\alpha}^2 \{\frac{7}{10} M\gamma^2\} \qquad \text{(D-10)}$$

With the total vehicle energy given in (D-10) and the damper dissipation function given in (D-9), the equation of motion of the vehicle and the damper system can be obtained as

$$\frac{d}{dt}\frac{\partial T}{2W_X} - W_Z\frac{\partial T}{2W_Y} + W_Y\frac{\partial T}{2W_Z} = 0$$

$$\frac{d}{dt}\frac{\partial T}{\partial W_Y} - W_X\frac{\partial T}{\partial W_Z} + W_Z\frac{\partial T}{\partial W_X} = 0$$

$$\frac{d}{dt}\frac{\partial T}{\partial W_Z} - W_Y\frac{\partial T}{\partial W_X} + W_X\frac{\partial T}{\partial W_Y} = 0$$

$$\frac{d}{dt}\frac{\partial T}{\partial \dot{\alpha}} - \frac{\partial T}{\partial \alpha} + \frac{\partial F}{\partial \dot{\alpha}} = 0 \qquad \text{(D-11)}$$

The rotational equation of motion of the vehicle can be written in the form of Euler's rigid body equation as

$$\begin{cases} A\dot{W}_X + (C - A)\, W_Z W_Y = T_X \\ A\dot{W}_Y - (C - A)\, W_X W_Z = T_Y \\ A\dot{W}_Z = T_Z \end{cases} \qquad \text{(D-12)}$$

where the torques T_X, T_Y, and T_Z are,

$$\begin{aligned} T_X = -M\,[&\dot{W}_X\,(\gamma^2 + b^2 + a^2 + 2b\gamma\sin\alpha - 2a\gamma\cos\alpha) \\ &+\dot{\alpha}\,(2W_X + \dot{\alpha})\,(b\gamma\cos\alpha + a\gamma\sin\alpha) \\ &+\ddot{\alpha}\,(\gamma^2 - a\gamma\cos\alpha + b\gamma\sin\alpha) \\ &+W_Y W_Z\,(a^2 - b^2 - 2a\gamma\cos\alpha - 2b\gamma\sin\alpha - \gamma^2\sin^2\alpha + \gamma^2\cos^2\alpha) \\ &+ (W_Y^2 - W_Z^2)\,(ab + a\gamma\sin\alpha - b\gamma\cos\alpha - \gamma^2\sin\alpha\cos\alpha)] \end{aligned} \qquad \text{(D-13)}$$

$$\begin{aligned} T_Y = -M\,[&\dot{W}_Y\,(b^2 + 2b\gamma\sin\alpha + \gamma^2\sin^2\alpha) \\ &+ (\dot{W}_Z - W_X W_Y)\,(ab + a\gamma\sin\alpha - b\gamma\cos\alpha - \gamma^2\sin\alpha\cos\alpha) \end{aligned}$$

$$+ W_X W_Z (\gamma^2 + b^2 + 2b\gamma \sin\alpha - \gamma^2 \cos^2\alpha)$$

$$+ 2W_Y \dot{\alpha} (b\gamma \cos\alpha + \gamma^2 \sin\alpha \cos\alpha)$$

$$+ 2W_Z \dot{\alpha} (b\gamma \sin\alpha + \gamma^2 \sin^2\alpha)] \qquad \text{(D-14)}$$

$$T_Z = -M [\dot{W}_Z (a^2 - 2a\gamma \cos\alpha + \gamma^2 \cos^2\alpha)$$

$$+ (\dot{W}_Y + W_X W_Y) (ab + a\gamma \sin\alpha - b\gamma \cos\alpha - \gamma^2 \sin\alpha \cos\alpha)$$

$$+ W_X W_Y (-a^2 + 2a\gamma \cos\alpha - \gamma^2 \cos^2\alpha)$$

$$+ 2W_Z \dot{\alpha} (a\gamma \sin\alpha - \gamma^2 \sin\alpha \cos\alpha)$$

$$- 2W_Y \dot{\alpha} (b\gamma \sin\alpha + \gamma^2 \sin^2\alpha)] \qquad \text{(D-15)}$$

With ball's equation of motion in tube given as,

$$\frac{7}{5} \gamma\ddot{\alpha} + \dot{W}_X (\gamma - a \cos\alpha + b \sin\alpha)$$

$$- W_X^2 (b \cos\alpha + a \sin\alpha) - W_Y^2 (b \sin\alpha + \gamma \sin\alpha \cos\alpha)$$

$$- W_Z^2 (a \sin\alpha - \gamma \sin\alpha \cos\alpha)$$

$$- W_Y W_Z (a \cos\alpha + b \sin\alpha - \gamma \cos^2\alpha + \gamma \sin^2\alpha)$$

$$+ W_X \dot{\alpha} (a \sin\alpha + b \cos\alpha - a \sin\alpha - b \cos\alpha)$$

$$+ \left(\frac{C_D \gamma}{N}\right) \dot{\alpha} = 0 \qquad \text{(D-16)}$$

The drag force on the ball consists of two components: the pressure drag and the viscous drag. For the case where the gap between tube and ball is small, as in the GPS nutation damper, and the speed of the ball in the tube is small compared with the speed of sound, it has been determined in Ref. D-3 that the drag force is primarily due to pressure drag. The drag force D,

can be written as

$$D = \frac{135}{4x64}\left(\frac{\pi^3 \mu \gamma_b}{g^{5/2}}\right) S \triangleq C_D S$$

where

μ = viscosity of gas in tube

$g = (\gamma_i - \gamma_b)\gamma_b$ = gap parameter

γ_i = inside radius of tube

S = speed of ball relative to gas

C_D = dissipation coefficient

$$= \frac{135}{4x64} \frac{\pi^3 \mu \gamma_b}{g^{5/2}}$$

For GPS nutation damper,

$\mu = 178.1 \times 10^{-6} \times 2.089 \times 10^{-3}$ lb_f sec/ft^2

$g = (0.633 - 0.625) / 0.625$

$\gamma_i = 0.633$ in.

Hence, value of dissipation coefficient,

$C_D = .0171$ lb_f/(ft/sec)

To handle the discontinuity at either end of the damper tube, let

$\dot{\alpha} = -\varepsilon\dot{\alpha}$ at $\alpha = \pm \alpha$ max

where

α max $\approx$ (8/159) rad = 2.9 deg.

ε = 0 for inelastic collision

= 1 for elastic collision.

The GPS requirement on half cone angle of nutation is to be less than 2 deg. The discontinuity situation is not expected to be encountered often if the 2 deg. requirement is met. The value of $\varepsilon = 1$ would give a conservative result in that less precession energy is dissipated at bottoming. Hence, use of $\varepsilon = 1$ is recommended for this reason.

NUTATION DAMPING TIME CONSTANT VERIFICATION

Nominal Solution Undamped Rigid Body Motion

Consider a rigid body with symmetric moment of inertia about the traverse axes, i.e., $I_{XX} = I_{YY}$ in a torque free situation. The Euler's equation is reduced to:

$$\begin{cases} \dot{W}_X = -A\, W_Y W_Z \\ \dot{W}_Y = A\, W_Z W_X \\ \dot{W}_Z = 0 \end{cases} \qquad \text{(D-17)}$$

where

$$A = \left(\frac{I_{ZZ} - I_{XX}}{I_{XX}} \right) = \left(\frac{I_{ZZ}}{I_{XX}} - 1 \right) \triangleq (n - 1)$$

The solution of the above equation can be written as:

$$\begin{cases} W_X = -B \sin \Omega t \\ W_Y = B \cos \Omega t \\ W_Z = W_Z(0) \end{cases} \qquad \text{(D-18)}$$

with $\Omega = A\, W_Z(0)$ (D-19)

The angular momentum vector is written as:

$$\underline{H} = I_{XX} W_X \underline{X}_B + I_{YY} W_Y \underline{Y}_B + I_{ZZ} W_Z \underline{Z}_B \qquad \text{(D-20)}$$

Since there is no external torque, the angular momentum is constant. The nominal motion of the rigid body can be visualized as a constant precession about the angular momentum vector with a precession rate Ω and a nutation angle θ which is defined as:

$$\tan \theta = \frac{H_I}{H_S} = \frac{\sqrt{I_{XX}^2 W_X^2 + I_{YY}^2 W_Y^2}}{I_{ZZ} W_Z} = \frac{I_{YY} B}{I_{ZZ} W_Z} \qquad \text{(D-21)}$$

Therefore:

$$B = \left(\frac{I_{ZZ}}{I_{YY}} \times \tan \theta \right) W_Z \qquad \text{(D-22)}$$

For small value of θ, (6) becomes

$$B \approx \left(\frac{I_{ZZ}}{I_{YY}} \times \theta \right) W_Z \qquad \text{(D-23)}$$

A relationship between the rigid body's angular momentum and rotational energy useful for later development of the energy sink approximation is:

$$\begin{cases} T = \frac{1}{2} I_{XX} (W_X^2 + W_Y^2) + \frac{1}{2} I_{ZZ} W_Z^2 = \dfrac{H_t^2}{2I_{XX}} + \dfrac{H_s^2}{2I_{ZZ}} \\ H^2 = H_t^2 + H_s^2 \end{cases} \qquad \text{(D-24)}$$

$$\text{Hence } H_t^2 = \left(\frac{I_{XX} I_{ZZ}}{I_{ZZ} - I_{XX}} \right) \left(2T - \frac{H^2}{I_{ZZ}} \right) \qquad \text{(D-25)}$$

From (5)

$$\sin^2 \theta = \frac{H_t^2}{H^2} = \left(\frac{I_{XX} I_{ZZ}}{I_{ZZ} - I_{XX}} \right) \left(\frac{2T}{H^2} - \frac{1}{I_{ZZ}} \right) \qquad \text{(D-26)}$$

Nutation Damping Time Constant

The GPS nutation damper consists of a tube aligned with respect to the vehicle spin axis. A ball inside the tube is dissipating the nutation energy via viscous drag force retarding the ball's motion. An approximation procedure known as the energy sink concept assumes that the dissipation of nutation energy does not change the system's angular momentum (which is dominantly spin angular momentum). Hence equation (D-26) can be differentiated with terms $\dot{H}$ neglected in this approximation, i.e.,

$$2 \sin \theta \cos \theta \dot{\theta} = \frac{2I_{ZZ}\dot{T}}{(n-1)H^2} \qquad \text{(D-27)}$$

For small value of θ,

$$\theta \dot{\theta} \quad \frac{2I_{ZZ}\dot{T}}{(n-1)H^2} \qquad \text{(D-28)}$$

A further approximation involves

$$H^2 \approx H_S^2 = I_{ZZ}^2 W_Z^2 \qquad \text{(D-29)}$$

Hence

$$\dot{\theta} \approx \left[\frac{1}{(n-1)I_{ZZ}W_Z^2\theta}\right] \dot{T} \qquad \text{(D-30)}$$

The energy dissipation $\dot{T}$ can be expressed as the product of the drag force the ball experienced and the velocity of the ball, i.e.,

$$\dot{T} = -fv \qquad \text{(D-31)}$$

with drag force,

$$f = C_D V$$

and the ball velocity,

$$V = \gamma\dot{\alpha}$$

Hence the energy dissipation rate,

$$\dot{T} = -C_D \gamma^2 \dot{\alpha}^2 \qquad \text{(D-32)}$$

where α is the position of ball in tube defined as in Figure D-2,

γ = is radius of damper tube,

C_D = is dissipation coefficient

From analysis of nutation damper, the motion of the ball in tube was obtained as

$$\frac{7}{5}\gamma\ddot{\alpha} + \dot{W}_X(\gamma - a\cos\alpha + b\sin\alpha) - W_Y^2(b\cos\alpha + \gamma\sin\alpha\cos\alpha)$$
$$-W_X^2(b\cos\alpha + a\sin\alpha) - W_Z^2(a\sin\alpha - \gamma\sin\alpha\cos\alpha)$$
$$-W_Y W_Z(a\cos\alpha + b\sin\alpha - \gamma\cos^2\alpha + \gamma\sin^2\alpha)$$
$$+ \frac{C_D\gamma}{M}\dot{\alpha} = 0 \qquad \text{(D-33)}$$

With the geometry of mounting such that b = 0 and introducing the small angle approximations $\sin\alpha \approx \alpha$, $\cos\alpha \approx 1$ and neglecting terms W_X^2 and W_Y^2 as they are small for small nutation angle θ, equation (17) becomes

$$(\frac{7\gamma}{5})\ddot{\alpha} + (\frac{C_D\gamma}{M})\dot{\alpha} + W_Z^2(\gamma - a)\alpha = W_Y W_Z(a - \gamma) - \dot{W}_X(\gamma - a) \qquad \text{(D-34)}$$

Using the expression of W_Y as given in equations (2) and (7)

$$W_Y = \theta n\, W_Z \cos\Omega t \qquad \text{(D-35)}$$

Similarly,

$$\dot{W}_X = -\theta n\, W_Z\, \Omega \cos \Omega t$$

Equation (18) can be reduced to the following form:

$$\ddot{\alpha} + \left(\frac{5C_D}{7M}\right)\dot{\alpha} + \left[\frac{5(\gamma - a)W_Z^2}{7\gamma}\right]\alpha = -\theta\left[\frac{5(\gamma - a)\,(2n - n^2)W_Z^2}{7\,\gamma}\right]\cos \Omega t \qquad \text{(D-36)}$$

The solution of the standard second order linear differential equation of the form

$$\ddot{\alpha} + 2\underline{b}\,\dot{\alpha} + \underline{a}^2\,\alpha = \underline{c}\,\theta \cos \Omega t \qquad \text{(D-37)}$$

has been obtained in standard textbooks as:

$$\alpha = \frac{c\theta}{\sqrt{(\underline{a}^2 - \Omega^2)^2 + 4\underline{b}^2\,\Omega^2}} \cos(\Omega t + \phi) \triangleq \theta\alpha_o \cos(\Omega t + \phi) \qquad \text{(D-38)}$$

Compare (20) and (21),

$$2\underline{b} = 5\,C_D/(7M)$$
$$\underline{a}^2 = 5(\gamma - a)W_Z^2/(7\gamma)$$
$$\underline{c} = -5(\gamma - a)\,(2n - n^2)W_Z^2/(7\gamma) \qquad \text{(D-39)}$$

From (22),

$$\dot{\alpha} = -\theta\,\alpha_o\,\Omega \sin(\Omega t + \phi) \qquad \text{(D-40)}$$

Substitute (24) into (16)

$$\dot{T} = -\theta^2\, C_D\, \gamma^2\, \alpha_o^2\, \Omega^2 \sin^2(\Omega t + \phi) \qquad \text{(D-41)}$$

The average value over a full period, i.e.,

$\Omega t_p = 2\pi$, is

$$\bar{\dot{T}} = -\tfrac{1}{2} C_D \gamma^2 \alpha_o^2 \Omega^2 \theta^2 \qquad \text{(D-42)}$$

since $\frac{1}{t_p} \int_o^{t_p} \sin^2 (\Omega t + \phi) dt = \tfrac{1}{2}$

Substitution of (26) into (14) gives

$$\dot{\theta} = \left[\frac{1}{(n-1) I_{ZZ} W_Z^2 \theta}\right] \left[-\tfrac{1}{2} C_D^2 \alpha_o^2 \Omega^2 \theta^2\right]$$

or

$$\dot{\theta} = -\left[\frac{C_D \gamma^2 \alpha_o^2 \Omega^2}{2(n-1) I_{ZZ} W_Z^2}\right] \theta \qquad \text{(D-43)}$$

The time constant of nutation damping can now be written as:

$$T_c = \frac{2(n-1) I_{ZZ} W_Z^2}{C_D \gamma^2 \alpha_o^2 \Omega^2} \qquad \text{(D-44)}$$

where

$$\begin{cases} \alpha_o = \dfrac{c}{\sqrt{(\underline{a}^2 - \Omega^2)^2 + 4\underline{b}^2 \Omega^2}} \\ 2\underline{b} = 5 C_D/(7M) \\ \underline{a}^2 = 5(\gamma - a) W_Z^2/(7\gamma) \\ \underline{c} = -(2n - n^2)\underline{a}^2 \\ \Omega = (n - 1) W_Z \end{cases}$$

The predicted nutation damping time constant for the two cases of W_Z = 100 RPM and W_Z = 10 RPM are computed as follows:

Case 1:

$r = 13.25$ ft.

$a = 10.25$ ft.

$m = 0.018$ slug

$C_D = 0.0171\ lb_f/(ft/sec)$

$I_{XX} = I_{YY} = 77$ slug-ft^2

$I_{ZZ} = 94$ slug-ft^2

$W_Z = 100$ RPM $= 10.47$ rad/sec.

$n = 1.22$

$\Omega = 2.31$

$2\underline{b} = 0.6789$

$\underline{a}^2 = 17.728$

$\underline{c}^2 = -16.84$

$\alpha_o = -1.348$

$T_c = 155.755$ sec.

Case 2:

$W_Z = 10$ RPM $= 1.047$ rad/sec.

$n = 1.22$

$\Omega = 0.231$

$2\underline{b} = 0.6786$

$\underline{a}^2 = 0.17728$

$\underline{c}$ = -0.1684

α_o = -0.84275

T_c = 398.497 sec.

The nutation half cone angle history corresponding to Case 1 and Case 2 considered above are plotted in Figures D-3 and D-4 respectively. These results are obtained using the nutation damping simulation program where the detailed dynamics of the damper ball and rigid body dynamics are considered.

100 RPM

$$\begin{cases} I_{xx} = 76.3 \\ I_{yy} = 78.3 \\ I_{zz} = 94.1 \end{cases}$$

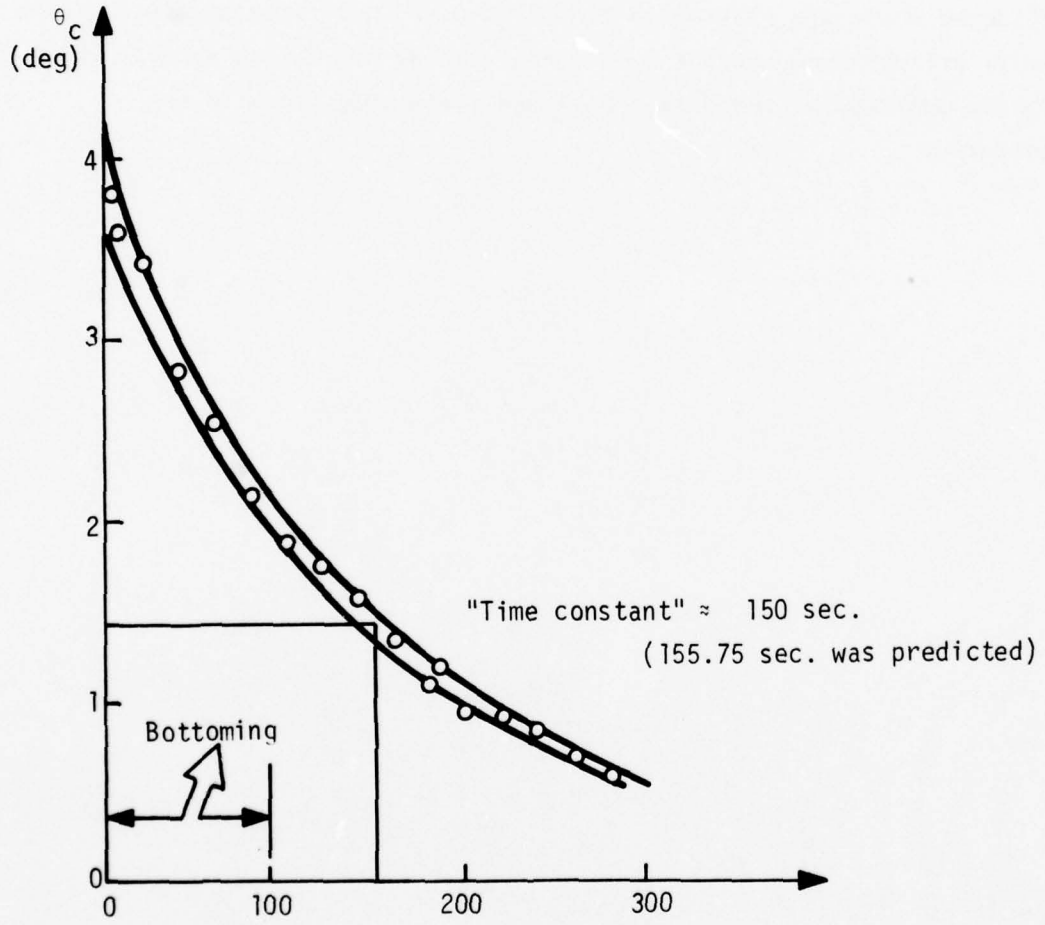

Figure D-3. Simulation Data

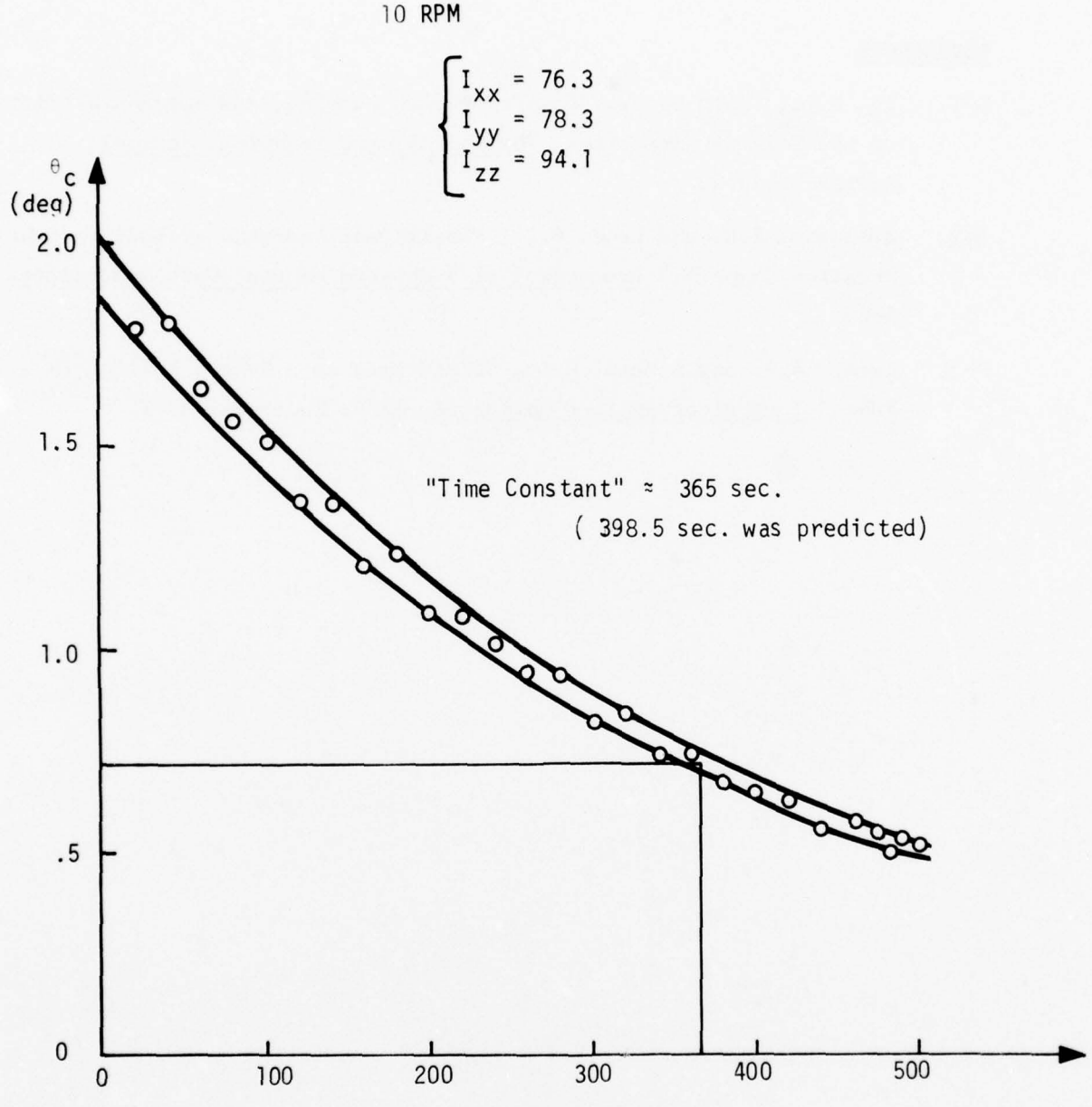

Figure D-4. Simulation Data

REFERENCES

D-1. Yu, E.Y., "Spin Decay, Spin-Precession Damping, and Spin-Axis Drift of the Telstar Satellite," The Bell System Technical Journal, September 1963.

D-2. Auelmann, R.R. and Lane, P.T., "Design and Analysis of Ball-In-Tube Nutation Dampers," Proceeding of Symposium on Dual Spin Spacecraft, 1967.

D-3. Bauer, A.B. and DuPuis, R.A., "Fluid Drag on a Sphere Rolling in a Tube," Journal of Applied Mechanics, ASME, September 1967.

APPENDIX E

APPENDIX E

ATTITUDE CONTROL ELECTRONICS SYSTEM MODEL

The unmodified model of the Attitude Control Electronics system as implemented in the computer simulation differs only from that shown on the Spacetac blueprints in the absence of voltage units and wheel signal monitoring elements. It is given in block diagram form in Figures E-1, E-2, E-3, and E-4.

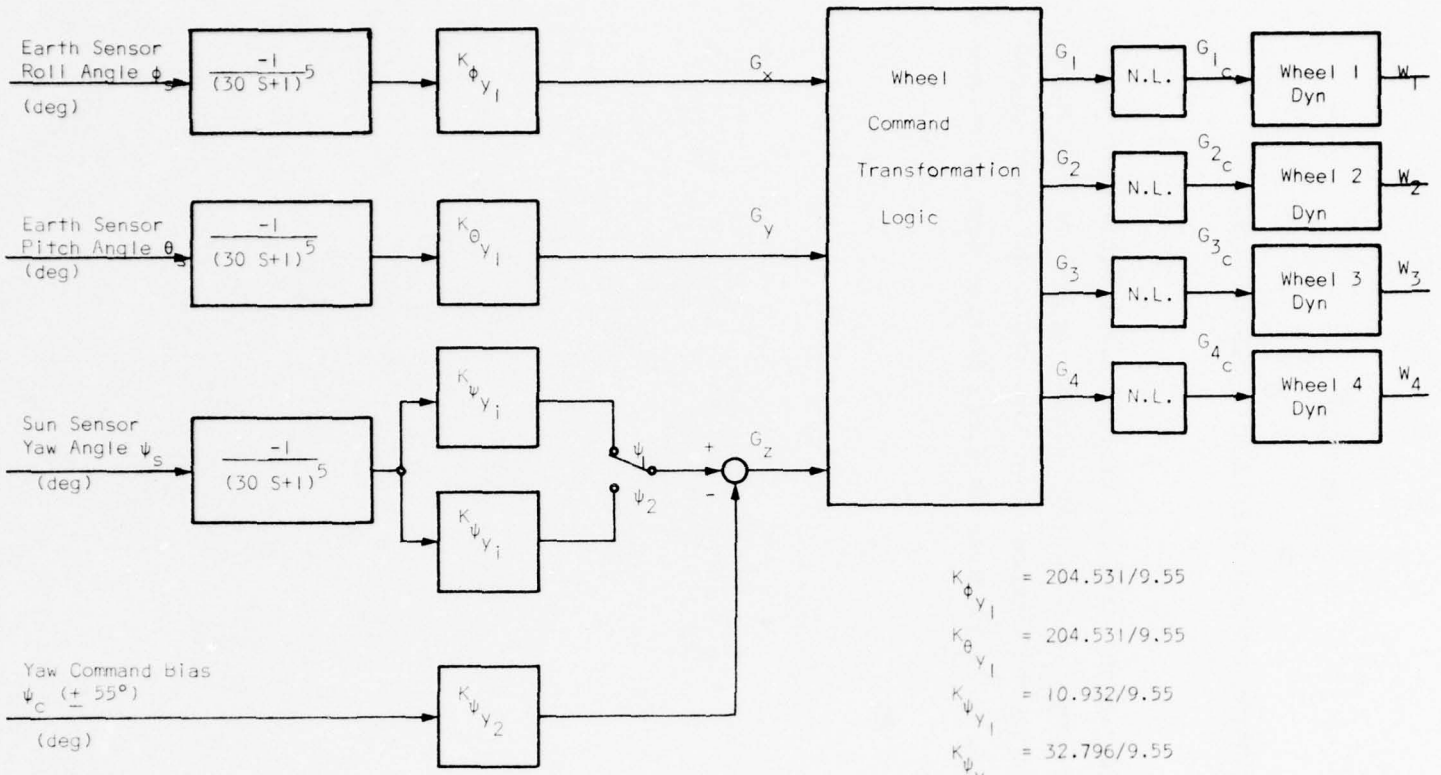

Figure E-1. ACE Systems Block Diagram

Nominal

$$\begin{bmatrix} G_1 \\ G_2 \\ G_3 \\ G_4 \end{bmatrix} = \begin{bmatrix} K & 0 & -K \\ 0 & -K & -K \\ -K & 0 & -K \\ 0 & K & -K \end{bmatrix} \begin{bmatrix} G_x \\ G_y \\ G_z \end{bmatrix}$$

Wheel 1 off

$$\begin{bmatrix} G_1 \\ G_2 \\ G_3 \\ G_4 \end{bmatrix} = \begin{bmatrix} 0 & 0 & 0 \\ +K & -K & -2K \\ -2K & 0 & 0 \\ +K & K & -2K \end{bmatrix} \begin{bmatrix} G_x \\ G_y \\ G_z \end{bmatrix}$$

Wheel 2 off

$$\begin{bmatrix} G_1 \\ G_2 \\ G_3 \\ G_4 \end{bmatrix} = \begin{bmatrix} K & -K & -2K \\ 0 & 0 & 0 \\ -K & -K & -2K \\ 0 & +2K & 0 \end{bmatrix} \begin{bmatrix} G_x \\ G_y \\ G_z \end{bmatrix}$$

$K = .707$

Figure E-2. Wheel Command Transformation Logic

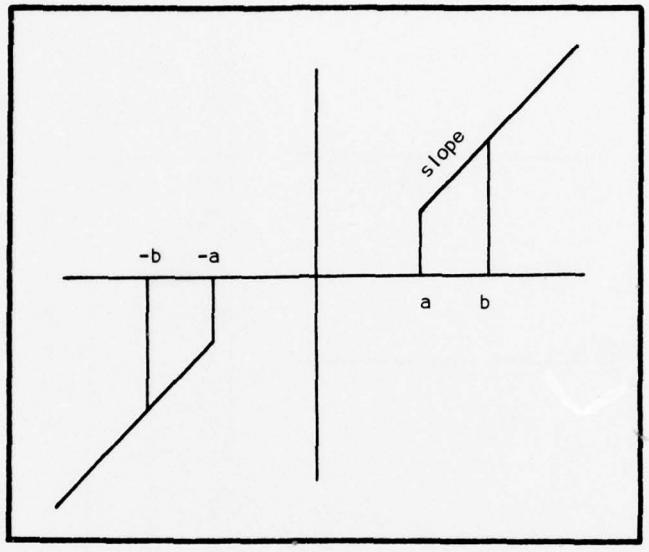

a = 1.57 rad/sec

b = 2.09 rad/sec

slope = 1.0

(equivalent to .14° db in pitch and roll,
2.58° db in yaw, for single axis inputs)

Figure E-3. Nonlinear Element

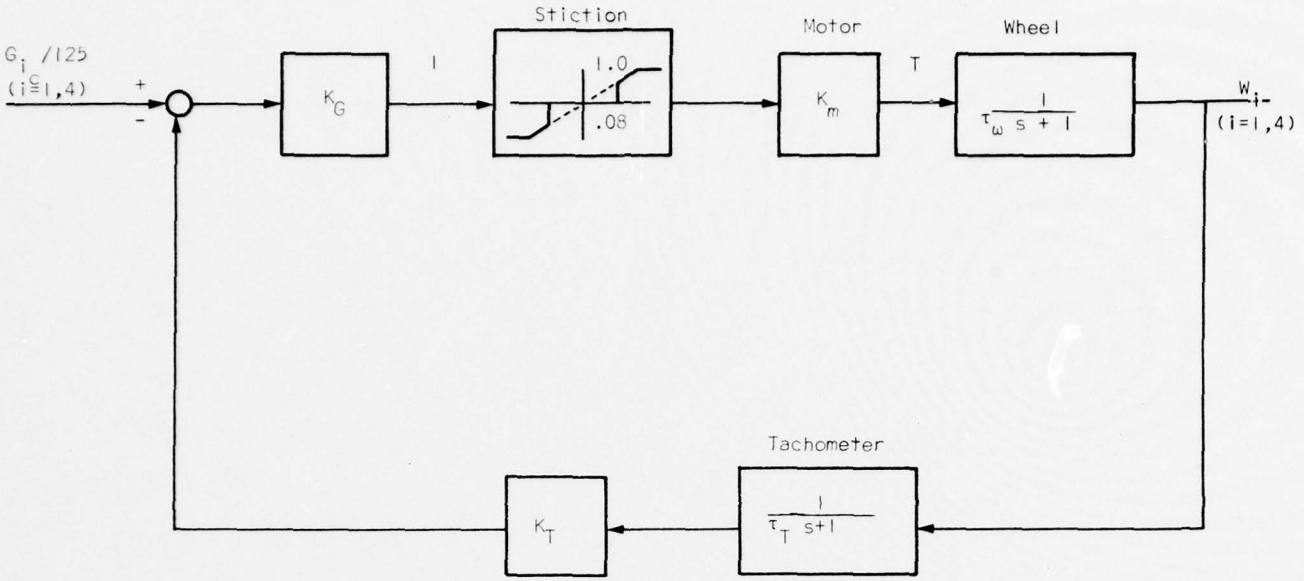

K_G = 33.333

K_m = 125

K_T = .00776

τ_ω = 30 - 50 sec.

τ_T = 1.0

Stiction Gain = $\begin{matrix} 0 \\ \frac{1}{3.93} \\ 1 \end{matrix}$ $\begin{matrix} 1 \\ 1 \\ 1 \end{matrix}$ $\begin{matrix} 1 < .314 \\ .314 \leq 1 \leq 3.93 \\ 1 > 3.93 \end{matrix}$

Figure E-4. Wheel Dynamics with Tach Feedback

APPENDIX F

APPENDIX F

TILTED, CENTERED DIPOLE MAGNETIC TORQUE MODEL

The instantaneous magnetic disturbance torque is $\underline{T}_m = \underline{M} \times \underline{B}$ where

$\underline{M}$ is the spacecraft effective dipole moment

$\underline{B}$ is the local magnetic induction or flux density.

The tilted, centered dipole model is used to represent the flux density. The flux density is a function of latitude and longitude. These parameters were not being calculated in the previous model. Hence a new coordinate system, the E frame, was defined. The E frame has its center at the center of mass of the vehicle with the reference plane perpendicular to the earth's radius vector.

The x axis points east, the y points south, and the Z axis points towards the center of the earth.

The flux density, $\underline{B}$ is defined in the E frame as

$$B_{E_X} = -\left(\frac{Re}{R}\right)^3 \left(g_1^{\,1} \sin\lambda - h_1^{\,1} \sin\theta\right)$$

$$B_{E_Y} = \left(\frac{Re}{R}\right)^3 \left(g_1^{\,o} \cos\underline{\theta} + g'; \sin\theta \cos 2 + h_1^{\,1} \sin\theta \sin\lambda\right)$$

$$B_{E_z} = -2\left(\frac{Re}{R}\right)^3 \left(g_1^{\,o} \sin\theta + g_1^{\,1} \cos\theta \cos\lambda + h_1^{\,1} \cos\theta \sin\lambda\right)$$

where R_e = radius of earth = 2.09029×10^7 ft.

R = orbit radius 8.71627×10^7 ft.

θ = latitude

λ = longitude

where if $\underline{B}$ is in webers/m^2

$$g_1^0 = -3.04012 \times 10^{-5}$$

$$g_1^1 = -2.1638 \times 10^{-6}$$

$$h_1^1 = 5.7782 \times 10^{-6}$$

Latitude and longitude may be calculated from the following expressions.

$$\dot{\theta} = \omega_o \cos \psi_{\underline{H}}$$

$$\dot{\lambda} = \omega_o \frac{\sin \psi_H}{\cos} - \omega_e$$

where ω_o = orbital rate = 1.454441×10^{-4} rad/sec = $\sqrt{\frac{R}{R^3}}$

ω_e = earth spin rate = 7.272205×10^{-5} rad/sec

ψ_H = heading angle

The rate of change of the heading angle is given by

$$\dot{\psi}_H = \sin \psi_H \tan \theta \, \omega_o$$

Initial conditions may be defined as

$\theta_o = o$

$\lambda_o = o$

$\psi H_o = (90^o - i)$, i = inclination angle - 63^o

The flux density must be transformed into body coordinates or

$$\underline{B_B} = T_{LV/B} \; T_{E/LV} \; \underline{B_E}$$

where

TE/LV = transformation from E frame to local vertical frame

$$= \begin{bmatrix} \sin \psi_H & -\cos \psi_H & o \\ \cos \psi_H & -\sin \psi_H & o \\ o & o & 1 \end{bmatrix}$$

$T_{LV/B}$ = transformation from local vertical frame to body frame (already computed in program)

The resulting torque expression then is

$$\underline{T_B'} = \underline{M_B} \times \underline{B_B}$$

Prior to launch the spacecraft dipole moment will be calculated and reduced to less than .5 ampere-meter^2 (500 pole-cm) per axis. Thus if $\underline{M_B}$ is given ampere-meter^2 and $\underline{B_B}$ is in Weber/m^2, $\underline{T_B}$ is in newton meter. The conversion factor between newton meters and ft. lbs. is .737757 ft-lb/nt-m, which will be applied to T_B', or

$$\underline{T_B} \text{ (ft. lbs.)} = .73757 \; \underline{T_B} \text{ (nt m)}$$

Operating Range

Although it is planned to measure the spacecraft dipole moment prior to launch and compensate to obtain values less than 500 pole-cm per axis. Table F-1, which was taken from NASA SP-8018 indicates there may be a large disparity between prelaunch measurements and on-orbit values. In magnitude alone, the values given in Table F-1 range from a factor of .25 to 12. for spin axis.

Table F-1. Change in Spacecraft Dipole Moment

Spacecraft	Spin-axis dipole moment measured prior to transportation to launch site		Spin-axis dipole moment in orbit (computed from motion of spin axis)	
	$A\text{-}m^2$	(pole-cm)	$A\text{-}m^2$	(pole-cm)
Tiros II	+0.1	(+100)	+0.9	(+900)
Tiros III	+0.34	(+340)	-0.45	(-450)
Tiros V	-0.40	(-400)	-0.56	(-560)
Tiros IX	+0.08	(+ 80)	-0.02	(- 20)
ESSA II	+0.01	(+ 10)	+0.10	(+100)
ESSA III	0.00		+0.10	(+100)
ESSA IV	+0.03	(+ 30)	+0.35	(+350)
ESSA V	(a)	(a)	+0.05	(+ 50)
ESSA VI	+0.17	(+170)	-0.15	(-150)

NOTE: Specified spin axis dipole moment for all spacecraft listed is 0.1 $A\text{-}m^2$ (100 pole-cm).

(a) Information is not available.

Table F-2. Factors for Estimating Spacecraft Dipole Moment (M)

Category of magnetic properties control	Estimate of dipole moment per unit mass for non-spinning spacecraft		Estimate of dipole moment per unit mass for spinning spacecraft	
	$A\text{-}m^2/kg$	(pole-cm/lb)	$A\text{-}m^2/kg$	(pole-cm/lb)
Class I	1.0×10^{-3}	(0.45)	0.4×10^{-3}	(0.18)
Class II	3.5×10^{-3}	(1.6)	1.4×10^{-3}	(0.63)
Class III	10×10^{-3} and higher	(4.5)	4.0×10^{-3} and higher	(1.8)

Table F-2, also taken from NASA SP-8018 suggests using a value of 1.6 pole cm. per lb. of spacecraft which would suggest a value of 1600 pole-cm. for NTS-2. The Class I category is for cases where magnetic torques are comparable to other torques.

Although Table F-1 does indicate factor of 10 variations, it appears that these occurred for systems who were tuned to finer than 500 pole cm. An operating range of $\pm$ 5000 pole cm. is clearly unreasonable. However, based on Table F-2, an operating range of $\pm$ 2000 pole-cm. would be realistic if slightly conservative value.

APPENDIX G

APPENDIX G

SOLAR TORQUE MODEL

The relative position of the satellite's surfaces are given in Figure G-1 below.

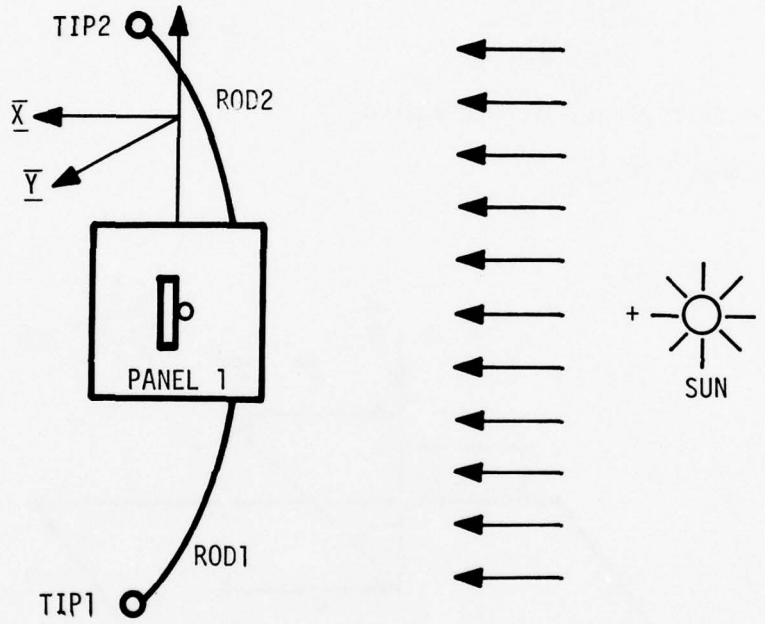

Figure G-1. Relative Position of Satellite's Surface

The solar force on a flat surface is given by:

$$\vec{F} = -F_N\vec{N} + F_T\vec{T} \qquad \text{where:} \qquad \text{(G-1)}$$

$$F_N = \left[(1+\sigma\rho)\cos\psi + \frac{2}{3}(1-\sigma)\right] P\ A\ \cos\psi$$

$$F_T = (1-\sigma\rho)\cos\psi\sin\psi\ P\ A$$

$$P = \text{Solar Pressure Constant} = 1. \times 10^{-7}\ \text{lb/ft}^2$$

A = Area of the flat surface

ρ = Total reflected of the incident light

σ = That part of ρ that is specular reflection (there is also the diffused reflection δ and $\rho = (\sigma + \delta)$

$\vec{N}$ = Normal unit vector to the flat surface

$\vec{T}$ = Shear (tangent) unit vector on the flat surface given by:

$$\vec{T} = \frac{(\vec{N}.\vec{S})\ \vec{N}-\vec{S}}{(\vec{N}.\vec{S})\ \vec{N}-\vec{S}} \qquad \text{(See Figure G-2)}$$

$\vec{S}$ = Unit vector on the sun LOS.

$\psi = \cos^{-1}(\vec{N}.\vec{S})$

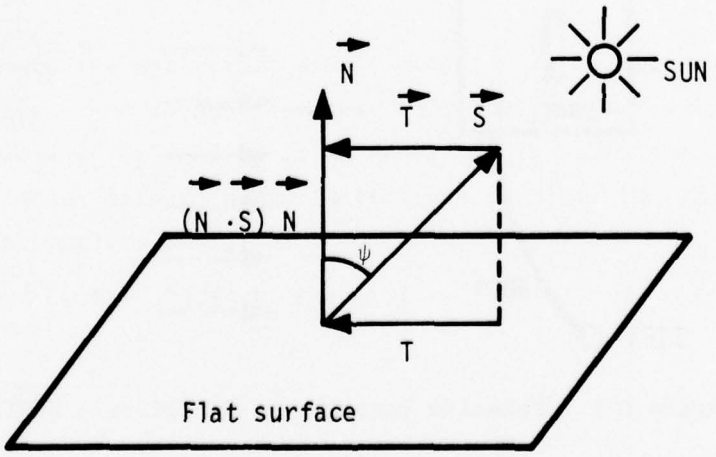

Figure G-2. Unit Vector on Flat Surface

The torque due to (1) is:

$\vec{T} = \vec{C} \times \vec{F}$ where: (G-2)

$\vec{C}$ = Vector of the center of pressure of the surface (usually the geometrical center).

The force and the torque on a full cylindrical surface are given by:

$\vec{F} = -F_N\vec{N} + F_T\vec{T}$ where: (G-3)

$\vec{T}$ = Unit vector along cylinder axis

$\vec{N}$ = Normal unit vector in middle of the cylindrical surface given by:

$$\vec{N} = \frac{\vec{S} - (\vec{S}.\vec{T})\ \vec{T}}{\vec{S} - (\vec{S}.\vec{T})\ \vec{T}}$$

$\vec{S}$ = Unit vector on LOS to the sun

$F_N = \left[(1 + \sigma\rho/3)\ \cos\ \psi + \rho\ (1-\sigma)\ \frac{\pi}{6}\right] P\ A\ \cos\ \psi$

$F_T = (1-\sigma\rho)\ \cos\ \psi\ \sin\ \psi\ P\ A$

A = Projected area of the cylinder = 2 R H

R = Cylinder radius

H = Cylinder Height

$\psi = \cos^{-1}\ (\vec{S}.\vec{N})$

P = Solar constant ($1. \times 10^{-7}$ lb/ft^2)

The torque due to G-3 is:

$\vec{T} = \vec{D} \times \vec{F}$ where: (G-4)

$\vec{D} = \vec{C} + R\vec{N}$

$\vec{C}$ = Vector to the geometrical center of the cylinder (see Figure G-3)

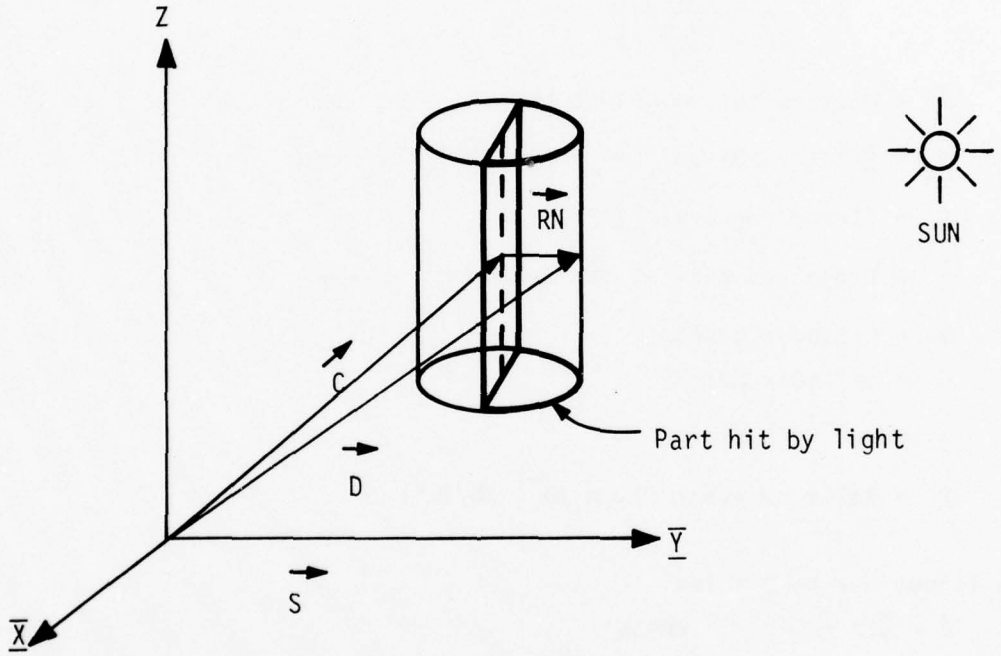

Figure G-3. Vector to Geometrical Center of Cylinder

TIP MASSES

The total solar force on a sphere goes through its geometrical center. Due to the symmetry each quarter (of the half surface of the sphere hit by the sunlight) will produce one quarter of this force along LOS.*

Let us divide this quarter into k equal slices by means of k meridians at $\boxed{\Delta \Phi = \frac{\pi}{2k}}$ angle intervals (Figure G-4).

Then let us divide each slice into n spherical trapezia by means of n parallel circles at $\boxed{\Delta\theta = \frac{\pi}{2n}}$ angle intervals, from the equator to the north pole.

As $(k \to \infty)$ and $(n \to \infty)$ the spherical trapezia can be approximated by flat trapezia.

The dimensions of the ith trapezium on a slice are: The two equal sides:

$$\boxed{\ell_{\theta_r} = r\Delta\theta} \quad , \; r = \text{radius of sphere} \tag{G-5}$$

the unequal sides of the trapezium (its bases):

$\ell_{\Phi_{r_i}} = r_i \Delta\phi$, r_i = radius of ith parallel circle

or

*Other forces (tangential) cancel out due to the symmetry of the sphere and the assumption that sun rays are parallel at ∞.

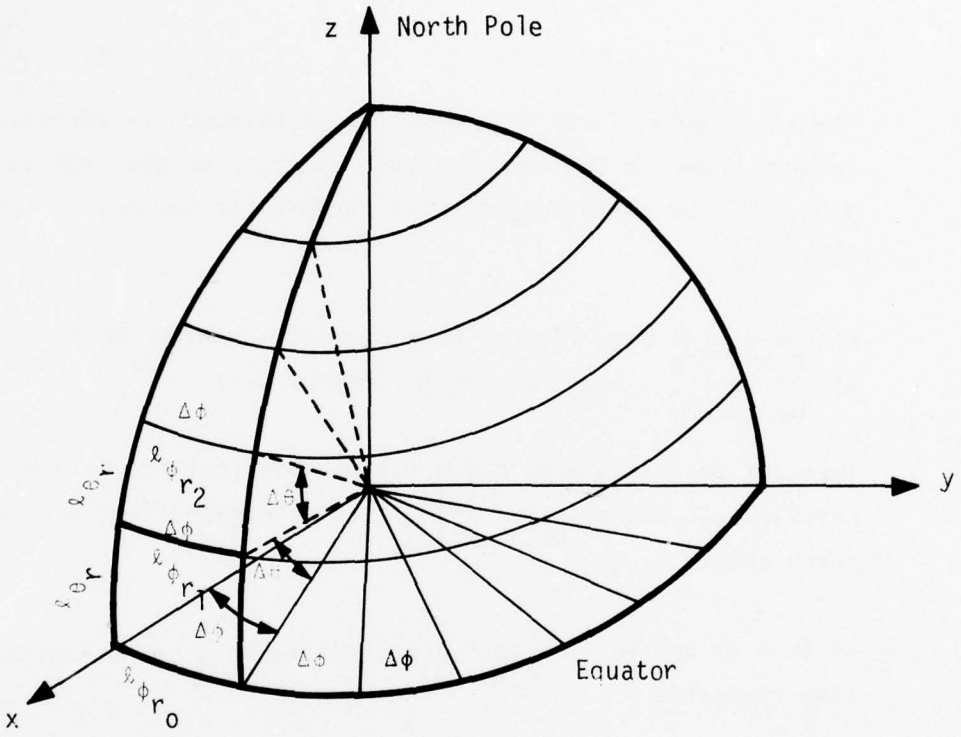

Figure G-4. Angle Intervals

$$\boxed{\ell_{\phi_{r_i}} = r \cos(i\Delta\theta) * \Delta\phi}, \quad i = 1, 2, \ldots, n \tag{G-6}$$

A. From (G-5) and (G-6) we find the area of the ith trapezium:

$$A_i = \frac{(\ell_{\phi_{r_{i-1}}} + \ell_{\phi_{r_i}}) \sqrt{\ell^2_{\theta_r} - (\ell_{\phi_{r_{i-1}}} - \ell_{\phi_{r_i}})^2 / 4}}{2} \tag{G-7}$$

$i = 1, 2, \ldots, n$; where $r_o = r$.

B. CG Location

We have: $\vec{W} = \vec{R} + \vec{U}$ (See Figure G-5)

$$\vec{R} = (r\cos\Phi, r\sin\Phi, 0) \tag{G-8}$$

$$U = (-X\cos\Phi, -X\sin\Phi, r\sin((i-1)\Delta\theta)) \tag{G-9}$$

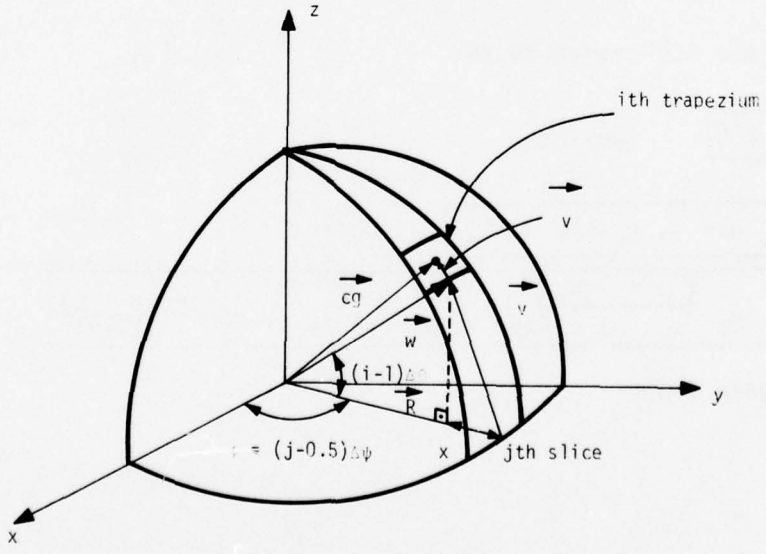

Figure G-5. CG Location

From Figure G-6: $X = r - r\cos((i-1)\Delta\theta)$ or $X = r(1-\cos((i-1)\Delta\theta))$ (G-10)

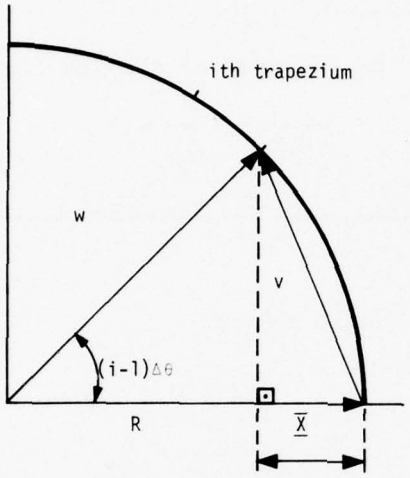

Figure G-6. Value of X

$$\therefore \vec{W} = \vec{R} + \vec{U} = ((r-X)\cos\Phi, (r-X)\sin\phi, r\sin((i-1)\Delta\theta)) \quad \text{(G-11)}$$

Now the CG of the ith trapezium is:

$$\boxed{\vec{CG} = \vec{W} + \vec{V}} \quad \text{where:} \quad \text{(G-12)}$$

$$\boxed{V = (c_x \cos\Phi, c_x \sin\Phi, c_z)} \quad \text{where:} \quad \text{(G-13)}$$

$$\boxed{c_z = \frac{c'}{h} z_i \quad \boxed{c = h-c}, \quad c_x = \frac{c}{h}\sqrt{h^2 - z_i^2}, \quad c = \frac{h(2\alpha+\beta)}{3(\alpha+\beta)}} \quad \text{(G-14)}$$

See Figure G-7.

where:

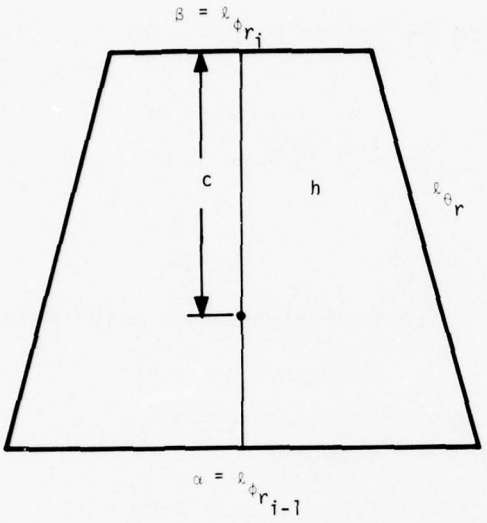

Figure G-7

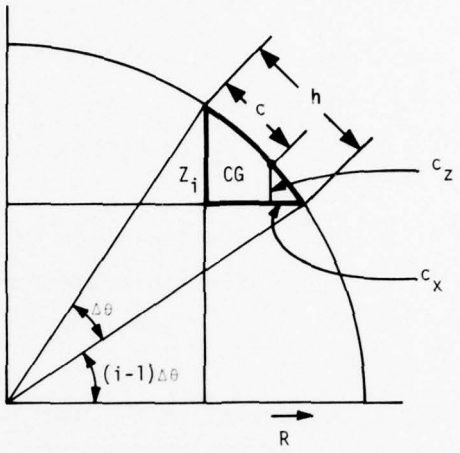

Figure G-8

$$h = \sqrt{\ell^2_{\theta_r} - \frac{(\ell_{\phi_{r_{i-1}}} - \ell_{\phi_{r_i}})^2}{4}}$$

See also G-6 and G-7 (G-15)

and:

$$z_i = r \sin(i\Delta\theta) - r \sin((i-1)\Delta\theta)$$
$$= r\,[\sin(i\Delta\theta) - \sin((i-1)\Delta\theta)] \qquad \text{(G-16)}$$

Substituting G-11 and G-13 into G-12 we obtain the $\overrightarrow{CG}$ vector of the ith trapezium

$$CG = (x\cos\Phi,\ x\sin\Phi,\ c_z + r\sin((i-1)\Delta\theta)) \qquad \text{(G-17)}$$

where: $x = r - X - c_x$

1) c_x and c_z are given by G-14, G-15, and G-16

2) X is given by (5a) and

3) $\Phi = (j-1)\Delta\phi + \frac{\Delta\phi}{2}$, $j = 1, 2, \ldots, (k-1)$
$= (j-0.5)\Delta\phi$

j = jth slice ($j = 1, 2, \ldots, k$)

i = ith trapezium on this slice from equator to north pole.
($i = 1, 2, \ldots, n$)

C. The normal unit vector to the ith trapezium is:

$$\vec{U}_i = \frac{\vec{CG}}{\vec{CG}} \qquad \text{(G-18)}$$

where $\vec{CG}$ is given by G-17 and the norm:

$\vec{CG} \simeq r$ or

$$\vec{CG} = \sqrt{[x\cos\Phi]^2 + [x\sin\Phi]^2 + [c_z + r\sin((i-1)\Delta\theta)]^2}$$

$$= \sqrt{x^2 + [c_z + r\sin((i-1)\Delta\theta)]^2}$$

GRAVITY GRADIENT RODS

Let S be the length of the rod. The rod is a full cylindrical surface and when it is curved due to thermal bending we can approximate it by N equal small cylinders, each having height S/N and which we assume to be right cylinders. See Figure G-9.

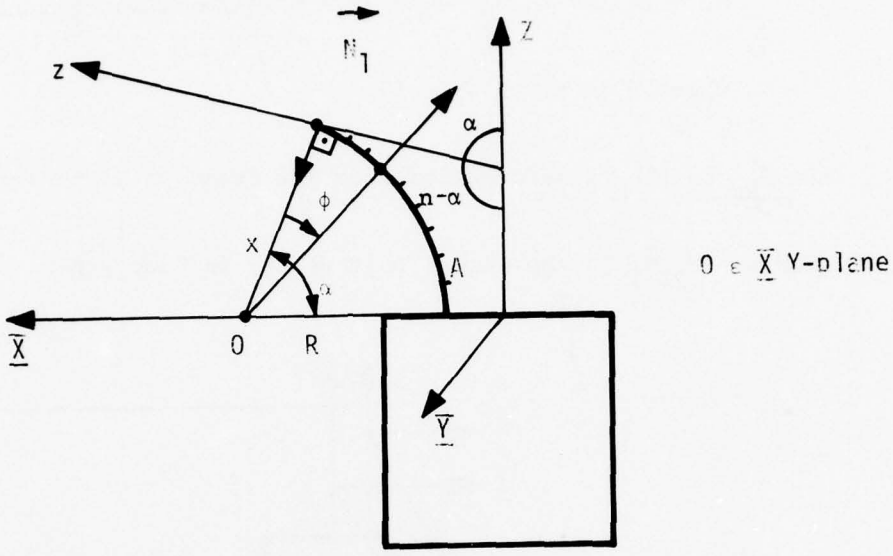

Figure G-9

Let:

X Y Z - Body Frame

x y z - Rod Frame (same as XYZ at nominal position)

R = Radius of curvature of rod.

We have: $\alpha = \frac{S}{R}$, $\Delta\psi = \frac{\alpha}{N}$ and

$$\boxed{\Phi = i\Delta\psi + \frac{\Delta}{2}} \quad , \; i = 0, 1, 2, \ldots, (N-1) \qquad \text{(G-19)}$$

$0 < \Phi < \alpha$

From Figure G-9 we determine the normal unit vector $\vec{N}_1$ to the ith subdivision in Rod Frame.

$$\vec{N}_1 = (-R\cos\Phi,\ 0,\ -R\sin\Phi)/R = (-\cos\Phi,\ 0,\ -\sin\Phi)$$

where Φ is given by G-19.

Let T_{RB} be the transformation from Rod Frame to Body Frame.

Then $\vec{N} = T_{RB}\vec{N}_1$ is the normal unit vector in Body Frame.

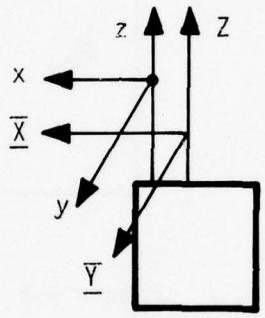

We must determine T_{RB}, i.e., the three Euler angles.

Let $\vec{S} = (S_1, S_2, S_3)$ be the sun unit vector, and $\vec{S}_{XY}$ its projection vector on the XY plane. Then(see Figure G-10) we have

$$\tan\theta = \frac{-S_2}{-S_1}$$

$$\theta = \tan^{-1}(S_2/S_1) \qquad \text{(G-20)}$$

ψ = (see Figure 8) and

$\varphi = 0$

and we have the Euler angles for T_{RB}.

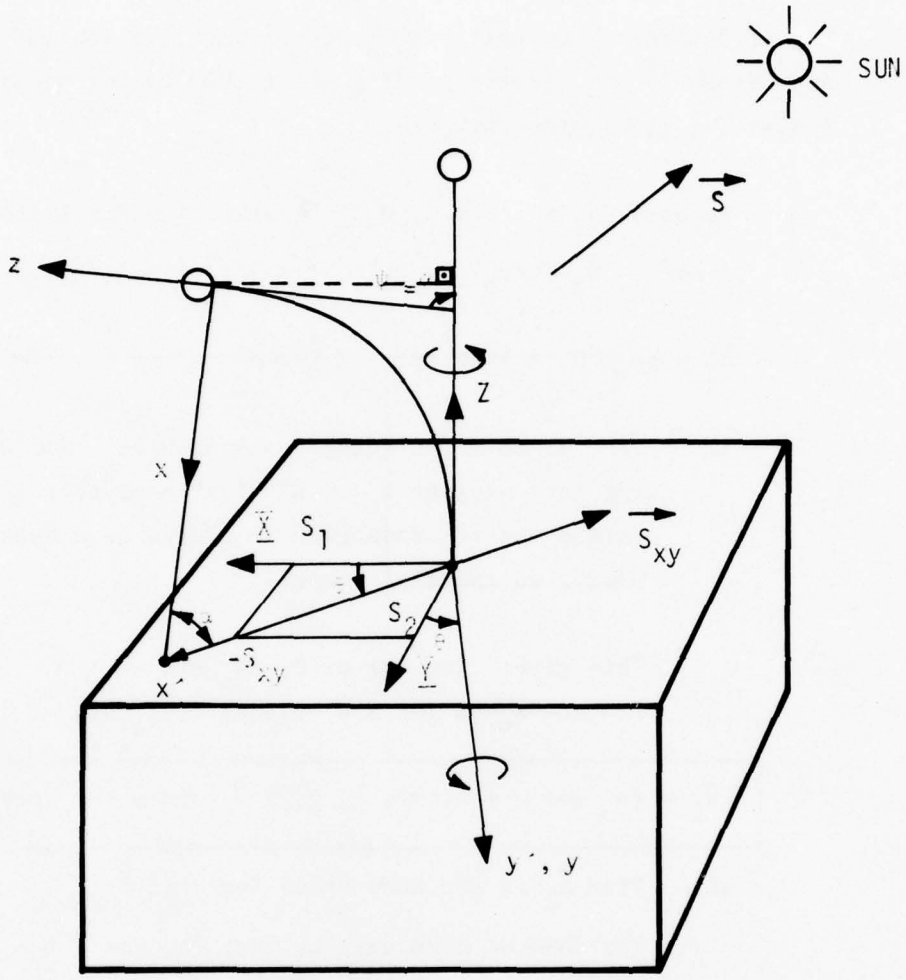

Figure G-10

Let us determine the unit normal vector $\vec{N}$ of the ith rod element in Body Frame from $\vec{N}_1$ (corresponding one in Rod Frame) and the known Euler angles (θ, ψ, φ) given by G-20.

We had: $\vec{N}_1 = (-\cos \Phi, 0, \pm \sin \Phi)$, $\Phi = (i-.5)\Delta\varphi$ (G-23)

or $\vec{N}_1 \quad (x_o, 0, z_o)$ $i = 1, 2, \ldots, N$

$\vec{N}_1 = (x_o, 0, z_o)$ in xyz rod frame

i) Find $\vec{N}_1$ in x'y'z'frame(call it $\vec{N}_2$). See also Figure G-11. For this project x_o on x'-y'-z' axes actually x'-z'-axes (since the y' projection is always zero because $\vec{N}_1$ is always on the x'z' plane).

This gives: $(x_o \cos \alpha, 0, \pm x_o \sin \alpha)$

Project z_o on the x'z'-plane: $(\mp z_o \sin \alpha, 0, z_o \cos \alpha)$

$$\therefore \vec{N}_2 = (x_o \cos \alpha \mp z_o \sin \alpha, 0, \pm x_o \sin \alpha + z_o \cos \alpha) \quad \text{(G-24)}$$

ii) Find $\vec{N}_2$ in XYZ Body Frame (call it $\vec{N}$)

For this we need only project $(x_o \cos \alpha + z_o \sin \alpha)$ on the X, Y axes since Z and z' are identical.

$$\therefore \vec{N} = ((x_o \cos \alpha \mp z_o \sin \alpha) \cos \theta, (x_o \cos \alpha \mp z_o \sin \alpha) \sin \theta, \pm x_o \sin \alpha + z_o \cos \alpha) \quad \text{(G-25)}$$

where:

$x_o = -\cos \Phi$; $\Phi = (i-0.5)\Delta\varphi$, $i = 1, 2, \ldots, N$

$z_o = \pm \sin \Phi$; $\Delta\varphi = \frac{\alpha}{N}$

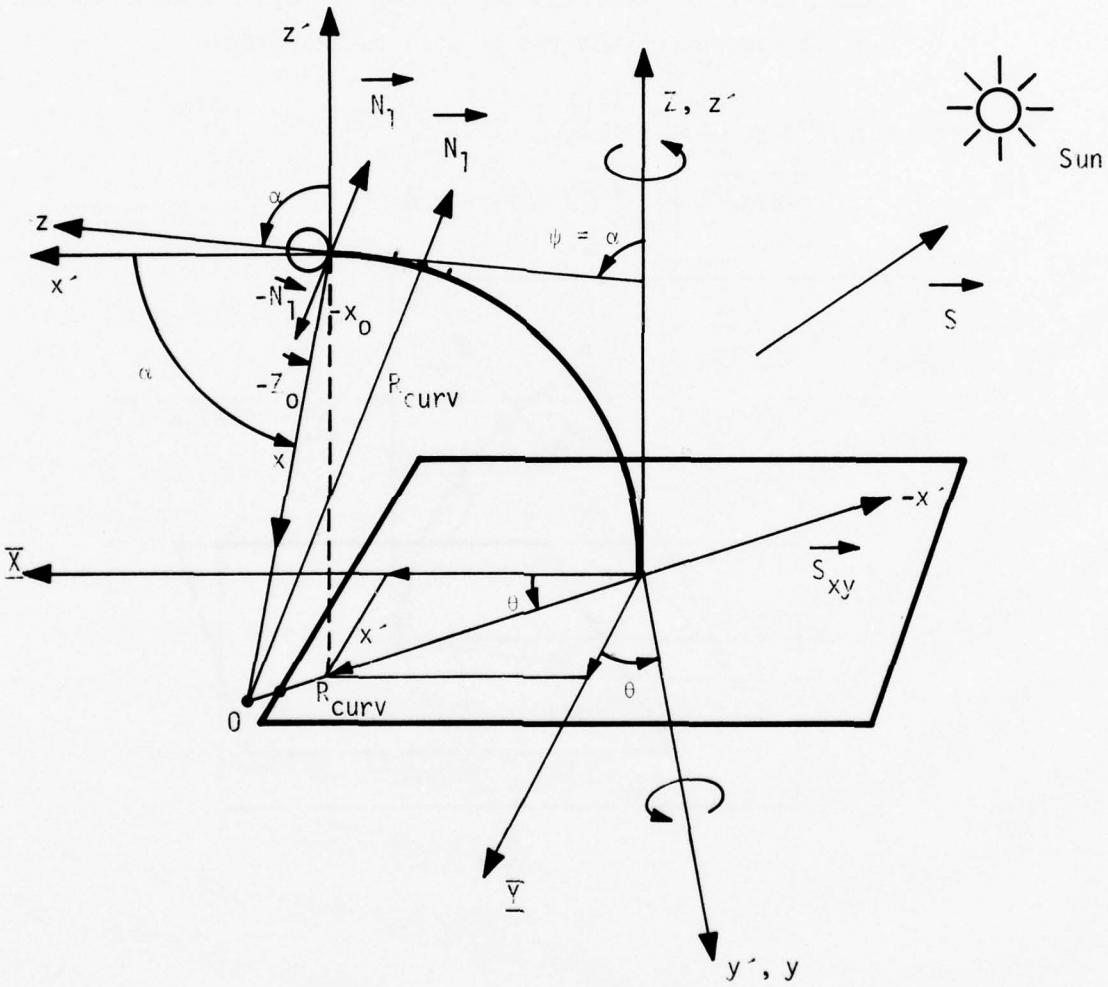

Figure G-11

where: the top sign applies to the rod on -Z axis and the bottom sign applies to the rod on +Z axis.

Finally we must determine the $\overrightarrow{\text{CENTER}}$ vector in body frame at the ith element of the rod as well as its AREA.

From Figure G-12 we have

$$\overrightarrow{\text{CENTER}} = R_{curv} (\vec{N} + \vec{T}) + R \vec{N}$$

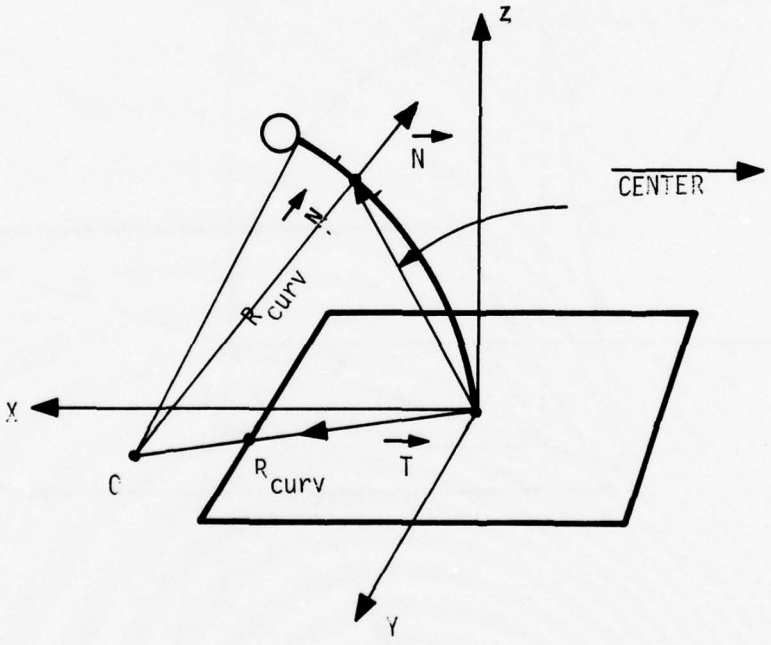

Figure G-12

where $\vec{T} = (-\frac{S_1}{\|\vec{S}\|}, -\frac{S_2}{\|\vec{S}\|}, 0)$, $\vec{S} = (S_1, S_2, 0_3)$ unit vector on LOS to sun.

R = Rod Radius

$\vec{N}$ is given by G-23 and R_{curv} is the input radius of curvature of the rod due to the thermal bending.

$AREA_i = \Delta\varphi * R_{curv} * WR\emptyset D$

$WR\emptyset D$ = Rod Diameter

When R_{curv} = i.e., straight rod the formulae above must be modified as follows:

$\theta = \tan^{-1} (S_2/S_1)$

$\alpha = 0$

$\Delta\varphi = 0$

$\Phi = 0$

$\vec{N}_1 = (-1, 0, 0)$

$\vec{N} = (-\cos\theta, -\sin\theta, 0)$

$\longrightarrow$

CENTER = $(0, 0, \mp SR\emptyset D/2 + RBIAS)$

$SR\emptyset D$ = S (Rod Height)

AREA = $SR\emptyset D * WR\emptyset D$

.

SOLAR PANELS

Definition 1: θ_ρ = angle between the panel normal and LOS to the sun and is positive if rotation is CCW from LOS to the sun, when standing at the origin of the body frame and looking at +Y axis.

Definition 2: Panels are at nominal position when their normal unit vector is $\vec{N} = (1, 0, 0)$

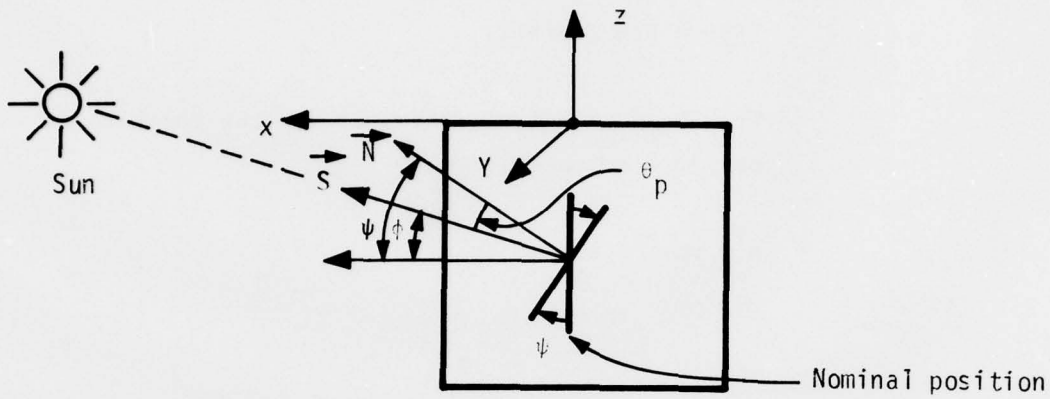

Figure G-13

From Figure G-13 we have: $\phi = \cos^{-1} \left(\frac{S_1}{\| \vec{S} \|}\right)$

$\vec{S} = (S_1, S_2, S_3)$ unit vector along LOS.

Then $\psi = \phi + \theta$ and

$\vec{N} = (\cos \psi, 0, \sin \psi)$ is the normal unit vector to the panel

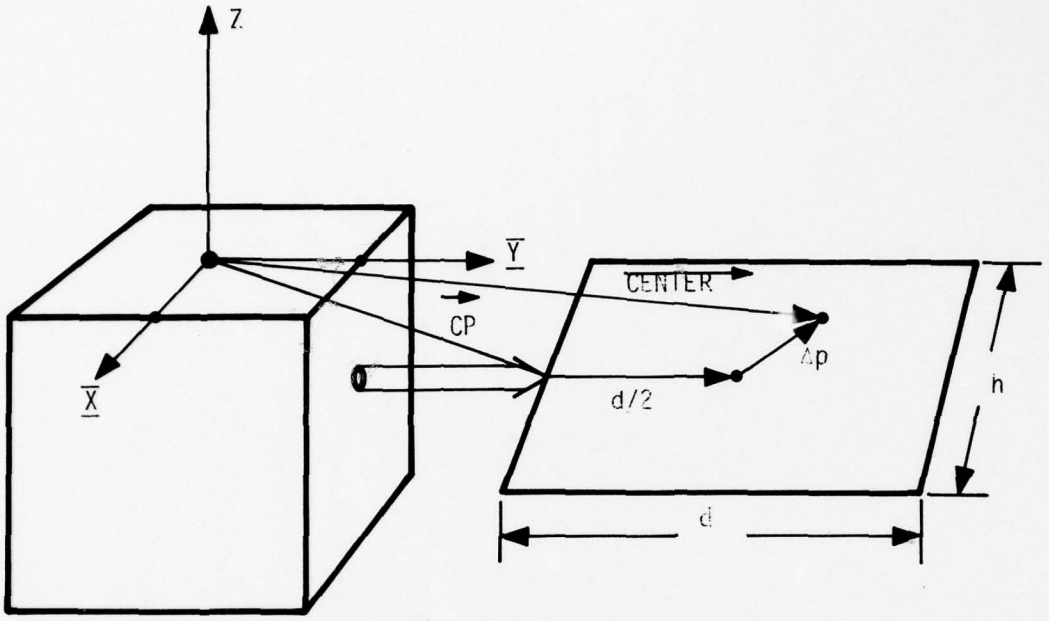

Figure G-14

From Figure G-14 we see that:

$$\overrightarrow{\text{CENTER}} = \vec{CP} + \vec{D}_2 + \vec{\Delta\rho}$$

where:

$\vec{CP}$ is input

$\vec{\Delta\rho}$ = Solar pressure shift vector from the panel geometrical center (given in Body Frame when panel is at nominal position) and is input.

$\vec{D}_2$ = (0, d/2, 0)

d = length of panel

h = width of panel

AREA = d*h

APPENDIX H

APPENDIX H

NTS-2 GRAVITY GRADIENT ROD THERMAL ANALYSIS

The BI-STEM boom configuration and 2-D thermal model are shown in Figure H-1. The NRL specification quotes a maximum solar absorptivity of 0.15; no emissivity data was available - a nominal value of 0.05 was assumed. Preliminary calculations showed that compared with peripheral conduction. internal radiation could be neglected. Radiation was included between the overlapping sections of the boom elements. A hot case solar flux of 455 Btu/hr. ft.^{2} was assumed. Earth-albedo and IR fluxes were excluded, providing a major analysis simplification. Inclusion of these terms would result in a slight reduction of the predicted temperature gradients.

Note that the model is two dimensional, i.e., axial temperature gradients in the boom are not considered.

Temperature Predictions

Figures H-2 to H-7 show steady state temperature for two solar orientations and for various values of α, ε. Figure H-2 is for nominal α, ε and indicates a gradient of only 2^{o}F from sunside to backside. Figure H-3 shows the effect of severe degradation in both α and ε: the gradient increases to 4.1^{o}F. (Note that the mean boom temperature is unchanged because the α/ε ratio is the same.) Figure H-4 shows the effect of increasing the emissivity only; although the mean boom temperature drops significantly, the gradient is still only 2^{o}F.

Figures H-5, H-6 and H-7 show temperatures for the same property combinations but for a different solar orientation. Hot side to cold side gradients are unchanged.

DIAMETER 0.5"

ELEMENT THICKNESS 0.002"
MATERIAL BeCu Alloy No. 25

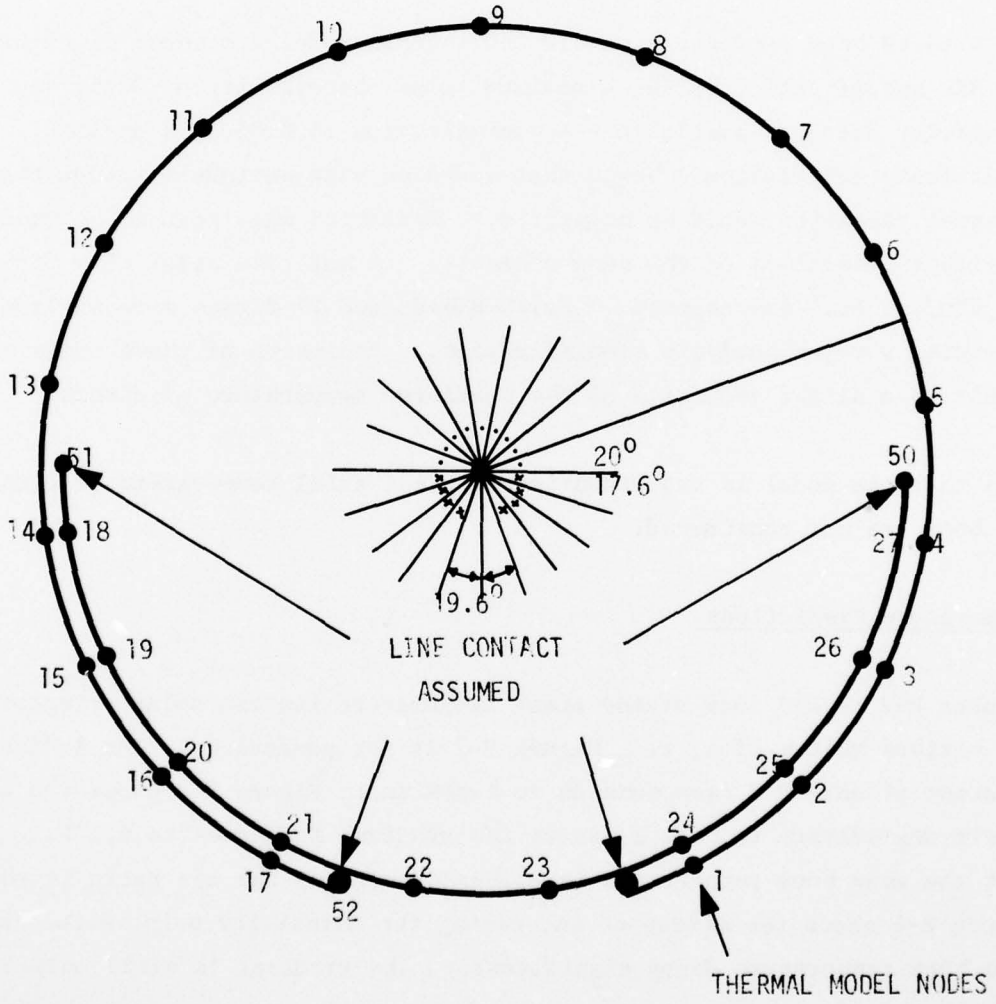

Figure H-1. Bi-Stem Boom Configuration and Thermal Model

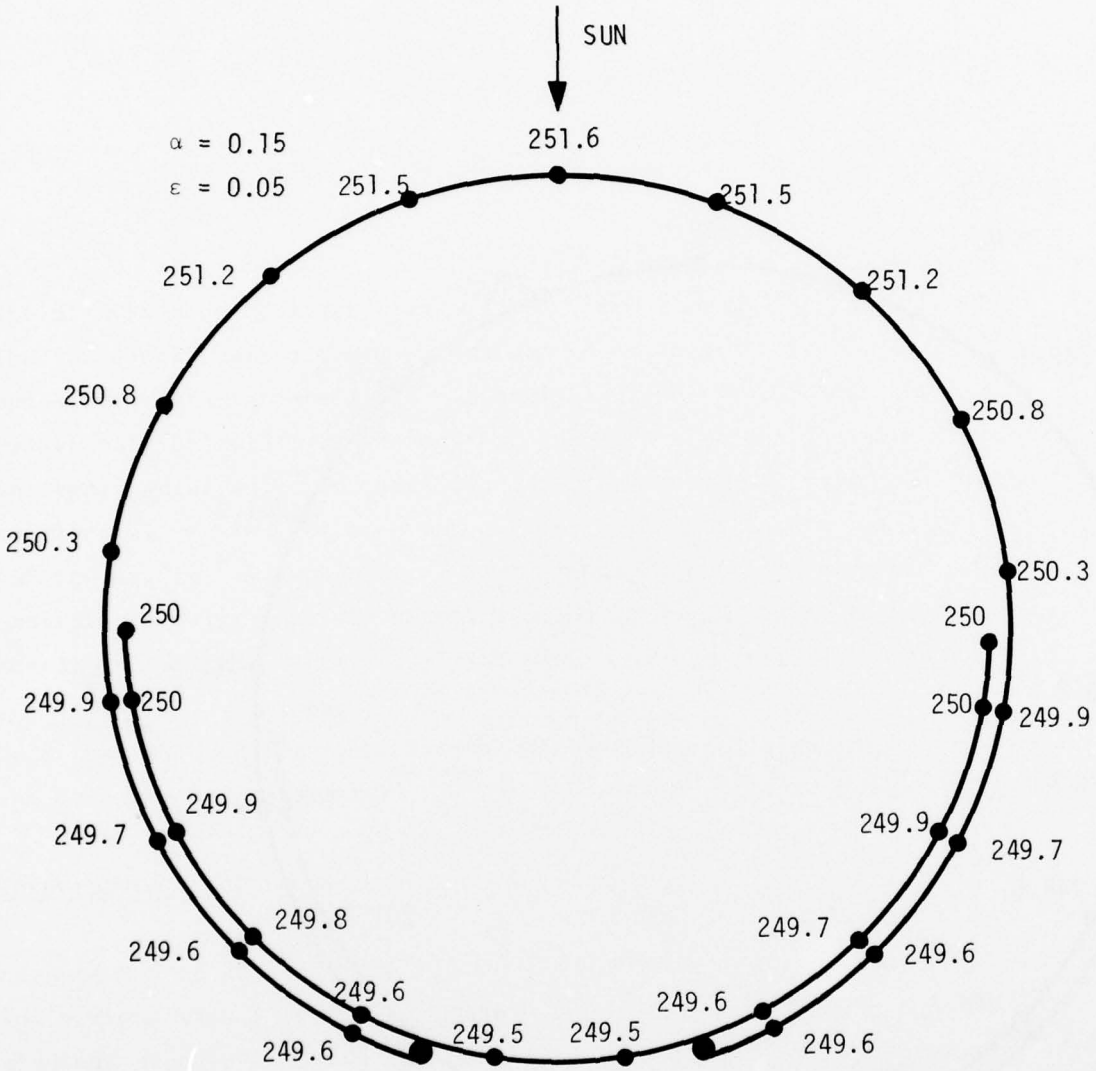

Figure H-2. Nominal α and ε

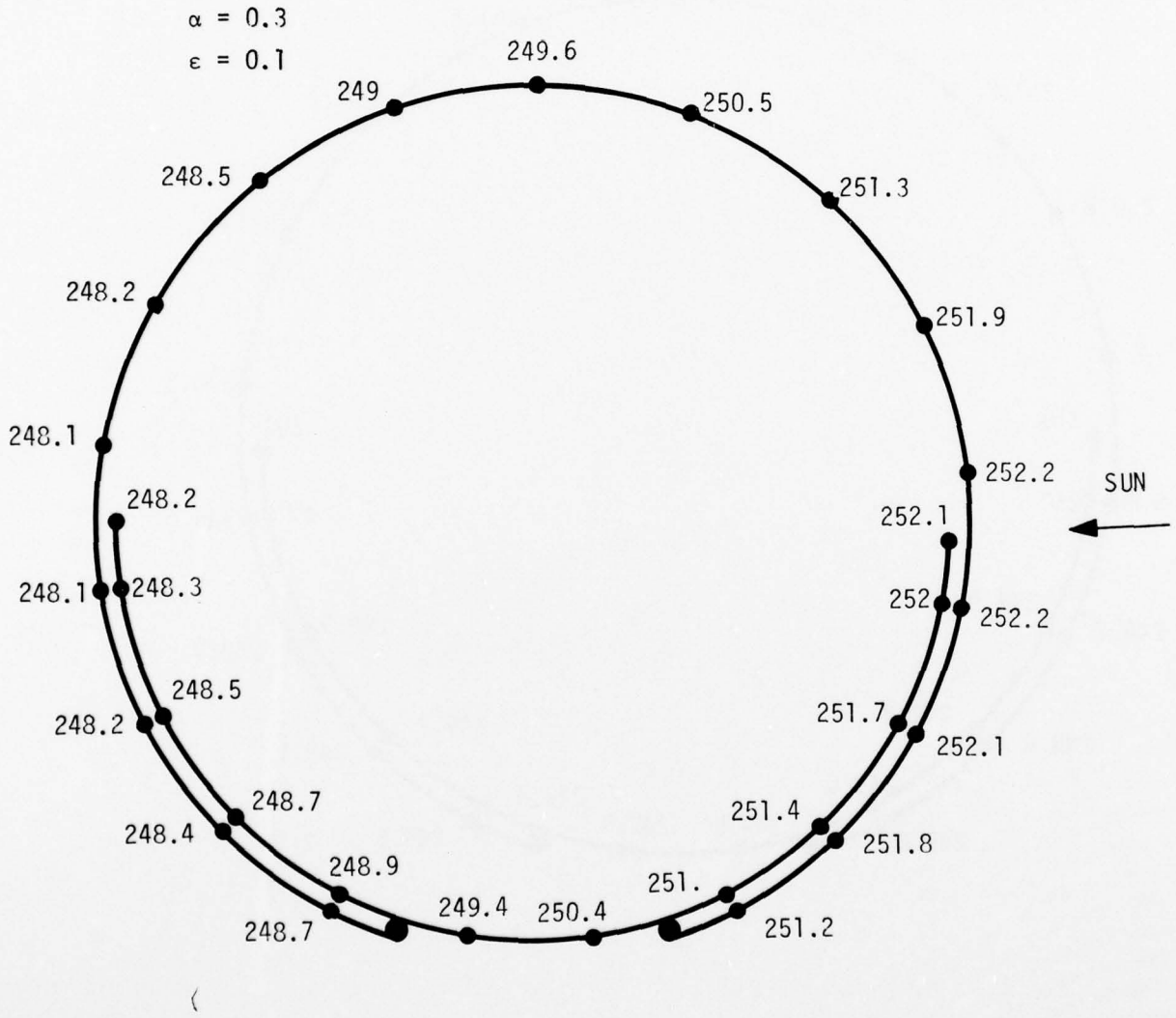

Figure H-3. Degraded α and ε

α = 0.15

ε = 0.1

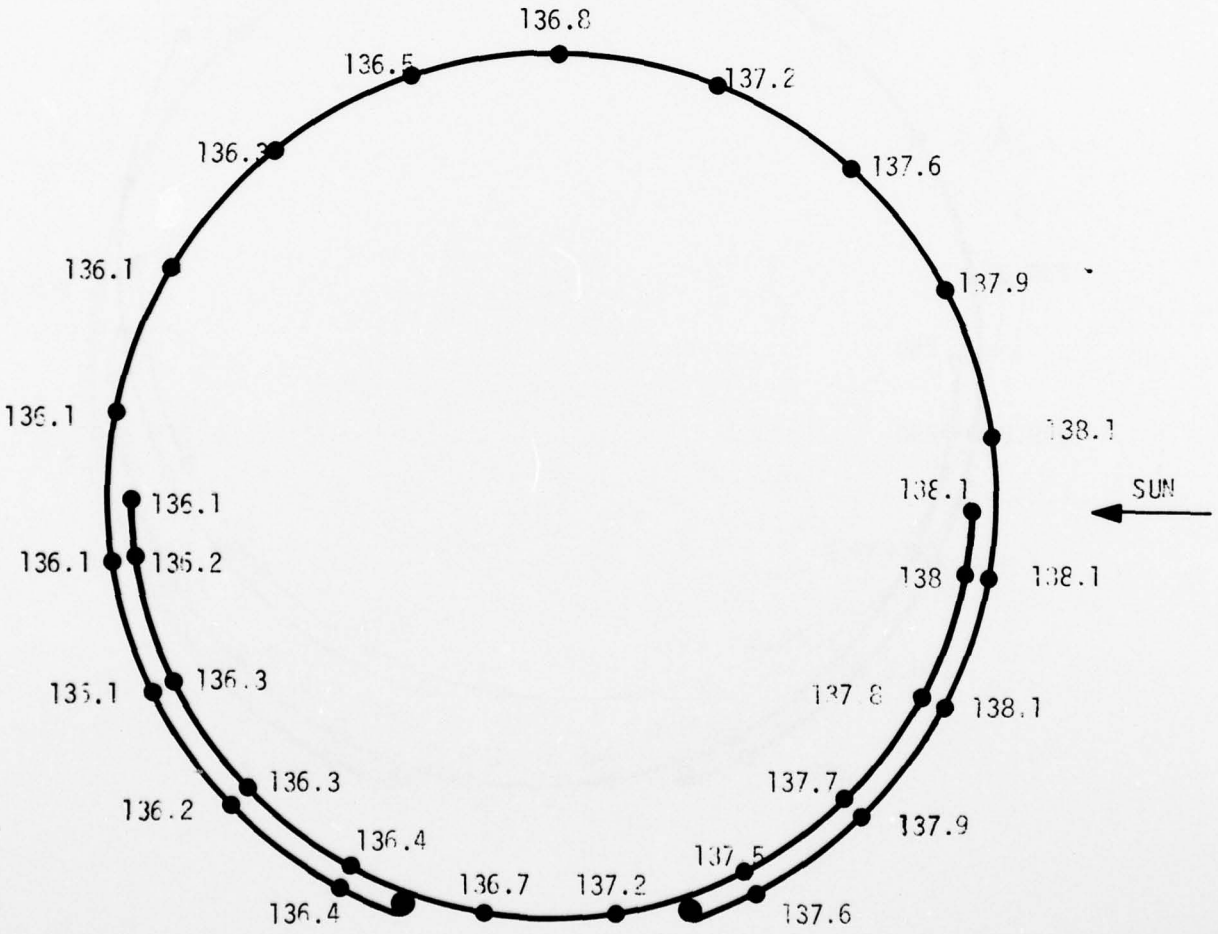

Figure H-4. Degraded ε

α = 0.15

ε = 0.05

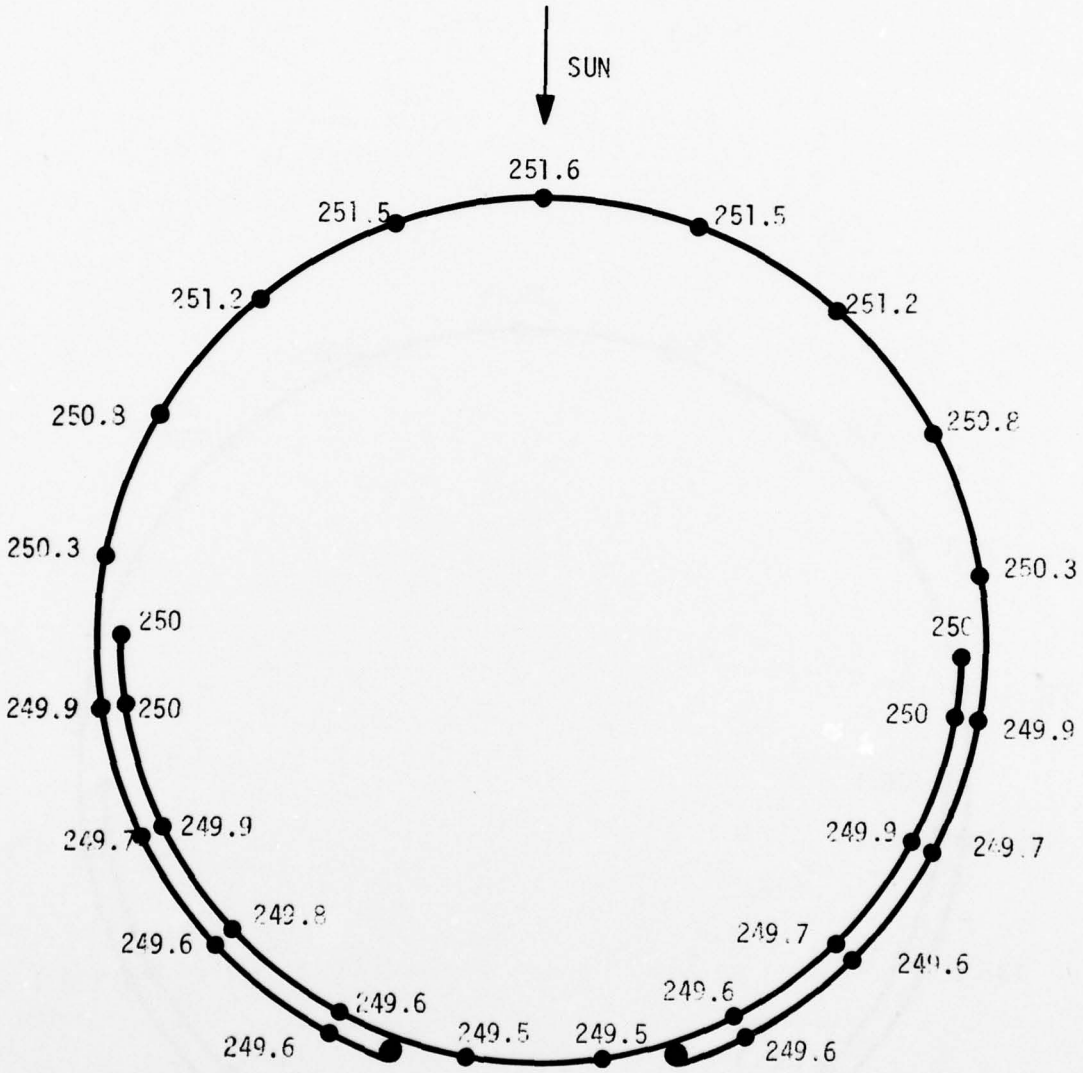

Figure H-5. Nominal α and ε

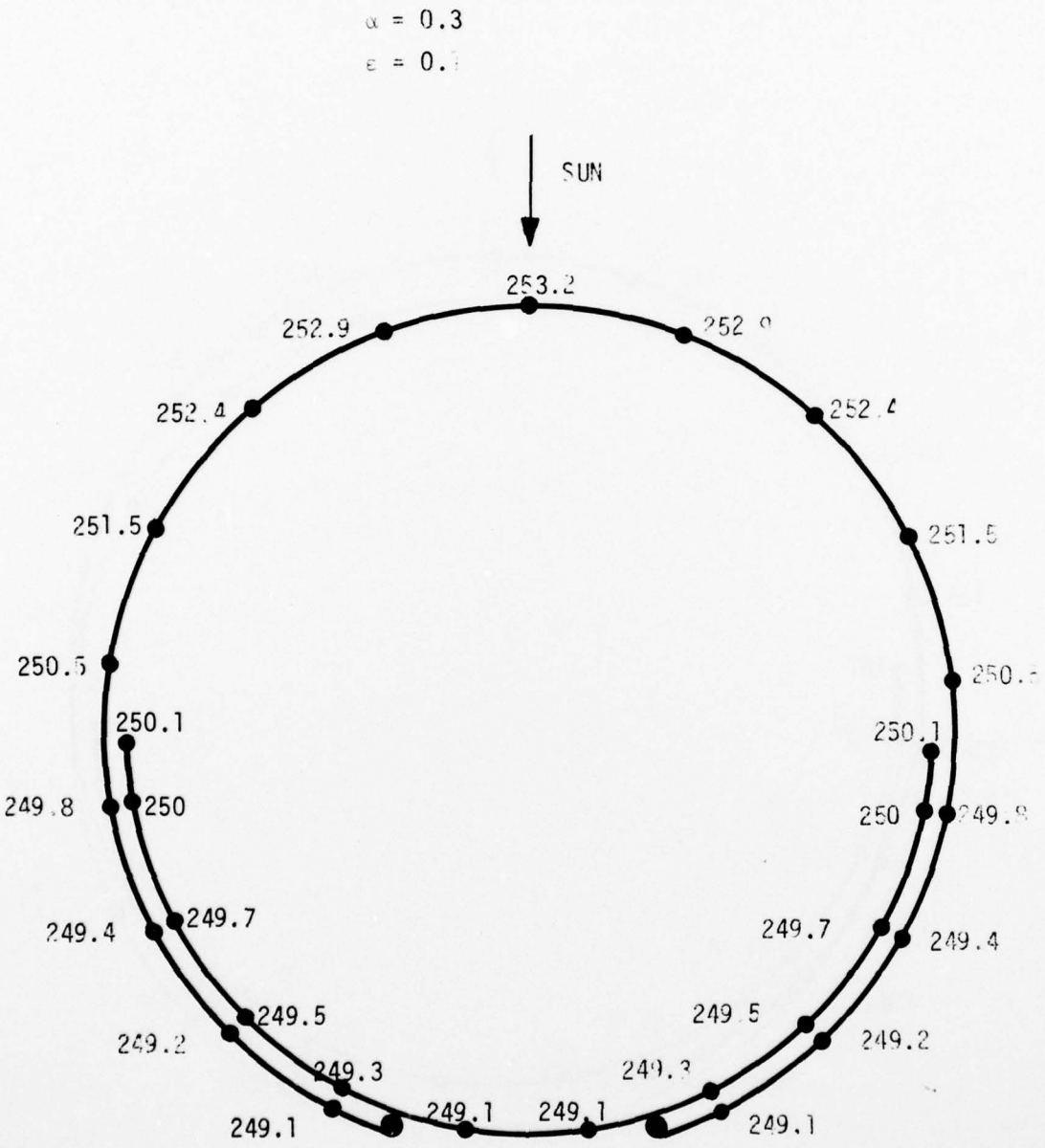

Figure H-6. Degraded α and ε

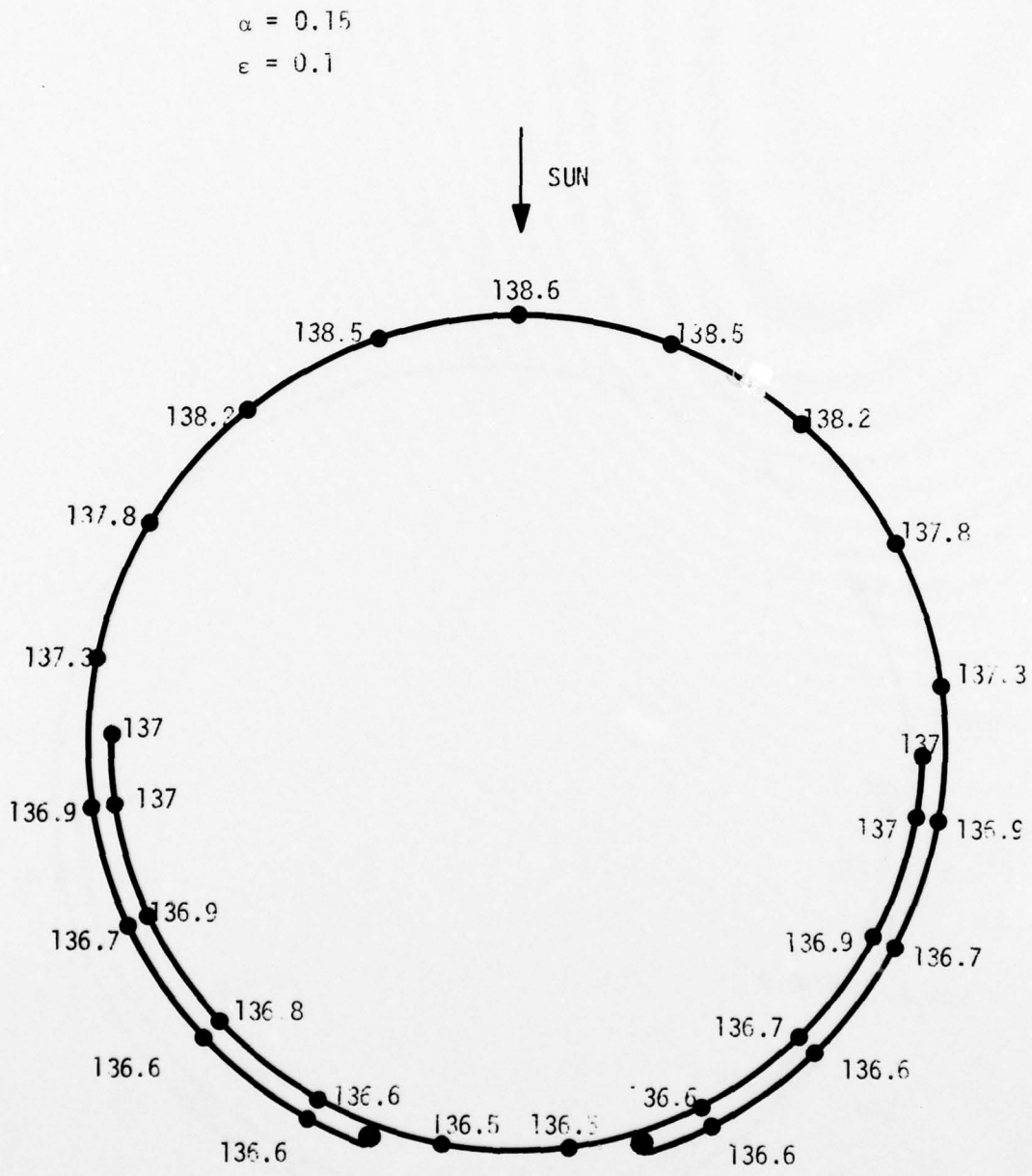

Figure H-7. Degraded ε

Figure H-8 shows the transient response for entering and leaving a 55 minute period in the earth's shadow. Initial temperatures were assumed to be those shown in Figure H-5; at time zero the solar flux was removed and the temperature histories computed for 55 minutes. At this time the sun was switched on again and the response computed for a further 200 seconds. The results in Figure H-8 show that the $2^{\circ}F$ gradient decays within 10 seconds of eclipse and re-establishes within 10 seconds of re-entering sunlight. In actuality, the change would be slower, since the transition from sunlight to darkness (and vice versa) would take a minute or so rather than being a step function as assumed in the analysis.

Boom Deflections

To get an estimate of tip deflection, consider the relative expansion of "strips" on the sunside and shadeside:

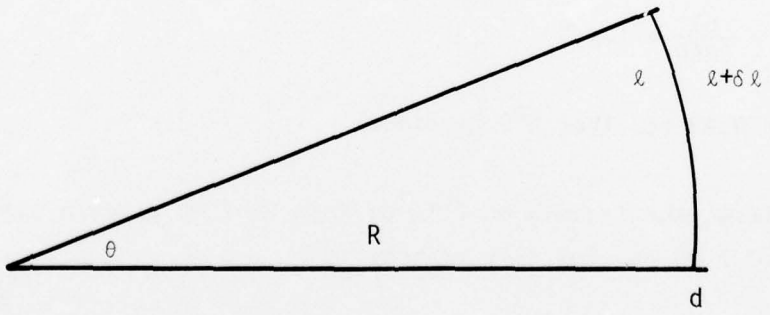

$$\theta = \frac{\ell}{R} = \frac{\ell + \delta\ell}{R + d}$$

i.e.

$$\frac{R + d}{R} = \frac{\ell + \delta\ell}{\ell}$$

$$\therefore R = \frac{d \times \ell}{\delta\ell}$$

But

$$\delta \ell = B \times \Delta T \times \ell$$

where B is the coefficient of expansion

$$\therefore R = \frac{d}{B \times \Delta T}$$

For Beryllium Copper Alloy No. 25,

$$B = 9.3 \times 10^{-6} \text{ in/in}^{\circ}\text{F}$$

Thus for a ΔT of $2^{\circ}F$, and d = 0.5"

$$R = \frac{0.5}{9.3 \times 10^{-6} \times 2} = 26{,}881.7 \text{ inches} = 2240 \text{ ft.}$$

The tip deflection,

$$\delta = R\,(1-\cos\theta)$$

$$\text{and } \theta = \frac{61}{2240} = 1.56^{\circ}$$

$$\therefore \delta = 0.83 \text{ ft. (For } 2^{\circ}F \text{ gradient)}$$

[For comparison, the formula on P.13 of NASA CR-2516 gives a static tip deflection of 1.05 ft. for this geometry.]

It had been planned to generate a STARDYNE model of a finite length of the boom and impose the computer cross section temperature profile and determine displacements. In view of the small gradients and tip deflection, this is not presently considered necessary.

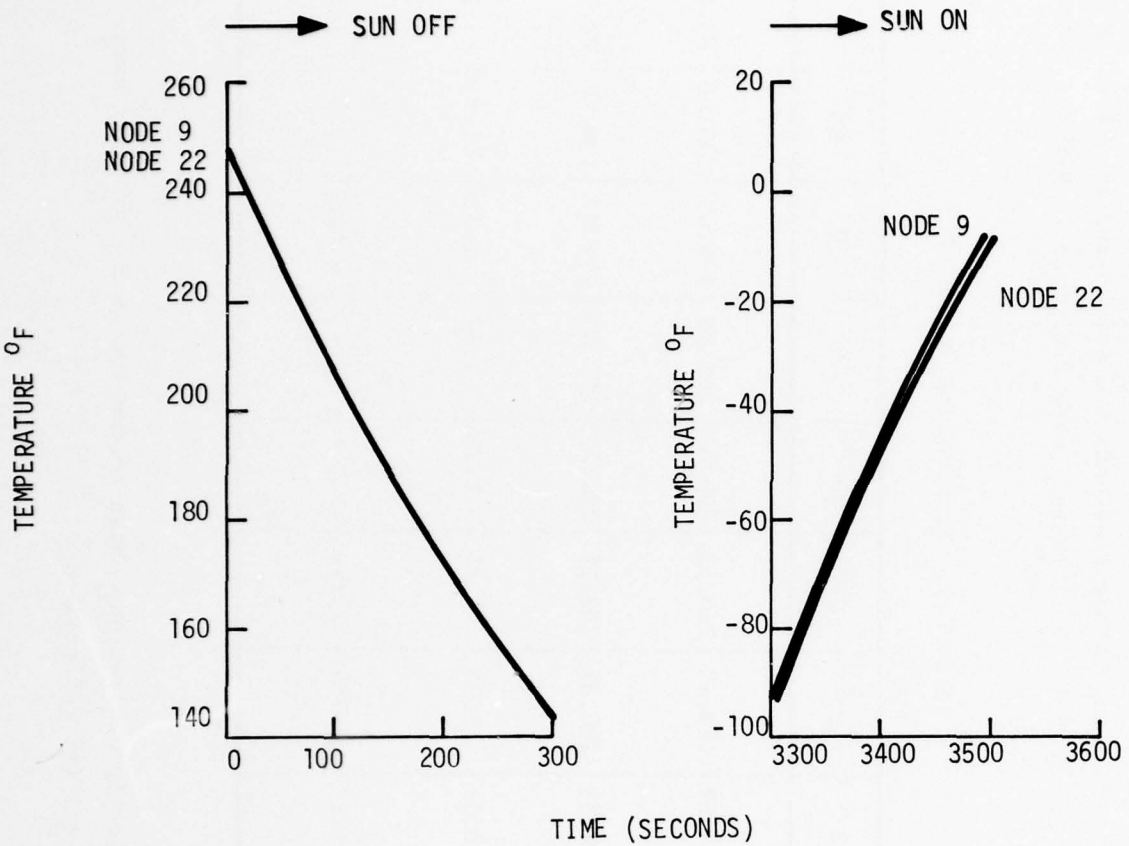

Figure H-8. Transient Response

Implementation

The thermal model was set up to run a series of cases for solar incidence angles verying from 0^{o} to 80^{o}. The configuration was simulated with "nominal" thermal properties. Temperature gradients are summarized in the table below and plotted in Figure H-9. Full thermal maps are given in Figures H-10 through H-18.

Table H-1. Temperature Gradients

SOLAR INCIDENCE	0	10^{o}	20^{o}	30^{o}	40^{o}	50^{o}	60^{o}	70^{o}	80^{o}
Sunside Temp. ^{o}F	251.59	248.42	240.12	225.89	205.06	176.40	137.52	83.26	-1.51
Shadeside Temp. ^{o}F	249.53	246.39	238.18	224.11	203.49	175.07	136.49	82.56	-1.86
T ^{o}F	2.06	2.03	1.94	1.78	1.57	1.33	1.03	0.70	0.35
Static Tip Deflection (Feet)	1.0	0.985	0.942	0.864	0.762	0.646	0.50	0.34	0.17

The boom static tip deflections shown assume that a $2^{o}F$ gradient gives approximately a 1 ft. deflection.

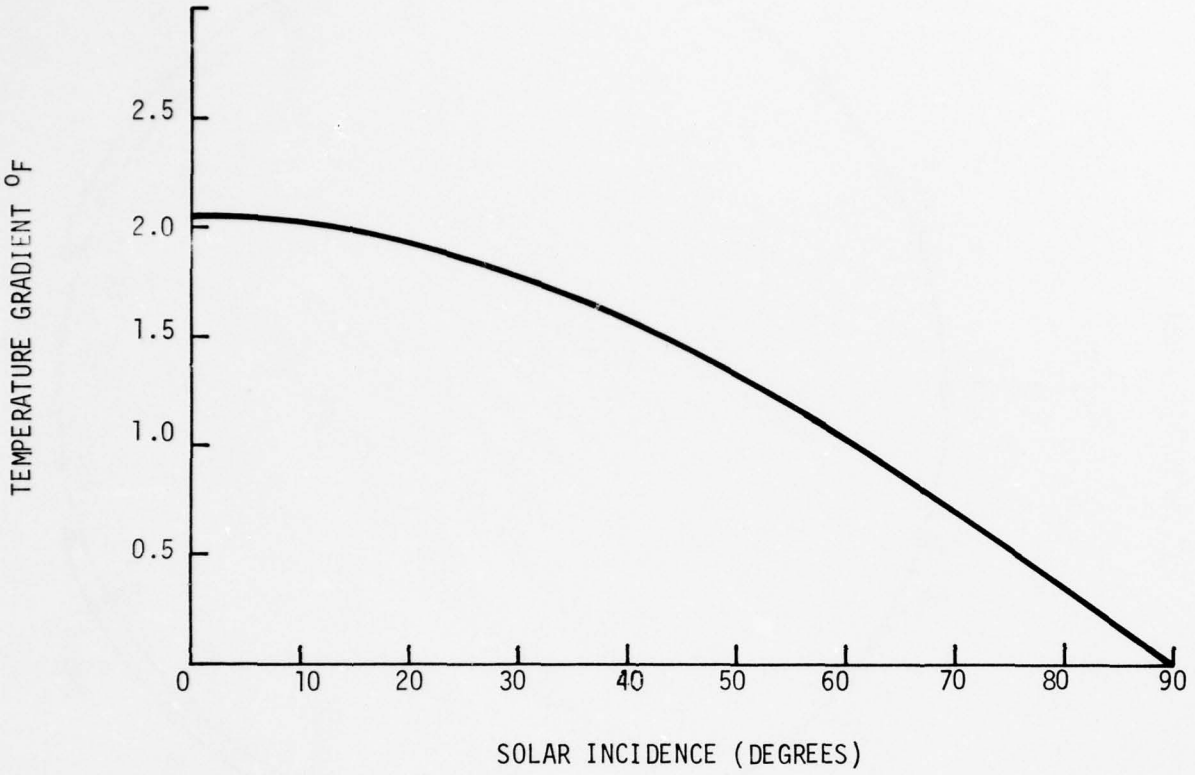
TEMPERATURE GRADIENT °F
2.5
2.0
1.5
1.0
0.5
0
10
20
30
40
50
60
70
80
90
SOLAR INCIDENCE (DEGREES)

Figure H-9

AD-A052 634 HONEYWELL INC MINNEAPOLIS MINN SYSTEMS AND RESEARCH --ETC F/G 22/2
NTS-2 INDEPENDENT STABILITY AND CONTROL ANALYSIS. VOLUME II. AP--ETC(U)
MAR 77 R E POPE, M D WARD, S M SCHWANTES

UNCLASSIFIED 77SRC17-VOL-2 NL

2 OF 3
AD A052834

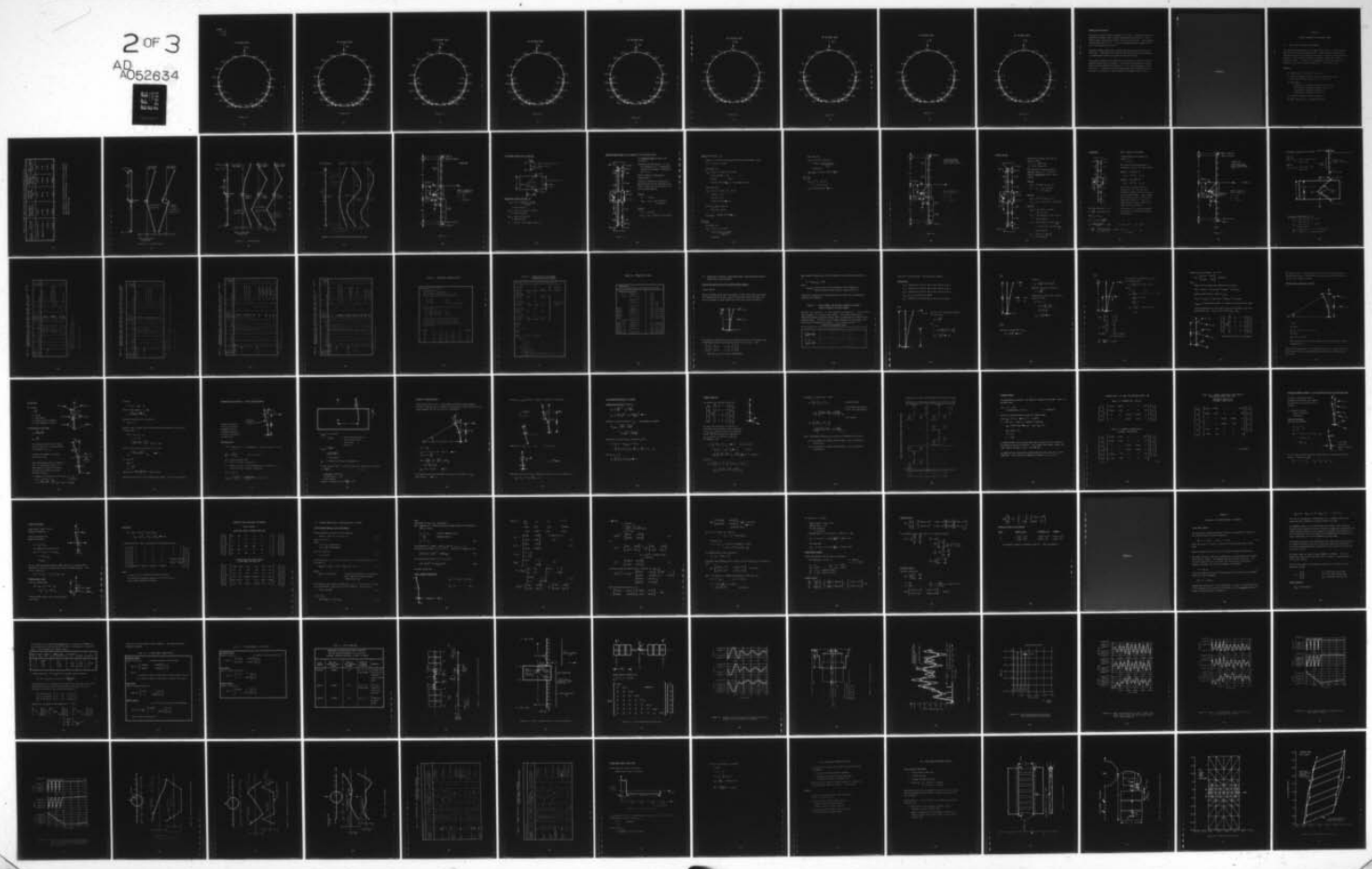

NOMINAL α, ε

α = 0.15

ε = 0.05

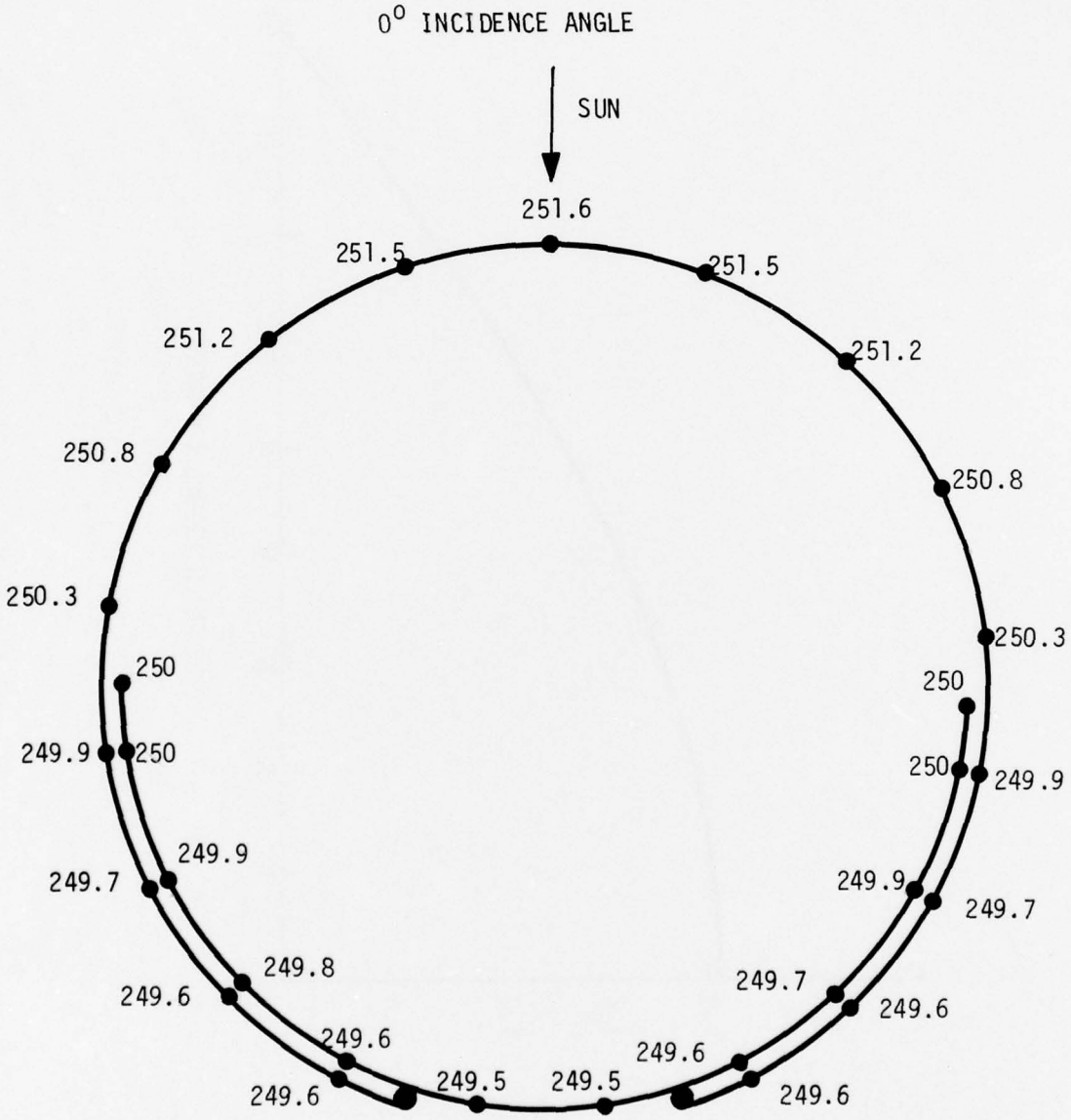

Figure H-10

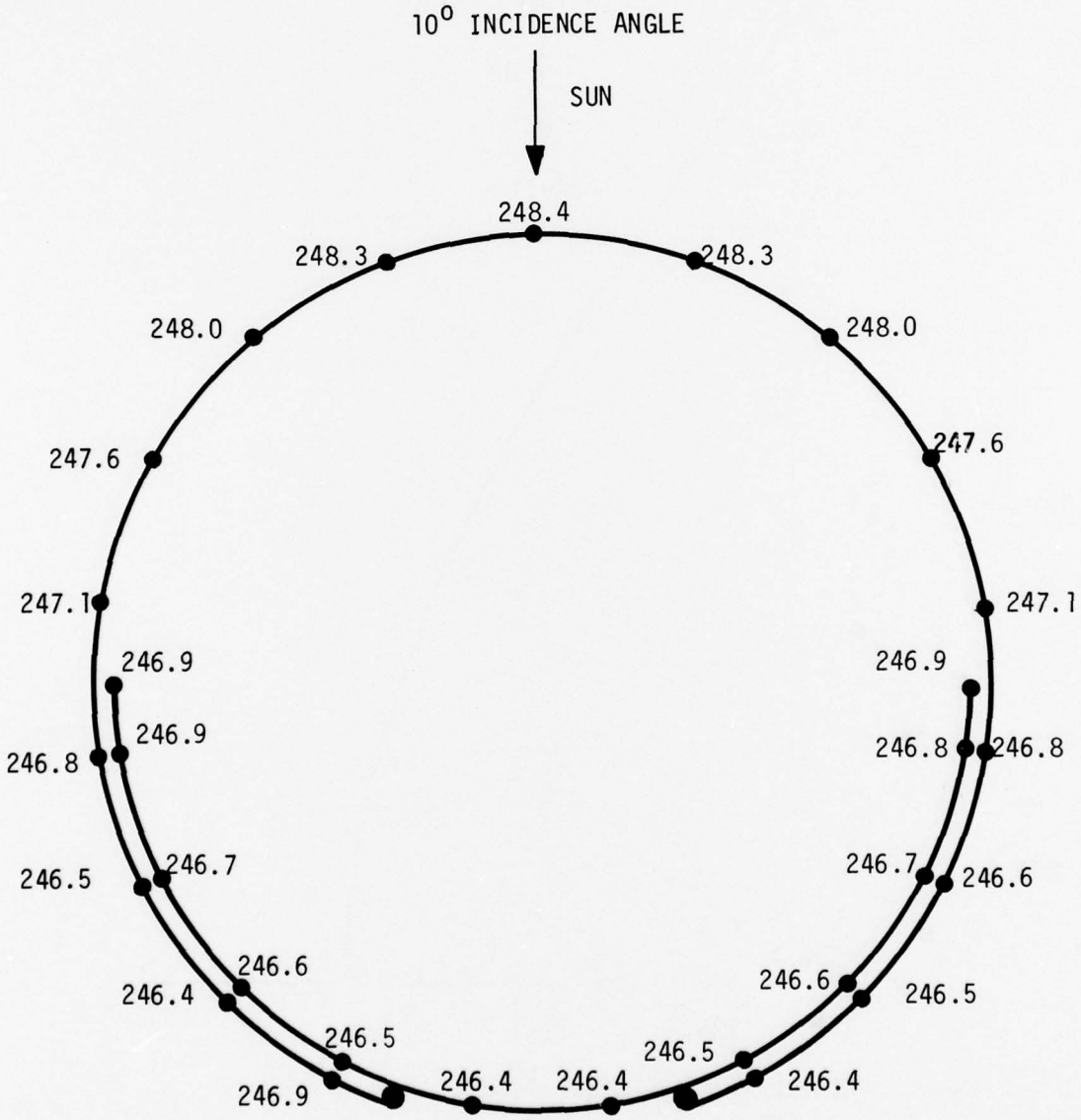
10° INCIDENCE ANGLE
SUN
248.4
248.3
248.3
248.0
248.0
247.6
247.6
247.1
247.1
246.9
246.9
246.9
246.8
246.8
246.8
246.7
246.7
246.5
246.6
246.6
246.6
246.4
246.5
246.5
246.5
246.9
246.4
246.4
246.4

Figure H-11

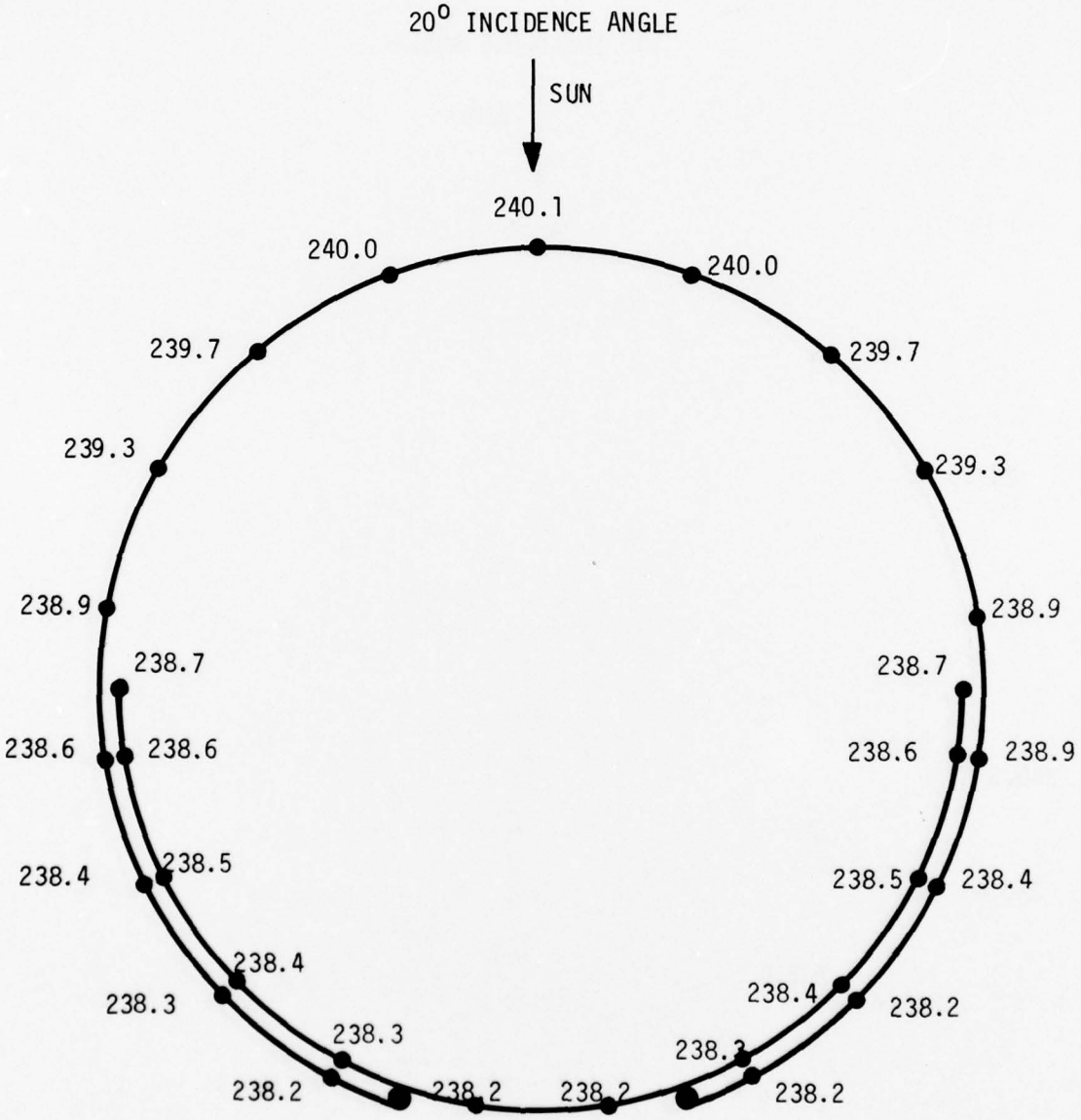
20° INCIDENCE ANGLE
SUN
240.1
240.0
240.0
239.7
239.7
239.3
239.3
238.9
238.9
238.7
238.7
238.6
238.6
238.9
238.4
238.5
238.5
238.4
238.4
238.3
238.2
238.3
238.3
238.2
238.2
238.2
238.2

Figure H-12

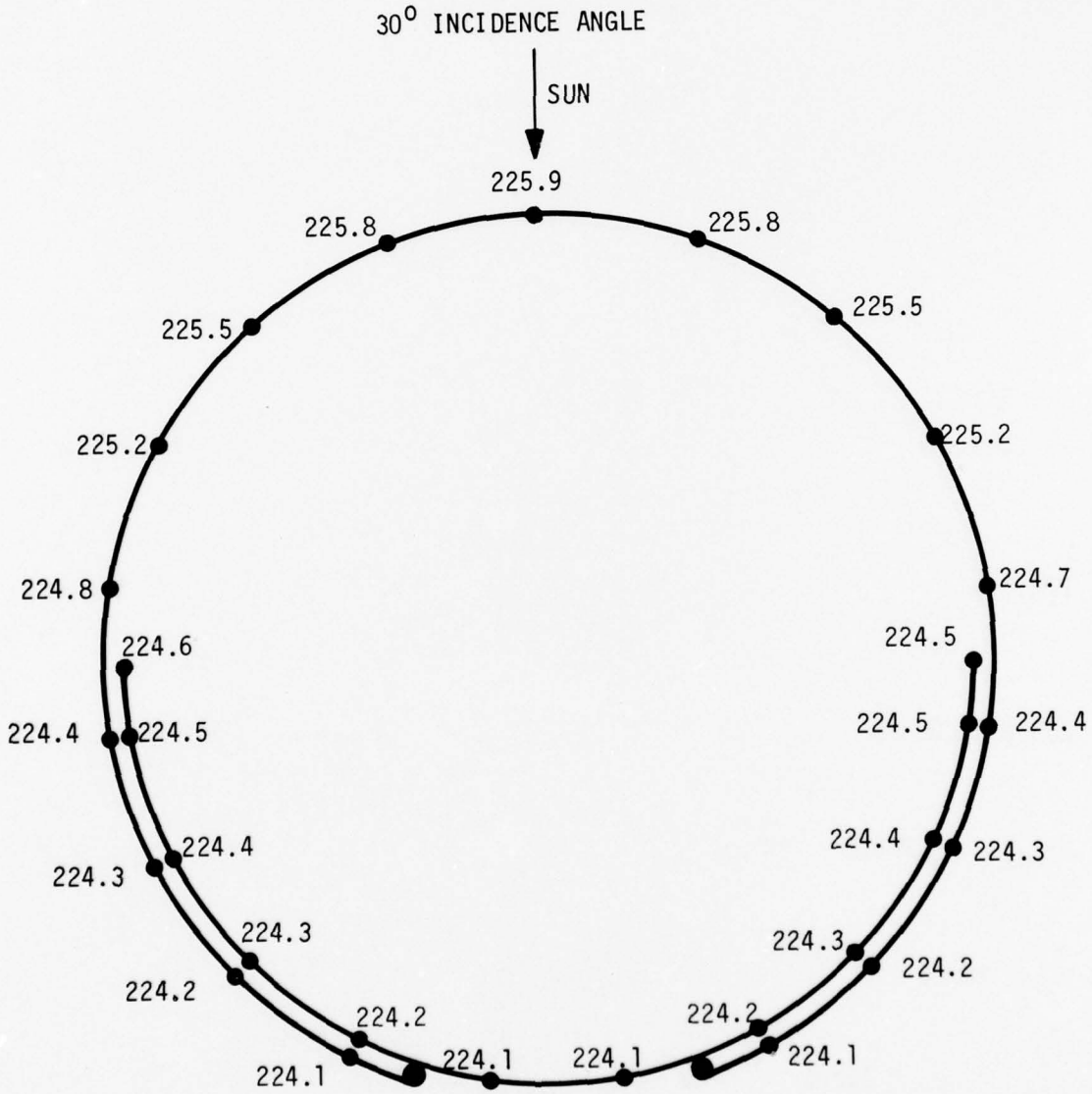
30° INCIDENCE ANGLE
SUN
225.9
225.8
225.8
225.5
225.5
225.2
225.2
224.7
224.8
224.5
224.6
224.5
224.4
224.4
224.5
224.4
224.3
224.3
224.3
224.2
224.3
224.2
224.2
224.2
224.1
224.1
224.1
224.1

Figure H-13

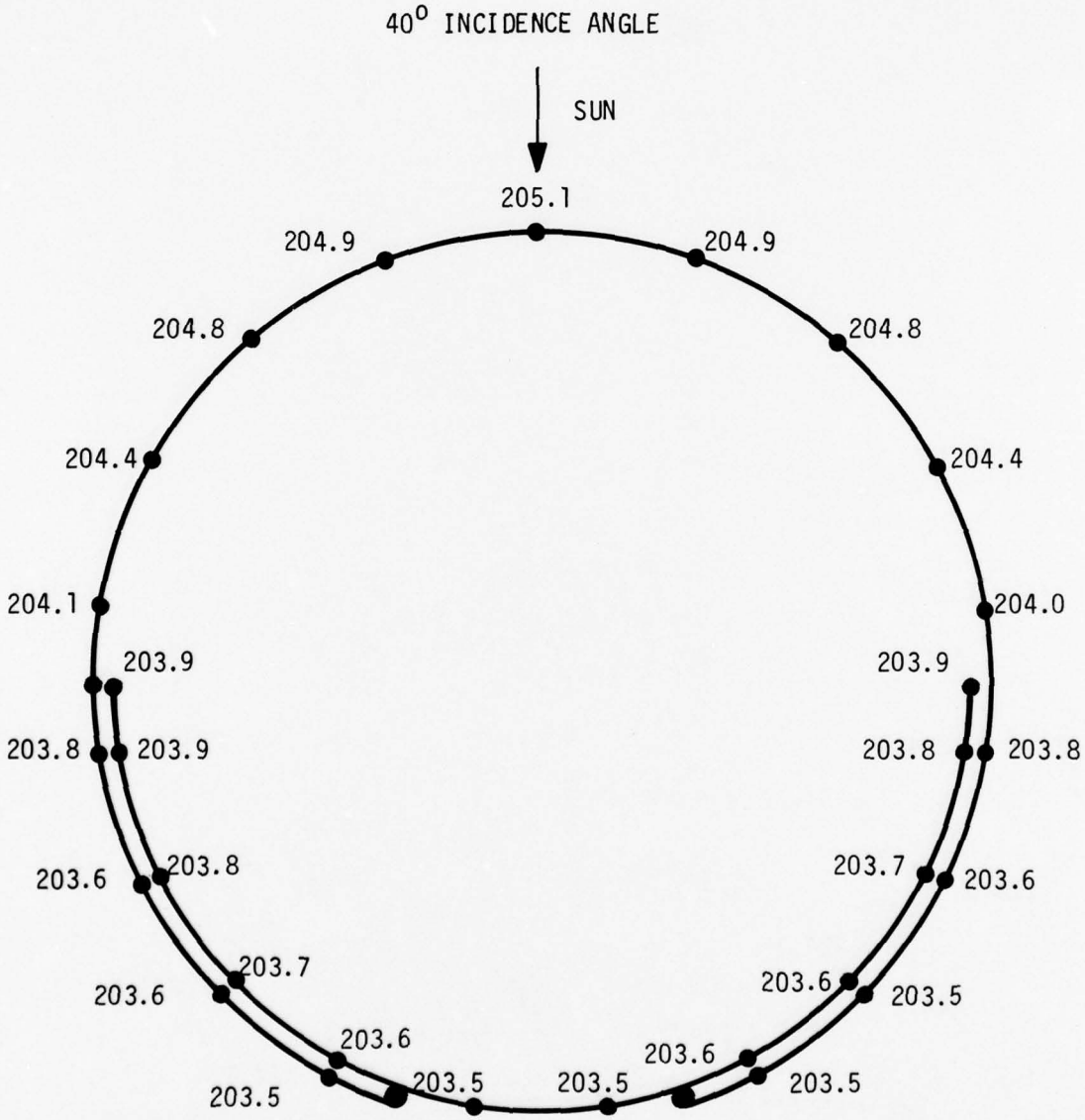
40° INCIDENCE ANGLE
SUN
205.1
204.9
204.9
204.8
204.8
204.4
204.4
204.1
204.0
203.9
203.9
203.8
203.9
203.8
203.8
203.6
203.8
203.7
203.6
203.7
203.6
203.6
203.5
203.6
203.6
203.5
203.5
203.5
203.5

Figure H-14

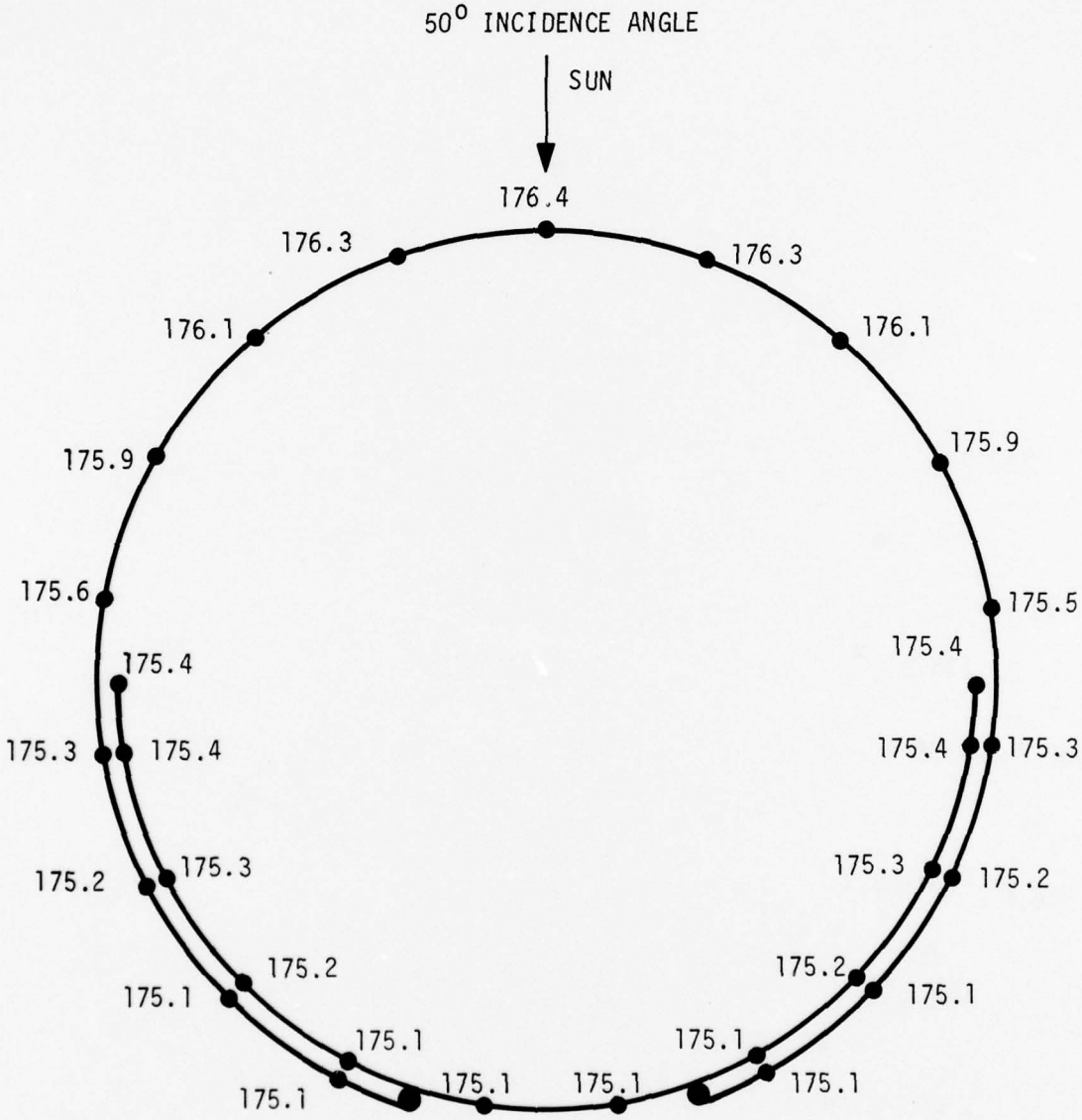
50° INCIDENCE ANGLE
SUN
176.4
176.3
176.3
176.1
176.1
175.9
175.9
175.6
175.5
175.4
175.4
175.3
175.4
175.4
175.3
175.2
175.3
175.3
175.2
175.2
175.2
175.1
175.1
175.1
175.1
175.1
175.1
175.1
175.1

Figure H-15

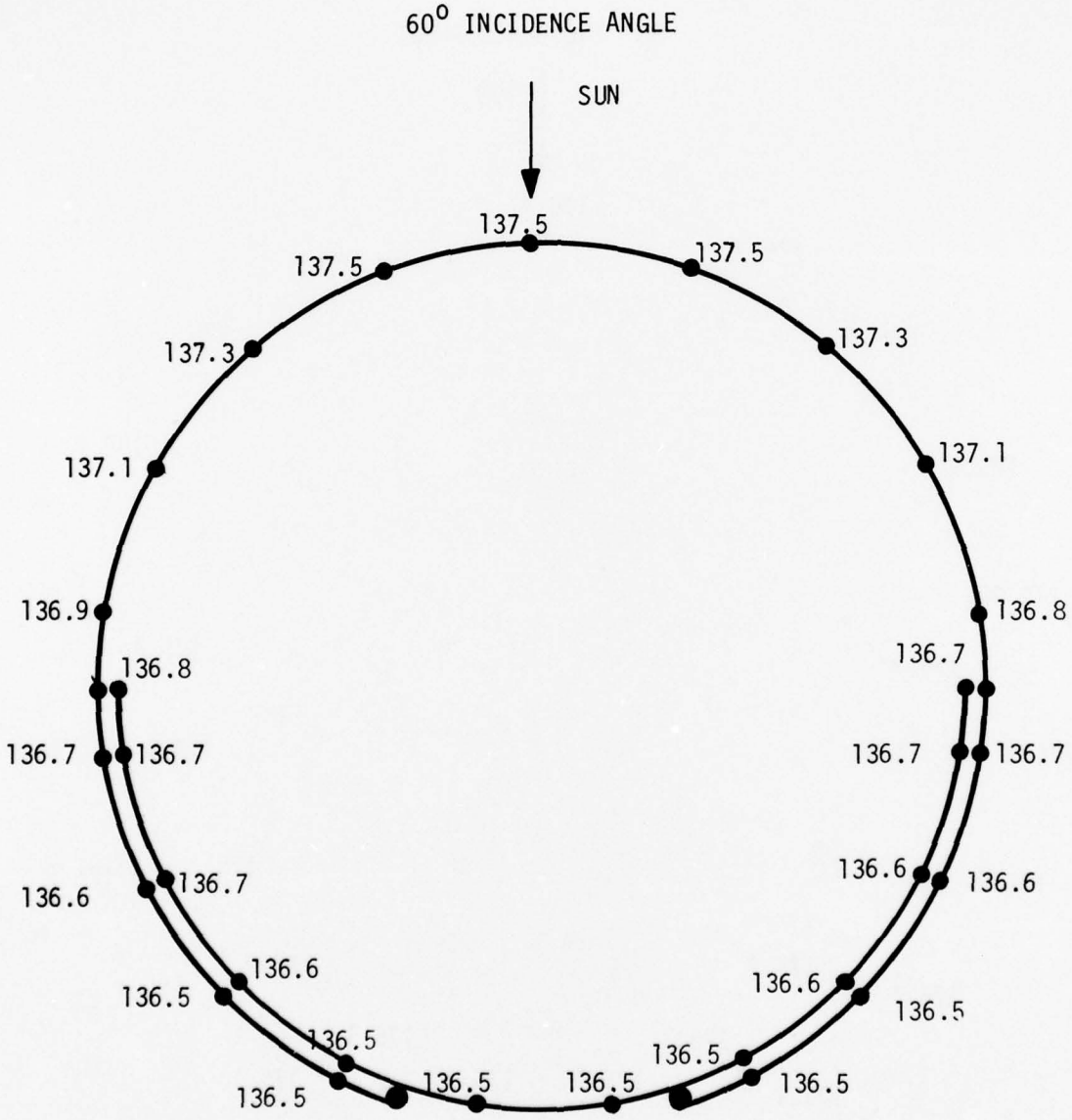
60° INCIDENCE ANGLE
SUN
137.5
137.5
137.5
137.3
137.3
137.1
137.1
136.9
136.8
136.8
136.7
136.7
136.7
136.7
136.7
136.6
136.6
136.7
136.6
136.6
136.5
136.6
136.5
136.5
136.5
136.5
136.5
136.5

Figure H-16

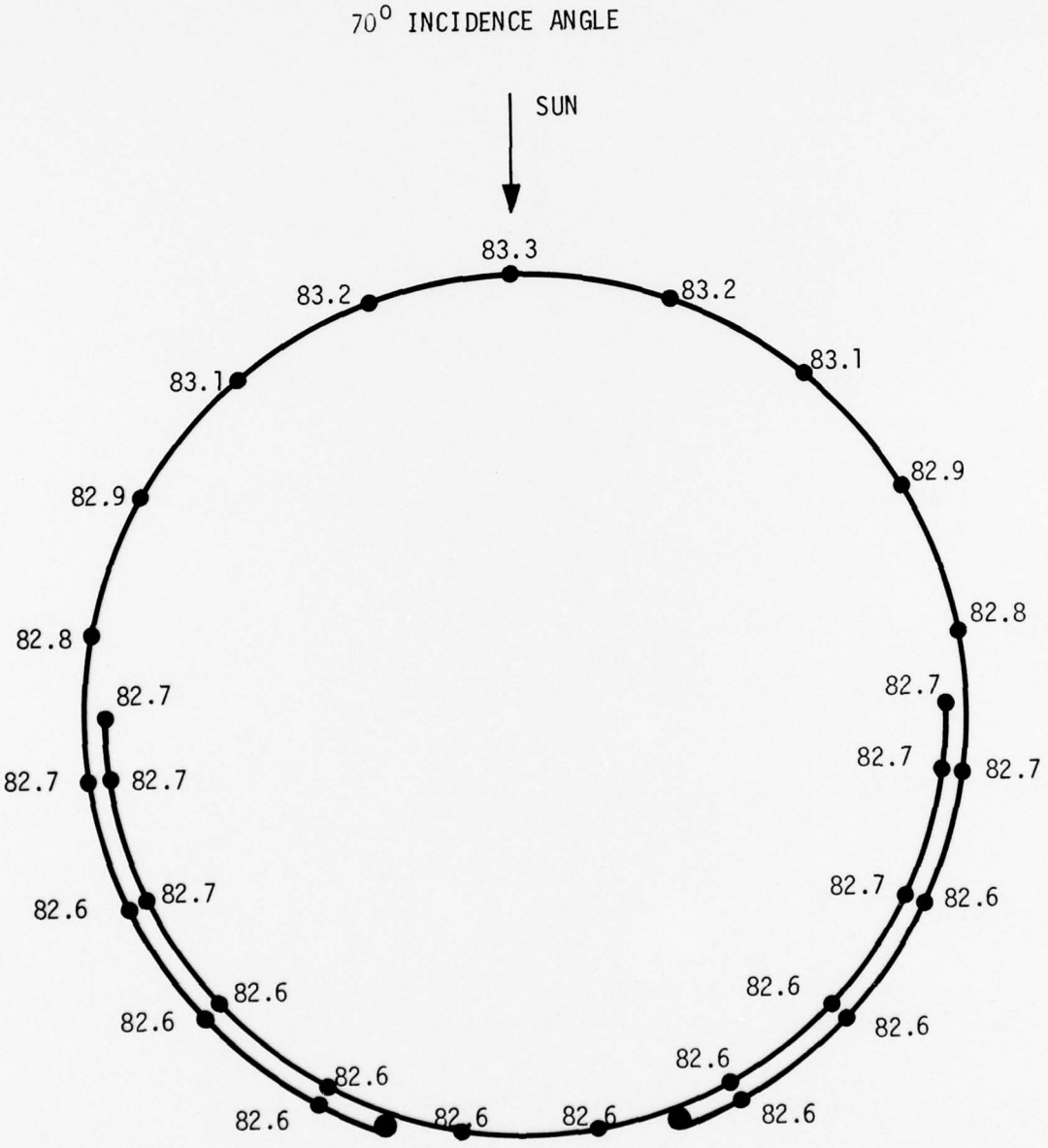
70° INCIDENCE ANGLE
SUN
83.3
83.2
83.2
83.1
83.1
82.9
82.9
82.8
82.8
82.7
82.7
82.7
82.7
82.7
82.7
82.7
82.6
82.7
82.6
82.6
82.6
82.6
82.6
82.6
82.6
82.6
82.6
82.6
82.6

Figure H-17

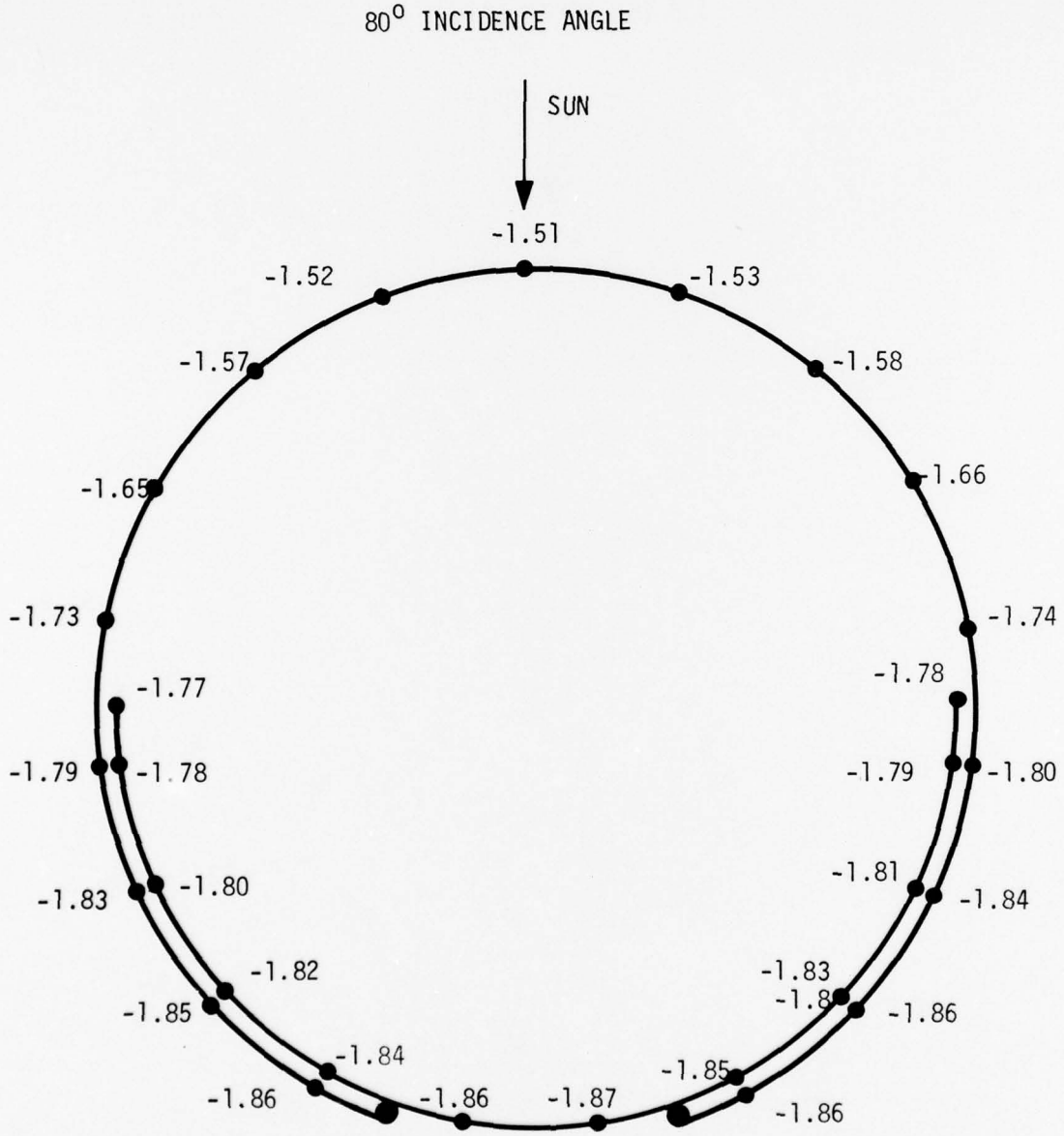
80° INCIDENCE ANGLE
SUN
-1.51
-1.52
-1.53
-1.57
-1.58
-1.65
1.66
-1.73
-1.74
-1.77
-1.78
-1.79
-1.78
-1.79
-1.80
-1.83
-1.80
-1.81
-1.84
-1.82
-1.83
-1.85
-1.86
-1.84
-1.85
-1.86
-1.86
-1.87
-1.86

Figure H-18

Summary and Conclusions

For nominal external thermal properties ($\alpha = 0.15$, $\varepsilon = 0.05$) the steady state temperature gradient across the boom is predicted to be only $2^{o}F$. This would produce a deflection of about 1 foot at the boom tips. With degraded thermal properties ($\alpha = 0.3$, $\varepsilon = 0.1$) this gradient would increase to $4^{o}F$ and the tip deflection to 2 feet.

Transient thermal response was evaluated for step function sun on/sun off conditions. The results show that the $2^{o}F$ sun side to back side gradient is established/or decays very rapidly (within 10 seconds).

This analysis suggests that deflection of the booms as a result of thermal gradients should not be a problem. The effect on the spacecraft control system could be assessed by imposing a 1 - 2 ft. step displacement on the boom tips. If problems occur the displacement could be ramped over time periods of 10 seconds to 1 minute instead of assuming a step function.

APPENDIX I

APPENDIX I

GRAVITY GRADIENT ROD FLEXIBILITY MODEL

I-1 NTS-2 GRAVITY GRADIENT ROD DYNAMICS

This appendix contains details of Stardyne simulations of a rigid satellite with two flexible gravity gradient rods. These simulations showed that modeling each rod with one flexible beam and one tip mass gives questionable results. Using two-beam elements or four-beam elements gives almost identical results. Therefore, a two-beam model was further explored for addition to the orbit simulation model (GPS). (See Section I-2).

Contents

- Summary Table - Key Results (Table I-1)
- Deformed Geometry Sketches, for modes responsive to solar array drive torques (Figures I-1, I-2, and I-3)
- Math Models:
  - 2 Nodes/Rod (1 beam/rod), original (Figure I-4)
  - 2 Nodes/Rod (1 beam/rod), updated (Figure I-5)
  - 3 Nodes/Rod (2 beam/rod) (Figure I-6)
  - 5 Nodes/Rod (4 beam/rod) (Figure I-7)
- Modal Data Summaries, Tables I-6 and I-7
- Mass Property Calc. for Dynamic Rod Models

TABLE I-1. SUMMARY TABLE--RESULTS OF FLEXIBLE GRAVITY GRADIENT ROD STUDIES

No. of Beams/Rod	1st Elastic Freq., H_z	Major Response Mode Freq. (4th Elastic) H_z	Generalized WT, 4th Elastic Mode, Lbs.	Spacecraft Rotation in 4th Mode, about array drive axis	Freq. of Next Highest Response Mode, H_z
1 (Original)	0.00546	0.02878	446.18	0.03677	1.858
1 (Updated)	0.00554	0.02442	303.42	0.02533	1.799
2	0.00553	0.02808	16.54	-0.00686	0.1424
4	0.00554	0.02804	16.8	-.006899	0.1479

Good agreement in these parameters for both 2 and 4 beam/rod models shown that 2 beams are adequate. Also see transient response simulations.

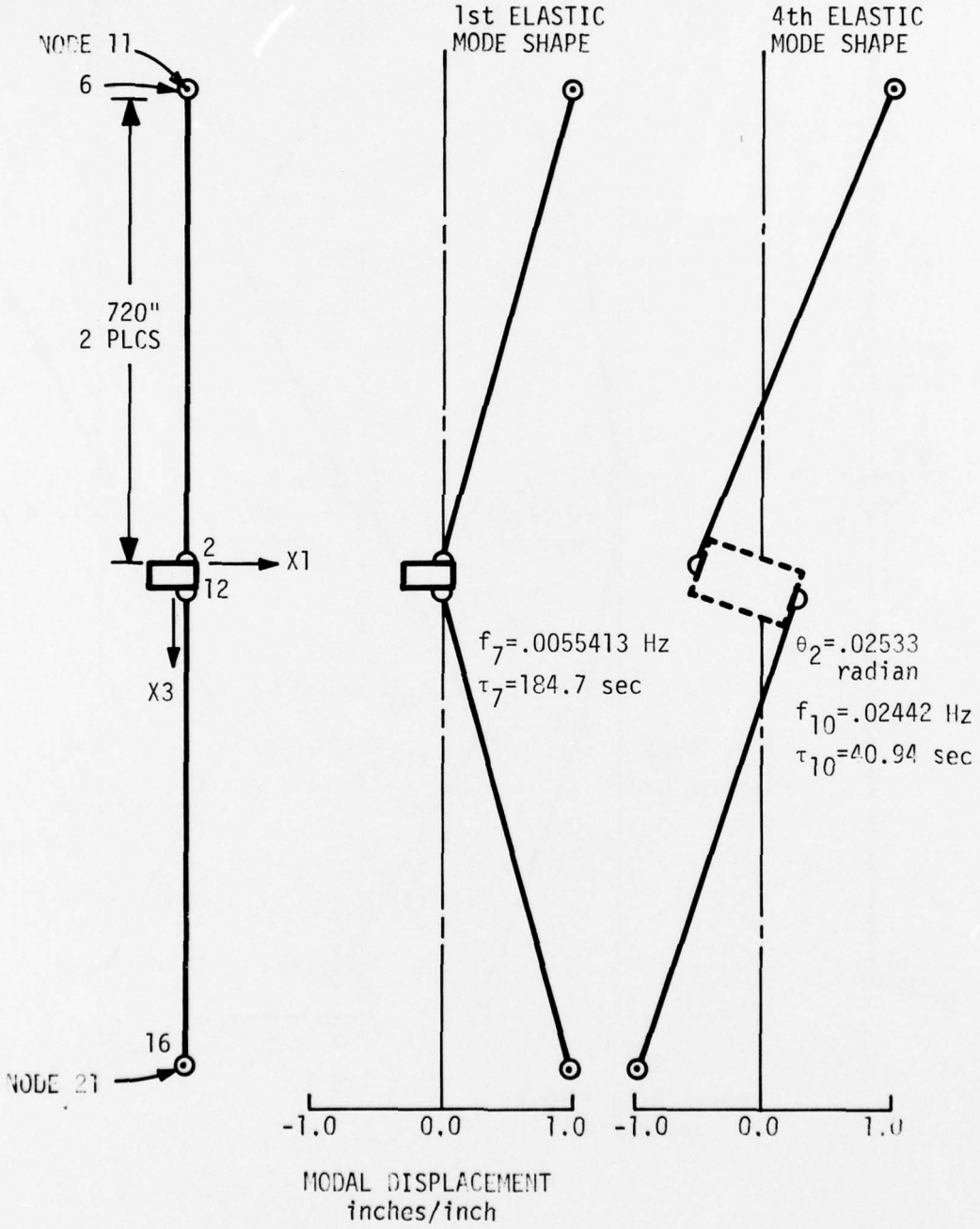

Figure I-1. 1 Beam/Rod Model

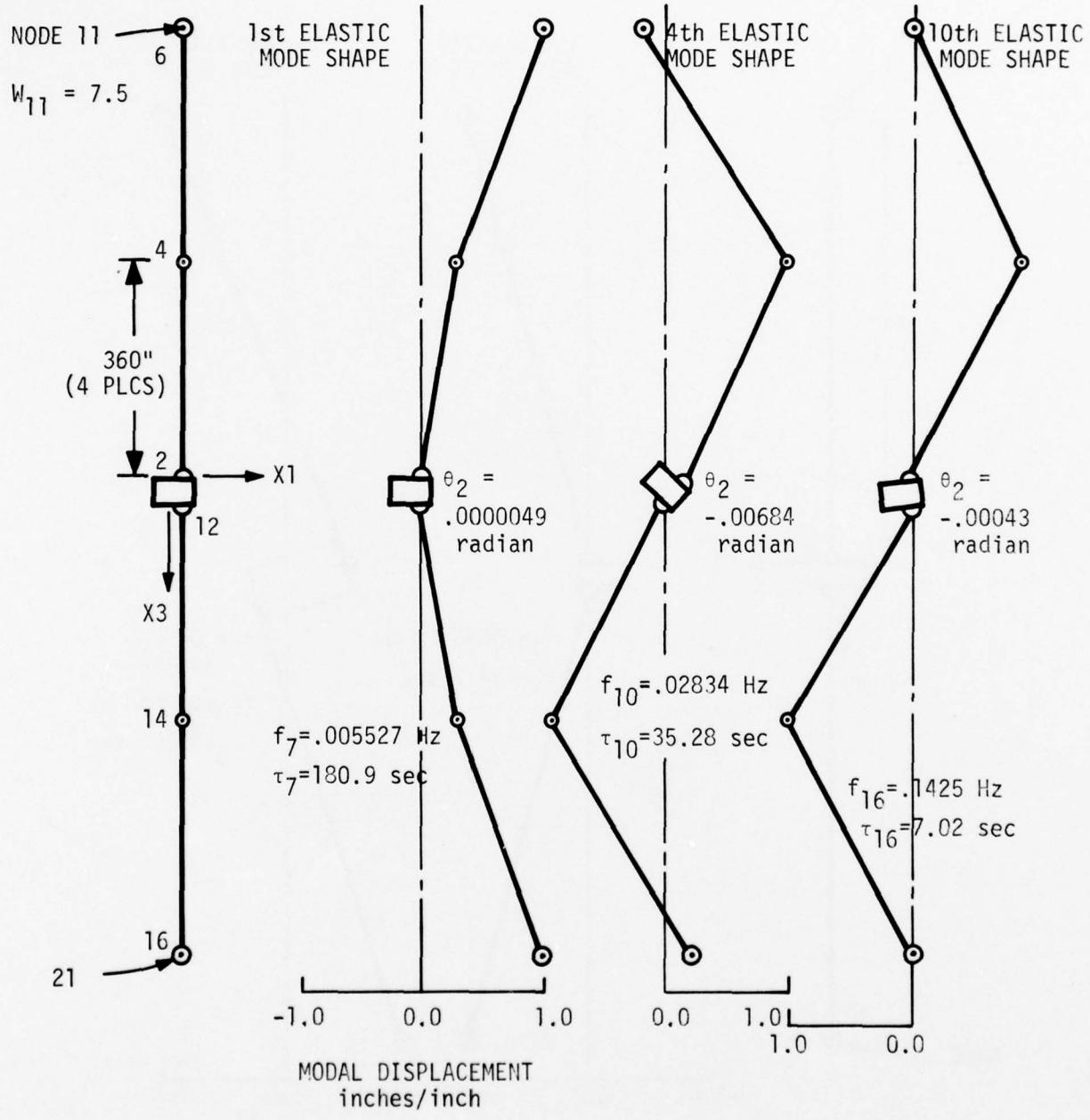

Figure I-2. 2 Beam/Rod Model

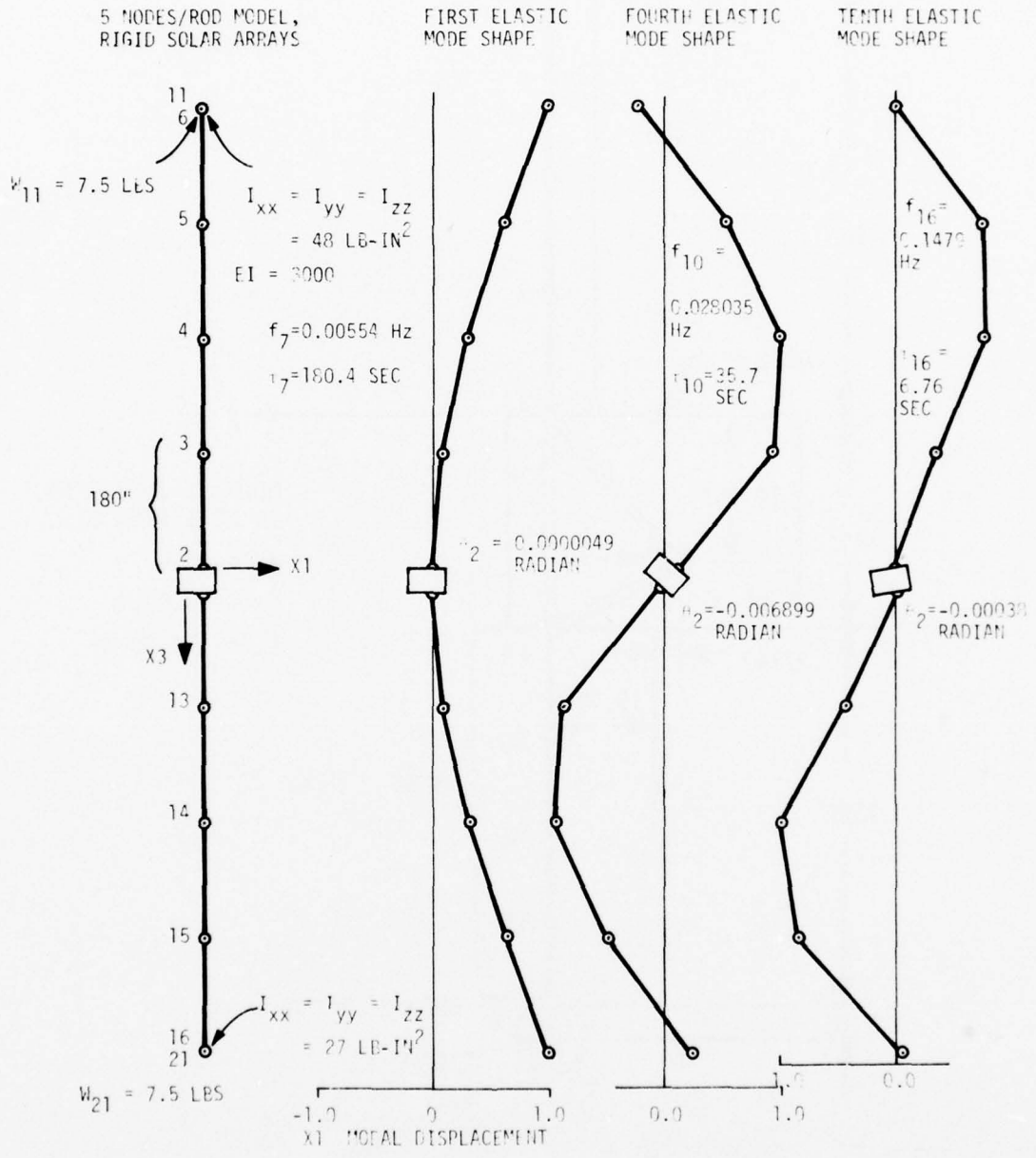

Figure I-3. Gravity Gradient Rod Bending Mode Shapes

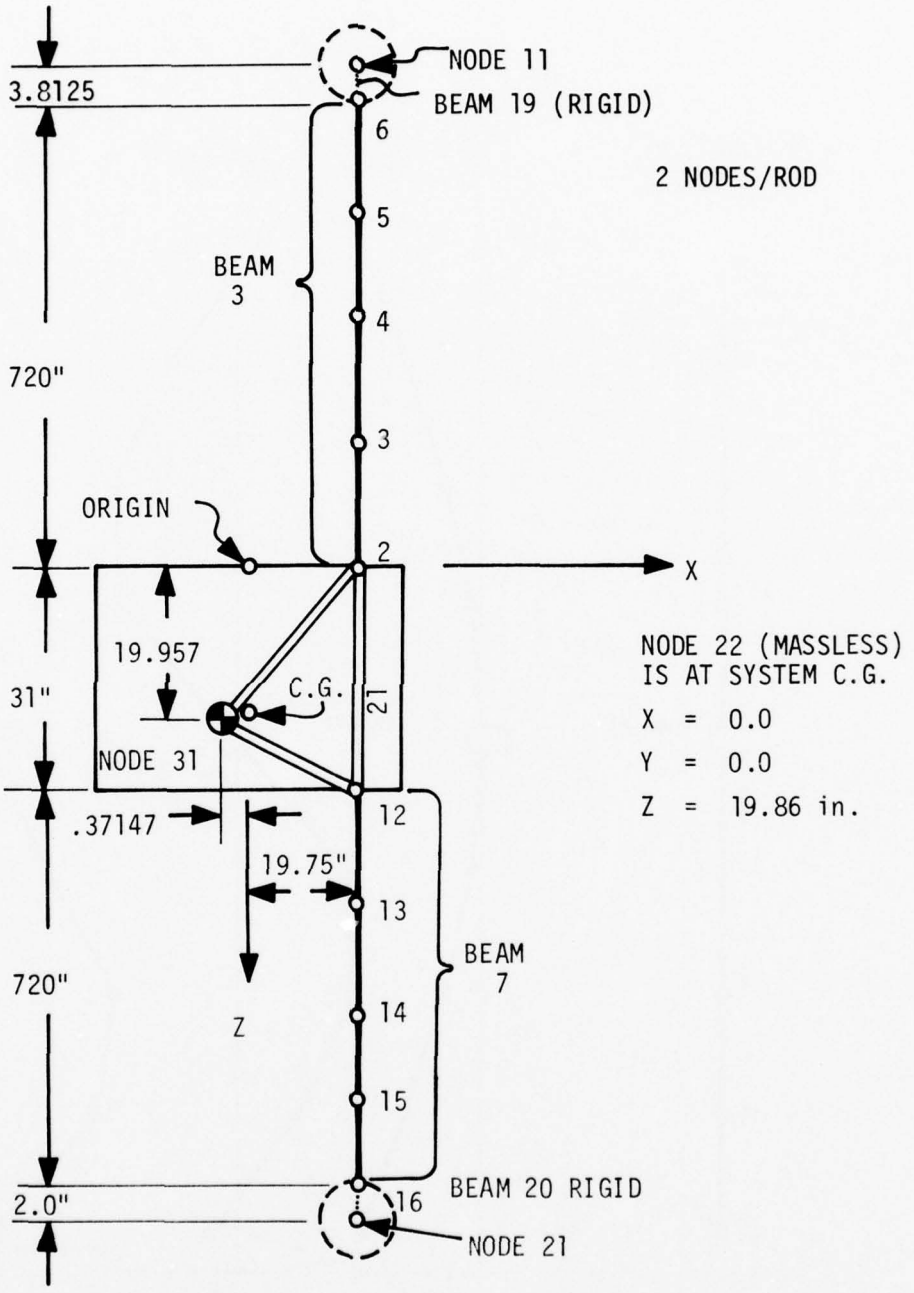
NODE 11
3.8125
BEAM 19 (RIGID)
6
2 NODES/ROD
5
BEAM
3
4
720"
3
ORIGIN
2
X
19.957
NODE 22 (MASSLESS)
IS AT SYSTEM C.G.
X = 0.0
Y = 0.0
Z = 19.86 in.
31"
C.G.
21
NODE 31
.37147
12
19.75"
13
BEAM
7
720"
Z
14
15
2.0"
16
BEAM 20 RIGID
NODE 21

Figure I-4

FOR DYNAMIC MODEL WITH 2 NODES/ROD

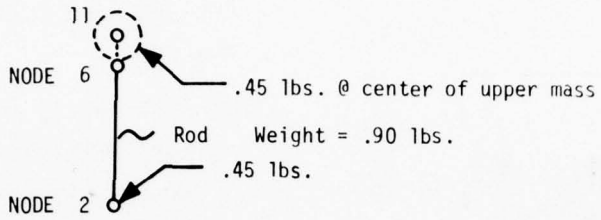

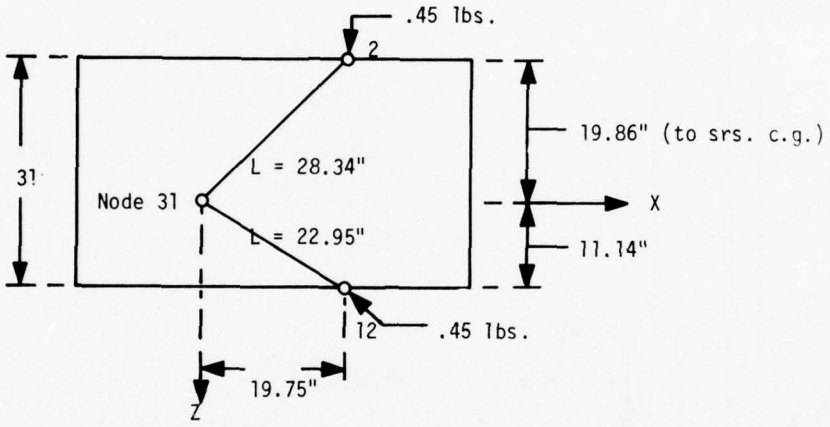

ADDITIONAL INERTIA FOR NODE 31:

$$\Delta I_{XX} = (.45)\ 2\ \underbrace{(19.86^2 + 11.14^2)}_{518.5}$$

$$= 466.67 \text{ lbs-in}^2$$

$$\Delta I_{YY} = (.45)\ (2)\ (28.34^2 + 22.95^2)$$

$$= 1196.87 \text{ lbs-in}^2$$

$$\Delta I_{ZZ} = (.45)\ (2)\ [19.75]^2$$

$$= 351.06 \text{ lbs-in}^2$$

$$\Delta W = .90 \text{ lbs. total added to Node 31}$$

UPDATED DYNAMIC MODEL, 2 NODES/ROD (TIP and SPACECRAFT END)

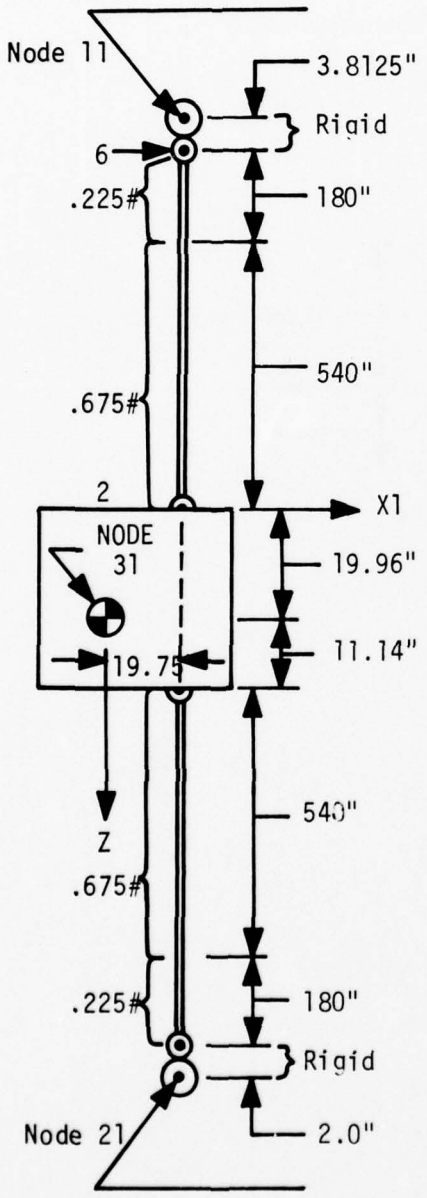

Figure 1-5

For cantilever beam of mass m_b and tip mass m

Equivalent tip mass weight = $m + \frac{1}{4}m_b$

Ref. MyKlestad, N.O., "Fundamentals of Vibration Analysis," McGraw-Hill, 1956, p. 40.

Above is based on Rayleigh-Ritz energy method.

Therefore, transform ¼ beam weight to end of beam but do not transform ¼ beam inertia, since this is accounted for in the $\frac{1}{4}\ m_b$ approximation.

Node 11

$\Delta W = .225$ lbs.

$\Delta I_{XX} = I_{YY} = .225(3.8125)^2 = 3.27$ lbs-in^2

Node 21

$\Delta W = .225$ lbs.

$\Delta I_{XX} = \Delta I_{YY} = .225(2)^2 = 0.9$ lbs-in^2

Node 31 (Spacecraft c.g.)

Assume 3/4 of rods attached and full inertia transformed to base.

$\Delta W = 2 \times .675 = 1.35$ lbs.

From upper rod

$\Delta I_{YY} = 1/3\ W\ \ell^2 + W(19.96^2 + 19.75^2)$

$= 1/3(.675)540^2 + .675(\quad) =$

$= 65{,}610 \quad + \quad 532.2 \quad =$

$= 66{,}142.2$ lbs-in^2 ← from upper rod only

From lower rod

$\Delta I_{YY} = 1/3\ W\ \ell^2 + W(11.14^2 + 19.75^2)$

$= 65{,}610. + .675\ (\quad)$

$= 65{,}610. + 347.$

$= 65{,}957.$ lbs-in^2 ←

Total I_{YY} added to Node 31

$= 66{,}142.2 + 65{,}957$

$\Delta I_{YY\ TOTAL} = 132{,}099.$ lbs-in^2 ←

For ΔI_{XX}:

From upper rod

$\Delta I_{YY} = 1/3\ W\ \ell^2 + W\ 19.96^2$

$= 65{,}610 + \underbrace{.675\ (19.96)^2}_{268.9} =$

$= 65{,}878.9$

From lower rod

$$\Delta I_{YY} = 1/3\ W\ \ell^2 + W(11.14)^2$$

$$= 65{,}610. + \underbrace{.675\ (11.14)^2}_{83.76}$$

$$= 65{,}693.76$$

$$\Delta I_{XX\ TOTAL} = 131{,}572.7\ \text{lbs-in}^2 \longleftarrow$$

For ΔI_{ZZ}:

$$\Delta I_{ZZ} = 2 \times W \cdot (19.75)^2$$

$$= 2 \times .675 \times 19.75^2$$

$$\Delta I_{ZZ} = 526.584\ \text{lbs-in}^2 \longleftarrow$$

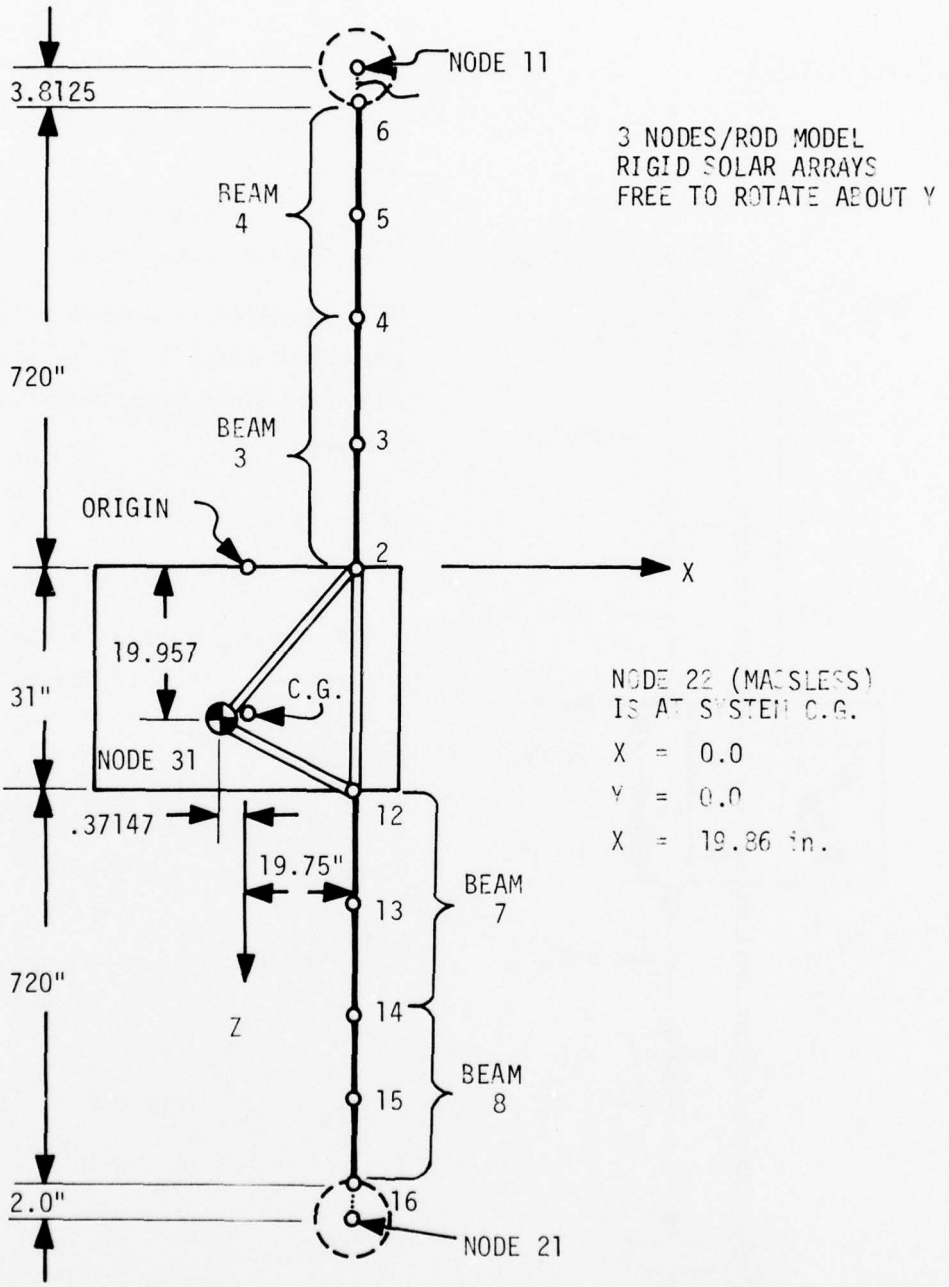
NODE 11
3.8125
6
BEAM
4
5
4
720"
BEAM
3
3
ORIGIN
2
X
19.957
31"
C.G.
NODE 31
.37147
12
19.75"
BEAM
7
13
720"
Z
14
BEAM
8
15
2.0"
16
NODE 21
3 NODES/ROD MODEL
RIGID SOLAR ARRAYS
FREE TO ROTATE ABOUT Y
NODE 22 (MASSLESS)
IS AT SYSTEM C.G.
X = 0.0
Y = 0.0
X = 19.86 in.

Figure I-6

3 NODES PER ROD

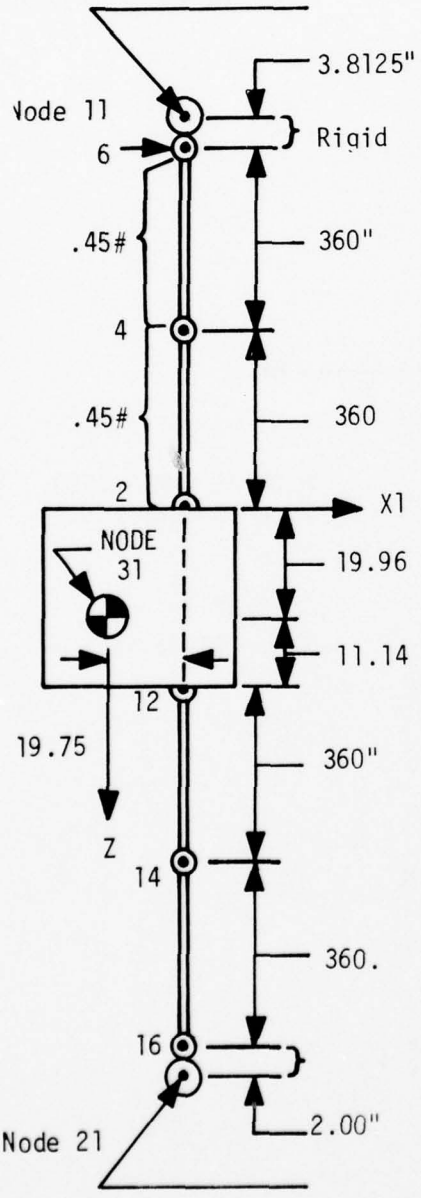

Program will automatically lump rod masses to Nodes

2, 4, 6 (upper rod)

12, 14, 16 (lower rod)

Will manually transform weights at dependent nodes 2, 6, 12 and 16 to adjacent <u>independent</u> nodes of rigid systems.

<u>Node 11:</u>

$$\Delta W_{11} = .225 \text{ lbs. } (W_x, W_y, W_z)$$

$$\Delta I_X = \Delta I_Y = .225\ (3.8125)^2 = 3.27 \text{ lbs-in}^2$$

<u>Node 21:</u>

$$\Delta W_{21} = .225 \text{ lbs. } (W_x, W_y, W_z)$$

$$\Delta I_X = \Delta I_Y = .225\ (2.0)^2 = .90 \text{ lbs-in}^2$$

<u>Node 31</u>:

$$\Delta W_{31} = 2 \times (.225) = .450 \text{ lbs. } (W_x, W_y, W_z)$$

$$\Delta I_x = .225\ (19.96)^2 + .225\ (11.14)^2 = 117.56 \text{ lbs-in}^2$$

$$\Delta I_Y = .225\ (19.96^2 + 19.75^2) \text{ upper rod} + .225\ (11.14^2 + 19.75^2) \text{ lower rod} = 293.09 \text{ lbs-in}^2$$

$$\Delta I_Z = .225 \times 2 \times (19.75)^2 = 175.53 \text{ lbs-in}^2$$

3 NODES/ROD

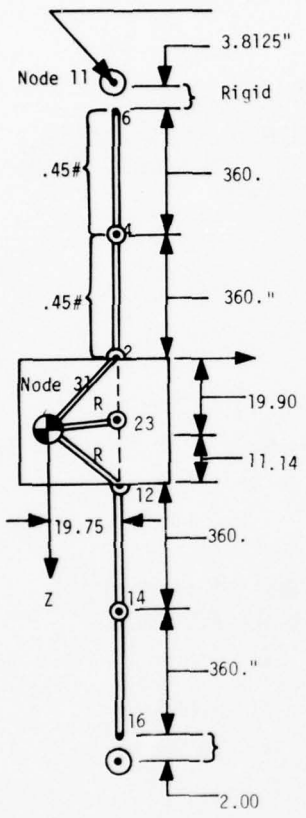

For beam from Node 23 - 31

$K = \frac{3EI}{\ell^3}$ - cantilever beam

Want $f_n = 50.\ H_z$

$W_n^2 = (2\pi\ 50)^2 \frac{K\ 386.4}{16.8}$

$K = \frac{16.8 \times (100\pi)^2}{386.4} = 4291.$ $\quad E = 18.5 \times 10^6$ $\quad b = 12kI^{\frac{1}{2}}$

$I = \frac{K\ell^3}{3E} = \frac{4291\ (19.75)^3}{3 \times 18.5 \times 10^6} = 0.03016$ for b = d $\quad b = .775$

$I = 1/12\ b^4$

MOVE Z MASSES TO SPACECRAFT

Program generates rod weights at nodes 2, 4, 6

12, 14, 16

Must manually transform weight to independent nodes of any rigid systems.

Node 11: (from Node 6)

$\Delta W_{11} = .225$ lbs. $\quad W_x, W_y$

Node 21: (from Node 16)

$\Delta W_{21} = .225$ lbs. $\quad W_x, W_z$

Total rod + tip mass weight in Z direction = 7.5 + .90 = 8.4 lbs. Transform to Nodes 2 and 12, which are part of rigid systems. Hang Z weight on new Nodes at ends of stiff elastic beams tied to Node 31. Node 23 at same location as Node 2, Node 24 at same location as Node 12.

Thus total c.g. is correctly modeled and inertia of Z weight contribution is retained.

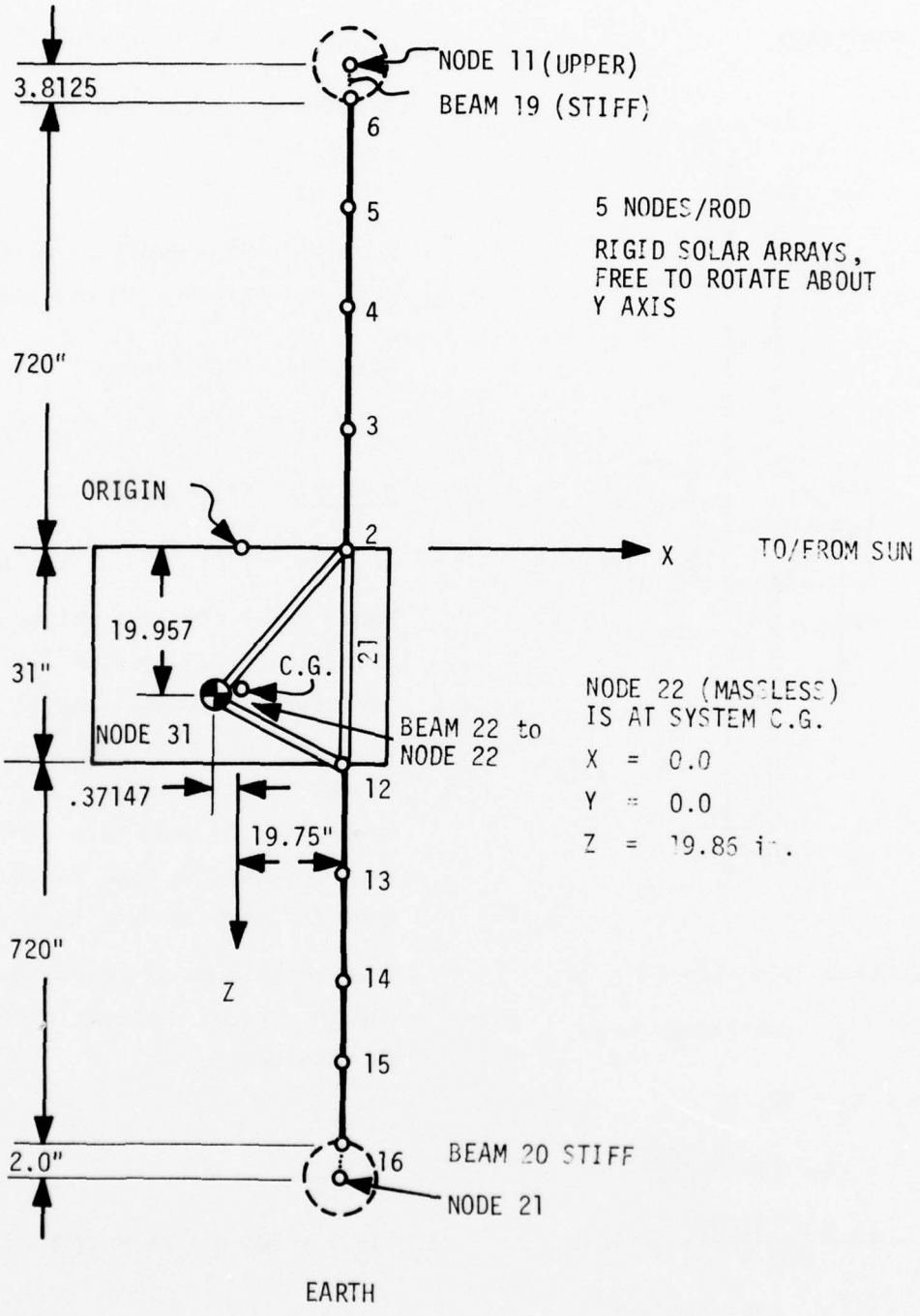
NODE 11 (UPPER)
BEAM 19 (STIFF)
3.8125
6
5
4
5 NODES/ROD
RIGID SOLAR ARRAYS, FREE TO ROTATE ABOUT Y AXIS
720"
3
ORIGIN
2
X
TO/FROM SUN
19.957
31"
C.G.
21
NODE 31
BEAM 22 to NODE 22
NODE 22 (MASSLESS) IS AT SYSTEM C.G.
X = 0.0
Y = 0.0
Z = 19.86 in.
.37147
12
19.75"
13
720"
Z
14
15
2.0"
16
BEAM 20 STIFF
NODE 21
EARTH

Figure I-7

FOR DYNAMIC MODEL WITH 5 NODES/ROD

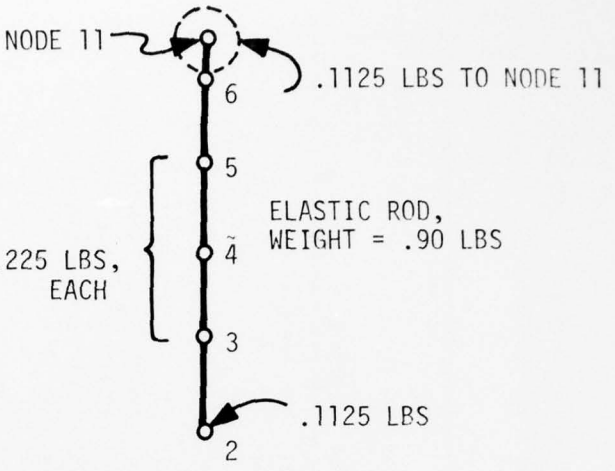

Nodes 11

$$\Delta I_{xx} = \Delta I_{yy} = .1125 \times 3.8125^2 \times 50\%$$
$$= .8176 \text{ lb-in}^2$$

Node 21

$$\Delta I_{xx} = \Delta I_{yy} = .1125 (2.0)^2 \times 50\%$$
$$= .225 \text{ lb-in}^2$$

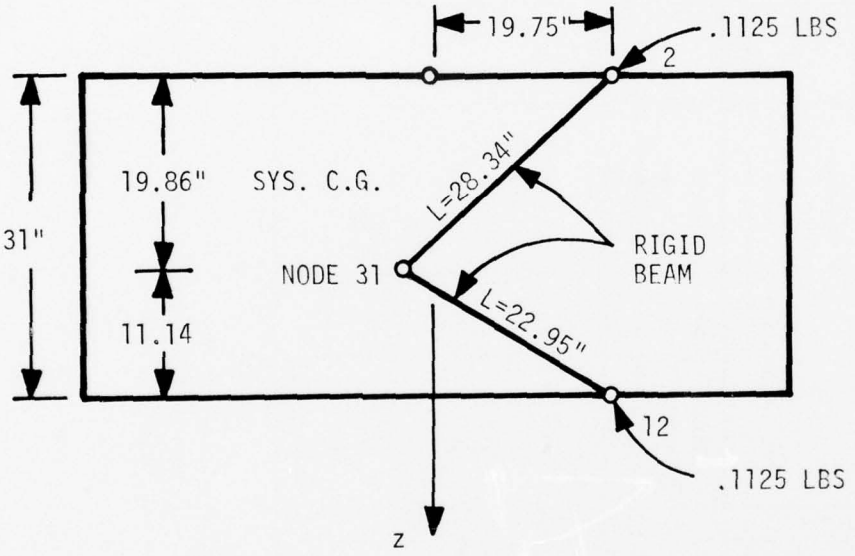

ADDITIONAL INERTIA FOR NODE 31:

$$\Delta I_{xx} = .1125 (2) \quad 19.86^2 + 11.14^2$$
$$= 116.67 \text{ lb-in}^2$$

$$\Delta I_{yy} = .1125 (2) \quad 28.34^2 + 22.95^2$$
$$= 299.22 \text{ lb-in}^2$$

$$\Delta I_{zz} = .1125 (2) \quad 19.75^2 = 87.764 \text{ lb-in}^2$$

$$\Delta W = .1125 \times 2 = .225 \text{ lbs to Node 31}$$

TABLE I-2. STARDYNE MODAL DATA 1 BEAM PER GRAV. GRAD. ROD. ROD EI = 3000. LBS-IN^2.
SOLAR ARRAYS ASSUMED RIGID BUT FREE TO ROTATE ABOUT X2 AXIS.

Signif. Modes for Solar Array Torque Responses	Mode No. (Total)	Elastic Mode No.	Freq. H_z	Genr'lzd Wt. Lbs	Modal Rotation About Solar Array Drive Axis * Rad/Inch	Unsym.	Sym.	Comments	Node With Max Defl.
	7	1	.00546	15.96	.0000050		X1	1st Rod Bending Mode	21
	8	2	.00548	16.07	.0 →		X2	" " " "	21
	9	3	.01925	199.60	.0 →	X2		" " " "	11
Major →	10	4	.02878	446.18	.0367693	X1		" " " "	11
	11	5	.08405	48.00	.0 →	X3		Torsion Mode, Upper Tip	2
	12	6	.11206	27.0	.0 →		X3	Torsion Mode, Lower Tip mass	2
	13	7	1.858	3.28	.0 →		X2/ X1	"2nd" Rod/Spacecraft bend	6
	14	8	1.858	3.28	.0000213		X1/ X2	" " " "	6
	15	9	2.468	6.71	.0 →	X2/ X1		" " " "	16
	16	10	2.468	6.70	.0000221	X1/ X2		" " " "	16
	17	11	11.52	15.9	.0 →		X3	Rod axial mode	6
	18	12	11.74	16.5	.0010255	X3		" " "	16

NOTES: * at spacecraft c.g.

** Lumped 1/2 of each rod weight at tip mass

Lumped 1/2 of each rod weight at attach point on spacecraft

Ignored transfer of dristributed rod inertias

(HQR run TSNST65, not saved on tape)

TABLE I-3. STARDYNE MODAL DATA 1 BEAM PER GRAV. GRAD. ROD. ROD EI = 3000. LBS-IN^2.
SOLAR ARRAYS ASSUMED RIGID BUT FREE TO ROTATE ABOUT X2 AXIS (updated)**

Signif. Modes for Solar Array Torque Responses	Mode No. (Total)	Elastic Mode No.	Freq. H_z	Genr'lzd Wt. Lbs	Modal Rotation About Solar Array Drive Axis * Rad/Inch	Unsym.	Sym.	Comments	Node With Max Defl.
Included but not Signif. →	7	1	.00554	15.5	.0000050		X1	1st Rod Bending Mode	21
	8	2	.00556	15.6	.0 →		X2	" " " "	21
	9	3	.01789	162.96	.0 →	X2		" " " "	11
Major →	10	4	.02442	303.42	.0253276	X1		" " " "	11
	11	5	.08405	48.0	.0 →	X3		Torsion, Upper tip mass	2
	12	6	.11207	27.0	.0 →		X3	Torsion, Lower tip mass	2
	13	7	1.798	3.50	.0 →		X2	"2nd" Rod/Spacecraft bend	6
	14	8	1.799	3.50	.0000161		X1	" " " "	6
	15	9	2.428	6.92	.0 →	X2		" " " "	16
	16	10	2.428	6.92	.0000162	X1		" " " "	16
	17	11	11.69	15.45	.0 →		X3	Rod Axial Mode	6
	18	12	11.87	15.93	.000702	X3/X1		" " "	16

NOTES: * at spacecraft c.g.

** Lumped 1/4 of rod weight to tip mass

Wt. and inertia of 3/4 of rod adjacent to spacecraft lumped with spacecraft c.g. (Node 31)

(HQR run TSNST U, modes on tape X765)

TABLE I-4. STARDYNE MODAL DATA 2 BEAMS PER GRAV. GRAD. ROD. ROD EI = 3000. LBS-IN^2. SOLAR ARRAYS ASSUMED RIGID BUT FREE TO ROTATE ABOUT X2 AXIS.

Signif. Modes for Solar Array Torque Responses	Mode No. (Total)	Elastic Mode No.	Freq. H_z	Genr'lzd Wt. Lbs	Modal Rotation About Solar Array Drive Axis * Rad/Inch	Unsym.	Sym.	Comments	Node With Max Defl.
Included but not signif. →	7	1	.00553	15.58	.0000049		X1	1st Rod Bending Mode	21
	8	2	.00555	15.69	.0 →		X2	" " " "	21
	9	3	.01910	48.72	.0 →	X2		" " " "	4
Major →	10	4	.02808	16.54	-.0068569	X1		" " " "	4
	11	5	.08405	48.0	.0 →	⊕X3		Torsion, upper tip mass	4
	12	6	.11207	27.0	.0 →		⊕X3	Torsion lower tip mass	4
	13	7	.1382	.75	.0 →		X2	2nd Rod Bending Mode	4
	14	8	.1382	.85	.0000221		X1	" " " "	4
	15	9	.1399	.77	.0 →	X2		" " " "	14
Minor →	16	10	.1424	.91		X1		" " " "	14
	17	11	2.395	3.49	.0 →	X2		"3rd" Rod Bending/θX1 upper tip	6
	18	12	2.395	3.49		X1		"3rd" Rod Bending/θX2 upper tip	6
	19	13	3.224	6.89	.0 →	X2		"3rd" Rod Bending/θX1 lower tip	16
	20	14	3.224	6.89	.0000069	X1		"3rd" Rod Bending/θX2 lower tip	16
	21	15	11.6	15.68	.0 →		X3	Rod axial mode	6
	22	16	11.8	16.27	.0010278	X3		Rod axial/s-craft mode	16

NOTES: spacecraft c.g.

HQR run TSNSTL2, modes on tape X4176

TABLE I-5. STARDYNE MODAL DATA, 4 BEAMS PER GRAV. GRAD. ROD. ROD EI = 3000. LBS-IN^2. SOLAR ARRAYS ASSUMED RIGID BUT FREE TO ROTATE ABOUT X2 AXIS.

Signif. Modes for Solar Array Torque Responses	Mode No. (Total)	Elastic Mode No.	Freq. H_z	Genr'Izd Wt. Lbs	Modal Rotation About Solar Array Drive Axis * Rad/Inch	Unsym.	Sym.	Comments	Node With Max Defl.
Included but not signif. →	7	1	.00554	15.5	.0000049		X1	1st Rod Bending Mode	21
	8	2	.00556	15.6	.0000003		X2	" " " "	21
	9	3	.01910	48.1	.0	X2		" " " "	3
Major →	10	4	.02804	16.8	-.0068989	X1		" " " "	4
	11	5	.08405	48.0	.0 →	θX3		Torsion, Upper tip mass	4
	12	6	.11207	27.0	.0 →		θX3	Torsion, Lower tip mass	4
	13	7	.1436	.65	.0 →		X2	2nd Rod Bending Mode	4
	14	8	.1436	.77	.0000344		X1	" " " "	4
	15	9	.1456	.65	.0 →	X2		" " " "	14
Minor →	16	10	.1479	.81	-.0003841	X1		" " " "	14
	17	11	.4543	.50	.0 →		X2	3rd Rod Bending Mode	5
	18	12	.4546	.53	-.0000538		X1	3rd Rod Bending Mode	5
	19	13	.4567	.49	.0 →	X2		" " " "	15
3rd Order	20	14	.4573	.53	.0000901	X1		" " " "	15
	21	15	.8512	.50	.0 →		X2	4th Rod Bending Mode	3
	22	16	.8514	.51	.0000309		X1	" " " "	3
	23	17	.8534	.51	.0 →	X2		" " " "	13
	24	18	.8536	.51	-.0000368	X1		" " " "	13
	25	19	3.527	3.34	.0 →		X2	Upper Mass, θX1	6
	26	20	3.527	3.34	-.0000008		X1	Upper Mass. θX2	6
	27	21	4.645	6.71	.0 →	X2		Lower Mass, θX1	16
	28	22	4.645	6.71	.0000006	X1		Lower Mass, θX2	16

NOTES: *Spacecraft c.g.

(Run No. TSNSTA5, Moes on Tape X3381)

TABLE I-(b). SPACECRAFT PARAMETER VALUES

Mass Properties (orbital configuration)

Total weight (lbs) = 910

Orbit correction - 75% hydrazine usage

Spacecraft moments and products of inertia, solar arrays deployed, gravity gradient rods not deployed (slug - ft^2)

I_{XX} = 208.89 $\quad$ I_{XX} = 0

I_{YY} = 167.46 $\quad$ I_{XZ} = 0

I_{ZZ} = 78.98 $\quad$ I_{YZ} = -3.04 = 14082.73 lbs-in^2

Spacecraft moments and products of inertia with arrays and rods deployed (slug - ft^2)

I_{XX} = 209 = 968188.3 lbs-in^2 $\quad$ I_{XY} = 0

I_{YY} = 1998 = 9.2557 x 10^6 $\quad$ I_{XY} = 0

I_{ZZ} = 1909 = 8.8434 x 10^6 $\quad$ I_{YZ} = -3.04

Solar array moment of inertia about array axis of rotation = 3.28 slug - ft^2 (total for two arrays) = 15194.5 lbs-in^2.

Spacecraft weights, center of gravity, moments and products of inertia (slug-ft^2) and hydrazine usage for orbit connection in stowed condition.

Total WT (lbs)	C G_x (in)	I_{XX}	I_{YY}	I_{ZZ}	I_{YZ}	Hydrazine Usage
949	25.75	124.12	73.91	88.78	-3.31	0
936	25.58	122.55	71.92	88.34	-3.31	25%
923	25.44	120.94	70.08	88.05	-3.31	50%
910	25.33	119.34	68.33	87.85	-3.31	75%
897	25.26	117.75	66.69	87.76	-3.31	100%

TABLE I-7. INPUT TO RUN G2 MASS INERTIA PROPERTIES COMPUTER PROGRAM

```
NTS-2 with rigid deployed solar arrays less elastic grav. grad. rods
Total properties from G.E. report, NRL Table 4-1. c.g. from top of vehicle.

Total Weight              2   910.                                  } Start with
Total c.g.                                          19.86           } total rigid
Total Mi.          9255695.04  8843404.32   968188.32               } spacecraft
Total Prod.         -14082.73
Uprmass Weight            2   -7.5
Uprmass c.g.         19.75                        -723.8125
Uprmass Mi.          -48.        -48.            -48.

Upr rod Weight            2   -.90                                  Subtract elastic
Upr rod c.g.         19.75                        -360.             rods and tip
Upr rod Mi.          -38880.03   -38880.03        -.0558            masses

Lwrmass Weight            2   -7.5
Lwrmass c.g.         19.75                        753.0
Lwrmass Mi.          -27.        -27.            -27.

Lwr rod Weight            2   -.90
Lwr rod c.g.         19.75                        391.0
Lwr rod Mi.          -38880.03   -38880.03        -.0558

Endgroup
Endcase
Stop
$          ENDJOB
$*$DIS
$*$DIS

RESULTS       for Node 31, Flex Rod Models

     Wt. = 893.2
     c.g. =
           x = -.3714 in.
           y = 0.0
           z = 19.957 in.

     Inertias about c.g.

          I_XX = 744940. lbs-in^2
          I_YY = 325980 - 15,195
               = 310,785 lbs.-in^2 for solar arrays free to turn about drive axis
          I_ZZ = 961440. lbs-in^2
```

TABLE I-8. INPROP RUN G2 MASS

COMPUTED VALUES

NTS-2 with rigid deployed solar arrays less elastic grav. grad rods

RESULTS FOR THE TOTAL SYSTEM		
Wt. =	0.89320E 03 +- 0.	Pounds
c.g. Loc.	-0.37147E 00 +- 0.	Inches
	0. +- 0.	Inches
	0.19957E 02 +- 0.	Inches
	-0.33180E 03 +- 0.	Pound - Inches
	0. +- 0.	Pound - Inches
	0.17826E 05 +- 0.	Pound - Inches
Square =	0.11007E 07 +- 0.	Pound - Inches square
Square =	0.68185E 06 +- 0.	Pound - Inches square
Square =	0.96156E 06 +- 0.	Pound - Inches square
Square =	-0.14083E 05 +- 0.	Pound - Inches square
Square =	0. +- 0.	Pound - Inches square
Square =	-0.48744E 04 +- 0.	Pound - Inches square
Mass mom. of inertia about c.g.		
Square = I_{XX}	0.74494E 06 +- 0.	Pound - Inches square
Square = I_{YY}	0.32598E 06 +- 0.	Pound - Inches square
Square = I_{ZZ}	0.96144E 06 +- 0.	Pound - Inches square
Square = I_{XY}	-0.14083E 05 +- 0.	Pound - Inches square
Square = I_{YZ}	0. +- 0.	Pound - Inches square
Square = I_{XZ}	0.17474E 04 +- 0.	Pound - Inches square

I-2 DERIVATION OF INFLUENCE COEFFICIENT MATRIX, INCLUDING CROSS-COUPLING EFFECTS DUE TO ROD CURVATURE

Gravity Rod Simulation with Two Flexible Beam Elements

(Linear Theory)

Based on Stardyne model vibration analysis of NTS-2 with rigid solar arrays and flexible gravity gradient rods, the following flexible rod model with two beam elements of equal length was found to give very good results.

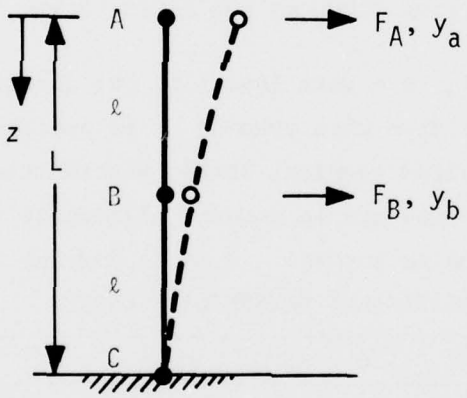

The influence coefficient matrix for the above case can be calculated using standard beam deflection equations, shown on the next page. Thus

$$\begin{Bmatrix} y_a \\ y_b \end{Bmatrix} = \begin{bmatrix} e_{1,1} & e_{1,2} \\ e_{2,1} & e_{2,2} \end{bmatrix} \begin{Bmatrix} F_A \\ F_B \end{Bmatrix}$$

where the $e_{i,j}$ are influence coefficients.

Under dynamic loading cases, the net applied force at each panel point will be

$$F_i = F_{external_i} - m_i \ddot{y}_i$$

where

$F_{external}$ could be due to solar pressures or the component of gravity gradient torque (forces) normal to the rod.

From Roark, "Formulas for Stress and Strain," 4th Ed., the following beam equations are presented.

TABLE I-9. SHEAR, MOMENT, AND DEFLECTION FORMULAS FOR BEAMS; REACTION FORMULAS FOR RIGID FRAMES

Notation: W = load (lb.); w = unit load (lb. per linear in.). M is positive when clockwise; V is positive when upward; y is positive when upward. Constraining moments, applied couples, loads, and reactions are positive when acting as shown. All forces are in pounds, allmoments in inch-pounds; all deflections and dimensions in inches. θ is in radians and tan $\theta = \theta$

STATICALLY DETERMINATE CASES

Loading, Support, and Reference Number	Reactions R_1 and R_2, Vertical Shear V	Bending Moment M and Maximum Bending Moment	Deflection y, Maximum Deflection, and End Slope
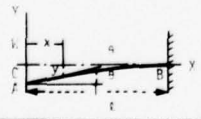	R2 = +W V = -W	M = -Wx MaxM = -W·at B	$y = -\frac{1}{6}\frac{W}{EI}(x^3 - 3\cdot^2 x + 2\cdot^3)$ Max $y = -\frac{1}{3}\frac{W\cdot^3}{EI}$ at A $\theta = +\frac{1}{2}\frac{W\cdot^2}{EI}$ at A
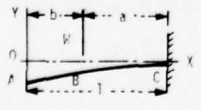	R2 = +W (A to B)V = 0 (B to C)V = -W	(A to B)M = 0 (B to C)M = -W(x-b) MaxM = -Wa at C	(A to B)$y = -\frac{1}{6}\frac{W}{EI}(-a^3 + 3a^2\cdot - 3a^2 x)$ (B to C)$y = -\frac{1}{6}\frac{W}{EI}(x-b)^3 - 3a^2(x-b) + 2a^3$ Max $y = -\frac{1}{6}\frac{W}{EI}(3a^2\cdot - a^3)$ $\theta = +\frac{1}{2}\frac{Wa^2}{EI}$ (A to B)

Note that no external beam torque loads are included.

Definitions:

$e_{1,1}$ = deflection of point A due to unit load at point A

$e_{1,2}$ = deflection of point A due to unit load at point B

$e_{2,2}$ = deflection of point B due to unit load at point B

$e_{2,1} = e_{1,2}$ by reciprocity theorem.

$e_{2,1}$ = deflection of point B due to unit load at point A

$e_{1,1}$

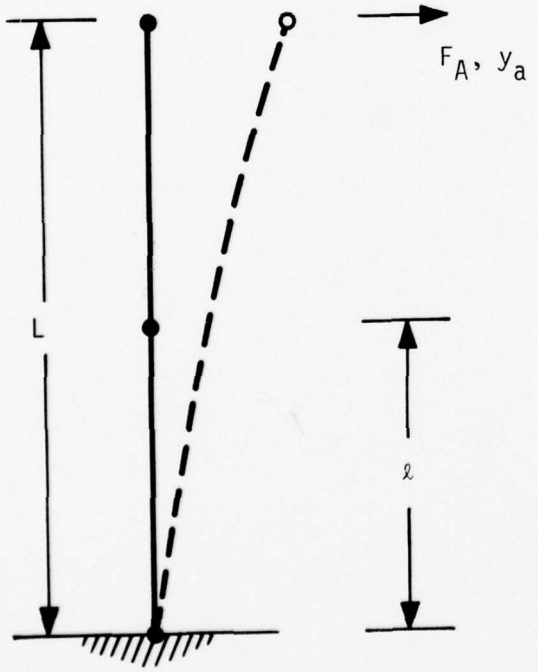

By Case 1, for F_A applied positive in y direction

$$y_a = \frac{1}{3}\frac{PL^3}{EI}$$

but

$$L = 2\ell$$

$$y_a = \frac{1}{3}\frac{(1.0)\ (2\ell)^3}{EI} = \frac{1}{3}\frac{8\ell^3}{EI}$$

$$e_{1,1} = \frac{8}{3}\frac{\ell^3}{EI} \longleftarrow$$

$e_{1,2}$

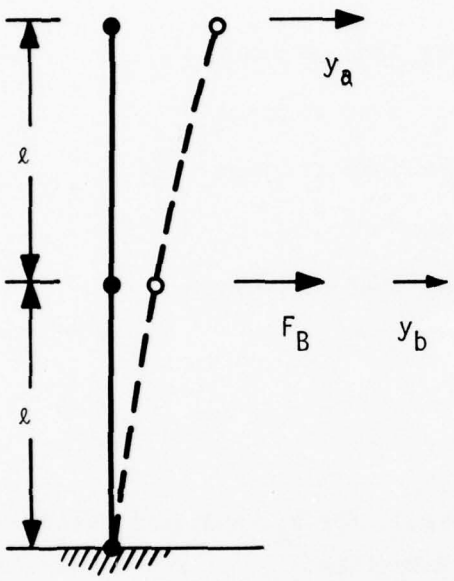

By Case 1

$$y_b = \frac{1}{3}\frac{P\ell^3}{EI} = \frac{1}{3}(1.0)\frac{\ell^3}{EI}$$

Rotation at point b, (by Case 1)

$$\theta = \tfrac{1}{2}\frac{P\ell^3}{EI}$$

Deflection at point A due to load at point B is then

$$y_A = y_b + \theta \cdot \ell$$

$$= (1.0)\frac{\ell^3}{3EI} + \frac{\ell^2}{2EI}\ell =$$

$$= (\frac{1}{3} + \frac{1}{2})\frac{\ell^3}{EI}$$

$$e_{1,2} = \frac{5}{6}\frac{\ell^3}{EI} \longleftarrow$$

$e_{2,2}$

From first calculation for $e_{1,2}$

$$e_{2,2} = \frac{1}{3}\frac{\ell^3}{EI} \longleftarrow$$

$e_{2,1}$

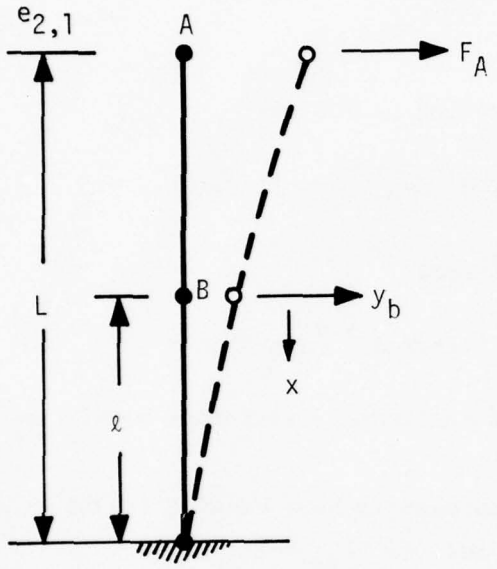

For load at A, deflection at point B is found by Case 2.

$$y_b = \frac{1}{6}\frac{P}{EI}(-a^3 + 3a^2L - 3a^2x)$$

but $a = \ell$

$L = 2L \qquad x = 0$

$$y_b = \frac{1}{6}\frac{P}{EI}(-\ell^3 + 3\ell^2 \cdot 2\ell - 3\ell^2 \cdot 0)$$

$$= \frac{1}{6}\frac{P}{EI}(-\ell^3 + 6\ell^3)$$

$$= \frac{5}{6}\frac{P}{EI}\ell^3$$

$$e_{2,1} = \frac{5}{6}\frac{\ell^3}{EI} \quad \text{for unit load P.}$$

$$= e_{1,2}$$

$$[E] = \begin{bmatrix} e_{1,1} & e_{1,2} \\ e_{2,1} & e_{2,2} \end{bmatrix}$$

$$E = \frac{\ell^3}{EI}\begin{bmatrix} \frac{8}{3} & \frac{5}{6} \\ \frac{5}{6} & \frac{1}{3} \end{bmatrix}$$

for NTS-2 $\ell = 720/2 = 360.$"

$EI = 3000.$ lbs-in^2

$$\frac{\ell^3}{EI} = \frac{(360)^3}{3000} = 15{,}552.0$$

Numerically, for straight rods, NTS-2

$$[E] = \begin{bmatrix} 41{,}472. & 12{,}960. \\ 12{,}960. & 5{,}184. \end{bmatrix} \quad \text{inches/lb.}$$

Note:

Define total rod panel point deflection as follows

$$y_{TOT} = y_{elastic} + y_{rigid\ body} + y_{thermal} + y_{non\text{-}linear}$$

Define inertia loads in terms of y_{total}

$$\ddot{y}_{total} = \ddot{y}_{elastic} + \ddot{y}_{rigid\ body} + \ddot{y}_{thermal} + \ddot{y}_{non\text{-}linear}$$

$y_{elastic}$ is determined by means of influence coefficient matrix above.

Similar expression will also govern elastic beam bending in the other beam bending axis. That is, for uniform $EI_{xx} = EI_{yy}$

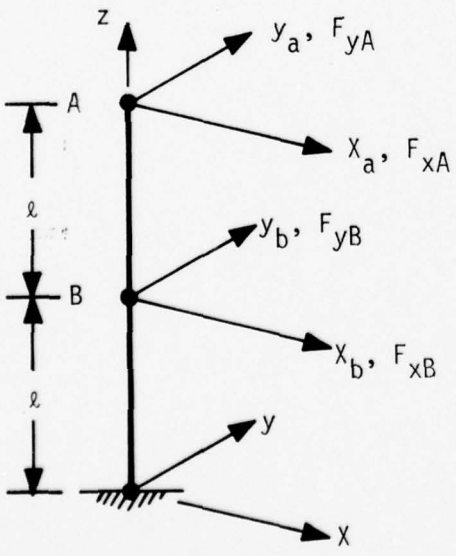

$$\begin{Bmatrix} x_a \\ x_b \\ y_a \\ y_b \end{Bmatrix} = \frac{\ell^3}{EI} \begin{bmatrix} \frac{8}{3} & \frac{5}{6} & 0 & 0 \\ \frac{5}{6} & \frac{1}{3} & 0 & 0 \\ 0 & 0 & \frac{8}{3} & \frac{5}{6} \\ 0 & 0 & \frac{5}{6} & \frac{1}{3} \end{bmatrix} \begin{Bmatrix} F_{x_A} \\ F_{x_B} \\ F_{y_A} \\ F_{y_B} \end{Bmatrix}$$

Note that x's and y's are uncoupled.

Now examine effect of slight bending of rod due to out-of-straightness, thermal deflections, or other sources, causing an equilibrium position of the rod with a slight curvature.

LINEAR ELASTIC CROSS-AXIS COUPLING

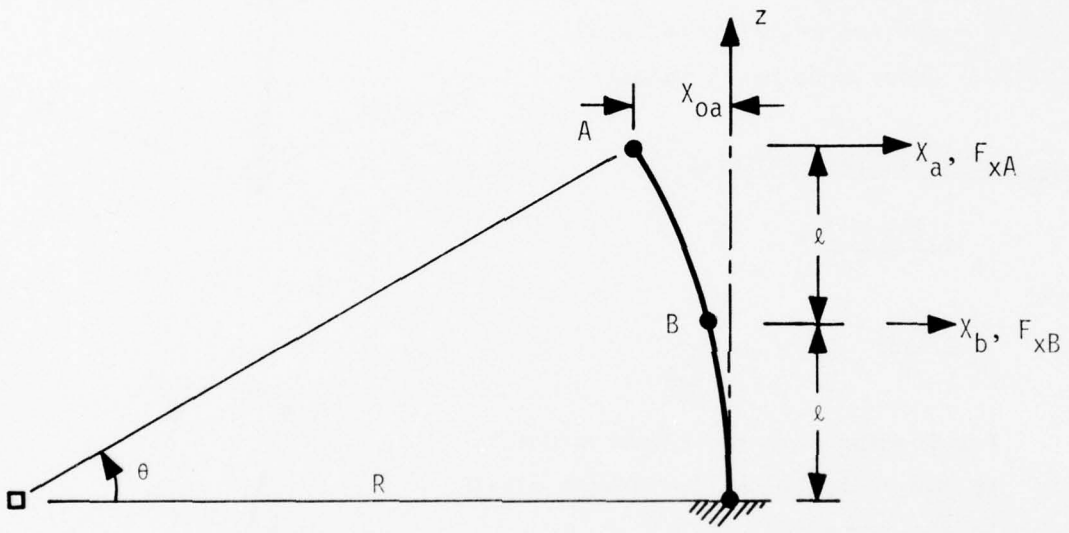

$$\theta = \frac{2\ell}{R}$$

at Node A

$$x_{0A} = R - R \cos \theta = R(1 - \cos \theta)$$

at Node B

$$x_{0B} = R\left(1 - \cos \left(\frac{\theta}{2}\right)\right)$$

Choose positive x in direction toward sun, resulting thermal bending is <u>away</u> from sun.

Now, a force perpendicular to x-z plane will result in a linear y direction deflection, as before plus additional deflections due to twisting about the z axis.

In 3-D View

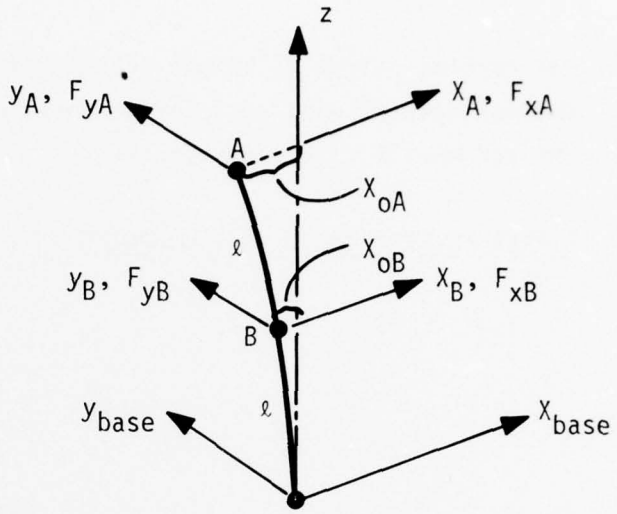

For torsion

$$\theta = \frac{TL}{JG}$$

T = torque

L = beam length

J = torsion section stiffness

G = shear modulus of material

In Side View, in X-Z Plane

$$\phi_A = \frac{x_{0A} - x_{0B}}{\ell}$$

$$\phi_B = \frac{x_{0B}}{\ell}$$

For loading into the plane of paper, in the y direction, no torsion exists in the beams if $\phi_A = \phi_B$.

In upper beam segment, no torsion exists due to F_{yA}.

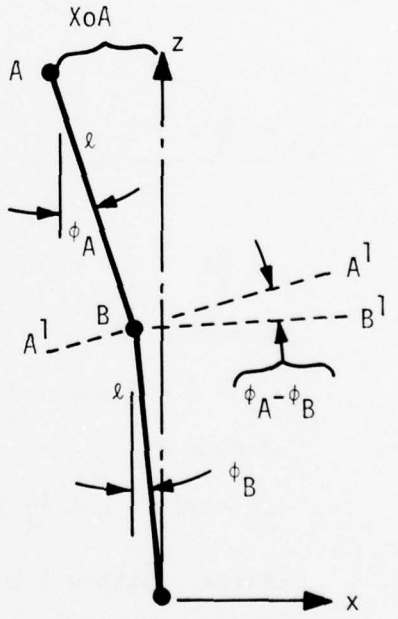

Pure bending about point B is about an axis to upper beam, line A' - A'. This moment at B about A'A' must be resolved into a moment about axis B'-B and a torque.

$$T = (\text{Moment at B referred to A'-A'}) * \sin(\phi_A - \phi_B)$$

$$= F_{ya} \cdot \ell \sin(\phi_A - \phi_B) \qquad \text{for small } \phi$$

$$= \ell \sin \frac{x_{0A} - x_{0B}}{\ell} - \frac{x_{0B}}{\ell} \; F_{yA} = (x_{0A} - 2\,x_{0B}) F_{yA}$$

At Node B

$$T = (x_o - 2\, x_{0B}) \cdot F_{yA}$$

Twist of lower beam is $\theta_B = \frac{T\ell}{JG}$

$$\theta_B = \frac{\left[(x_{0A} - 2\, x_{0B})\right]\ell}{JG} F_{yA}$$

Additional deflection in y direction at

Node B = 0

However, twist θ_B about lower beam will cause some additional y deflection at upper node.

$$\text{Arm} = \ell \sin (\phi_A - \phi_B)$$

$$= \ell(\phi_A - \phi_B)$$

$$= \ell\left(\frac{x_{0A} - x_{0B}}{\ell} - \frac{x_{0B}}{\ell}\right) = (x_{0A} - 2\, x_{0B})$$

Deflection at end of arm (Node A) is $\theta_B \cdot$ arm

$$\Delta_{y_A} = \frac{(x_{0A} - 2\, x_{0B})^2 \ell}{JG} F_{yA} \longleftarrow$$

for $x_{0A} = 36$

$x_{0B} = 9$

$\ell = 360.$

$JG = 25$

above term is $\frac{(36 - 18)^2\ 360.}{25.} = 4665.6$ in/lb.

Checks very well with 3 node Stardyne static model. Low for 5 Node static.

Coupling with Accelerations along Z Axis (Rod Axis)

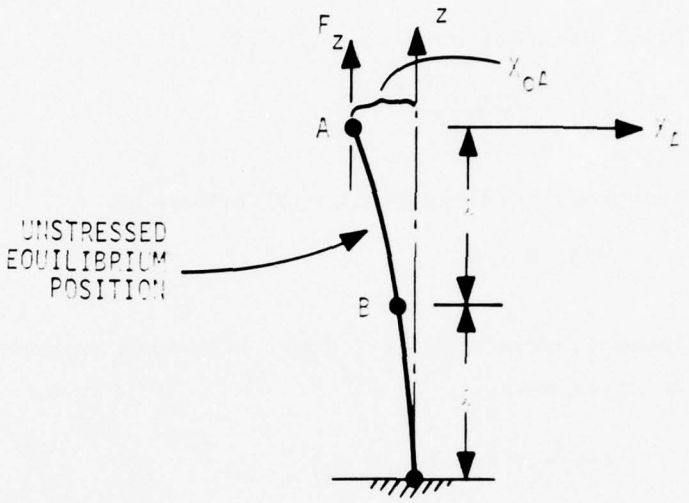

As shown, a positive force F_z will tend to straighten the rod. A negative oriented Z force will increase the rod deflection.

Buckling check:

From: Myklestad, N.O., "Fundamentals of Vibration Analysis," 1956, p. 28.

$$\frac{W}{P_{cr}} = \frac{4 L^2 mg}{-^2 EI} \qquad \text{for } F_z = mg \text{ down}$$

P_{cr} = column buckling load

$m = (7.5 + .45)/386.4$ lbs-sec^2/in.

g = dynamic load factor acting downward due to reactions from solar array drive torques, inches/sec^2.

$$mg = -^2 EI/4 L^2$$

$$g_{allow} = \frac{-^2 EI\, g_c}{4 L^2} = \frac{-^2 (3000.) 386.4}{-(720)^2} = 5.51 \text{ in/sec}^2$$

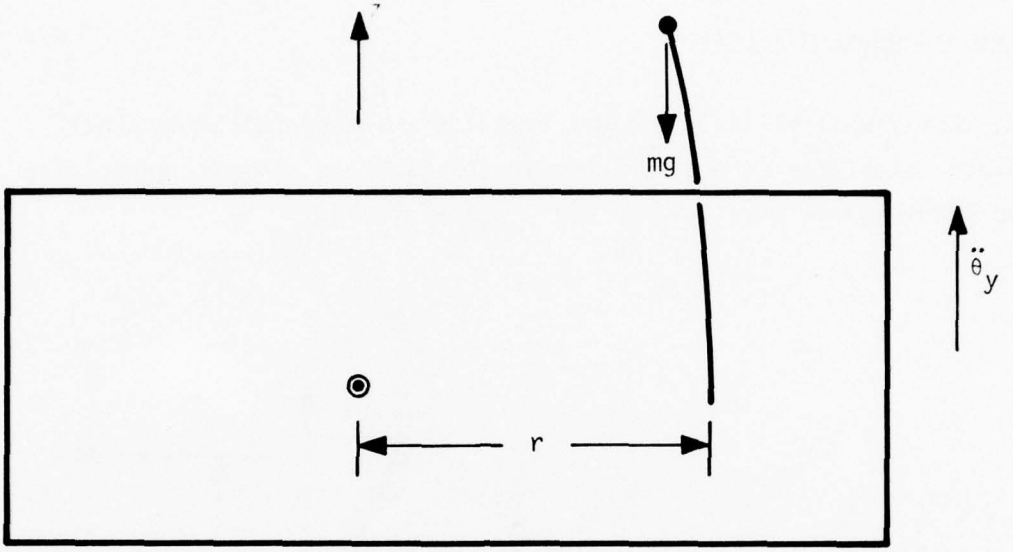

$g_{allow} = 5.51 \text{ in/sec}^2$

$r\ddot{\theta} = g_{allow}$ r = dist. from spacecraft c.g. to rod attack point, $\perp$ to Z axis

= 19.75 in.

$$\ddot{\theta}_{allow} = \frac{g_{allow}}{r}$$

$$= \frac{5.51}{19.75} \frac{\text{in/sec}^2}{\text{in}}$$

$$= .279 \text{ rad/sec}^2$$

I_{YY} = 311,160 lb-in^2 input to Stardyne run

If peak applied torque = 1 ft-lb for max pulse duration of 45 millisec

$$\ddot{\theta} = \frac{\text{Torque}}{I} \qquad T = I\ddot{\theta}$$

$$= \frac{12.0 \text{ lb-in} \times 386.4 \text{ in}}{311{,}160 \text{ lb-in}^2 \quad \text{sec}^2}$$

$$= .0149 \text{ rad/sec}^2$$

Fraction of buckling load = $\frac{.0149}{.279} = .0534$

Coupled X-Z Beam Deflection

Linear theory will be used. Exact buckling solution involving theory of elastic stability is not suitable for application at hand, especially since column loadings are very low, by prev. calculations.

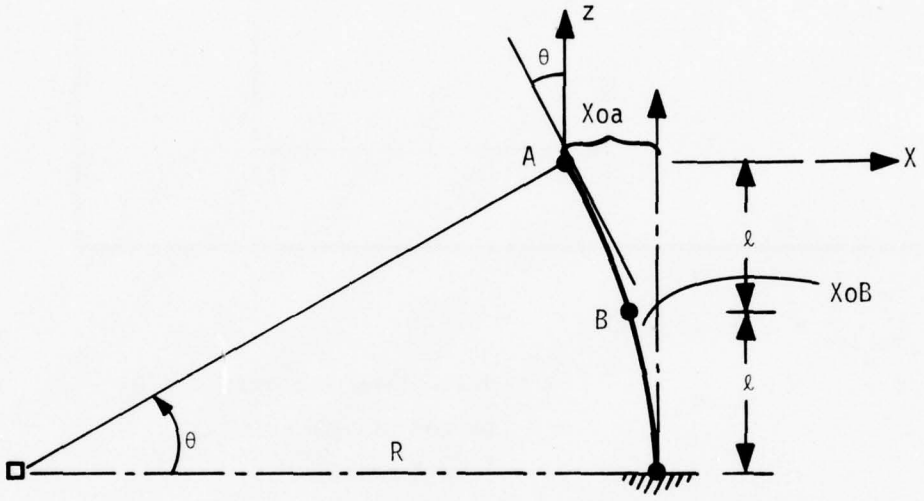

$$\sin\theta = \frac{2\ell}{R}$$

$$x_{0A} = R - R\cos\theta = R(1 - \cos\theta) \quad \longleftarrow$$

$$\cos\theta = 1 - \frac{x_{0A}}{R}$$

$$\tan\theta = \left(\frac{2\ell}{R}\right) \Big/ \left(1 - \frac{x_{0A}}{R}\right) = \frac{L}{R - x_0}$$

$$\theta = \tan^{-1}\left(\frac{L}{R - x_o}\right)$$

$$x_{0B} = R\left(1 - \cos\frac{\theta}{2}\right) \quad \longleftarrow$$

No closed form solution available to solve for R in terms of ℓ, x_{0A}. Must iterate. ←

Assume γ_{0A}, γ_{0B} are known, estimated, or previously calculated.

$$\phi_A \cong \frac{X_{oA} - X_{oB}}{\ell}$$

for ϕ small

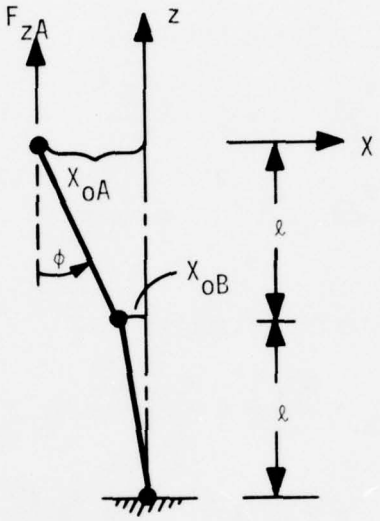

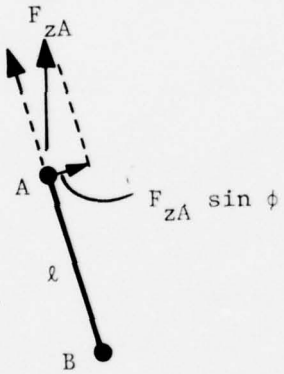

Moment at B = $F_{zA} \cdot \phi_A \cdot \ell = M_B$ for sin $\phi_A \approx \phi_B$

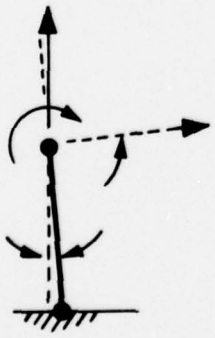

$$\phi_B = \frac{x_{OB}}{\ell} \leftarrow$$

Resolving vertical force F_{zA} transferred to point B, lateral component is

$$F_{xB} = F_{zA} \cdot \sin \phi_B \approx F_{zA} \cdot \phi_B$$

Z-X Coupled Deflections, continued

Deflections of point B (elastic)

$$x_B = \frac{1}{3} \frac{F_{xB}}{EI} \ell^3 + \frac{1}{2} \frac{M_{yB}}{EI} \ell^2$$

$$x_B = \frac{1}{3} \frac{F_{zA} \cdot \phi_B}{EI} \ell^3 + \frac{1}{2} \frac{F_{zA} \phi_A}{EI} \ell^3 \longleftarrow$$

Rotation of point B (elastic) = α_B (intermediate variable)

$$\alpha_{B_{elastic}} = \frac{M_{yB} \ell}{EI} + \frac{F_{xB}}{2 EI} \ell^2$$

$$= F_{zA} \frac{\phi_A}{EI} \ell^2 + \frac{F_{zA} \phi_B}{2 EI} \ell^2$$

Deflection of point A due to vertical F_{zA} force

$$x_A = x_B + \ell \cdot \alpha B_{elastic} \cdot \cos \phi_A$$

$$= \frac{\ell^3}{EI} (\frac{1}{3} \phi_B + \frac{1}{2} \phi_A) F_{zA} + \frac{\ell^3}{EI} (\phi_A + \frac{\phi B}{2}) \cos \phi_A \cdot F_{zA}$$

For $\cos \phi_A$ 1.0

$$x_A = \frac{\ell^3}{EI} (\frac{3}{2} \phi_A + \frac{5}{6} \phi_B) F_{zA} \longleftarrow$$

SUMMARY EQUATIONS

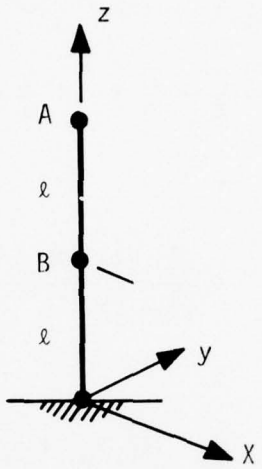

For un-bent rod, EI same in both axes

$$\begin{Bmatrix} x_A \\ x_B \\ y_A \\ y_B \end{Bmatrix} = \frac{\ell^3}{EI} \begin{bmatrix} \frac{8}{3} & \frac{5}{6} & 0 & 0 \\ \frac{5}{6} & \frac{1}{3} & 0 & 0 \\ 0 & 0 & \frac{8}{3} & \frac{5}{6} \\ 0 & 0 & \frac{5}{6} & \frac{1}{3} \end{bmatrix} \begin{Bmatrix} F_{x_A} \\ F_{x_B} \\ F_{y_A} \\ F_{y_B} \end{Bmatrix}$$

For bent rod, with point A initially at unstressed position having x and y components of x_{0A}, y_{0A} and point B having corresponding initial unstressed deflection components of x_{0B}, y_{0B} write out deflection equations in algebraic form.

$$x_A = \frac{\ell^3}{EI_y}\left(\frac{8}{3} F_{x_A} + \frac{5}{6} F_{x_B}\right) \longleftarrow \text{in-plane bending}$$

$$+ \frac{\ell}{JG}\left(y_{0A} - 2\, y_{0B}\right)^2 F_{x_A} \longleftarrow \text{torsion}$$

$$+ \frac{\ell^3}{EI_y}\left(\frac{3}{2}\,\frac{(x_{0A} - x_{0B})}{\ell} + \frac{5}{6}\cdot\frac{x_{0B}}{\ell}\right) F_{z_A} \longleftarrow \text{Z-X coupling}$$

Similarly:

$$y_A = \frac{\ell^3}{EI_y}\left(\frac{8}{3} F_{y_A} + \frac{5}{6} F_{y_B}\right) + \frac{\ell}{JG}\left(x_{0A} - 2\, x_{0B}\right)^2 F_{y_A}$$

$$\cdot \frac{\ell^3}{EI_y}\left(\frac{3}{2}\left(\frac{y_{0A} - y_{0B}}{\ell}\right) + \frac{5}{6}\,\frac{y_{0B}}{\ell}\right) F_{z_A}$$

For Point B (elastic deflections)

$$x_B = \frac{\ell^3}{EI_y}\left(\frac{5}{6} F_{x_A} + \frac{1}{3} F_{x_B}\right)$$ in-plane bending

$$+$$ (no torsional contribution at B) (1st order approx.)

$$+ \frac{\ell^3}{EI_y}\left(\frac{1}{2}\left(\frac{x_{0A} - x_{0B}}{\ell}\right) + \frac{1}{3}\left(\frac{x_{0B}}{\ell}\right)\right) F_{z_A}$$ z-x coupling

$$y_B = \frac{\ell^3}{EI_x}\left(\left(\frac{5}{6} F_{y_A} + \frac{1}{3} F_{y_B}\right)\right)$$

$$+ \frac{\ell^3}{EI_x}\left(\left(\frac{1}{2}\left(\frac{y_{0A} - y_{0B}}{\ell}\right) + \frac{1}{3}\left(\frac{y_{0B}}{\ell}\right)\right) F_{z_A}\right.$$

Note: Rod bending stiffnesses EI_x and EI_y are designated as follows:

EI_x is stiffness for bending rotations about x axis, resulting in y deflections

EI_y is stiffness for bending rotations about y axis, resulting in x deflections.

FINAL 2-BEAM GRAVITY ROD INFLUENCE COEFFICIENT MATRIX

$$
\begin{Bmatrix} x_A \\ x_B \\ y_A \\ y_B \end{Bmatrix} =
\left[\begin{array}{cc|cc|c}
\left[\frac{8}{3}\frac{\ell^3}{EI_y} + \frac{\ell}{JG}(y_{0A} - 2\,y_{0B})^2\right] & \frac{5}{6}\frac{\ell^3}{EI_y} & 0 & 0 & \left[\frac{1}{6}\frac{\ell^2}{EI_y}\cdot\right. \\
 & & & & \left.\cdot\,(9\,x_{0A} - 4\,x_{0B})\right] \\
\frac{5}{6}\frac{\ell^3}{EI_y} & \frac{1}{3}\frac{\ell^3}{EI_y} & 0 & 0 & \frac{1}{6}\frac{\ell^2}{EI_y}\cdot \\
 & & & & \cdot\,(3\,x_{0A} - x_{0B}) \\
\hline
0 & 0 & \left[\frac{8}{3}\frac{\ell^3}{EI_x} + \frac{\ell}{JG}(x_{0A} - 2\,x_{0B})^2\right] & \frac{5}{6}\frac{\ell^3}{EI_x} & \left[\frac{1}{6}\frac{\ell^2}{EI_x}\cdot\right. \\
 & & & & \left.\cdot\,(9\,y_{0A} - 4\,y_{0B})\right] \\
0 & 0 & \frac{5}{6}\frac{\ell^3}{EI_x} & \frac{1}{3}\frac{\ell^3}{EI_x} & \frac{1}{6}\frac{\ell^2}{EI_x}\cdot \\
 & & & & \cdot\,(3\,y_{0A} - y_{0B}) \\
 & & & & 4 \times 5
\end{array}\right]
\begin{Bmatrix} F_{xA} \\ F_{xB} \\ F_{yA} \\ F_{yB} \\ F_{zA} \end{Bmatrix}
$$

Numerical Check

For manufacturing tolerance, min radius of curvature for BI-STEM > 1800. foot per NTS-2 spec.

For $L = 2\ell = 720"$

tie deflection = 12.0 in. $\theta = 1.91021317^{o}$

Add 24 in. thermal deflection (per R.G. Langton memo)

Total $x_{0A} = 36.$ in. $\longleftarrow \theta = 5.7248^{o}$

$R = 601.5$ ft. $= 7218.$ in. (radius of curvature)

$x_{0B} = 9.005$ inches $\longleftarrow y_{0A} = y_{0B} = 0.0$

$EI_x = 3000. = EI_y$

$JG = 25.$

$\ell = 360.$

A 2-beam Stardyne finite element model was run using the above parameters, including the radius of curvature. Two straight beam element connect the base, Node B, and Node A (top). Run TSNS T6Z.

An additional run, using twice as many beams and nodes, was also run (Run TSNS T9D). Both results are presented in Tables I-1, I-2, and I-3.

STARDYNE CHECK CASE, GRAV. ROD INFLUENCE MATRIX. [E]

TABLE I-10. COMPUTED [E] ~ lbs/inch

$$\begin{Bmatrix} x_A \\ x_B \\ y_A \\ y_B \end{Bmatrix} = \begin{bmatrix} 41,472. & 12,960. & 0 & 0 & 2073. \\ 12,960. & 5,184. & 0 & 0 & 713. \\ 0 & 0 & 46,138. & 12,960. & 0 \\ 0 & 0 & 12,960. & 5,184. & 0 \end{bmatrix} \cdot \begin{Bmatrix} F_{x_A} \\ F_{x_B} \\ F_{y_A} \\ F_{y_B} \end{Bmatrix}$$

TABLE I-11. STARDYNE 2 BEAM SOLUTION
(INCLUDES Z DEFLECTIONS)

$$\underset{6 \times 1}{\begin{Bmatrix} x_A \\ x_B \\ y_A \\ y_B \\ z_A \\ z_B \end{Bmatrix}} = \begin{bmatrix} 41,498. & 12,993. & 0 & 0 & 2464. \\ 12,993. & 5,205. & 0 & 0 & 715. \\ 0 & 0 & 46,294. & 13,011. & 0 \\ 0 & 0 & 13,011. & 5,208. & 0 \\ +2,465. & 715. & 0 & 0 & 149. \\ +\ 325. & 130. & 0 & 0 & 18. \end{bmatrix} \underset{5 \times 1}{\begin{Bmatrix} F_{x_A} \\ F_{x_B} \\ F_{y_A} \\ F_{y_B} \\ F_{z_A} \end{Bmatrix}}$$

TABLE I-12. STARDYNE 4 BEAM STATIC CHECK RESULTS
FOR FLEXIBLE GRAVITY GRAD. ROD

(COMPARE TO TABLE 2 & 1)
(INCLUDES Z DEFLECTIONS)

$$\begin{Bmatrix} x_A \\ x_B \\ y_A \\ y_B \\ z_A \\ z_B \end{Bmatrix} = \begin{bmatrix} 41{,}494. & 12{,}992. & 0 & 0 & 2{,}562. \\ 12{,}992. & 5{,}204. & 0 & 0 & 739. \\ 0 & 0 & 48{,}336. & 13{,}886. & 0 \\ 0 & 0 & 13{,}886. & 5{,}354. & 0 \\ 2{,}562. & 739. & 0 & 0 & 162. \\ 398. & 154. & 0 & 0 & 23. \end{bmatrix} \begin{Bmatrix} F_{x_A} \\ F_{x_B} \\ F_{y_A} \\ F_{y_B} \\ F_{z_A} \end{Bmatrix}$$

Run TSidST9D

SHEARS AND MOMENTS TRANSMITTED TO ROD ATTACH POINT BY FLEXIBLE ROD MODEL

In terms of previously defined parameters the dynamic loads imposed on spacecraft by rod motions are as follows:

For loads in Y-Z plane:
(shown in positive direction)

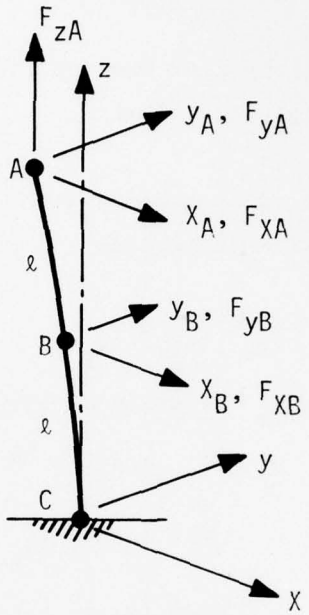

Loads on spacecraft are equal and opposite:

$$V_y = F_{y_A} + F_{y_B}$$

$$V_z = F_z$$

$$M_x = -(\ell \cos \phi_A + \ell \cos \phi_B) \cdot F_{y_A} - \ell \cos \phi_B \cdot F_{y_B} - (y_{0A}) F_{z_B}$$

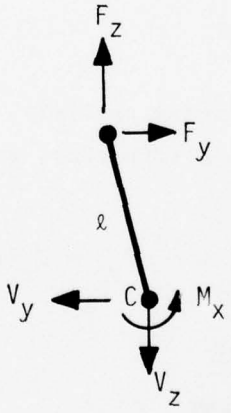

+ F_y causes negative M_x applied to spacecraft.

For 1st order non-linear analysis, update moment to include deflection of point A. Assume $\cos \phi_A \approx 1$

$$M_x = -2 \cdot \ell \cdot F_{y_A} - \ell \cdot F_{y_B} - (y_{0A} - y_a) \cdot F_{z_A}$$

Loads in X-Z Plane

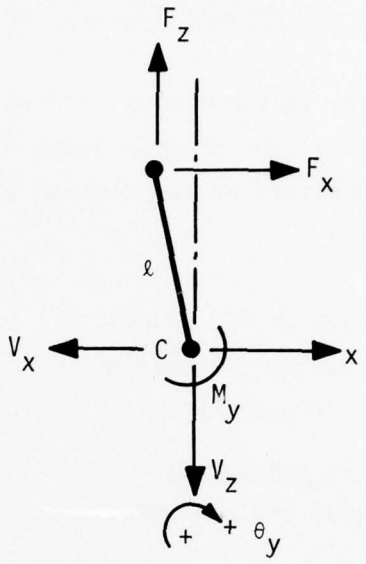

Loads shown at base of rod to maintain equilibrium.

Loads on spacecraft are opposite and equal.

$$V_x = F_{x_A} + F_{x_B}$$

V_z (previously calculated = F_z

$$M_y = +(\ell \cos \phi_A + \ell \cos \phi_B) F_{x_A} + \ell \cos \phi_B F_{x_B} + F_z(x_{0A})$$

For 1st order non-linear analysis, update last term to include current deflection of point A (tip mass) which could be changing fastest. Also $\cos \phi_A = \cos \phi_B \approx 1$

$$M_y = 2\ell F_{x_A} + \ell F_{x_B} + F_z(x_{0A} - x_A)$$

Moments about Z Axis

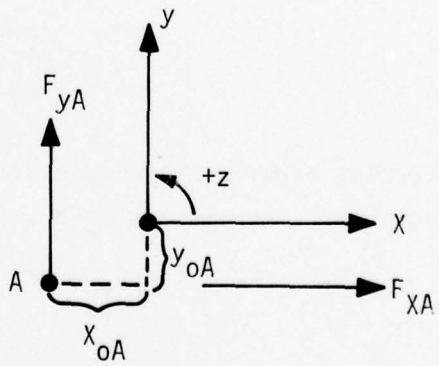

From top, looking down

$$M_z = y_{0A} \cdot F_{x_A} + y_{0B} \cdot F_{x_B} - x_{0A} \cdot F_{y_A} - x_{0B} F_{y_B}$$

For non-linear effects, update total distance from Z axis.

Non-linear

$$M_z = (y_{0A} - y_A)\, F_{x_A} + (y_{0B} - y_B) F_{x_B}$$
$$- (x_{0A} - x_A)\, F_{y_A} - (x_{0B} - x_B) F_{y_B} \longleftarrow$$

In matrix notation, loads on spacecraft at rod attach point are:

$$\begin{Bmatrix} V_x \\ V_y \\ V_z \\ M_x \\ M_y \\ M_z \end{Bmatrix} = \begin{bmatrix} 1 & 1 & 0 & 0 & 0 & 0 \\ 0 & 0 & 1 & 1 & 0 & 0 \\ 0 & 0 & 0 & 0 & 1 & 1 \\ 0 & 0 & -2\ell & -\ell & (y_{0A}-y_A) & (y_{0B}-y_B) \\ 2\ell & \ell & 0 & 0 & (x_{0A}-x_A) & (x_{0B}-x_B) \\ (y_{0A}-y_A) & (y_{0B}-y_B) & -(x_{0A}-x_A) & -(x_{0B}-x_B) & 0 & 0 \end{bmatrix} \begin{Bmatrix} F_{x_A} \\ F_{x_B} \\ F_{y_A} \\ F_{y_B} \\ F_{z_A} \\ F_{z_B} \end{Bmatrix}$$

where

x_A, x_B, y_A, y_B are updated rod elastic deflection.

For non-linear Lagrangian analysis or do not include for linear (small deflection) analysis.

NUMERICAL CHECK, REACTIONS AND MOMENTS

Linear analysis

CALCULATED VALUES, STARDYNE CHECK CASE

$$\begin{Bmatrix} V_x \\ V_y \\ V_z \\ M_x \\ M_y \\ M_z \end{Bmatrix} = \begin{bmatrix} 1.0 & 1.0 & 0 & 0 & 0 & 0 \\ 0 & 0 & 1.0 & 1.0 & 0 & 0 \\ 0 & 0 & 0 & 0 & 1 & 1 \\ 0 & 0 & -720 & -360 & 0 & 0 \\ 720 & 360 & 0 & 0 & 36 & 9 \\ 0 & 0 & -36 & -9 & 0 & 0 \end{bmatrix} \begin{Bmatrix} F_{x_A} \\ F_{x_B} \\ F_{y_A} \\ F_{y_B} \\ F_{z_A} \\ F_{z_B} \end{Bmatrix}$$

COMPUTED REACTIONS FROM STARDYNE
2 BEAM MODEL (RUN USNS T6Z)

$$\begin{Bmatrix} V_x \\ V_y \\ V_z \\ M_x \\ M_y \\ M_z \end{Bmatrix} = \begin{bmatrix} 1.00 & 1.00 & 0.0 & 0.0 & 0.0 & 0.0 \\ 0.0 & 0.0 & 1.00 & 1.00 & 0.0 & 0.0 \\ 0.0 & 0.0 & 0.0 & 0.0 & 1.0 & 1.0 \\ 0.0 & 0.0 & -720.00 & -360.45 & 0.0 & 0.0 \\ 720.0 & 360.45 & 0.0 & 0.0 & 36.0 & 9.006 \\ 0.0 & 0.0 & -36.00 & -9.006 & 0.0 & 0.0 \end{bmatrix} \begin{Bmatrix} F_{x_A} \\ F_{x_B} \\ F_{y_A} \\ F_{y_B} \\ F_{z_A} \\ F_{z_B} \end{Bmatrix}$$

I-3 DISCRETE DAMPING MATRIX DERIVATION AND CALCULATION

Convert Modal Damping to Discrete Damping

Matrix equations of motion for free vibration:

$$[M]\{\ddot{x}\} + [C]\{\dot{x}\} + [K]\{x\} = \{0\} \tag{I-1}$$

Let $\{x\} = [\phi]\{q\}$ (I-2)

where

$[\phi]$ = set of mode shapes

$\{q\}$ = modal displacements

Also $\{\dot{x}\} = [\phi]\{\dot{q}\}$ (I-3)

$$\{\ddot{x}\} = [\phi]\{\ddot{q}\} \tag{I-4}$$

Substituting Eqs. I-2, I-3, and I-4 into Eq. I-1 and premultiplying by $[\phi]^T$, the result is

$$[M_{EQ}]\{\ddot{q}\} + [M_{EQ}\ 2\beta\omega_n]\{\dot{q}\} + [M_{EQ}\ \omega_n^2]\{q\} = \{0\} \tag{I-5}$$

where

$[M_{EQ}] = [\phi^T][M][\phi]$ (Generalized Mass Matrix) or equivalent (Ref. STARDYNE Theoretical Manual, DYNRE1 Analytics)

For solution by the normal mode method, Eq. I-5, the damping must be assumed to be proportional to the mass or to the stiffness. For the first,

$$[C] = 2[\beta][M] \tag{I-6}$$

If so, then

$$[\phi]^T[C][\phi] = 2[\beta][M_{EQ}] \tag{I-7}$$

Note:

(Corollary for one d.o.f., oscillator)

Ref: Thomson, W.T., "Vibration Theory and Applications," Prentice-Hall, 1965, p. 51-55.

$$C_c = 2\ m\ \omega_n \qquad \text{(critical damping coeff.)}$$

$$\rho = \frac{C'}{C_c} \qquad \text{(damping factor),}$$

$$C' = 2\ \rho\ m\ \omega_n \tag{8}$$

From Equation I-7, assume a value of .005 for $\beta_1, \beta_2, \ldots, \beta_n$.
Premultiply both sides of I-7 by $[\phi]^{T\ -1}$. (Inverse at transpose of $[\phi]$).

$$[I]\ [C]\ [\phi] = [[\phi]^{T\ -1}\ 2\ [\beta]\ [M_{EQ}] \tag{9}$$

Post-multiply both sides of Eq. I-9 by $[\phi]^{-1}$.

$$[C] = [[\phi]^T]^{-1}\ [2\ \beta][M_{EQ}]\ [\phi]^{-1} \tag{10}$$

Evaluate numerically.

EQUIV. DAMPING CALCULATION

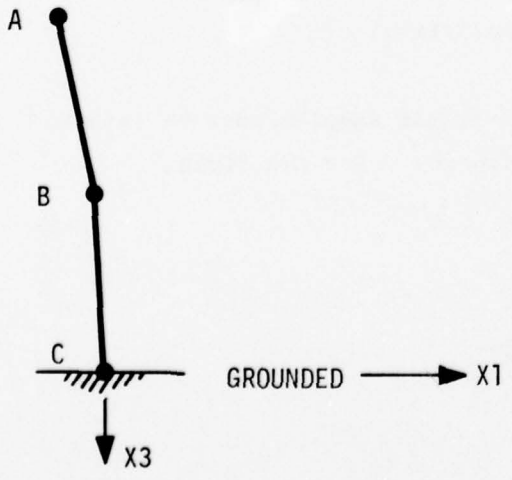

$W_A = 7.5 + .225 = 7.725$ lbs.

$W_B = .45$ lbs.

Mode No., n	M_{EQ_n} lbs.	x_{1_A}	x_{1_B}	f_n, H_z
1	7.7969	1.000	.31352	.00550005
2	.47307	-.01526	1.000	.13555

$$[\phi] = \begin{bmatrix} 1.0000 & -.01526 \\ .31352 & 1.0000 \end{bmatrix}$$ Columns are for a mode (11)

$$[\phi]^T = \begin{bmatrix} 1.0000 & .31352 \\ -.01526 & 1.0000 \end{bmatrix} \quad (12)$$

$$[2\beta] = \begin{bmatrix} .01 & 0 \\ 0 & .01 \end{bmatrix}$$

$$[M_{EQ}] = \begin{bmatrix} 7.7969 & 0 \\ 0 & .47307 \end{bmatrix} \text{ lbs.}$$

$$[2\beta][M_{EQ}] = \begin{bmatrix} .01 & 0 \\ 0 & .01 \end{bmatrix} \begin{bmatrix} 7.7969 & 0 \\ 0 & .47307 \end{bmatrix}$$

$$= \begin{bmatrix} .077969 & 0 \\ 0 & .0047307 \end{bmatrix} \quad (13)$$

$$[[\phi]^T]^{-1} = \begin{bmatrix} 1.000 & .31352 \\ -.01526 & 1.000 \end{bmatrix}^{-1} = \frac{1}{A} \begin{bmatrix} 1.000 & -.31352 \\ +.01526 & 1.000 \end{bmatrix}$$

→ where

$$A = \text{determinant}$$

$$= a_{11}a_{22} - a_{12} \cdot a_{21}$$

$$= (1.0)^2 + (.31352)(.01526)$$

$$= 1.004\ 7843$$

$$[[\phi]^T]^{-1} = \begin{bmatrix} .995238 & -.312027 \\ .0151873 & .995238 \end{bmatrix} \tag{14}$$

and

$$[\phi]^{-1} = \begin{bmatrix} 1.000 & -.01526 \\ .31352 & 1.000 \end{bmatrix}^{-1} = \frac{1}{|A|} \begin{bmatrix} 1.000 & .01526 \\ -.31352 & 1.000 \end{bmatrix}$$

$$|A| = (1.0)^2 + (.01526)(.31352)$$

$$= 1.0047843$$

$$[\phi]^{-1} = \begin{bmatrix} .995238 & .0151873 \\ -.312027 & .995238 \end{bmatrix} \tag{15}$$

Performing numerical multiplication, from Eqs. I-13 and I-14,

$$[[\phi]^T]^{-1}\ [2\ \beta]\ [M_{EQ}] = \begin{bmatrix} .995238 & -.312027 \\ .0151873 & .995238 \end{bmatrix} \begin{bmatrix} .077969 & 0 \\ 0 & .0047307 \end{bmatrix}$$

$$= \begin{bmatrix} .0775977 & -.001476 \\ .0011841 & .00470817 \end{bmatrix}$$

Then post-multiplying by Eq. I-15,

$$\begin{bmatrix} .0775977 & -.001476 \\ .0011841 & .00470817 \end{bmatrix} \begin{bmatrix} .995238 & .0151873 \\ -.312027 & .995238 \end{bmatrix} = [C_M]$$

$$[C_M] = \begin{bmatrix} .07768884 & -.00029057 \\ -.00029057 & .00470374 \end{bmatrix} \times \frac{1}{386.4} \text{ lb-sec/inch}$$

(Divide by 386.4)

For 1 d.o.f. system, $f_n = .0055$ Hz

$\omega_n = 2\pi f_n = .0346$ rad/sec.

Using Eq. I-8

$C' = 2 \beta m_A \omega_n = 2 (.005) (7.725/386.4) (.0346)$

$= 6.917 \times 10^{-6}$ lb-sec^2/in. $\frac{1}{\text{sec}}$

If divided between Node A and Node B

$C_A = C_B = 3.4586 \times 10^{-6}$

Dividing coupled damping matrix by 386.4 (since Stardyne M_{EQ} is expressed in lbs.)

$$[C] = \begin{bmatrix} 2.01058 \times 10^{-4} & -.75199 \times 10^{-6} \\ -.75199 \times 10^{-6} & 1.21732 \times 10^{-5} \end{bmatrix} \text{ lb-sec/in.}$$

Note: if single d.o.f. damping were based on second mode only

$C' = 2 \beta m_B \omega_2$ $\omega_2 = 2\pi (.13555)$

$C' = (.01) \frac{.45}{386.4} 2\pi (.13555)$

$= 9.9187 \times 10^{-6}$ (see below)

For single d.o.f. system

Damping factor = C lb-sec/in

Damping force = $C\dot{x}$

For sine vibration

$\dot{x} = \omega X$ in/sec

Damping force = C ω X lb-sec/in · rad/sec in. = lbs.

$$\therefore \quad C'_{1,1} = 2\beta m_A = 2 \times (.005) \frac{7.725}{386.4} = 1.9992 \times 10^{-4}$$

For large mass.

$$C'_{2,2} = 2\beta m_B = 2 \times .005 \times \frac{.45}{386.4} = 1.1646 \times 10^{-5}$$

CHECK DAMPING MATRIX

Assume constrained vibration mode, at resonance,

tip amplitude = 1.0 sin ω t $\qquad f = .0055$ Hz

$\omega = 2\pi f = .03455$

$x_A = 1.0 \qquad \dot{x}_A = \omega x_A = .03455$

$x_B = .31352 \qquad \dot{x}_B = \omega x_B = .010834$

$\ddot{x}_A = -\omega^2 x_A = -.0011942$ in/sec^2

$\ddot{x}_B = -\omega^2 x_B = -.00037441$ in/sec^2

Inertia forces:

$$\begin{bmatrix} M_A & 0 \\ 0 & M_B \end{bmatrix} \begin{Bmatrix} \ddot{x}_A \\ \ddot{x}_B \end{Bmatrix} = \begin{Bmatrix} -\frac{7.725}{386.4} \times .0011942 \\ -\frac{.45}{386.4} \times .00037441 \end{Bmatrix} = \begin{Bmatrix} -2.3875 \times 10^{-5} \\ -4.3604 \times 10^{-7} \end{Bmatrix} \text{ lbs.}$$

Damping Forces:

$$[C]\begin{Bmatrix}\dot{x}_A\\ \dot{x}_B\end{Bmatrix} = \begin{bmatrix}2.01058 \times 10^{-4} & -.75199 \times 10^{-6}\\ -.75199 \times 10^{-6} & 1.21732 \times 10^{-5}\end{bmatrix}\begin{Bmatrix}.03455\\ .010834\end{Bmatrix} = \begin{Bmatrix}6.9384 \times 10^{-6}\\ 1.059 \times 10^{-7}\end{Bmatrix} \text{ lbs.}$$

For stiffness forces, must invert 2 x 2 influence matrix

$$[E] = \frac{\ell^3}{EI}\begin{bmatrix}\frac{8}{3} & \frac{5}{6}\\ \frac{5}{6} & \frac{1}{3}\end{bmatrix}$$

$$[K] = [E]^{-1}$$

$$= \frac{EI}{\ell^3}\begin{bmatrix}\frac{1}{3} & -\frac{5}{6}\\ -\frac{5}{6} & \frac{8}{3}\end{bmatrix}\frac{1}{\left|\frac{8}{3}\cdot\frac{1}{3} - \frac{5}{6}\cdot\frac{5}{6}\right|}$$

$$= \frac{EI}{\ell^3}\ \frac{36}{7}\begin{bmatrix}\frac{1}{3} & -\frac{5}{6}\\ -\frac{5}{6} & \frac{8}{3}\end{bmatrix}$$

$$[K] = \frac{EI}{7\ell^3}\begin{bmatrix}12 & -30\\ -30 & 96\end{bmatrix}$$

Stiffness forces:

Evaluate numerically:

$$[K] = \frac{EI}{7\ell^3}\begin{bmatrix}12 & -30\\ -30 & 96\end{bmatrix}$$

$\ell = 360$

$EI = 3000$

$$\frac{EI}{7\ell^3} = \frac{3000}{7 \times (360)^3} = 9.18577 \times 10^{-6}$$

$$[K] = \begin{bmatrix}1.10225 \times 10^{-4} & -2.7557 \times 10^{-4}\\ -2.7557 \times 10^{-4} & 8.8183 \times 10^{-4}\end{bmatrix} \text{ lbs/inch}$$

$$[K]\begin{Bmatrix} \times_A \\ \times_B \end{Bmatrix} = [K] \quad \begin{Bmatrix} 1.0 \\ .31352 \end{Bmatrix} = \begin{Bmatrix} 2.38315 \times 10^{-5} \\ 8.9947 \times 10^{-7} \end{Bmatrix}$$

Summary of check at 1st Natural

NODE	INERTIA, lbs.	STIFFNESS, lb.	DAMPING
A	-2.3875×10^{-5}	2.38315×10^{-5}	6.9384×10^{-6}
B	-4.3604×10^{-7}	8.9947×10^{-7}	1.059×10^{-7}

At resonance, inertia + stiffness forces are equal and opposite.

APPENDIX J

APPENDIX J

DETAILS OF SOLAR ARRAY FLEXIBILITY MODELING

SOLAR ARRAY TORSION

The solar array torsional equations of motion are described by a solution of the following system of matrix equations

$$[M]\{\ddot{\theta}\} + [C]\{\theta\} + [K]\{\theta\} = \{T(t)\} \qquad \text{(J-1)}$$

where the vector $\{\theta\}$ is the θ_y rotation of each solar panel and the drive motor.

Applied torques T(t) may be zero at all locations except the drive motor.

The above equations in discrete coordinates are coupled because the stiffness matrix [K] is coupled. The damping matrix [C] may also be coupled. For six solar panels plus the drive motor, the equation has at least seven degrees of freedom. Now make the following transformation:

$$\{\theta\} = [\phi]\{q\} \qquad \text{(J-2)}$$

where the columns of $[\phi]$ are the eigen vectors which result from the STARDYNE solution of the relationship

$$[K]\{\phi\} = \omega^2 [M]\{\phi\}$$

Substituting equation J-2 and its derivatives into Eqn. J-1 and premultiplying by the transpose of $[\phi]$ results in the following set of <u>uncoupled</u> equations in terms of the generalized coordinates {q}:

$$[M_{eq}]\{\ddot{q}\} + [M_{eq}\ 2\rho\omega_n]\{\dot{q}\} + [M_{eq}\ \omega^2_n]\{q\} = [\phi]^T\{T(t)\} \qquad (J-3)$$

Note that by orthogonality relationships, the off-diagonal terms of the teneralized mass, damping and stiffness matrices are zero.

The STARDYNE solution for the NTS-2 model with flexible solar arrays and flexible gravity gradient rods has six rigid body modes and one mechanism type rigid body mode because the solar arrays are considered free-wheeling in θ_y. The "free-wheeling" solar array mode in the STARDYNE modes is included as a linear combination of all seven STARDYNE rigid-body modes.

For simulation purposes, the free-wheeling solar array mode will be replaced by a single equivalent rigid body θ_y mode whose amplitude is normalized to 1.0 and whose generalized mass is thus equal to its total inertia about the solar array θ_y axis.

The elastic modes are taken from the STARDYNE run TSNSTRL. The only significant solar array elastic modes are the symmetric torsional modes at 1.095 H_z and 1.898 H_z.

Thus the total number of generalized coordinates to be solved is three, defined as follows:

$$\{q\} = \begin{Bmatrix} q_1 \\ q_2 \\ q_3 \end{Bmatrix}$$

q_1 = rigid body torsion mode
q_2 = first symm. torsion mode
q_3 = second symm. torsion mode

Generalized Mass

$$[M_{eq}] = [\phi]^T [M] [\phi]$$

The diagonals of the generalized weight matrix are printed by STARDYNE and are claculated for modes normalized to a maximum displacement or rotation of unity. For the above three solution modes:

MODE NO.	EQUIV. WEIGHT M_{eq}, Lbs.	EQUIV. MASS M_{eq}, lb-sec^2/ft	FREQUENCY H_z	ω_n rad/sec	ω_n^2 (rad/sec)^2
1	13956.7	3.01	0	0	0
2	9284.	2.002	1.095	6.880	47.339
3	6971.	1.5034	1.898	11.925	142.2

Premultiplying Eqn. J-3 by $[M_{eq}]^{-1}$, the response equation becomes

$$[I]\{\ddot{q}\} + [2\rho\omega_n]\{\dot{q}\} + [\omega_n^2]\{q\} = \frac{[\phi^T]\{T(t)\}}{[M_{eq}]} \qquad (J\text{-}4)$$

Extracting only the θ_y rotations at the drive motor (node 20), the -Y outer panel center (node 2), and the +Y outer panel center (node 31), these rotations are related to the generalized responses by

$$\begin{Bmatrix} \theta_y \text{ drive motor} \\ \theta_y \text{ -Y tip mass} \\ \theta_y \text{ +Y tip mass} \end{Bmatrix} = \begin{bmatrix} 1.0 & -1.0 & -.5 \\ 1.0 & 1.0 & -.5 \\ 1.0 & 1.0 & -.5 \end{bmatrix} \begin{Bmatrix} q_1 \\ q_2 \\ q_3 \end{Bmatrix} \qquad (J\text{-}5)$$

Equation J-4 in numerical form reduces to (ρ = .005):

$$\begin{bmatrix} 1.0 & & \\ & 1.0 & \\ & & 1.0 \end{bmatrix} \begin{Bmatrix} \ddot{q}_1 \\ \ddot{q}_2 \\ \ddot{q}_3 \end{Bmatrix} + \begin{bmatrix} 0.0 & & \\ & .0688 & \\ & & .11925 \end{bmatrix} \begin{Bmatrix} \dot{q}_1 \\ \dot{q}_2 \\ \dot{q}_3 \end{Bmatrix} + \begin{bmatrix} 0.0 & & \\ & 47.334 & \\ & & 142.2 \end{bmatrix} \begin{Bmatrix} q_1 \\ q_2 \\ q_3 \end{Bmatrix}$$

$$= \begin{bmatrix} .33222 \\ -.4995 \\ -.3326 \end{bmatrix} (T_{\substack{\text{drive} \\ \text{motor}}}(t)) \qquad (J\text{-}6)$$

Equation J-6 can be solved as three uncoupled second order linear differential equations.

TABLE J-1. -Y SOLAR ARRAY, (BENDING ONLY)

STIFFNESS MATRIX

(Units = lbs./ft.) For motion relative to drive motor

$$[K]\{x\} = \begin{bmatrix} .0085617 & -.004860 \\ -.004860 & .630218 \end{bmatrix} \begin{Bmatrix} x_1 \\ z_1 \end{Bmatrix}$$

where

x_1 = motion of center of outer panel, normal to plane of panel

z_1 = motion of center of outer panel, in plane of the panel

MASS MATRIX

(Units = slugs ($lb\text{-}sec^2/ft$)

$$[M]\{\ddot{x}\} = \begin{bmatrix} .42176 & 0 \\ 0 & .52608 \end{bmatrix} \begin{Bmatrix} \ddot{x}_1 \\ \ddot{z}_1 \end{Bmatrix}$$

DAMPING MATRIX

$\rho_R = .005$ (½ of 1 percent crticial damping)

$$[C]\{\dot{x}\} = \left(\frac{\rho}{.005}\right) \begin{bmatrix} .0006009 & 0 \\ 0 & .005758 \end{bmatrix} \begin{Bmatrix} \dot{x}_1 \\ \dot{z}_1 \end{Bmatrix}$$

(Units of [C] are lb-sec/ft.)

TABLE J-2. +Y SOLAR ARRAY, (BENDING ONLY)

STIFFNESS MATRIX

(Units = lbs./ft.) For motion relative to drive motor

$$[K]\{x\} = \begin{bmatrix} .008670 & -.010705 \\ -.010705 & 1.37791 \end{bmatrix} \begin{Bmatrix} x_2 \\ z_2 \end{Bmatrix}$$

MASS MATRIX

(Units = slugs (lb-sec^2/ft))

$$[M]\{\ddot{x}\} = \begin{bmatrix} .42176 & 0 \\ 0 & .52608 \end{bmatrix} \begin{Bmatrix} \ddot{x}_2 \\ \ddot{z}_2 \end{Bmatrix}$$

DAMPING MATRIX

(Units = (lb-sec/ft)

$$[C]\{x\} = \begin{bmatrix} .0006047 & 0 \\ 0 & .008514 \end{bmatrix} \begin{Bmatrix} \dot{x}_2 \\ \dot{z}_2 \end{Bmatrix}$$

TABLE J-3. NTS-2 SOLAR ARRAYS

COMPARISON OF MAXIMUM OUTER PANEL DEFLECTIONS FOR STEP INPUT YAW TORQUE OF .04 FT-LBS FOR 3 SECONDS, RESPONSES ARE NORM. TO PANEL, AT CENTER				
DYNREI RUN NO.	MAX. REL. RESPONSE, NODE 2 INCHES	TIME OF MAX. RESPONSE, SECONDS	MODE NOS. INCLUDED IN SOLUTION	COMMENTS
TSNSTCO	-.009843	1.40	10, 14, 17, 24 (Tape X3350)	Includes 1st and 2nd anti-symmetric array bending modes
TSNSTI1	-.009855	1.40	10, 14, 17 (Tape X3350)	2nd anti-symmetric array mode deleted
TSNSTJ0	-.009916	1.40	10, 14, 17	Simplified bending model

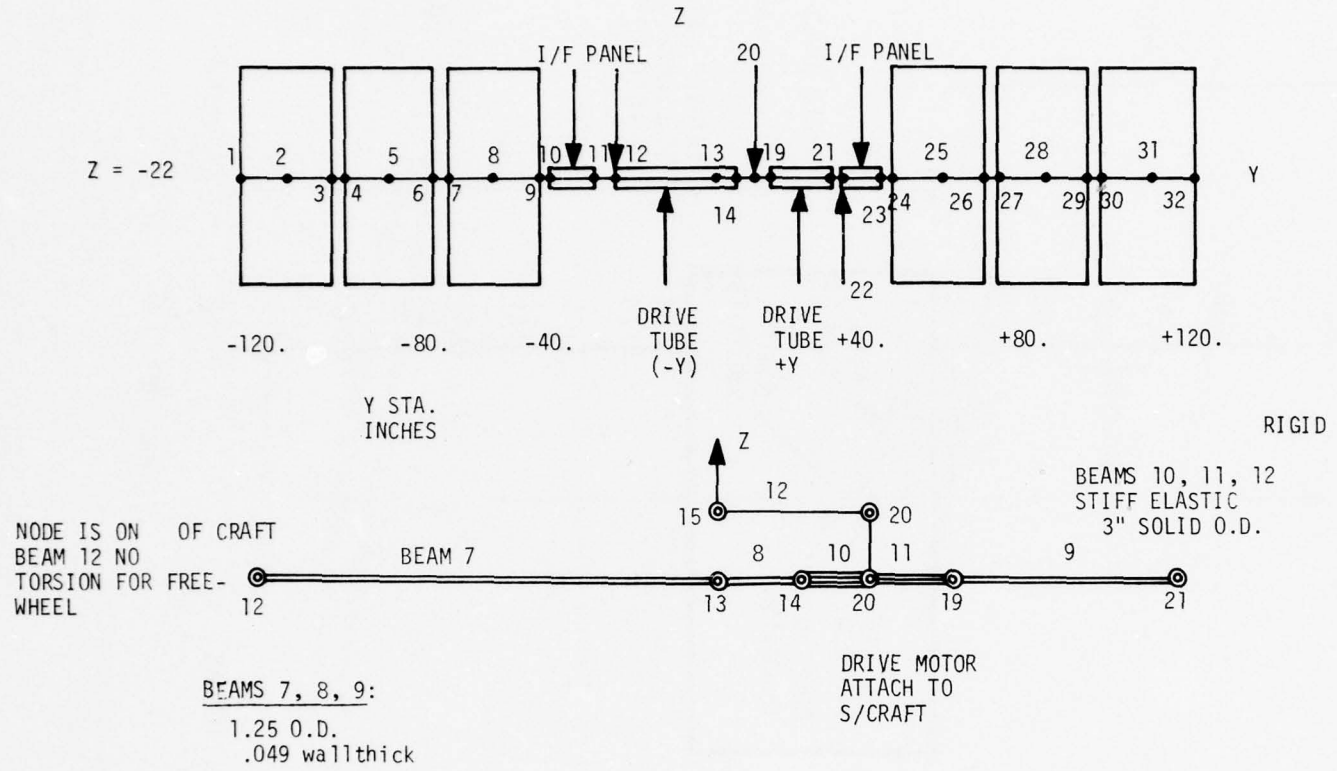

Figure J-1. Stardyne Math Model for Flexible Solar Arrays

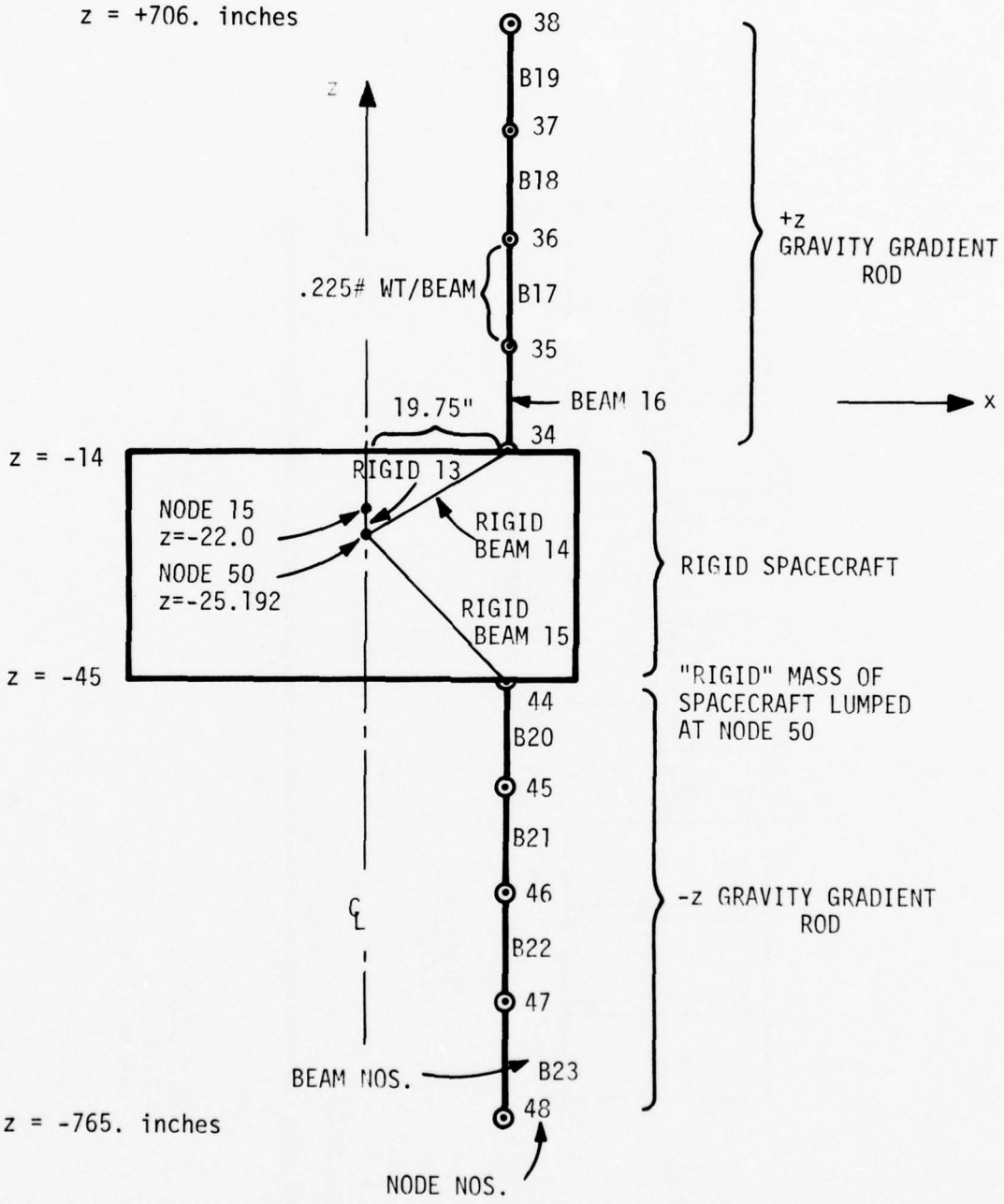

Figure J-2. Gravity Gradient Rod and Spacecraft Definition

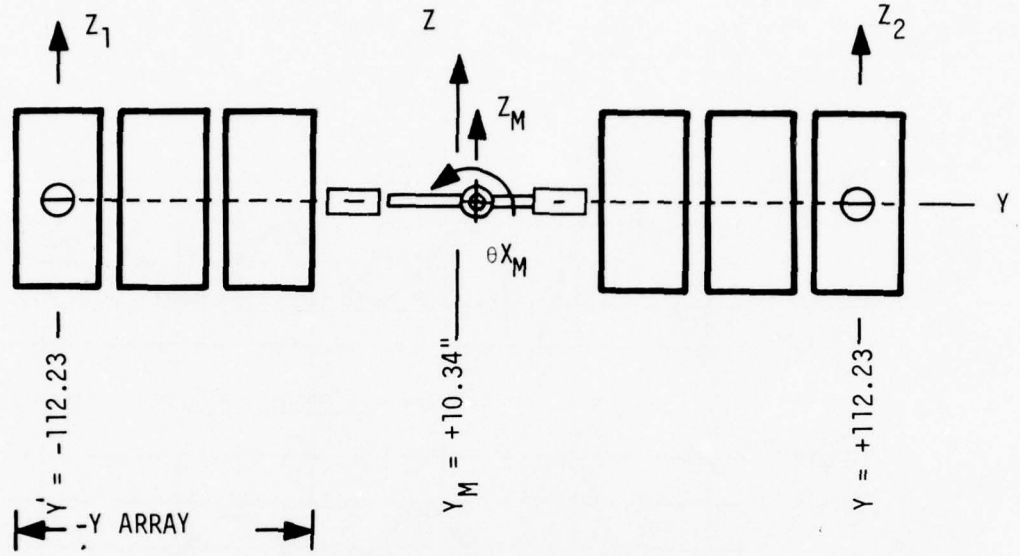

WEIGHTS MATRIX (DIVIDE BY g_c)

$$\frac{1}{g_c}\left[W\right]\{\ddot{X}\} = \left[M\right]\{\ddot{X}\}$$

$$\frac{1}{32.17}\begin{bmatrix} 13.568 & & & & & & & \\ 0 & 16.924 & & & & & & \\ 0 & 0 & 33.784 & & & & & \\ 0 & 0 & 0 & 27.072 & & & & \\ 0 & 0 & 0 & 0 & 272.34 & & & \\ 0 & 0 & 0 & 0 & 0 & 768.24 & & \\ 0 & 0 & 0 & 0 & 0 & 0 & 13.568 & \\ 0 & 0 & 0 & 0 & 0 & 0 & 0 & 16.924 \end{bmatrix} \begin{Bmatrix} \ddot{X}1 \\ \ddot{Z}1 \\ \ddot{X}M \\ \ddot{Z}_M \\ \theta\ddot{X}_M \\ \theta\ddot{Z}_M \\ \ddot{X}2 \\ \ddot{Z}2 \end{Bmatrix}$$

(SYMMETRIC)

Figure J-3. Solar Array Bending Flexure Model

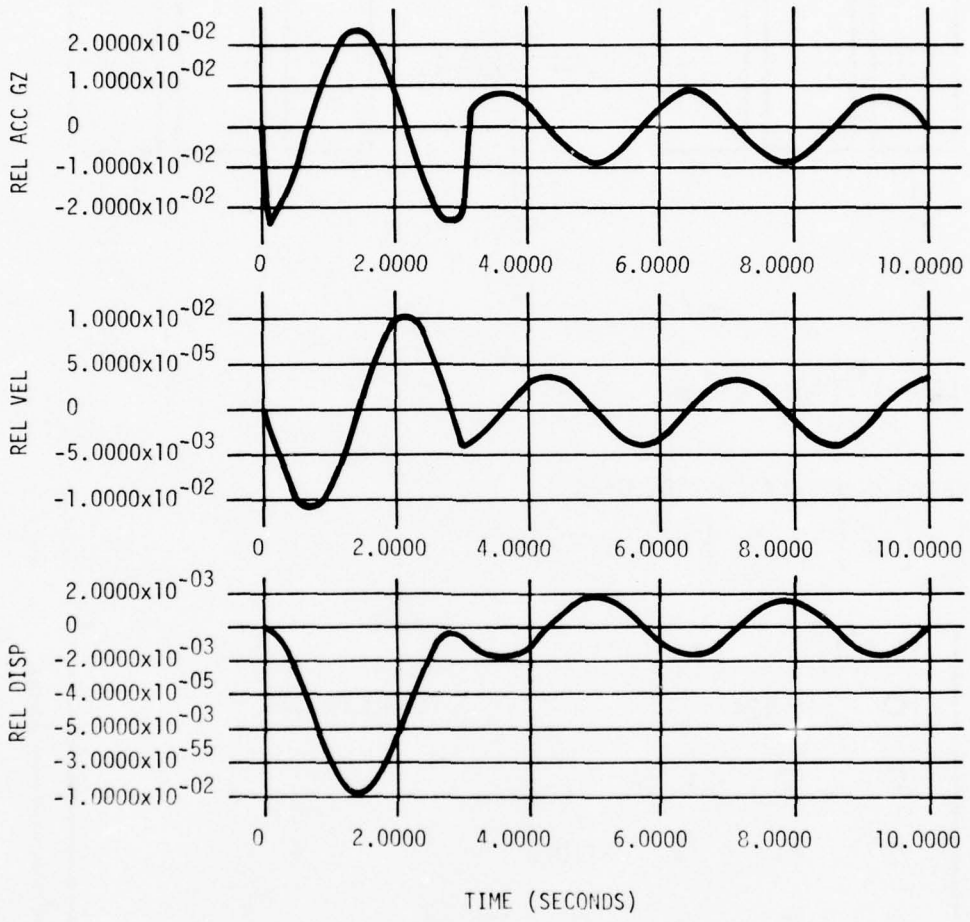

Figure J-4. Dynamic Response of Outer Panel (Node 2) to Step Yaw Torque Input of .04 ft-lbs for 3 seconds

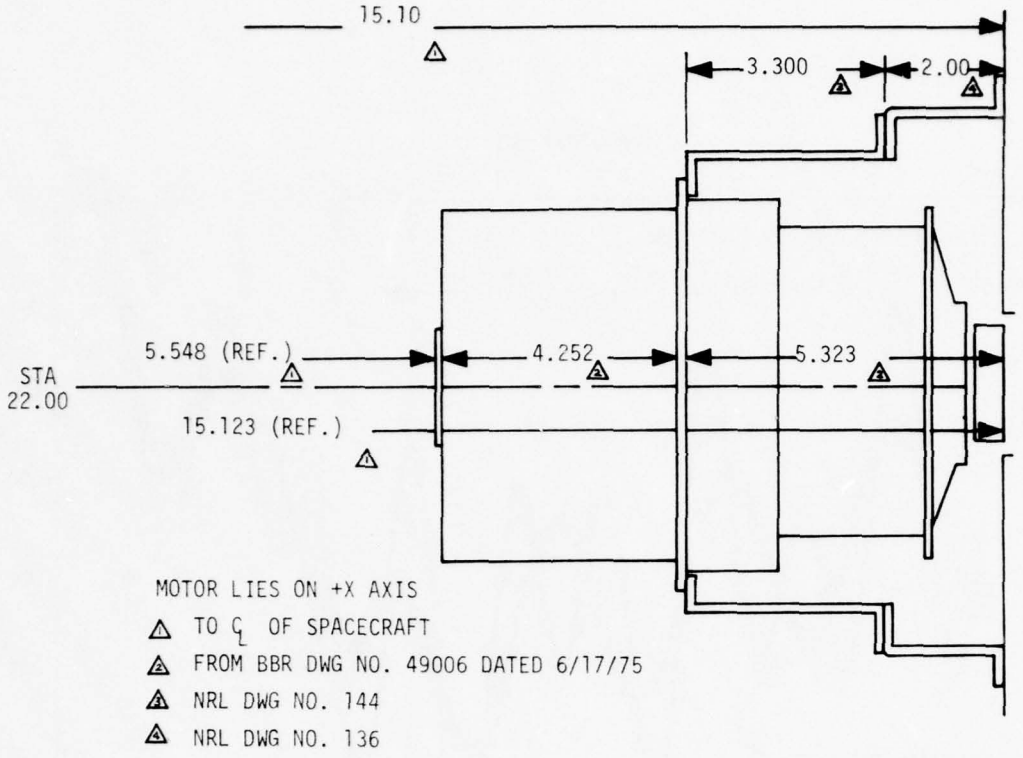

Figure J-5. Solar Array Drive Motor

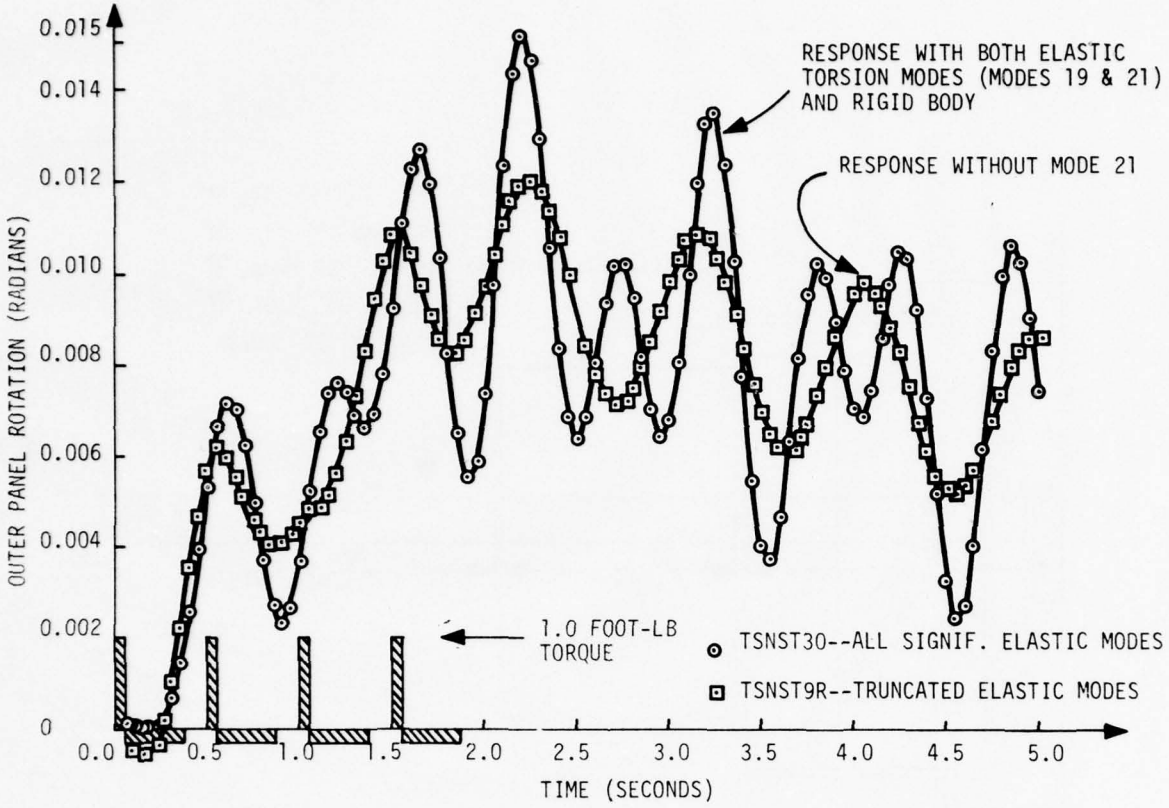

Figure J-6. Stardyne Model Mode 2, θY Response vs. Time

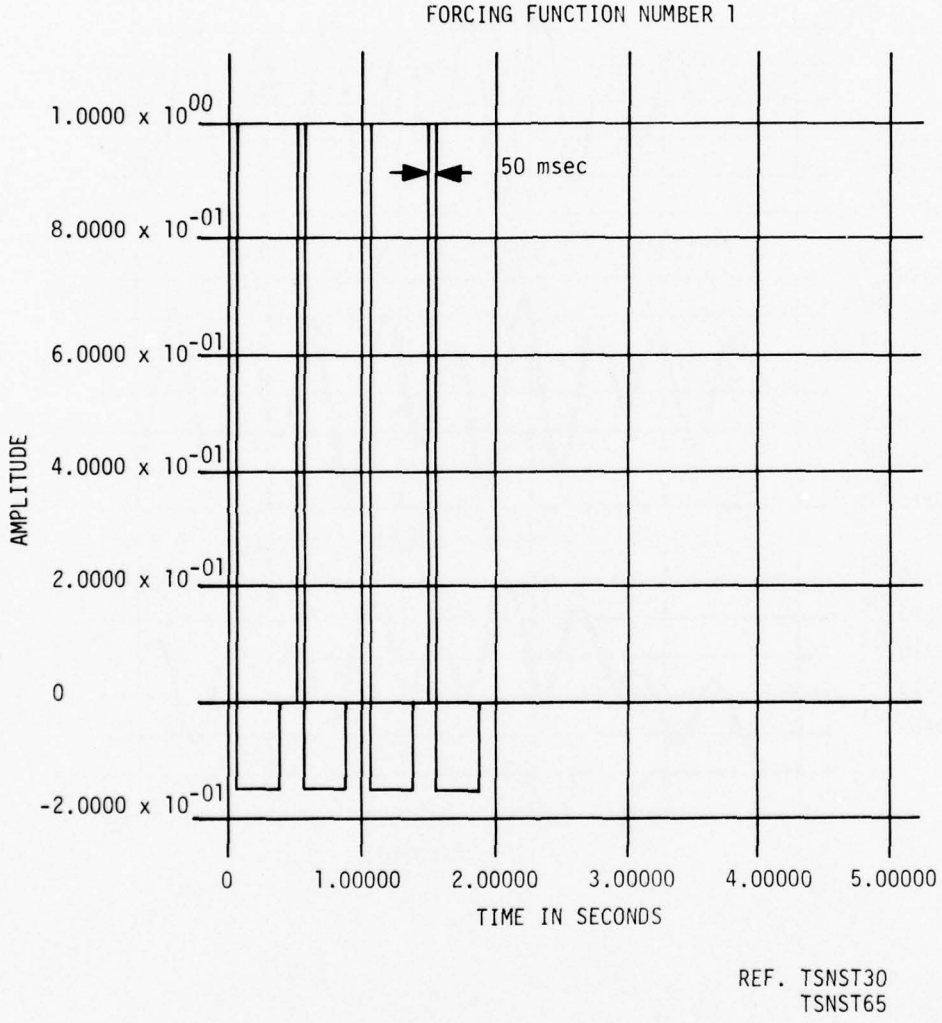

Figure J-7. Solar Array Torsion Model, 4-Pulse, Input Forcing Function (Normalized)

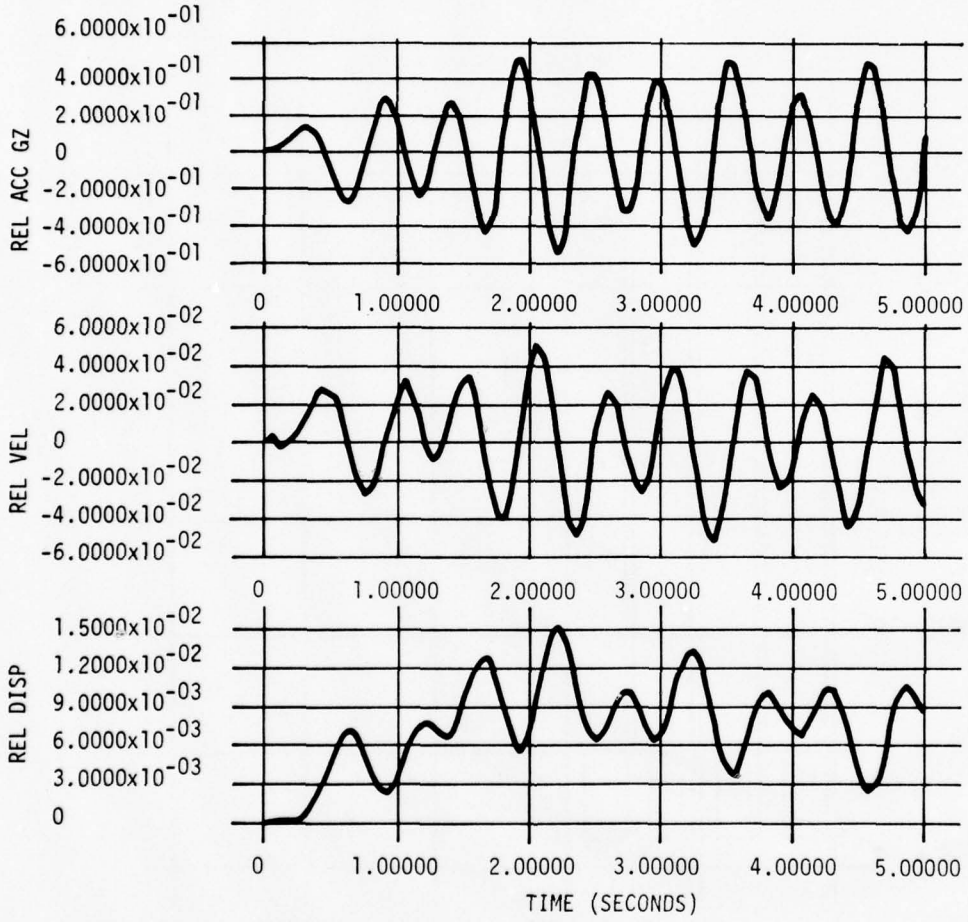

Figure J-8. Solar Array Torsion Model, Node 2 = Outer Panel Disp., Vel., & Accel. Response in Radian Units to Four-Pulse Excitation

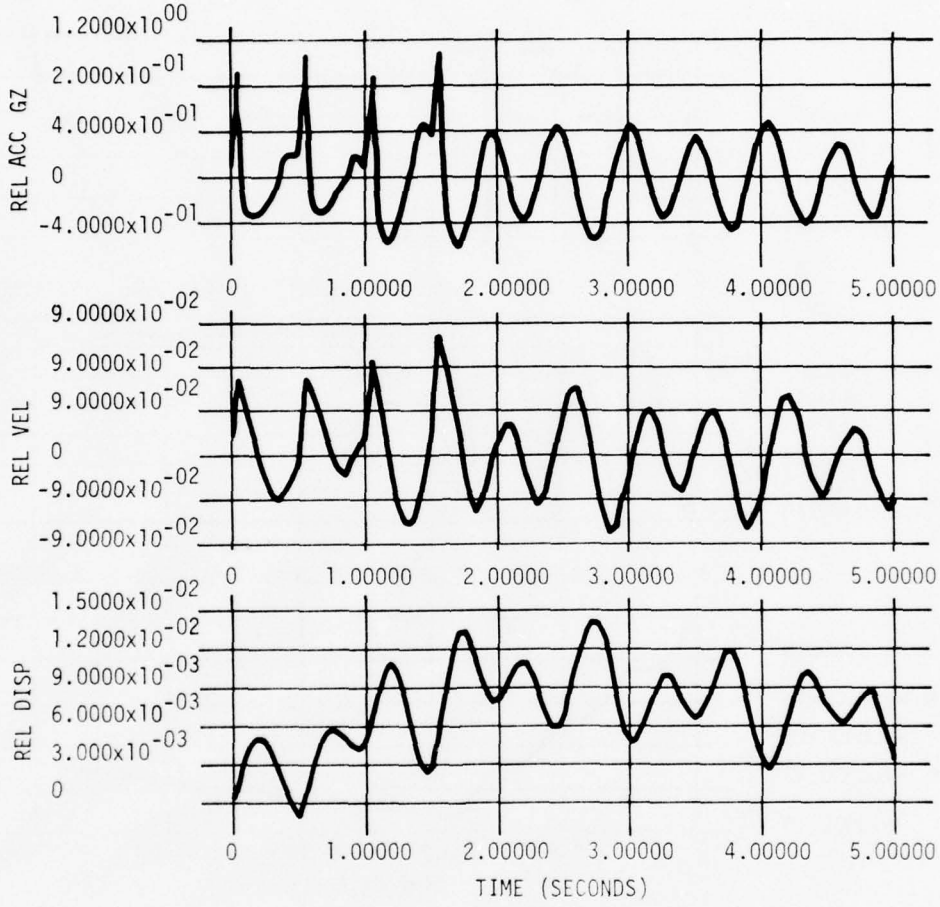

Figure J-9. Solar Array Torsion Model Response at Drive Motor to 4 Pulses Applied to Drive Motor

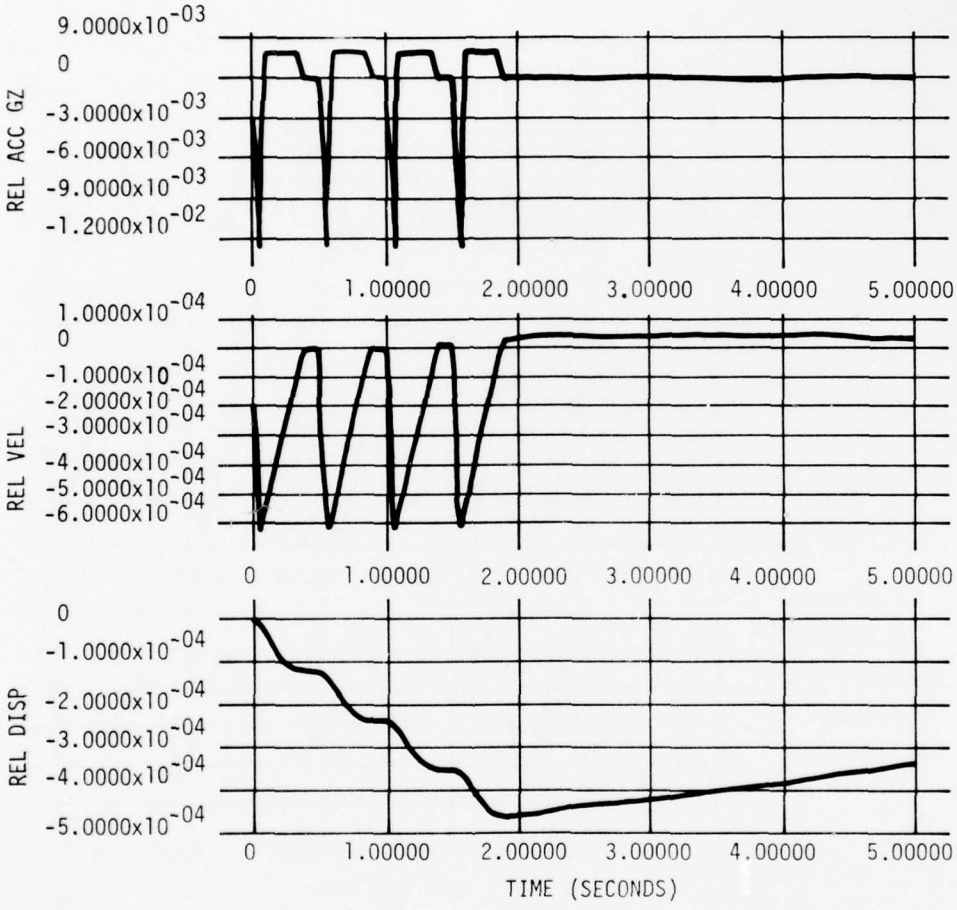

Figure J-10. Solar Array Torsion Model Response of Rigid Spacecraft to 4 Pulses

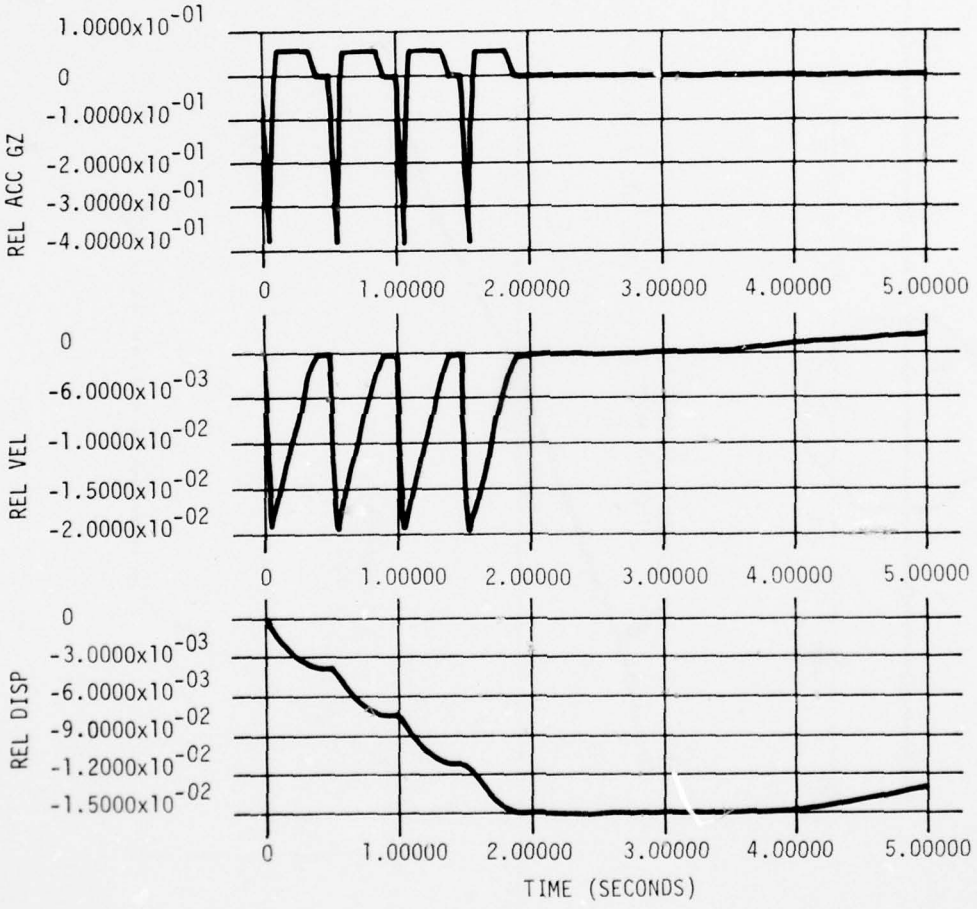

Figure J-11. Response of -Z Gravity Rod Tip Mass (Node 48) X Direction Response (Inch Units) Relative to Spacecraft Attach Point, 4 Pulses on Solar Array Drive Motor

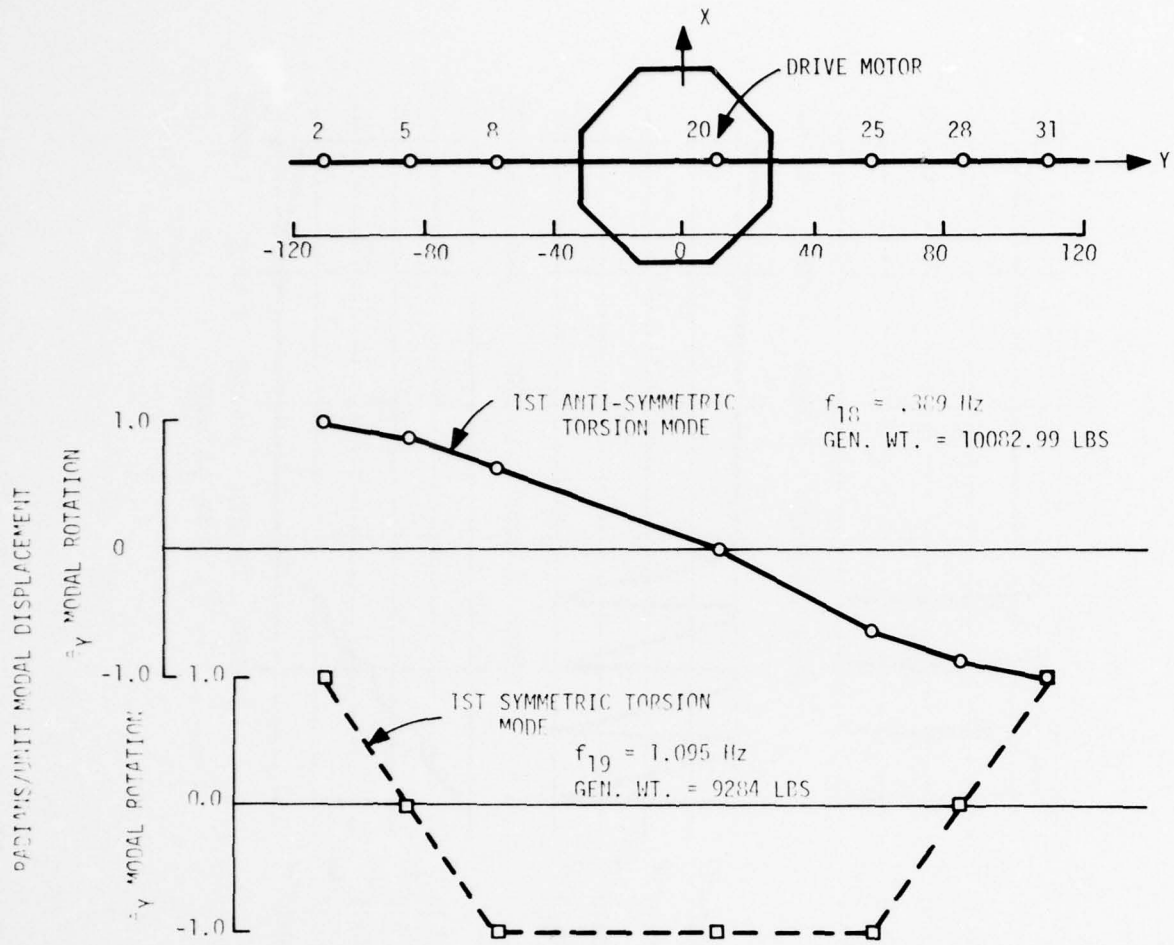

Figure J-12. Mode Plots--Torsion (First Order Modes)

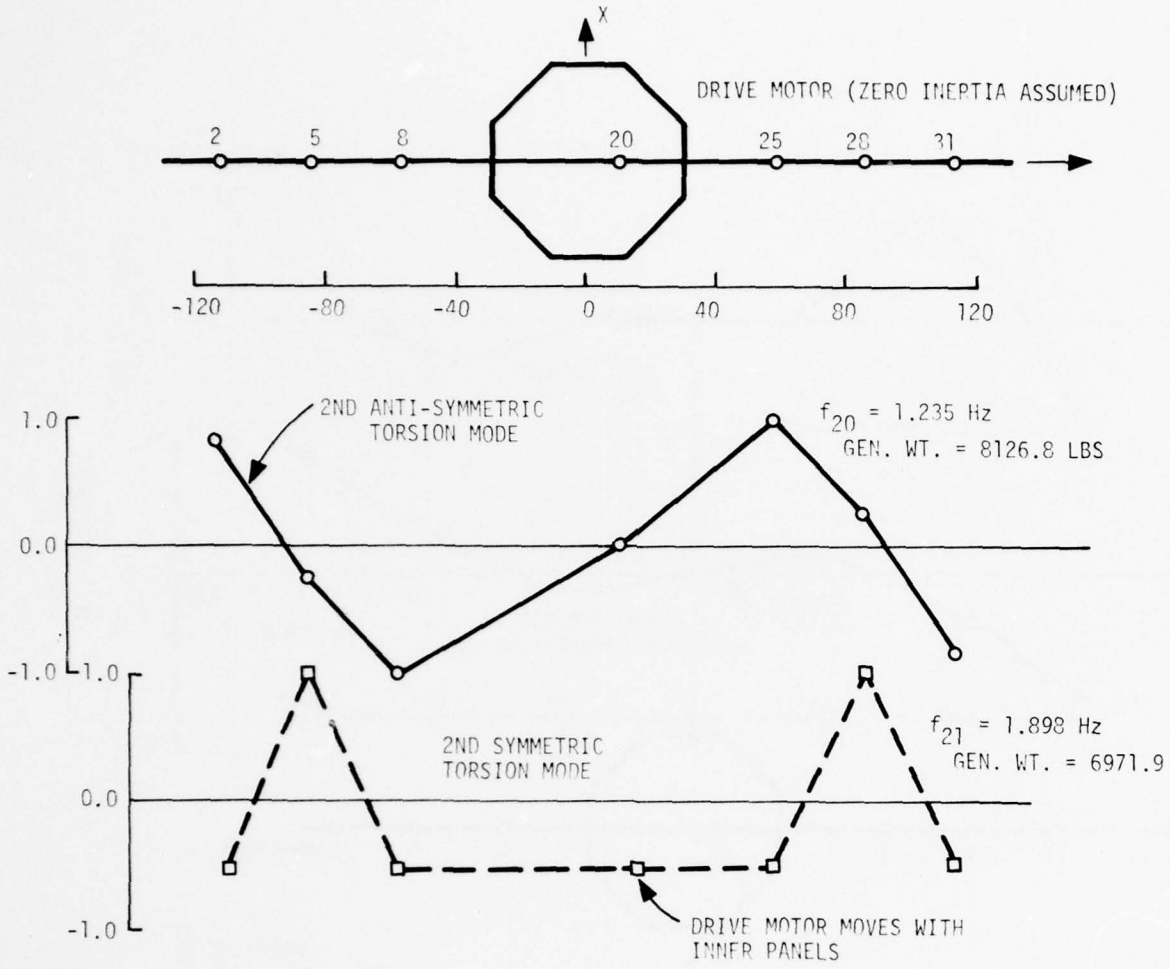

Figure J-13. Mode Plots--Torsion (Second Order Modes)

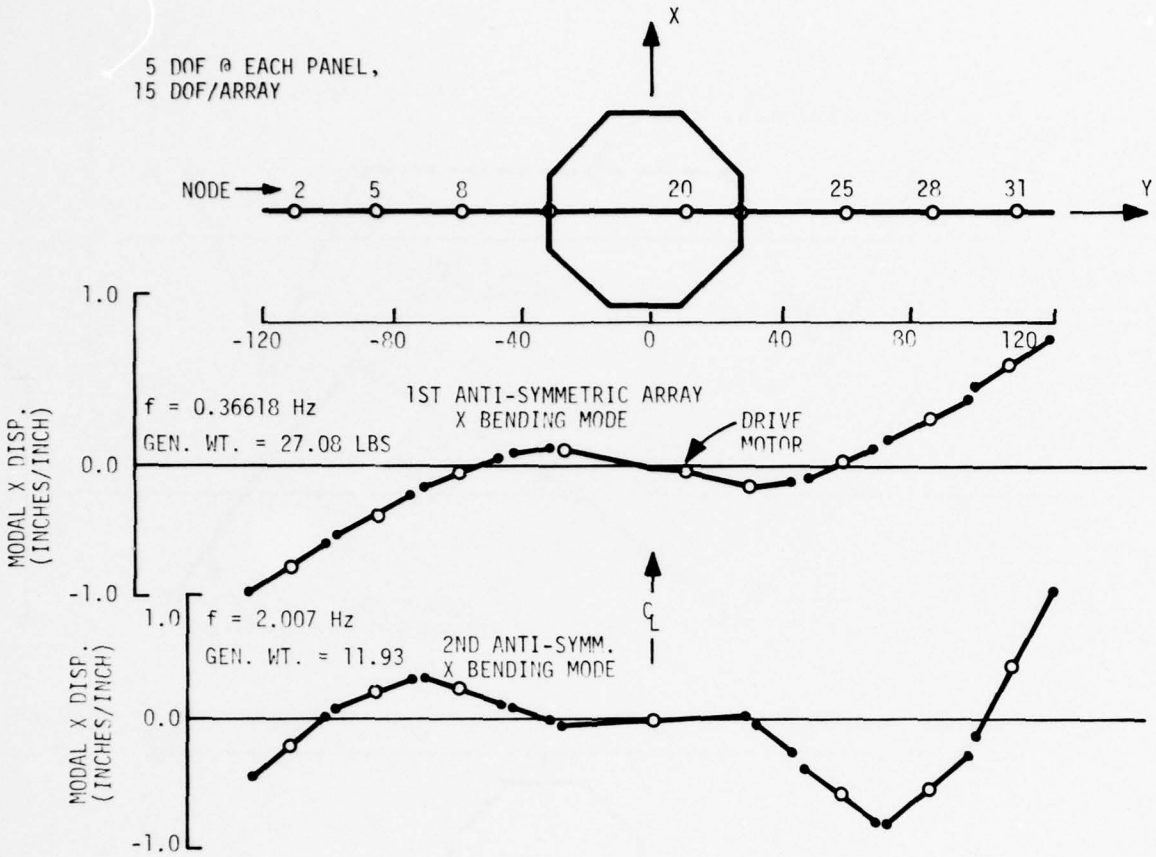

Figure J-14. Mode Plots--Bending

TABLE J-4. STARDYNE MODAL DATA: FLEXIBLE RODS--2 BEAMS/ROD
FLEXIBLE ARRAYS--5 DOF/PANEL (EACH PANEL)

Ref. TSNSTRL MODES ON TAPE X3350

SIGIF. MODES FOR ARRAY/ROD RESPONSES	MODE NO. TOTAL	MODE NO. ELAS.	NAT. FREQ. H_z	GEN'RLZD WEIGHT LBS.	MODAL ROTATIONS OF SPACECRAFT C.G. (NODE 50) RADIANS $\theta_x, \times 10^6$	$\theta_y, \times 10^6$	$\theta_z, \times 10^6$	MODE SHAPE DESCRIPTION UNSYMM.	SYMM.	COMMENTS
	7	0	.00018	283.8	-7.0	74.95	7632.			Rigid Body
	8	1	.00556	15.61	.15	.14	.52		X1	1st Rod Bending
	9	2	.00558	15.72	-.33	.002	-333.2		X2	" " "
Major Rod →	10	3	.01904	50.88	7753.	.20	.78	X2		" " "
Modes →	11	4	.0264	19.97	.18	-7020.	.05	X1		" " "
	12	5	.1389	.87	.002	-.06	-.01		X1	2nd Rod Bending
	13	6	.1389	.87	.089	-.001	10.99		X2	" " "
Minor Rod Modes	14	7	.1406	.89	-172.1	-.001	-.43	X2		" " "
	15	8	.1425	.92	-.005	361.	-.01	X1		" " "
Some Coupling → (Pitch)	16	9	.2795	19.59	.35	-253.9	-33.7		X1	1st Solar Array Bend.
Couples with Yaw	17	10	.366	27.08	-49.55	-2.0	4845.	X1		" " " "
	18	11	.389	10083.	-1.6	-.05	140.8	θ_y pan		Array Torsion -Y Array Opposes +Y Array
Major Array Torsion →	19	12	1.095	9284.	-.021	.30	-.003		θ_y pan	Array Torsion, Outer End 180° Out of Phase With Inner Panels
	20	13	1.235	8126.	.027	.001	2.25	θ_y pan		3rd Array Torsion
	21	14	1.898	6971.	-.11	-3.3	-2.6		θ_y pan	" " "
	22	15	1.930	7511.	-.22	.6	35.0			4th Array Torsion
Minor Array →	23	16	1.978	11.93	.55	88.6	314.5		X1	2nd Array Bending
Bending →	24	17	2.007	11.93	5.04	32.	869.8	X1		" " "
	25	18	2.422	19.47	2320.	-37.8	10.2		X3	1st Array Bend (In-Plane of Array)
Major Array In-Plane Bend. →	26	19	4.279	22.60	-6106.	-16.	-27.8	X3		" "

TABLE J-5. STARDYNE MODAL DATA: FLEXIBLE RODS--2 BEAMS/ROD
FLEXIBLE ARRAYS--4 DOF/ARRAY (EACH ARRAY)

Run TSNST17 on TAPE X3719

SIGIF. MODES FOR ARRAY/ROD RESPONSES	MODE NO. TOTAL	MODE NO. ELAS.	NAT. FREQ. H_z	GEN'RLZD WEIGHT LBS.	MODAL ROTATIONS OF SPACECRAFT C.G. (NODE 50) RADIANS $\theta_x, \times 10^6$	$\theta_y, \times 10^6$	$\theta_z, \times 10^6$	MODE SHAPE DESCRIPTION UNSYMM.	SYMM.	COMMENTS
	7	0	.000257	884.9	7.5	48.	8.9			Rigid Body
	8	1	.00556	15.63	0.0	-.15	.06		X1	1st Rod Bending
	9	2	.00558	15.73	.2	0.0	-365.7		X2	" " "
Major Rod	10	3	.01919	49.55	7727.5	.21	.93	X2		" " "
Modes	11	4	.02638	19.97	.2	-7023.	.03	X1		" " "
	12	5	.1389	.87	0.0	-.07	0.0		X1	2nd Rod Bending
	13	6	.1389	.87	.09	0.0	-12.4		X2	" " "
Minor Rod	14	7	.1407	.89	-175.	-.003	-.48	X2		" " "
Modes	15	8	.1425	.92	-.008	361.5	-.009	X1		" " "
	16	9	.2766	19.45	.365	-202.4	-30.		X1	1st Array Bending
Array Bending Couples w/ Yaw →	17	10	.3528	29.015	-53.7	-1.8	4864.	X1		" " "
	18	11	.4078	10574.	-.88	-.015	59.4	θ_y pan		Array Torsion -Y Array Opposes +Y Array
Major Array Torsion →	19	12	1.088	13917.	-.035	.14	-.014		θ_y pan	◄► Outer Ends 180° Out Of Phase W/Inner Panels
	20	13	1.190	10577.	-.09	0.0	.65	θ_y pan		3rd Array Torsion
	21	14	2.381	19.55	2202.6	31.97	11.03		X3	1st Array Bend (In-Plane of Array)
	22	15	4.077	25.36	-6241.	-15.5	-31.3	X3		" " "

SOLAR ARRAY DRIVE TORQUE PULSE

Drive torque vs. time is as follows:

Torque pulses repeat at 2/second.

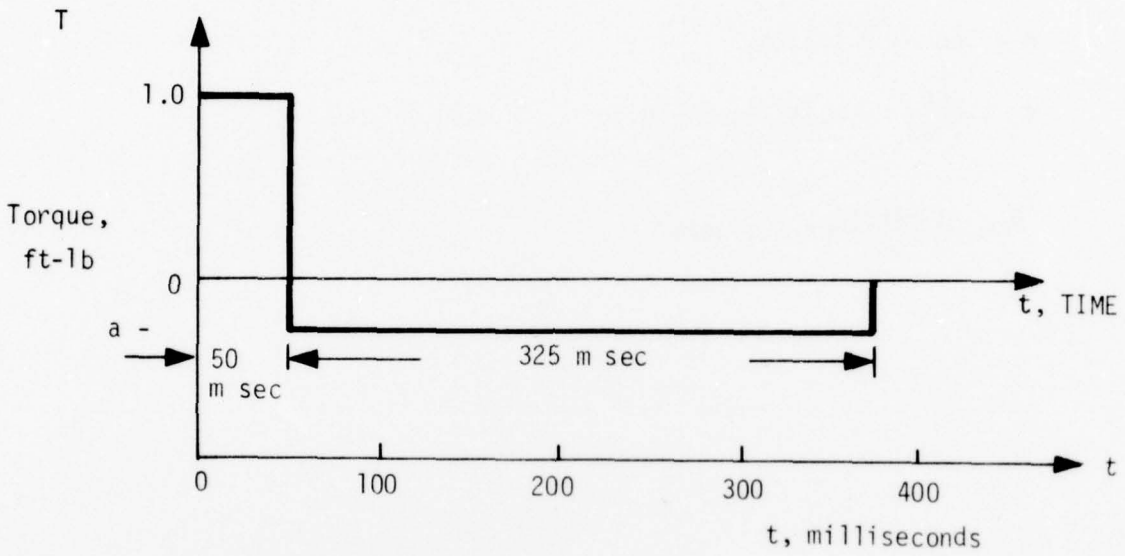

Figure J-15. Drive versus Torque

a is defined as level of stopping torque required to kill any rate built up during positive part of torque cycle.

$$\ddot{\theta} = \frac{T}{I} \qquad \text{for unit I}$$

$$\dot{\theta} = \ddot{\theta}t$$

after .050 sec.

$$\dot{\theta} = \frac{12.0 \text{ in-lb}}{1.0} \times .050 = .60 \text{ rad/sec}$$

To kill of .60 rad/sec in 325 msec.

$$\ddot{\theta} = \frac{T_B}{I}$$

$$\dot{\theta} = \dot{\theta}_o - \ddot{\theta}.t$$

$$0 = .60 - \frac{T_B}{I}\ (0.325)$$

$$T_B = \frac{.60}{.325} = 1.846154 \text{ in-lb.}$$

$$\frac{T_B}{T} = \frac{-1.846154}{12} = -.1538462$$

NTS-2 SOLAR ARRAY STRUCTURAL ANALYSIS

- A linear Open Loop model of total NTS-2 spacecraft was run on STARDYNE.
  - All sub-structure stiffnesses combined.
  - Combined with previous defined beam models (2 beams/rod) of gravity gradient rods.
- Above model was reduced to varying degrees of complexity by selecting fewer lumped mass points on solar arrays.

RESULTS

- Solar array flexible torsion model should have 4 D.O.F. + drive motor θY.
- Solar array flex. bending model can have
  2 DOF per array with good results,
  4 DOF per array with better results.
- Open-Loop transient response runs to be made to guide decision on bending model.

NTS-2 SOLAR ARRAY STRUCTURAL ANALYSIS

FOR EACH ARRAY, CONSIDERED

- o 3 Solar Panels (identical)
- o 1 Interface Panel
- o 4 Hinges (Assumed identical)
- o Drive Tube (L = 35.53 in., -Y Array)
  (L = 14.87 in., +Y Array)

Each identical structure was modeled in detail by finite element analysis (STARDYNE), and reduced to a sub-structure stiffness matrix element.

Substructures for -Y array checked out for comparison with NRL vibration test

- o When gravity field stiffness included, natural frequency in X and θY agreed well.
- o Model is somewhat stiffer in bending in Z direction (plane of panel) due to lack of defn. of brkt. at end of drive tube.

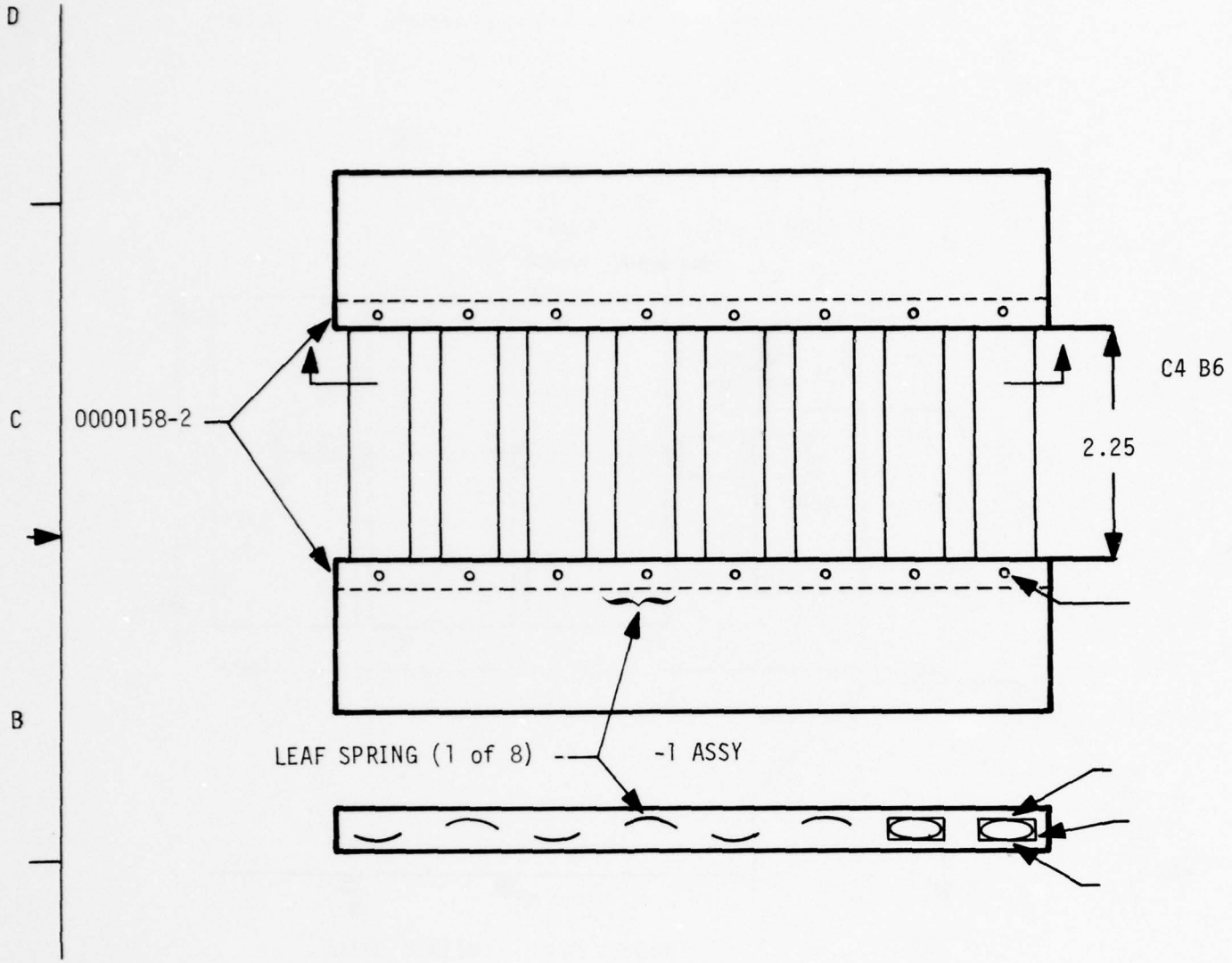

Figure J-16. Hinge Assembly

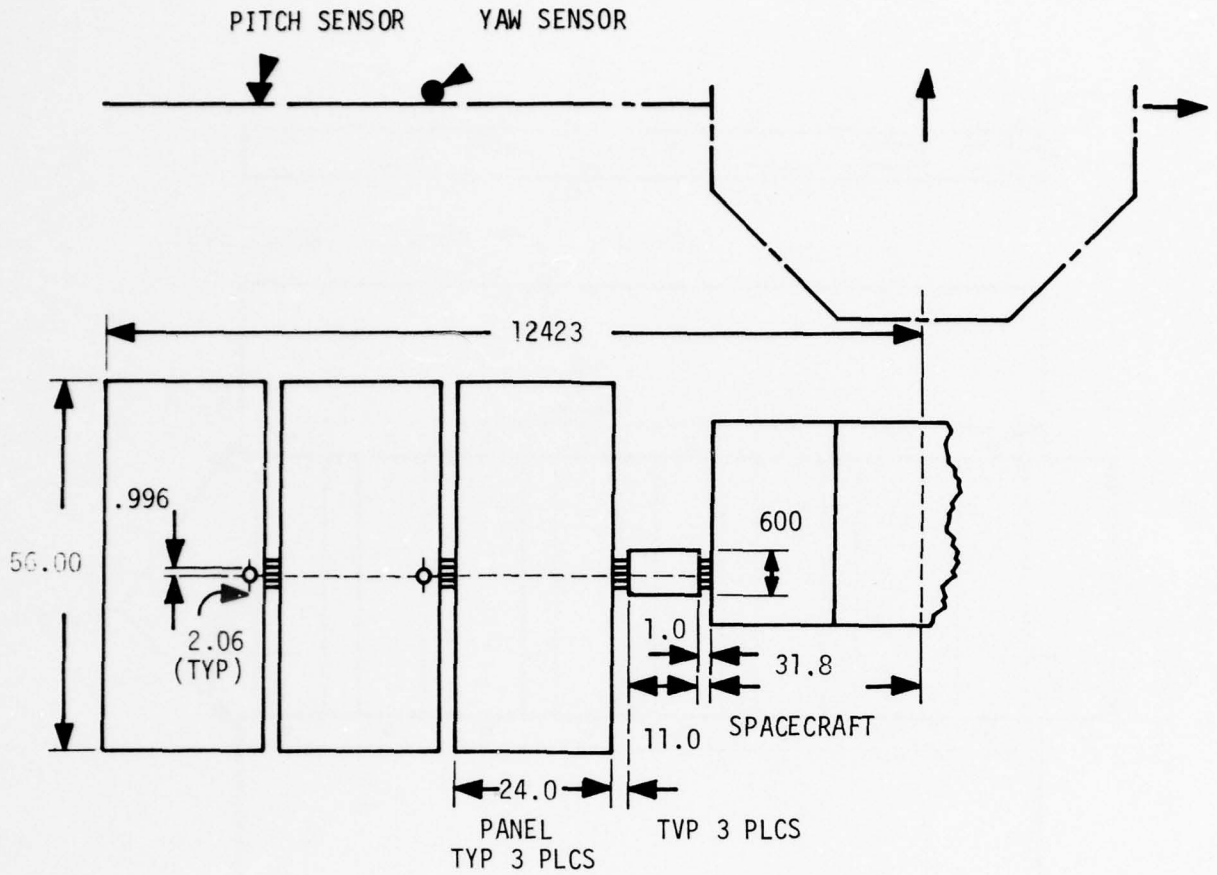

Figure J-17. Deployed Solar Array Configuration (NTS-2)

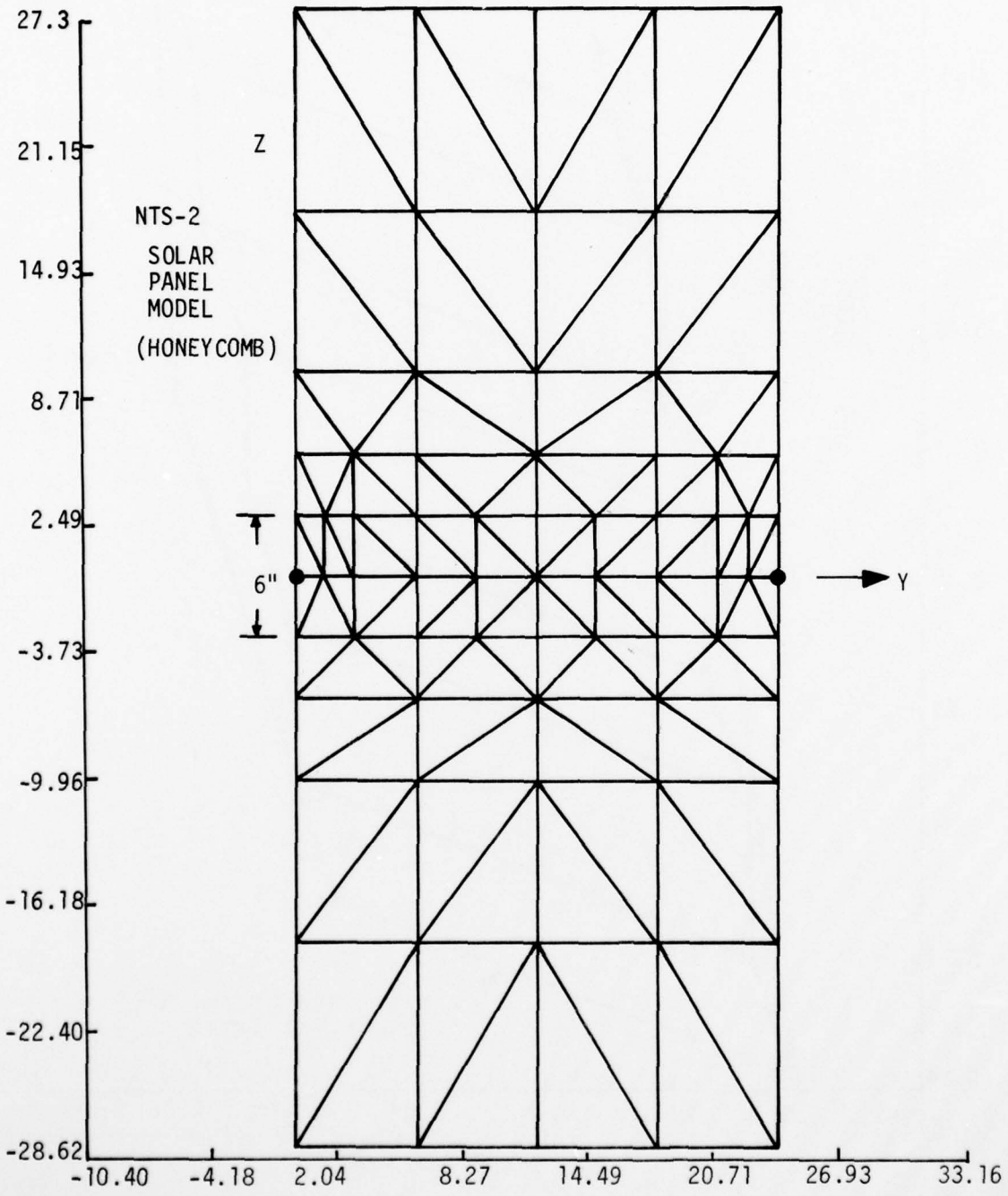

Figure J-18. NTS-2 Solar Panel Model

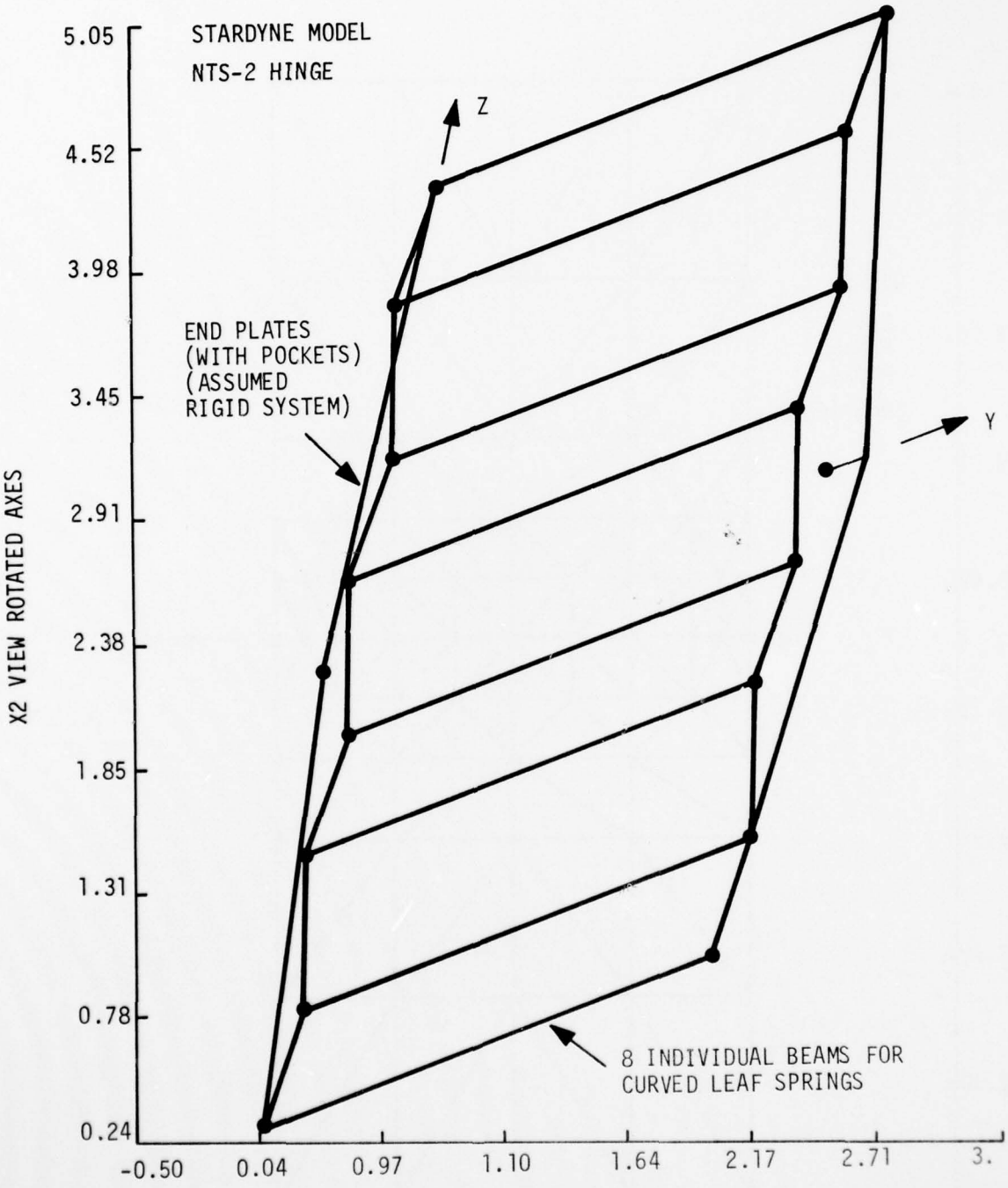

Figure J-19. Stardyne Model NTS-2 Hinge

AD-A052 634 HONEYWELL INC MINNEAPOLIS MINN SYSTEMS AND RESEARCH --ETC F/G 22/2
NTS-2 INDEPENDENT STABILITY AND CONTROL ANALYSIS. VOLUME II. AP--ETC(U)
MAR 77 R E POPE, M D WARD, S M SCHWANTES

UNCLASSIFIED 77SRC17-VOL-2 NL

3 OF 3
AD
A052634

END
DATE
FILMED
5 -78
DDC

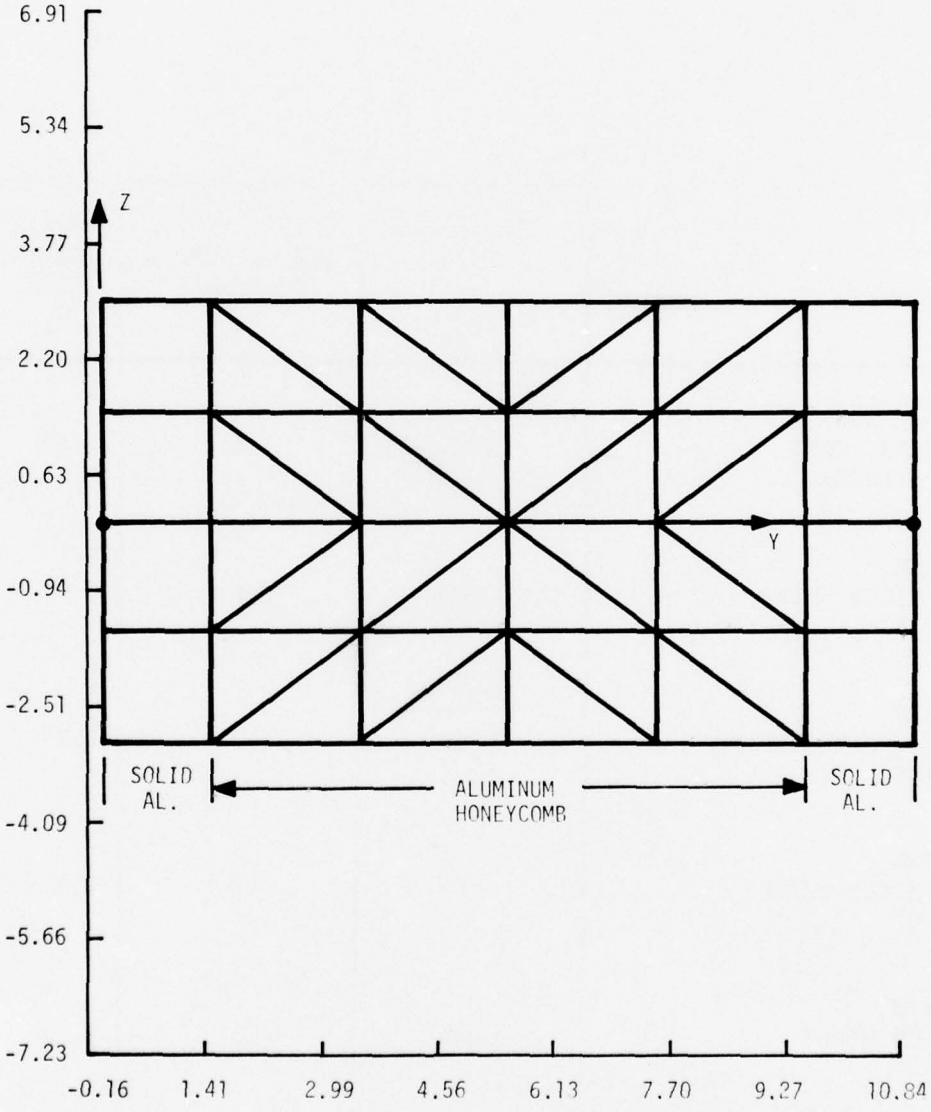

Figure J-20. NTS-2 Solar Array Interface Panel Model

TABLE J-6. SUMMARY OF SOLAR ARRAY CANTILEVER VIBRATION TEST RESULTS @ NRL VS. STARDYNE MODEL (GRAVITY VECTOR ALONG Y AXIS)

	1ST TORSION FREQ. θ_y H_z	1ST X BENDING FREQ., NORMAL TO PANELS H_z	1ST Z BENDING FREQ. H_z
INFORMAL NRL TEST DATA, (REF. LARRY TURNER)	.40	.44	.68
STARDYNE, ORIG. HINGE STIFF. I G FIELD	.408	.48	2.07
STARDYNE, MODIFIED HINGE STIFF. I G FIELD	.384	.47	2.05
STARDYNE, ORIG. HINGE STIFF "ZERO G"	.408	.28	2.04
STARDYNE, MODIFIED HINGE "ZERO G"	.384	.26	2.03

TABLE J-7. STARDYNE MODELS, TOTAL NTS-2 SPACECRAFT
EFFECTS OF COMPLEXITY OF SOLAR ARRAY
MODEL MAJOR MODES COMPARISON

MODEL DESCRIPTION (ARRAYS)	MAJOR ROD MODE, PITCH		1ST ARRAY BENDING MODE, YAW		MAJOR ARRAY TORSION MODE		1ST ARRAY ROLL (Z)
	FREQ. H_z	GENR'LZD WT., LBS	FREQ. H_z	GENR'LZD WT., LBS	FREQ. H_z	GENR'LZD WT., LBS	FREQ. H_z
6 DOF/PANEL	.0263	19.56	.366	27.08	1.095	9284.	2.422
5 DOF/PANEL	.0264	19.97	.366	27.08	1.095	9284.	2.422
6 DOF/ ARRAY (3 each @ Inner Outer)	.0264	19.96	.3499	30.59	1.095	9284.	2.427
4 DOF/ARRAY (2 Torsion) (2 Bending)	.0264	19.97	.3528	29.02	1.088	13917.	2.381

TABLE J-8. STARDYNE MODELS, TOTAL NTS-2 SPACECRAFT
EFFECTS OF COMPLEXITY OF SOLAR ARRAY
MODEL SECOND ORDER MODES COMPARISON

	SECOND ROD PITCH MODE		SECOND ARRAY BENDING MODE, YAW		SECOND/3RD ARRAY TORSION MODE		2ND ARRAY ROLL MODE
	FREQ. H_z	GENR'LZD WT., LBS	FREQ. H_z	GENR'LZD WT., LBS	FREQ. H_z	GENR'LZD WT., LBS	FREQ. H_z
6 DOF/PANEL	.1485	.872	1.979	11.95	1.235 1.898	8127. 6971.	4.286
5 DOF/PANEL	.1425	.92	1.978	11.93	1.235 1.898	8126. 6971	4.279
6 DOF/ARRAY 3 each @ Inner Outer	.1425	.92	2.224	11.92	1.235 (——)	6432. (——)	4.235
4 DOF/ARRAY (2 Torsion) (3 Bending)	.1425	.92	(——)	(——)	1.190 (——)	10577. (——)	4.077

TABLE J-9. STARDYNE MODAL DATA: FLEXIBLE RODS--4 BEAMS/ROD
FLEXIBLE ARRAYS--6 DOF/PANEL

Run TSNSTQE

SIGIF. MODES FOR SOLAR ARRAY RESPONSES	MODE NO. TOTAL	DIAS.	NAT. FREQ. H_z	GEN'RLZD WEIGHT LBS.	MODAL ROTATIONS OF SPACECRAFT C.G. (NODE 50) RADIANS θ_x	θ_y	θ_z	MODE SHAPE DESCRIPTION UNSYMM.	SYMM.	COMMENTS
	7	0	.00215	13.83	-.00103	.00011	-.00042	X2		Partial Rigid Body
	8	1	.00516	10.20	.00037	.00002	-.00013		X2	1st Rod Bending
	9	2	.00671	16.21	.00089	$.1x10^{-6}$	$.3x10^{-6}$		X1	" " "
Major Rod	10	3	.01866	52.13	.00762	$5.x10^{-6}$	$-14.x10^{-6}$	X2		" " "
Mode →	11	4	.02635	19.56	$.12x10^{-6}$	-.006926	$.5x10^{-7}$	X1		" " "
	12	5	.1449	.828	$-.55x10^{-6}$	$-.7x10^{-7}$	$-.87x10^{-7}$		X1	2nd Rod Bending
	13	6	.1449	.824	$1.x10^{-6}$	$.8x10^{-8}$	-.000011		X2	" " "
	14	7	.1466	.844	-.000166	$.11x10^{-6}$	$-.5x10^{-6}$	X2		" " "
Minor Rod Mode →	15	8	.1485	.872	$.2x10^{-8}$	.000349	$.15x10^{-7}$	X1		" " "
	16	9	.2795	19.59	$.35x10^{-6}$	-.00025	-.000034		X1	1st Array Bending
Arrays Excited by θ_z Torque →	17	10	.3662	27.08	-.00005	-.000002	.00484	X1		" " "
Not Sig., -Y Array Opposes +Y Array	18	11	.3891	10083.	$-.6x10^{-6}$	$2.x10^{-6}$	.00014	θ_y		Array Torsion Unsymm.
	19	12	.4592	.83	$.1x10^{-8}$	$4.8x10^{-6}$	$.87x10^{-7}$		X1	3rd Rod Bending
	20	13	.4593	.71	$-7.1x10^{-6}$	$-.5x10^{-7}$	.000021		X2	" " "
	21	14	.4598	.71	+.000049	$.9x10^{-7}$	$2.8x10^{-6}$	X2		" " "
3rd Order Rod Mode	22	15	.4605	.83	$-.5x10^{-8}$	-.000113	$-.25x10^{-7}$	X1		" " "
	23	16	.8558	.93	$-.4x10^{-8}$	$-.11x10^{-6}$	$-.14x10^{-7}$		X1	4th Rod Bending

(Continued On Next Page)

TABLE J-9. STARDYNE MODAL DATA (concluded)

SIGIF. MODES FOR SOLAR ARRAY RESPONSES	MODE NO. TOTAL	MODE NO. ELAS.	NAT. FREQ. H_z	GEN'RLZD WEIGHT LBS.	MODAL ROTATIONS OF SPACECRAFT C.G. (NODE 50) RADIANS θ_x	θ_y	θ_z	MODE SHAPE DESCRIPTION UNSYMM.	SYMM.	COMMENTS
	24	17	.8559	.9232	$.21\times10^{-6}$	$.1\times10^{-8}$	-8.54×10^{-6}		X2	4th Rod Bending
	25	18	.8561	.9229	-.000024	$-.3\times10^{-8}$	$-.17\times10^{-6}$	X2		" " "
	26	19	.8564	.9328	$.13\times10^{-7}$	+.000055	$-.1\times10^{-8}$	X1		" " "
High Array Response → No Rod Response	27	20	1.0954	9284.	$-.7\times10^{-7}$	$.57\times10^{-6}$	$-.1\times10^{-7}$		θ_y	Array Torsion 1st Symm.
	28	21	1.235	8126.8	$-.1\times10^{-6}$	$.53\times10^{-6}$	-.000002	θ_y		Array Torsion 2nd Unsymm.
→	29	22	1.898	6971.	$-.11\times10^{-6}$	$-.33\times10^{-6}$	-.0000027		θ_y	2nd Array Symm.
	30	23	1.930	7510.	$-.22\times10^{-6}$	$.47\times10^{-6}$	.000032	θ_y		3rd Array Torsion
	31	24	1.979	11.95	$.477\times10^{-6}$	.000089	.000315		X1	2nd Array Bending
Minor Array Bending →	32	25	2.007	11.95	$.499\times10^{-5}$	.000032	-.000872	X1		" " "
Couples Array Z To θ_x	33	26	2.422	19.54	.00233	-.000037	.00001		X3	1st Array Z Bending, In Plane of Panels
	34	27	4.286	22.64	-.00614	-.000015	-.000028	X3		1st Array Z Unsymm.

TABLE J-10. STARDYNE MODAL DATA: FLEXIBLE RODS--2 BEAMS/ROD
FLEXIBLE ARRAYS--3 DOF AT INNER, OUTER PANELS

Run TSNSTFZ, Tape X 4556

SIGIF. MODES FOR ARRAY/ROD RESPONSES	MODE NO. TOTAL	MODE NO. ELAS.	NAT. FREQ. H_z	GEN'RLZD WEIGHT LBS.	MODAL ROTATIONS OF SPACECRAFT C.G. (NODE 50) RADIANS $\theta_x, x10^6$	$\theta_y, x10^6$	$\theta_z, x10^6$	MODE SHAPE DESCRIPTION UNSYMM.	SYMM.	COMMENTS
	7	0	.00025	910.	16.5	48.4	-1624.			Rigid Body
	8	1	.00556	15.61	0.0	-.15	-.51		X1	1st Rod Bending
Minor Rod →	9	2	.00558	15.72	.131	0.0	-322.9		X2	" " "
Major Rod	10	3	.01889	52.19	7779.	.19	.86	X2		" " "
Modes	11	4	.02637	19.96	.17	-7020.	.05	X1		" " "
	12	5	.1389	.87	.002	-.07	-.01		X1	2nd Rod Bending
	13	6	.1389	.87	.09	-.001	-10.7		X2	" " "
Minor Rod	14	7	.1406	.89	-169.	-.001	-.43	X2		" " "
Modes	15	8	.1425	.92	-.005	361.	-.01	X1		" " "
	16	9	.2670	21.26	.31	-256.	-32.2		X1	1st Array Bending
Array Couples w/Yaw (Bending →	17	10	.3499	30.59	-49.2	-1.9	5095.	X1		" " "
	18	11	.4777	6430.	-.38	-.003	20.9	θ_y pan		Array Torsion (-Y Against +Y Array)
Major Array → Torsion	19	12	1.095	9284.	-.021	.32	.009		θ_y pan	Array Torsion Outer ends 180° out of Phase w/inner panels
	20	13	1.2525	6432.	.038	.001	1.71	θ_y pan		3rd Array Torsion
Minor Array	21	14	2.2244	11.92	7.3	-109.8	-464.4		X1	2nd Array X Bending
Bending	22	15	2.2773	11.69	-7.6	-49.6	1021.4	X1		" " " "
	23	16	2.4272	19.01	2273.	-36.8	9.99		X3	1st Array X3 Bending (In-Plane of Array)
Major Array In-Plane Bending →	24	17	4.2345	21.57	-5701	-16.4	-29.	X3		" " " "

θY3 ROTATION, INNER PANEL, +Y

θY4 ROTATION, OUTER PANEL, +Y

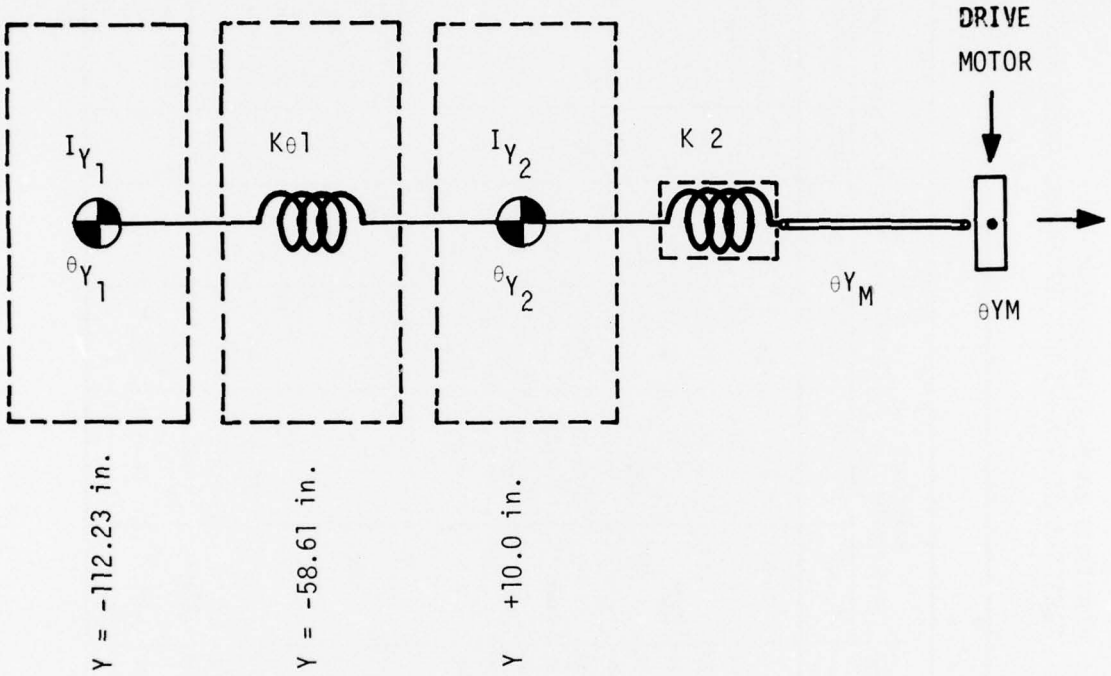

$C \times [K]\{\theta\} = C \times K$ in FT-LB/RADIAN)

where $C = 1/12$

$$\frac{1}{12}\begin{bmatrix} 211.065 & & & & \\ -211.131 & 352.756 & & \text{(SYMMETRIC)} & \\ 0 & -141.625 & 283.281 & & \\ 0 & 0 & -141.788 & 352.919 & \\ 0 & 0 & 0 & -211.131 & 211.065 \end{bmatrix} \begin{Bmatrix} \theta Y1 \\ \theta Y2 \\ \theta YM \\ \theta Y3 \\ \theta Y4 \end{Bmatrix}$$

(Final model is a modal solution using the more detailed structural model for torsion.)

Figure J-21. Solar Array Torsion Flexure Model

APPENDIX K

APPENDIX K

MODIFIED NTS-2 SOLAR ARRAY TORSION MODEL

Hinge stiffness increased from 326. to 92,000. in-lb/rad. Drive tube O.D. increased from 1.25 to 1.75 inches. Drive tube wall thickness increased from .049 to .063 inches. (Above information from Larry Turner, NRL by telephone calls 1/18/77 and 1/26/77.)

Previous model of solar arrays solved for torsion only (degree of freedom 5 = θY).

For existing S&R simulation model, update as follows:

Mode No. (Symmetric Only)	Equiv. Weight M_{eq} lb-in^2	M_{eq} Equiv. Mass Slug-ft.^{2}	Freq. H_z	ω_n rad/sec	ω_n^2 rad^2/sec^2
1	13944.	3.007	0	0	0
2 (3)	7152.5	1.5426	7.9635	50.036	2503.6
3 (5)	6289.1	1.3563	15.5315	97.587	9523.3

The differential equation of motion of the solar array drive system (open loo loop) is given in terms of the generalized coordinates, q, as:

$$I \{\ddot{q}\} + 2 \rho \omega_n \{\dot{q}\} + \omega_n^2 \{q\} = \frac{\phi^T \{T(t)\}}{M_{eq}}$$

For $\rho = 0.005$ (½ percent critical damping), the generalized equation reduces to

$$\begin{bmatrix} 1. & & \\ & 1. & \\ & & 1. \end{bmatrix} \begin{Bmatrix} \ddot{q}_1 \\ \ddot{q}_2 \\ \ddot{q}_3 \end{Bmatrix} + \begin{bmatrix} 0. & & \\ & .5004 & \\ & & .9759 \end{bmatrix} \begin{Bmatrix} \dot{q}_1 \\ \dot{q}_2 \\ \dot{q}_3 \end{Bmatrix} + \begin{bmatrix} 0. & & \\ & 2503.6 & \\ & & 9523.3 \end{bmatrix} \begin{Bmatrix} q_1 \\ q_2 \\ q_3 \end{Bmatrix} =$$

$$\left\{ \begin{Bmatrix} \frac{1.0}{3.007} \\ \frac{-1.00}{1.5425} \\ \frac{-.8856}{1.3563} \end{Bmatrix} \right\} (T_{\text{drive motor}}(t)) = \begin{Bmatrix} .33255 \\ -.64830 \\ -.65295 \end{Bmatrix} (T_{\text{drive motor}}(t))$$

This replaces Eq. 6 in previous memo. The discrete responses of several locations of interest are taken from the mode shapes and given below:

LOCATION	STARDYNE MODE NO.	θ_y Rotation (Radians) per Unit q		
		Mode 1 (Rigid Body)	Mode 2	Mode 3
Drive Motor	20	1.0	-1.0	-.8856
Tip of -Y outer panel	1	1.0	1.0	-.8856
Pitch sensor	3	1.0	.5683	.32105
Tip of +Y outer panel	32	1.0	1.0	-.8856

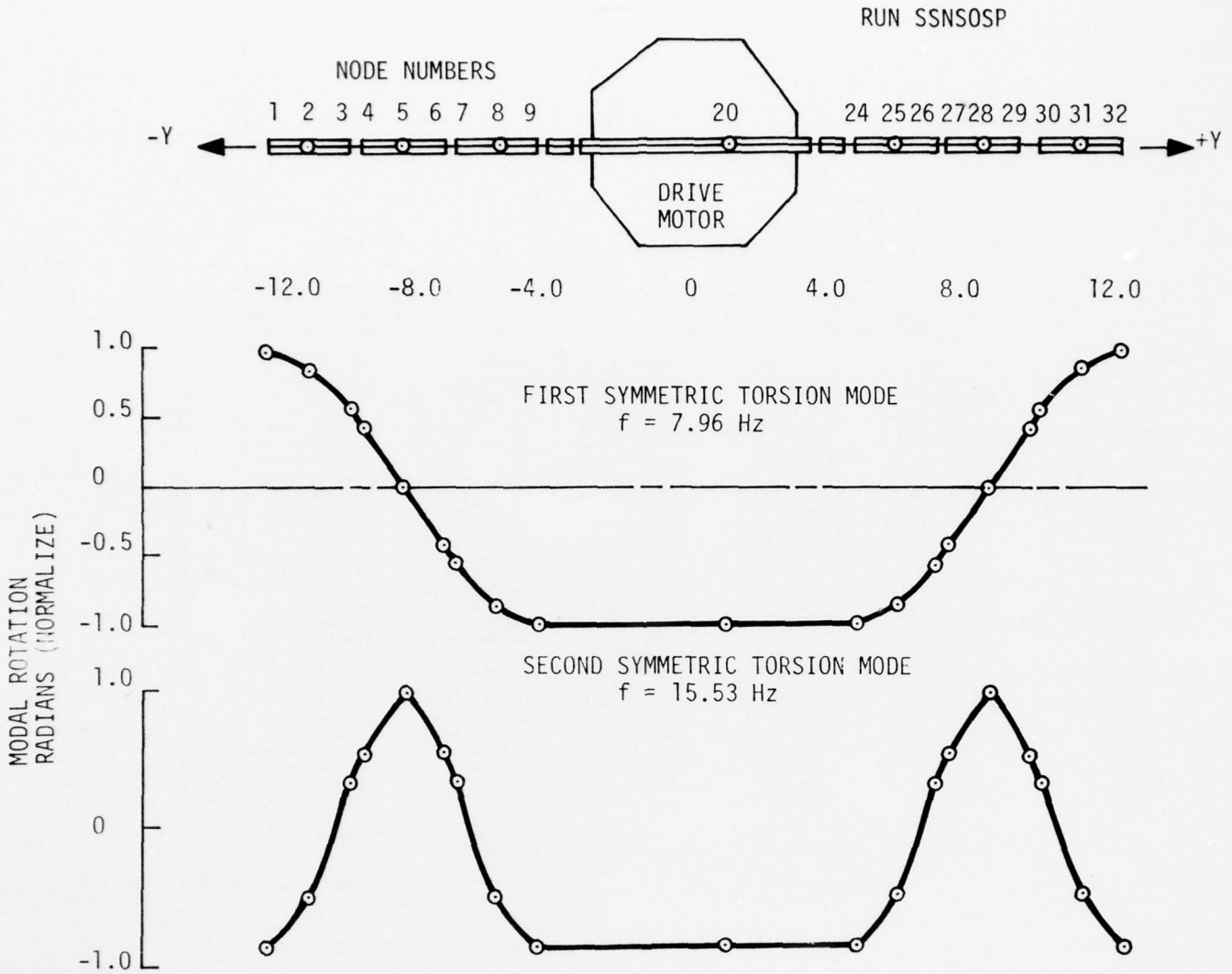

Figure K-1. Mode Shapes for Solar Array Stiff Hinges

TABLE K-1. RIGID BODY TORSION MODE

MODE SHAPE (EIGENVECTOR)

MODE NUMBER 1 • FREQUENCY = 0. • GENERALIZED WEIGHT = 1.3544.111

*MAXIMUM ROTATION IS AT NODE 1 *DOF = 5 VALUE = .1000000E+01

*MAXIMUM TRANSLATION IS AT NODE 1 *DOF = 1 VALUE = 0.

	********** TRANSLATIONS **********			********** ROTATIONS (RADIANS) **********		
NODE	X1	X2	X3	X4	X5	X6
1	0.000000000	0.000000000	0.000000000	0.000000000	1.000000000	0.000000000
2	0.000000000	0.000000000	0.000000000	0.000000000	1.000000000	0.000000000
3	0.000000000	0.000000000	0.000000000	0.000000000	1.000000000	0.000000000
4	0.000000000	0.000000000	0.000000000	0.000000000	1.000000000	0.000000000
5	0.000000000	0.000000000	0.000000000	0.000000000	1.000000000	0.000000000
6	0.000000000	0.000000000	0.000000000	0.000000000	1.000000000	0.000000000
7	0.000000000	0.000000000	0.000000000	0.000000000	1.000000000	0.000000000
8	0.000000000	0.000000000	0.000000000	0.000000000	1.000000000	0.000000000
9	0.000000000	0.000000000	0.000000000	0.000000000	1.000000000	0.000000000
10	0.000000000	0.000000000	0.000000000	0.000000000	1.000000000	0.000000000
11	0.000000000	0.000000000	0.000000000	0.000000000	1.000000000	0.000000000
12	0.000000000	0.000000000	0.000000000	0.000000000	1.000000000	0.000000000
13	0.000000000	0.000000000	0.000000000	0.000000000	1.000000000	0.000000000
14	0.000000000	0.000000000	0.000000000	0.000000000	1.000000000	0.000000000
19	0.000000000	0.000000000	0.000000000	0.000000000	1.000000000	0.000000000
20	0.000000000	0.000000000	0.000000000	0.000000000	1.000000000	0.000000000
21	0.000000000	0.000000000	0.000000000	0.000000000	1.000000000	0.000000000
22	0.000000000	0.000000000	0.000000000	0.000000000	1.000000000	0.000000000
23	0.000000000	0.000000000	0.000000000	0.000000000	1.000000000	0.000000000
24	0.000000000	0.000000000	0.000000000	0.000000000	1.000000000	0.000000000
25	0.000000000	0.000000000	0.000000000	0.000000000	1.000000000	0.000000000
26	0.000000000	0.000000000	0.000000000	0.000000000	1.000000000	0.000000000
27	0.000000000	0.000000000	0.000000000	0.000000000	1.000000000	0.000000000
28	0.000000000	0.000000000	0.000000000	0.000000000	1.000000000	0.000000000
29	0.000000000	0.000000000	0.000000000	0.000000000	1.000000000	0.000000000
30	0.000000000	0.000000000	0.000000000	0.000000000	1.000000000	0.000000000
31	0.000000000	0.000000000	0.000000000	0.000000000	1.000000000	0.000000000
32	0.000000000	0.000000000	0.000000000	0.000000000	1.000000000	0.000000000

MODAL PARTICIPATION FACTOR (X1) = 0.

MODAL PARTICIPATION FACTOR (X2) = 0.

MODAL PARTICIPATION FACTOR (X3) = 0.

GEN.WT. TIMES MODAL PART. FACT. (X1) = 0.

GEN.WT. TIMES MODAL PART. FACT. (X2) = 0.

GEN.WT. TIMES MODAL PART. FACT. (X3) = 0.

TABLE K-2. ANTI-SYMMETRIC TORSION MODE

* * * * * * * * * * * * * * * * * * * *

MODE SHAPE (EIGENVECTOR)

MODE NUMBER 2 , FREQUENCY = 2.5907912 , GENERALIZED WEIGHT = 10072.247

*MAXIMUM ROTATION IS AT NODE 32 *DOF = 5 VALUE = .100000E+01

*MAXIMUM TRANSLATION IS AT NODE 1 *DOF = 1 VALUE = 0.

	********** TRANSLATIONS **********			********** ROTATIONS (RADIANS) **********		
NODE	X1	X2	X3	X4	X5	X6
1	0.000000000	0.000000000	0.000000000	0.000000000	-1.000000000	0.000000000
2	0.000000000	0.000000000	0.000000000	0.000000000	-.987884188	0.000000000
3	0.000000000	0.000000000	0.000000000	0.000000000	-.951830340	0.000000000
4	0.000000000	0.000000000	0.000000000	0.000000000	-.934820397	0.000000000
5	0.000000000	0.000000000	0.000000000	0.000000000	-.875908244	0.000000000
6	0.000000000	0.000000000	0.000000000	0.000000000	-.795771411	0.000000000
7	0.000000000	0.000000000	0.000000000	0.000000000	-.763679591	0.000000000
8	0.000000000	0.000000000	0.000000000	0.000000000	-.664648745	0.000000000
9	0.000000000	0.000000000	0.000000000	0.000000000	-.549512380	0.000000000
10	0.000000000	0.000000000	0.000000000	0.000000000	-.505976266	0.000000000
11	0.000000000	0.000000000	0.000000000	0.000000000	-.054680043	0.000000000
12	0.000000000	0.000000000	0.000000000	0.000000000	-.011143929	0.000000000
13	0.000000000	0.000000000	0.000000000	0.000000000	.002116915	0.000000000
14	0.000000000	0.000000000	0.000000000	0.000000000	.004570105	0.000000000
19	0.000000000	0.000000000	0.000000000	0.000000000	.004570105	0.000000000
20	0.000000000	0.000000000	0.000000000	0.000000000	→ .004570105	0.000000000
21	0.000000000	0.000000000	0.000000000	0.000000000	.011143929	0.000000000
22	0.000000000	0.000000000	0.000000000	0.000000000	.054680043	0.000000000
23	0.000000000	0.000000000	0.000000000	0.000000000	.505976266	0.000000000
24	0.000000000	0.000000000	0.000000000	0.000000000	.549512380	0.000000000
25	0.000000000	0.000000000	0.000000000	0.000000000	.664648745	0.000000000
26	0.000000000	0.000000000	0.000000000	0.000000000	.763679591	0.000000000
27	0.000000000	0.000000000	0.000000000	0.000000000	.795771411	0.000000000
28	0.000000000	0.000000000	0.000000000	0.000000000	.875908244	0.000000000
29	0.000000000	0.000000000	0.000000000	0.000000000	.934820397	0.000000000
30	0.000000000	0.000000000	0.000000000	0.000000000	.951830340	0.000000000
31	0.000000000	0.000000000	0.000000000	0.000000000	.987884188	0.000000000
32	0.000000000	0.000000000	0.000000000	0.000000000	1.000000000	0.000000000

MODAL PARTICIPATION FACTOR (X1) = 0.

MODAL PARTICIPATION FACTOR (X2) = 0.

MODAL PARTICIPATION FACTOR (X3) = 0.

GEN.WT. TIMES MODAL PART. FACT. (X1) = 0.

GEN.WT. TIMES MODAL PART. FACT. (X2) = 0.

GEN.WT. TIMES MODAL PART. FACT. (X3) = 0.

TABLE K-3. SYMMETRIC TORSION MODE

MODE SHAPE (EIGENVECTOR)

MODE NUMBER 3 . FREQUENCY = 7.9635168 . GENERALIZED WEIGHT = 7152.4747

*MAXIMUM ROTATION IS AT NODE 32 *DOF = 5 VALUE = .100000E+01

*MAXIMUM TRANSLATION IS AT NODE 1 *DOF = 1 VALUE = 0.

NODE	********** TRANSLATIONS ********** X1	X2	X3	********** ROTATIONS (RADIANS) ********** X4	X5	X6
1	0.000000000	0.000000000	0.000000000	0.000000000	1.000000000	0.000000000
2	0.000000000	0.000000000	0.000000000	0.000000000	.885528468	0.000000000
3	0.000000000	0.000000000	0.000000000	0.000000000	.568321335	0.000000000
4	0.000000000	0.000000000	0.000000000	0.000000000	.431678665	0.000000000
5	0.000000000	0.000000000	0.000000000	0.000000000	.000000000	0.000000000
6	0.000000000	0.000000000	0.000000000	0.000000000	-.431678665	0.000000000
7	0.000000000	0.000000000	0.000000000	0.000000000	-.568321335	0.000000000
8	0.000000000	0.000000000	0.000000000	0.000000000	-.885528468	0.000000000
9	0.000000000	0.000000000	0.000000000	0.000000000	-1.000000000	0.000000000
10	0.000000000	0.000000000	0.000000000	0.000000000	-1.000000000	0.000000000
11	0.000000000	0.000000000	0.000000000	0.000000000	-1.000000000	0.000000000
12	0.000000000	0.000000000	0.000000000	0.000000000	-1.000000000	0.000000000
13	0.000000000	0.000000000	0.000000000	0.000000000	-1.000000000	0.000000000
14	0.000000000	0.000000000	0.000000000	0.000000000	-1.000000000	0.000000000
19	0.000000000	0.000000000	0.000000000	0.000000000	-1.000000000	0.000000000
20	0.000000000	0.000000000	0.000000000	0.000000000	-1.000000000	0.000000000
21	0.000000000	0.000000000	0.000000000	0.000000000	-1.000000000	0.000000000
22	0.000000000	0.000000000	0.000000000	0.000000000	-1.000000000	0.000000000
23	0.000000000	0.000000000	0.000000000	0.000000000	-1.000000000	0.000000000
24	0.000000000	0.000000000	0.000000000	0.000000000	-1.000000000	0.000000000
25	0.000000000	0.000000000	0.000000000	0.000000000	-.885528468	0.000000000
26	0.000000000	0.000000000	0.000000000	0.000000000	-.568321335	0.000000000
27	0.000000000	0.000000000	0.000000000	0.000000000	-.431678665	0.000000000
28	0.000000000	0.000000000	0.000000000	0.000000000	.000000000	0.000000000
29	0.000000000	0.000000000	0.000000000	0.000000000	.431678665	0.000000000
30	0.000000000	0.000000000	0.000000000	0.000000000	.568321335	0.000000000
31	0.000000000	0.000000000	0.000000000	0.000000000	.885528468	0.000000000
32	0.000000000	0.000000000	0.000000000	0.000000000	1.000000000	0.000000000

drive motor

MODAL PARTICIPATION FACTOR (X1) = 0. GEN.WT. TIMES MODAL PART. FACT. (X1) = 0.

MODAL PARTICIPATION FACTOR (X2) = 0. GEN.WT. TIMES MODAL PART. FACT. (X2) = 0.

MODAL PARTICIPATION FACTOR (X3) = 0. GEN.WT. TIMES MODAL PART. FACT. (X3) = 0.

TABLE K-4. 2ND ANTI-SYMMETRIC TORSION MODE

MODE SHAPE (EIGENVECTOR)

MODE NUMBER 4 , FREQUENCY = 4.0358543 , GENERALIZED WEIGHT = 7719.4047

*MAXIMUM ROTATION IS AT NODE 8 *DOF = 5 VALUE = .100000E+01

*MAXIMUM TRANSLATION IS AT NODE 1 *DOF = 1 VALUE = 0.

NODE	********** TRANSLATIONS ********** X1	X2	X3	********** ROTATIONS (RADIANS) ********** X4	X5	X6
1	0.000000000	0.000000000	0.000000000	0.000000000	-.984178388	0.000000000
2	0.000000000	0.000000000	0.000000000	0.000000000	-.839134325	0.000000000
3	0.000000000	0.000000000	0.000000000	0.000000000	-.446754100	0.000000000
4	0.000000000	0.000000000	0.000000000	0.000000000	-.282960028	0.000000000
5	0.000000000	0.000000000	0.000000000	0.000000000	.216962390	0.000000000
6	0.000000000	0.000000000	0.000000000	0.000000000	.652934803	0.000000000
7	0.000000000	0.000000000	0.000000000	0.000000000	.774379095	0.000000000
8	0.000000000	0.000000000	0.000000000	0.000000000	1.000000000	0.000000000
9	0.000000000	0.000000000	0.000000000	0.000000000	.930869333	0.000000000
10	0.000000000	0.000000000	0.000000000	0.000000000	.857119523	0.000000000
11	0.000000000	0.000000000	0.000000000	0.000000000	.092627532	0.000000000
12	0.000000000	0.000000000	0.000000000	0.000000000	.018877722	0.000000000
13	0.000000000	0.000000000	0.000000000	0.000000000	-.003586037	0.000000000
14	0.000000000	0.000000000	0.000000000	0.000000000	-.007741720	0.000000000
19	0.000000000	0.000000000	0.000000000	0.000000000	-.007741720	0.000000000
20	0.000000000	0.000000000	0.000000000	0.000000000	→ -.007741720	0.000000000
21	0.000000000	0.000000000	0.000000000	0.000000000	-.018877722	0.000000000
22	0.000000000	0.000000000	0.000000000	0.000000000	-.092627532	0.000000000
23	0.000000000	0.000000000	0.000000000	0.000000000	-.857119523	0.000000000
24	0.000000000	0.000000000	0.000000000	0.000000000	-.930869333	0.000000000
25	0.000000000	0.000000000	0.000000000	0.000000000	-1.000000000	0.000000000
26	0.000000000	0.000000000	0.000000000	0.000000000	-.774379095	0.000000000
27	0.000000000	0.000000000	0.000000000	0.000000000	-.652934803	0.000000000
28	0.000000000	0.000000000	0.000000000	0.000000000	-.216962390	0.000000000
29	0.000000000	0.000000000	0.000000000	0.000000000	.282960028	0.000000000
30	0.000000000	0.000000000	0.000000000	0.000000000	.446754100	0.000000000
31	0.000000000	0.000000000	0.000000000	0.000000000	.839134325	0.000000000
32	0.000000000	0.000000000	0.000000000	0.000000000	.984178388	0.000000000

MODAL PARTICIPATION FACTOR (X1) = 0. GEN.WT. TIMES MODAL PART. FACT. (X1) = 0.

MODAL PARTICIPATION FACTOR (X2) = 0. GEN.WT. TIMES MODAL PART. FACT. (X2) = 0.

MODAL PARTICIPATION FACTOR (X3) = 0. GEN.WT. TIMES MODAL PART. FACT. (X3) = 0.

TABLE K-5. 2ND SYMMETRIC TORSION MODE

MODE SHAPE (EIGENVECTOR)

MODE NUMBER 5 , FREQUENCY = 15.531520 , GENERALIZED WEIGHT = 6249.043

*MAXIMUM ROTATION IS AT NODE 5 *DOF = 5 VALUE = .100000E+01

*MAXIMUM TRANSLATION IS AT NODE 1 *DOF = 1 VALUE = 0.

	********** TRANSLATIONS			********** ROTATIONS (RADIANS) **********		
NODE	X1	X2	X3	X4	X5	X6
1	0.000000000	0.000000000	0.000000000	0.000000000	-.885625484	0.000000000
2	0.000000000	0.000000000	0.000000000	0.000000000	-.500000000	0.000000000
3	0.000000000	0.000000000	0.000000000	0.000000000	.321052751	0.000000000
4	0.000000000	0.000000000	0.000000000	0.000000000	.564572733	0.000000000
5	0.000000000	0.000000000	0.000000000	0.000000000	1.000000000	0.000000000
6	0.000000000	0.000000000	0.000000000	0.000000000	.564572733	0.000000000
7	0.000000000	0.000000000	0.000000000	0.000000000	.321052751	0.000000000
8	0.000000000	0.000000000	0.000000000	0.000000000	-.500000000	0.000000000
9	0.000000000	0.000000000	0.000000000	0.000000000	-.885625484	0.000000000
10	0.000000000	0.000000000	0.000000000	0.000000000	-.885625484	0.000000000
11	0.000000000	0.000000000	0.000000000	0.000000000	-.885625484	0.000000000
12	0.000000000	0.000000000	0.000000000	0.000000000	-.885625484	0.000000000
13	0.000000000	0.000000000	0.000000000	0.000000000	-.885625484	0.000000000
14	0.000000000	0.000000000	0.000000000	0.000000000	-.885625484	0.000000000
19	0.000000000	0.000000000	0.000000000	0.000000000	-.885625484	0.000000000
20	0.000000000	0.000000000	0.000000000	0.000000000	-.885625484	0.000000000
21	0.000000000	0.000000000	0.000000000	0.000000000	-.885625484	0.000000000
22	0.000000000	0.000000000	0.000000000	0.000000000	-.885625484	0.000000000
23	0.000000000	0.000000000	0.000000000	0.000000000	-.885625484	0.000000000
24	0.000000000	0.000000000	0.000000000	0.000000000	-.885625484	0.000000000
25	0.000000000	0.000000000	0.000000000	0.000000000	-.500000000	0.000000000
26	0.000000000	0.000000000	0.000000000	0.000000000	.321052751	0.000000000
27	0.000000000	0.000000000	0.000000000	0.000000000	.564572733	0.000000000
28	0.000000000	0.000000000	0.000000000	0.000000000	1.000000000	0.000000000
29	0.000000000	0.000000000	0.000000000	0.000000000	.564572733	0.000000000
30	0.000000000	0.000000000	0.000000000	0.000000000	.321052751	0.000000000
31	0.000000000	0.000000000	0.000000000	0.000000000	-.500000000	0.000000000
32	0.000000000	0.000000000	0.000000000	0.000000000	-.885625484	0.000000000

MODAL PARTICIPATION FACTOR (X1) = 0. GEN.WT. TIMES MODAL PART. FACT. (X1) = 0.

MODAL PARTICIPATION FACTOR (X2) = 0. GEN.WT. TIMES MODAL PART. FACT. (X2) = 0.

MODAL PARTICIPATION FACTOR (X3) = 0. GEN.WT. TIMES MODAL PART. FACT. (X3) = 0.

TABLE K-6. NODAL COORDINATE TABLE

	NODE	X1	X2 (Y)	X3 (Z)
NODES	1	0.	-.1242300E+03	-.2200000E+02
NODES	2	0.	-.1122300E+03	-.2200000E+02
NODES	3	0.	-.1002300E+03	-.2200000E+02
NODES	4	0.	-.9742000E+02	-.2200000E+02
NODES	5	0.	-.8542000E+02	-.2200000E+02
NODES	6	0.	-.7342000E+02	-.2200000E+02
NODES	7	0.	-.7061000E+02	-.2200000E+02
NODES	8	0.	-.5861000E+02	-.2200000E+02
NODES	9	0.	-.4661000E+02	-.2200000E+02
NODES	10	0.	-.4380000E+02	-.2200000E+02
NODES	11	0.	-.3280000E+02	-.2200000E+02
NODES	12	0.	-.2999000E+02	-.2200000E+02
NODES	13	0.	0.	-.2200000E+02
NODES	14	0.	.5548000E+01	-.2200000E+02
NODES	15	0.	0.	-.2200000E+02
NODES	16	0.	.1512300E+02	-.2200000E+02
NODES	20	0.	.1033600E+02	-.2200000E+02
NODES	21	0.	.2999000E+02	-.2200000E+02
NODES	22	0.	.3280000E+02	-.2200000E+02
NODES	23	0.	.4380000E+02	-.2200000E+02
NODES	24	0.	.4661000E+02	-.2200000E+02
NODES	25	0.	.5861000E+02	-.2200000E+02
NODES	26	0.	.7061000E+02	-.2200000E+02
NODES	27	0.	.7342000E+02	-.2200000E+02
NODES	28	0.	.8542000E+02	-.2200000E+02
NODES	29	0.	.9742000E+02	-.2200000E+02
NODES	30	0.	.1002300E+03	-.2200000E+02
NODES	31	0.	.1122300E+03	-.2200000E+02
NODES	32	0.	.1242300E+03	-.2200000E+02
NODES	33	0.	0.	0.

WARNING NODES 13 AND 15 HAVE IDENTICAL COORDINATES.

--- MAXIMUM ALLOWABLE NODE NUMBER BY ANALYSIS TYPE ---

STAR STATIC	2500
STAR HQR	1666
STAR INV.ITER.	1300
STAR SUBSTRUCT.	2500
DYNRE 1	1666
DYNRE 2	1300
DYNRE 3	300
DYNRE 4	1666
DYNRE 5	NO LIMIT

LARGEST NODE NUMBER CODED IN THIS MODEL = 33

NEXT TABLE HEADER (RESTG

APPENDIX L

APPENDIX L

SOLAR ARRAY TORSION MODES,
SOLUTION FOR RESPONSE TO TORQUE
MOTOR ANGULAR ACCELERATIONS

SUMMARY INPUT DATA

Based on updated solar array hinge torsional stiffness, the arrays are assumed to have symmetric responses for a rigid torque motor connection to the spacecraft.

The modes of interest are obtained from STARDYNE finite element structural model, using only the torsional masses and spring stiffness data, including updated hinge stiffness. For a locked-up or grounded torque motor, the following data is obtained for the two modes of interest:

Mode No. (STARDYNE)	Mode No. (S & R)	Equiv. Weight M_{eq} lb-in^2	M_{eq} Equiv. Mass Slug-ft.^{2}	Freq. H_z	ω_n rad/sec	ω_n^2 rad^2/sec^2
2	1	10072.297	2.17225	2.5908	16.2784	264.987
4	2	7719.405	1.6648	9.0358	56.774	3223.281

The differential equations of motion of the motor array drive system in terms of the generalized coordinates q is given by:

$$\left[I \right]\{\ddot{q}\} + \left[2 \rho \omega_n \right]\{\dot{q}\} + \left[\omega_n^2 \right]\{q\} = \frac{\left[-\phi \right]^T m}{\left[M_{eq} \right]} \ddot{\beta} \qquad \text{(L-1)}$$

where

$\ddot{\beta}$ = angular acceleration of drive motor (absolute)

$$\ddot{\beta} = \frac{\Sigma \text{ Torques applied to drive motor, not}}{I_{\substack{\text{arrays,} \\ \text{pitch,}}} \text{ total}} + \ddot{\beta}_{\text{spacecraft/pitch acceleration}} \qquad \text{(L-2)}$$

Note that if torque motor is moving and torque is applied to cause + β_{arrays}, then a negative torque is applied to the spacecraft.

If

$I_{p_{sc}}$ = pitch moment of inertia of spacecraft, without arrays

$$\ddot{\beta}_{sc} = \frac{-(\Sigma \text{ Torques applied to drive motor}) + \text{all other pitch torques}}{I_{p_{sc}}}$$

Also note that the net torque applied to drive motor = $T_{applied} - T_{brake\ torque}$

$$\ddot{\beta} = \frac{\text{Drive motor Torque}}{I_{array}} + \ddot{\theta}_A \qquad \text{(L-3)}$$

$$\begin{bmatrix} \ddot{q}_1 \\ \ddot{q}_2 \end{bmatrix} + \begin{bmatrix} .16278 & 0 \\ 0 & .56774 \end{bmatrix} \begin{bmatrix} \dot{q}_1 \\ \dot{q}_2 \end{bmatrix} + \begin{bmatrix} 264.987 & 0 \\ 0 & 3223.28 \end{bmatrix} \begin{bmatrix} q_1 \\ q_2 \end{bmatrix}$$

$$= \begin{bmatrix} -.8076 \\ -.2076 \end{bmatrix} (+ \ddot{\theta}_A)$$

$$\theta_{pitch\ sensor} = .95183\ q_1 - .46754\ q_2$$

$$\ddot{\theta}_A = \frac{T_m}{I} + \ddot{\theta}_{sc}$$

For $\rho = 0.005$ (½ percent critical damping) the generalized torsional equations of motion become

$$\begin{bmatrix} 1. & 0 \\ 0 & 1. \end{bmatrix} \begin{Bmatrix} q_1 \\ q_2 \end{Bmatrix} + \begin{bmatrix} .16278 & 0 \\ 0 & .56774 \end{bmatrix} \begin{Bmatrix} \dot{q}_1 \\ \dot{q}_2 \end{Bmatrix} + \begin{bmatrix} 264.987 & 0 \\ 0 & 3223.28 \end{bmatrix} \begin{Bmatrix} q_1 \\ q_2 \end{Bmatrix}$$

$$= \begin{Bmatrix} -.8076 \\ -.2076 \end{Bmatrix} \ddot{\beta} \qquad \text{(L-4)}$$

The discrete responses of several locations of interest on the solar panels are taken from the mode shapes and the generalized coordinate responses

$$\{\theta\} = \left[\phi\right] \{q\} + \beta \qquad \text{(L-5)}$$

where β = absolute angular displ. of drive motor

STARDYNE MODE NO.	LOCATION	ϕ MATRIX TERMS	
20	Drive motor	0.000	0.000
1	Tip of -Y outer panel	1.000	-.98418
3	Pitch sensor	.95183	-.46754
32	Tip of +Y outer panel	1.000	-.98418

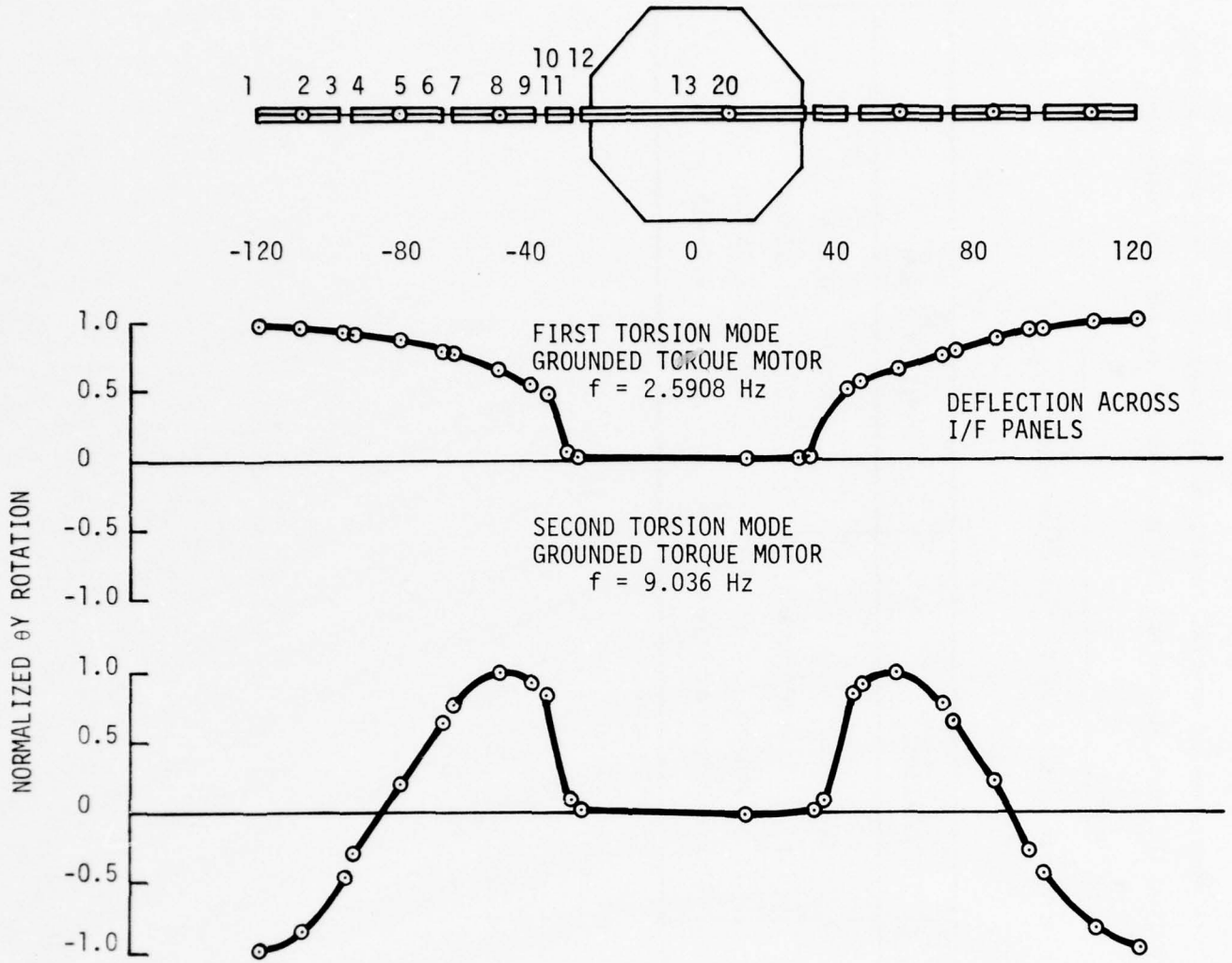

Figure L-1. Grounded Torsional Mode Shapes

TABLE I-1. NTS-2 SOLAR ARRAY TORSION--BASED ON ANTI-SYMETRIC MODES OF FREE-FREE MODEL WITH STIFF HINGES

NODE NO. n	M_n lb-in^2	$\left(f_2 = 2.59\ H_z\right)$ $\phi_{n,2}$ $= \left[\frac{\phi^T M}{\Sigma\ \phi_n \cdot M_n}\right]$	$f_4 = 9.035 H_z$ $\phi_{n,4}$ $\left[\phi^T M\right]$	
1	581.	1.000	-.98418	Note: Generalized forcing function for base excitation $-\frac{\left[\phi^T\right]\left[M\right]}{\left[M_{eq}\right]}$ is independent of units used for mass, as long as $\left[M\right]$ (mass matrix), and $\left[M_{eq}\right]$, generalized mass have same units.
2	1162.	.98788	-.83913	
3	581.	.95183	-.46754	
4	581.	.93482	-.28296	
5	1162.	.87591	.21696	
6	581.	.79577	.65293	
7	581.	.76368	.77438	
8	1162.	.66465	1.0000	
9	581.	.54951	.93087	
10	-	-.00457	-.00774	

Σ = 581. x 4.99561 + 1162. x 2.52844 = 4067. for 8 side only

Σ = 581. x .6235 + 1162. x .37783 = 801.3

$$\frac{\left[-\phi^h\right]^T\left[M\right]}{M_{eq}} = \frac{-4067.}{10072.3} = -.40378 \times 2 = .8076 \quad \text{for both sides}$$

$$\frac{-801.3 \times 2}{7719.4} = .2076$$

APPENDIX M

APPENDIX M

COMBINED EARTH SENSOR MODEL

INTRODUCTION

This appendix describes the model developed for the GPS combined earth sensor. The model can be used to evaluate acquisition as well as normal operation.

This model is based on information obtained from Barnes Engineering Company at a meeting in St. Petersburg, Florida on March 13, 1975, and a subsequent phone call, and the Rockwell procurement specification for the sensor.

SENSOR DESCRIPTION

The Combined Earth Sensor is a two-axis, static sensor which incorporates two horizon crossing indicators for spinning mode attitude sensing. The adjective static means the sensor uses no moving parts in the measurement of attitude.

The two-axis sensor consists of an optical system, 24 thermopile detectors, and processing electronics. The 24 detectors are arranged on the focal surface of the optical system. The earth image is tangent to the inner edges of the A detectors at null at the design altitude. Two roll and two pitch measurements are computed sequentially by switching sums and differences of various detector outputs to the input of an integrator. Each measurement is sampled and held for comparison check and possible output. A new roll and new pitch measurement is computed each 1/4 second. Roll and pitch computations are separated by 1/8 second. The S detectors are for space reference and are used with the A detectors for accurate

measurements over $+1^{\circ}$ in the track mode. The A and B detectors are used in the acquisition mode for $+4^{\circ}$ range. The thermopile detectors have a time constant of 1.4 seconds and are sensitive to the 14 to 16 micron wavelengths (CO_2 band). The sensor continuously tests all signals and rejects spurious or incorrect signals due to sun, moon, or other anomalies.

The two horizon crossing indicators consist of 3 degree by 3 degree square fields of view. One diagonal of each square is parallel to the scan path. One field is 10° from the -X axis toward +Z and the other is 10° from -X toward -Z (Spin rotation is about the Z axis). The detectors are pyroelectric with insignificant time constant.

MODEL DESCRIPTION

The model consists of an initialization and two normal operation sections. The initialization section performs one-time computations and clears outputs and counters. One normal operation section is for the horizon crossing indicators used in the spin phase. The other normal operation section is for two-axis earth sensing.

Characteristics of the horizon crossing indicator model are as follows:

- Inputs to the model are spacecraft position vector from center of earth, and spacecraft attitude direction cosine matrix. Both inputs must be relative to the same reference frame.
- When a sensor line of sight crosses the edge of the earth, the time from the crossing to the sample time is output. If no crossing occurs in the sample interval, the output is set to $-\Delta t$.
- If a sensor line of sight crosses the earth very close to a tangent, there may not be an output. The sample, Δt, should be small

enough so that this loss of output does not happen when attitude determination is critical. Select Δt as follows:

$$\Delta t \leq \frac{1}{W_s} \sqrt{1 - \frac{\ell}{r_e}^2} \quad \tan^{-1} \left[\frac{1}{\left[\left(1 - \frac{h}{r_e}\right)^2 - 1 \right]^{\frac{1}{2}}} \right]$$

where

W_s = spin rate in rad/sec

$= \frac{2\pi}{60} W_{RPM}$

W_{RPM} = spin rate in rev/min

h = satellite altitude in n. mi. ($100 \leq h \leq 10897$)

r_e = earth radius in n. mi. (3440)

ℓ = distance from earth center to chord of detector path in n. mi.

e.g.

let

W_{RPM} = 100

h = 10897

r_e = 3440

ℓ = 3405.6 = 0.99 r_e

then $\Delta t \leq 0.00326$ seconds.

o The equations used in the flow diagram are derived below

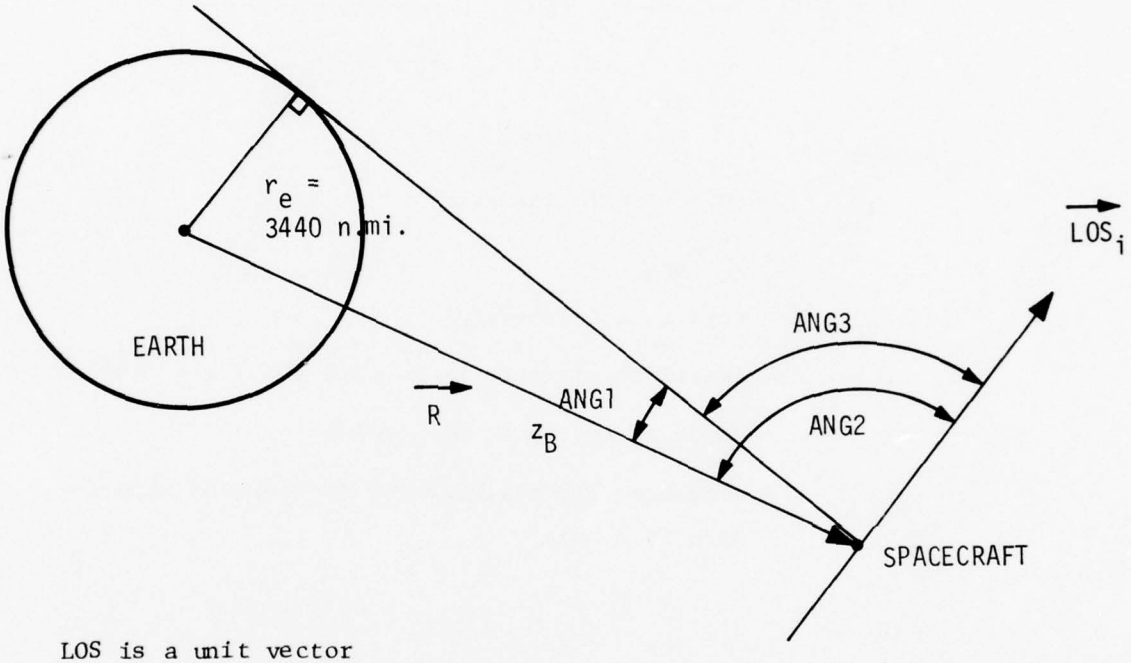

LOS is a unit vector

$$\frac{|\vec{R} \times \vec{LOS}|}{|\vec{R}|} = \text{SIN (ANG2)}$$

$$\frac{\vec{R} \cdot \vec{LOS}}{|\vec{R}|} = -\text{COS (ANG2)}$$

$$\text{ANG2} = \text{TAN}^{-1} \frac{\text{SIN (ANG2)}}{\text{COS (ANG2)}}$$

$$\text{ANG2} = \text{TAN}^{-1} \frac{|\vec{R} \times \vec{LOS}|}{-\vec{R} \cdot \text{LOS}}$$

$$ANG1 = SIN^{-1} \frac{r_e}{|\vec{R}|}$$

$$= TAN^{-1} \frac{r_e/|\vec{R}|}{[1 - (r_e/|\vec{R}|)^2]^{\frac{1}{2}}}$$

$$= TAN^{-1} \frac{r_e}{[|\vec{R}|^2 - r_e^2]^{\frac{1}{2}}}$$

$$ANG3 = ANG2 - ANG1$$

Note that $3440 + 100 \leq |\vec{R}| \leq 10897 + 3440$ n. mi.

$$13.8^{\circ} \leq ANG1 \leq 76.4^{\circ}.$$

Characteristics of the two-axis earth sensor model are as follows:

- The sensor output is updated every 1/8 second.
- The sensor model has four states which are:

State 1	Compute Roll 1, Output Pitch 2 if valid
State 2	Compute Pitch 1, Output Roll 1 if valid
State 3	Compute Roll 2, Output Pitch 1 if valid
State 4	Compute Pitch 2, Output Roll 2 if valid

  The state is advanced every 1/8 second.

- Each detector area is divided into $1^{\circ} \times 1^{\circ}$ squares. The area coverage of each $1^{\circ} \times 1^{\circ}$ square by the earth is computed from the distance between center of the earth circle on the focal surface and the center of the square. The orientation of the square is not considered.
- The position of the earth image on the focal surface (B&C) is computed from true attitude. The diameter of the earth image on the focal surface (RE) is computed from satellite altitude. Measurements on the focal surface are in equivalent radians.

- Each detector output is the sum of the coverages of $1^{o} \times 1^{o}$ squares within the detector.
- The sensor output is computed from the detector outputs according to the functions in the electronics.
- Functions of the system programmer to reject spurious or incorrect signals is included.
- Subroutine must be initialized by calling with MODE = 0 prior to operating in two-axis mode.
- The time increment, Δt, should be selected from one of the following to synchronize with the sensor update frequency:

Recommended Δt	Increments per Update	
0.125	1	
0.0625	2	
0.025	5	
0.0125	10	
0.01	12.5	Synchronization error 0.005 sec. is insignificant
$\leq$0.01	$\geq$12.5	

EARTH RADIANCE VARIATION

The variation of radiance over earth surface for the 14-16 μ CO_2 band has been calculated in Figure M-1. Plots of the radiance as function of latitude and time of year for various altitudes is shown in Figure M-2. The model for GPS simulation is deduced from these results. For maximum radiance variation a January situation is considered. The radiance is assumed to be a function of latitude but not longitude. The radiance variation for southern hemisphere is assumed to be that for northern hemisphere six months later. The radiance variation for earth disk is approximated by piecewise linear segments using the values corresponding to 20 Km altitude shown in Figure M-2. The radiance values and the normalized variations are summarized

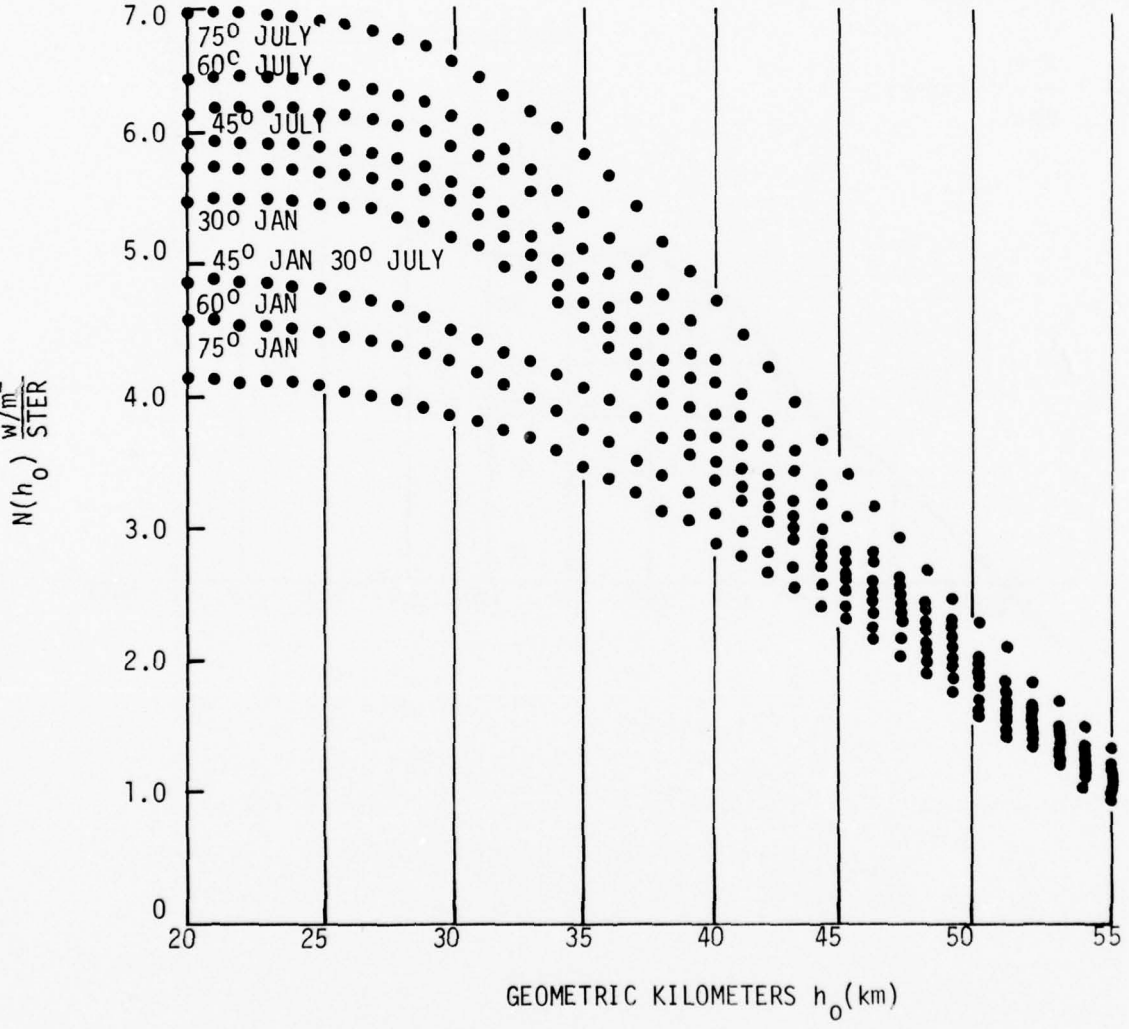

Figure M-1. Radiance CO_2 14-16μ

$$v = y_1 + L = y_1 + \frac{\beta - x_1}{x2 - x1} (y2 - y1)$$

$$\frac{L}{\frac{1}{2} - y_1} = \frac{\beta - x_1}{x2 - x1} (y2 - y1)$$

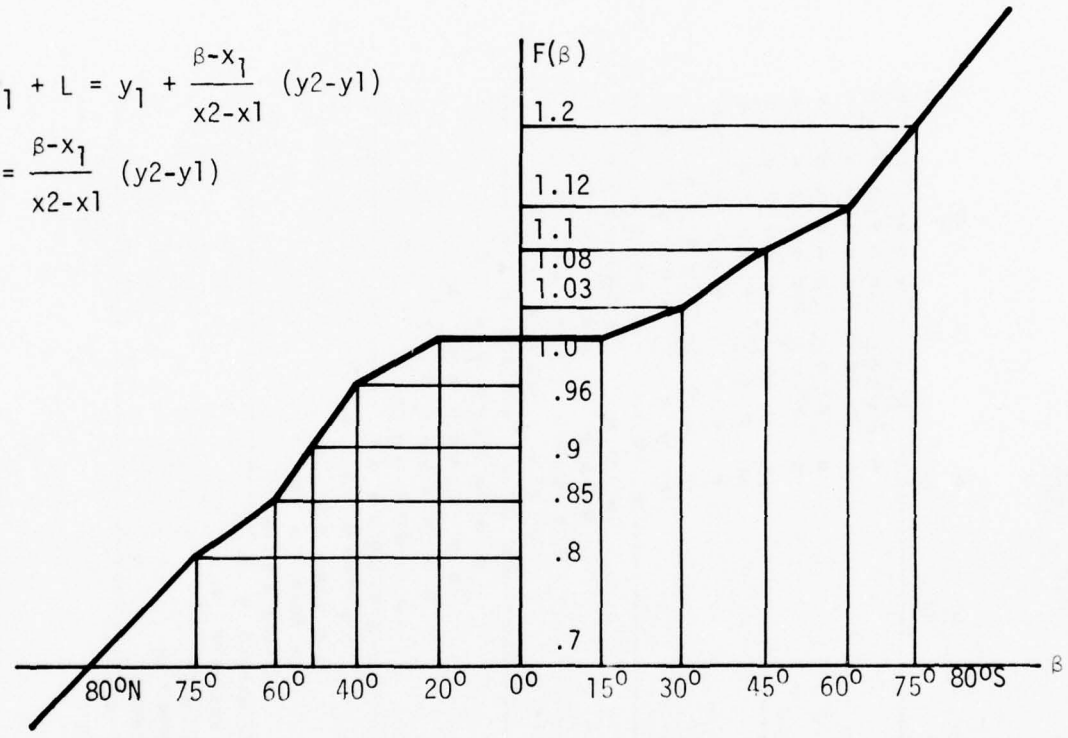

Figure M-2. Normalized Earth Radiance Variation with Latitude at January

in Table M-1. The normalized variation is used to be compatible with the existing earth sensor simulation that does not include the details of sensor optics and filter response. The radiance for the 15^{o} latitude band is taken as that corresponding to a $220^{o}K$ earth which, in conjunction with the sensor optics and filter response, provides 3.15 μw when the "A" detector FOV is fully illuminated.

TABLE M-1. EARTH RADIANCE VARIATION WITH LATITUDE AND TIME OF YEAR

LAT.	MON.	RADIANCE $\frac{W/M^2}{STER}$	NORMALIZED VARIATION
-75^{o}	JAN	4.13	0.72
-60^{o}	JAN	4.63	0.80
-45^{o}	JAN	4.88	0.85
-30^{o}	JAN	5.5	0.96
$\mp 15^{o}$	JAN/JUL	5.75	1.00
30^{o}	JUL	5.94	1.03
45^{o}	JUL	6.19	1.08
60^{o}	JUL	6.44	1.12
75^{o}	JUL	6.94	1.21

Implementation of the earth radiance variation into the sensor model requires the following computations which are based on the geometry given in Figure M-3.

(a) LOS-vector for detector cell element centered at (X_a, Y_a):

$$U = \sqrt{X_a^2 + Y_a^2}$$

$$X_s = \frac{X_a \sin U}{U}$$

$$Y_s = \frac{-Y_a \sin U}{U}$$

$$Z_s = \cos U$$

Denote

$$(\bar{L}_a^S) = \begin{bmatrix} X_s \\ Y_s \\ Z_s \end{bmatrix}$$

(b) Look point on earth surface along L_a:

$$(\bar{L}_a^I) = T_{IB}\, T_{SB}^I\, (\bar{L}_a^S)$$

$$(\bar{R}_a^I) = (\bar{R}_V^I) + S\, (\bar{L}_a^I)$$

where

$(\bar{R}_a^I)$ = look point on earth surface along $\underline{L}_a$.

$(\bar{R}_V^I)$ = vehicle position from center of earth

S = slant range from $\underline{R}_V$ to $\underline{R}_a$

$$= -(\bar{R}_V^I)^T(\bar{L}_a^I) - \{\gamma_e^2 - (\bar{R}_V^I)^T(\bar{R}_V^I) + [(\bar{R}_V^I)^T(\bar{L}_a^I)]^2\}^{\frac{1}{2}}$$

γ_e = 3590.95 n. mi.

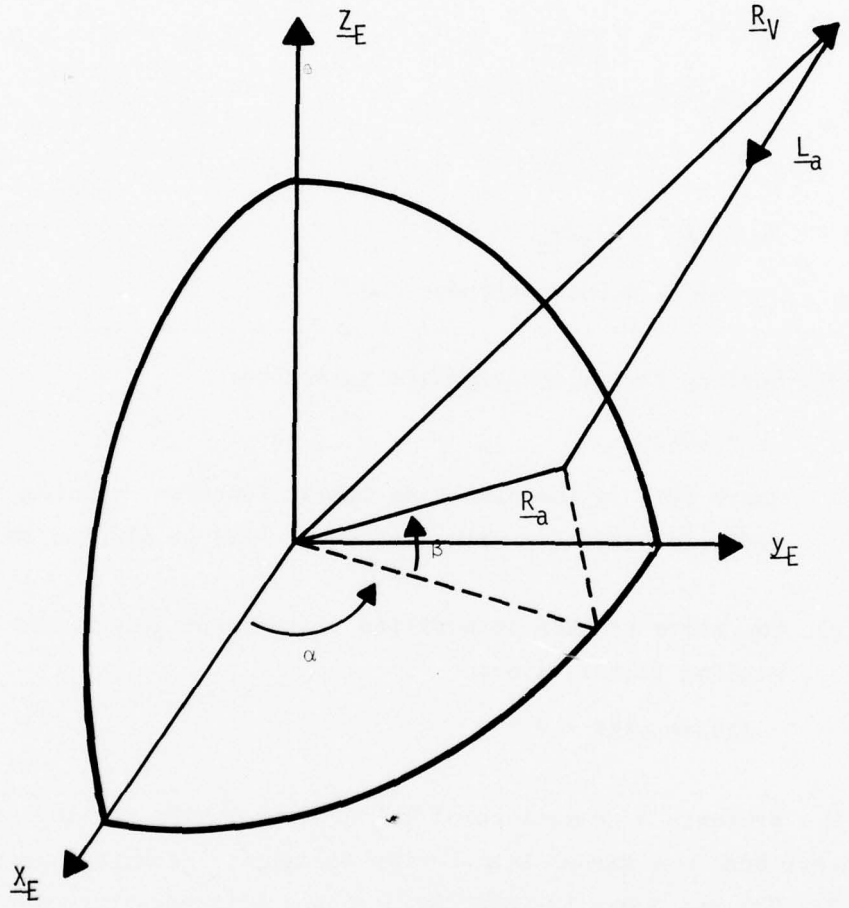

Figure M-3. Sensor Model Geometry

(c) Look point latitude:

$$(\underline{\bar{R}}_a^{-E}) = T_{EI}\ (\underline{\bar{R}}_a^{I})$$

Denote

$$(\underline{\bar{R}}_a^{-E}) = \begin{bmatrix} R_1 \\ R_2 \\ R_3 \end{bmatrix}$$

$$\beta = \sin^{-1}\ (R_3/\gamma_e)$$

= look point latitude

(d) Scaling factor for radiance variation:

$$V = F(\beta)$$

where $F(\beta)$ is the piecewise linear function defining the radiance variation with latitude; $F(\beta)$ is plotted in Figure M-1.

(e) The value of AREA is modified from the original value by the scaling factor, i.e.:

AREA←AREA * V

Figure M-4 presents a comparison of the GPS simulation radiance model and a model described in a Barnes Engineering document, "Technical Description Model 13-16901 and Model 13-16903 Synchronous Altitude Static-Sensors", 22 August, 1975. Models agree reasonably well.

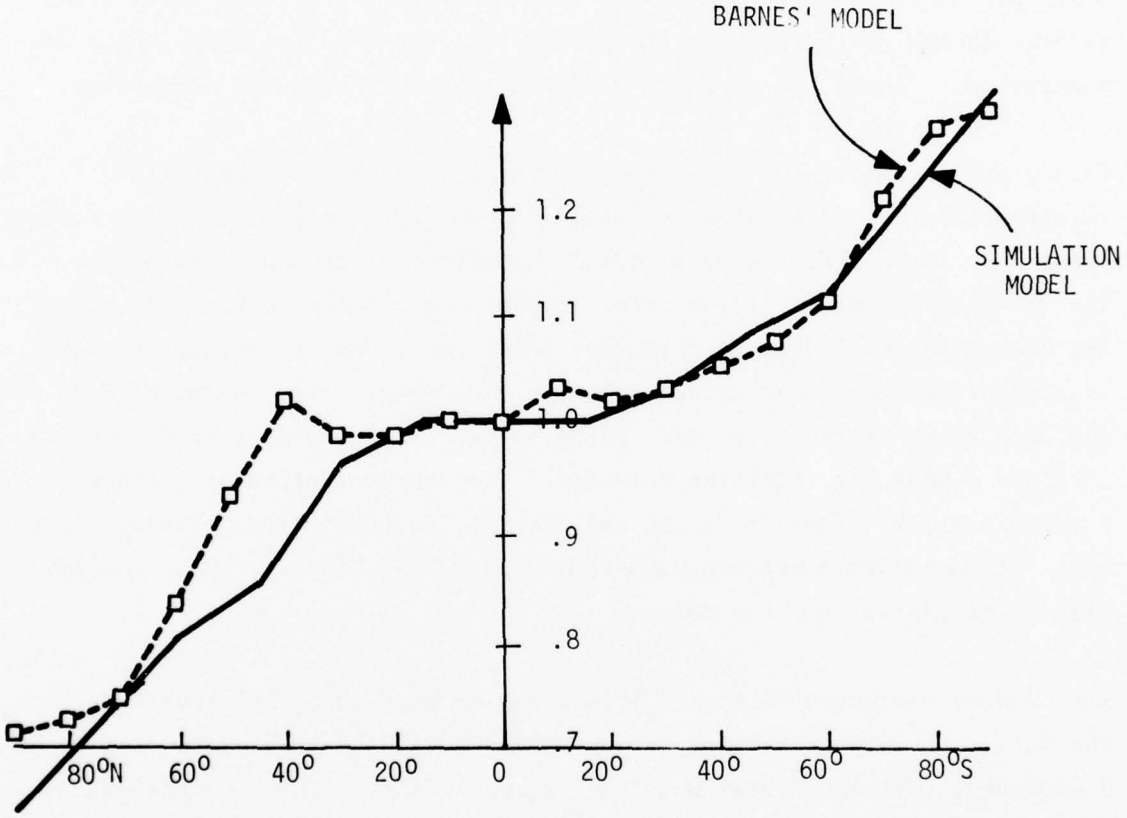

Figure M-4. Comparison of Models

SENSOR ERROR MODELING

The sensor error modeling considered here includes detector and pre-amp noises, electronics parameter shift error, error due to temperature gradient across detector and sensor alignment error. Horizon uncertainty errors, though not a sensor originated error, are also included in the consideration. These are errors that exist in all operational situations.

Errors due to sun or moon in sensor detector field of view and errors resulted from variation of earth disk size due to vehicle orbit eccentricity exist only for a specific operational condition and are not included here. The detector and preamplifier noise has been calculated to be 0.379 μV (3σ) for sensor in track mode (A detectors only) and 0.464 μV (3σ) for sensor in acquisition mode (A+B detectors) with a detector scale factor of 3.15 μW/deg. and responsivity of 20 V/W. These noises are equivalent to 0.0060 deg. (3σ) and 0.0074 deg. (3σ) respectively. Use the output scale factors of 5 V/deg and 1.25 V/deg for track and acquisition modes respectively. The noise at output then becomes 0.03 V(3σ) and 0.0093 V(3σ). The noise error will be simulated as white noise.

Electronics parameter shift has been analyzed by Barnes, Reference M-2. The values at initial setting and at end of life have been calculated to be 0.0034 deg. (3σ) and 0.0219 deg. (3σ) respectively. These correspond to output errors of 0.017 V (3σ) and 0.1095 V (3σ) for track mode and 0.0043 V (3σ) and 0.0274 V (3σ) for acquisition mode. The error due to electronics parameter shift will be simulated as bias errors.

The temperature gradient considered by Barnes amounts to a temperature difference of 0.00048^{o}F between A and S reference junctions. The corresponding attitude error evaluated for temperature of 70^{o}C is 0.0103^{o} or 0.0515 V

for track mode. For acquisition mode, the temperature change of 0.0028 deg. between detectors is calculated to cause attitude error of 0.0029 deg. which amounts to output error of 0.0035 V. All values quoted above are considered to be for worst case and will be treated as 3σ values. The error due to temperature gradient will be simulated as bias errors.

The achievable static sensor alignment accuracy has been estimated by Barnes to be in the order of 0.015 deg. (3σ). The equivalent output error is 0.075 V (3σ) for track mode and 0.019 V (3σ) for acquisition mode. The effect of alignment error will be simulated as bias errors. The horizon uncertainty error has been treated as an exponentially correlated noise with standard deviation 0.88 Km, correlation time 10 days and correlation distance 2500 N. Mi in Reference M-1, i.e.,

$$E[h(t,s)h(t+T, S+d)] = \sigma_h^2 e^{-T/10} e^{-d/2500}$$

where

σ_h = 0.88 Km

T = time in days

d = distance in n. mi.

The term $e^{-T/10}$ can be approximated by 1 if T is much less than 10 days. Factoring in the GPS orbit altitude of 10897 N. Mi the horizon uncertainty error amounts to 0.0020 deg. of earth disk angle error. In the evaluation of P_1 and R_1 detectors at opposite sides of the earth disk are involved. The separation between the look points of these detectors is:

$$d = \frac{(180^o - 14^o)X\pi}{180^o} \times 3461.6 \text{ N. Mi.}$$

$$= 10029 \text{ N. Mi.}$$

The separation is approximately four times the correlation distance. Hence the effects of horizon uncertainty error at opposing detectors are essentially uncorrelated. The equivalent error in evaluation of P_1 and R_1 is then $0.0020^o \times \sqrt{2} = 0.0028^o$ (1σ) or 0.0085^o (3σ). The output error becomes 0.0424 V for track mode and 0.0106 V for acquisition mode. The same values can be used for P_2 and R_2. (The distance between look points of every other detector cell is approximately 5383.1 N.Mi. The correlation of horizon uncertainty at points separated by this distance is only 0.12. It is neglected for simplicity of model.) For vehicle points at nadir and spins at a yaw rate of W RPM, the sensor detector scans the earth surface at a rate of 358.87 W N.Mi/sec. The 2500 N. Mi correlation distance would then be equivalent to a correlation time of 6.97/W sec.

The sensor output error e(t) due to the horizon uncertainty will be modeled as an exponentially correlated noise as follows:

$$E[e(t)\ e(t+T)] = \sigma_0^2\ e^{-T/T_c}$$

where

σ_0 = 0.0424 V for track mode
= 0.0106 V for acquisition mode

T_c = 6.97/W sec
= 3.485 sec for W = 2 RPM

The above model will be used to account for the effect of horizon uncertainty even for cases where vehicle is not quite pointing at the nadir. (The change of correlation time due to the pointing offset from nadir by $\pm 4^o$ is expected to be small. For large offset from nadir the effect of detector not seeing the earth disk will be much more significant than the effect of horizon uncertainty.)

In summary, the sensor error will be simulated as an additive output error consists of a white noise component, a bias component and an exponentially

correlated random noise. The white noise is used to simulate the effect of detector and preamplifier noises. The equivalent attitude error of the white noise is 0.0060^{o} (3σ). The exponentially correlated noise is used to simulate the effect of horizon uncertainty error. The equivalent attitude error is 0.0085^{o} (3σ). The correlation time of this error for the vehicle spin rate of 2 RPM at initiation of earth acquisition is 3.485 sec.

The bias error is introduced to account for the total effects of electronics error, temperature gradient error and sensor alignment error. The equivalent attitude error is 0.0285^{o} (3σ) evaluated as the RSS value of each individual effects.

CONCERNS

- The detector geometry and output computations may not be correct since Barnes has two different designs. The one used here (Figure M-5) is one of their designs. The other has detector pattern rotated $22\frac{1}{2}^{o}$ about the line of sight from the one shown here.
- The output update frequency for GPS is not certain. The one used here is the one proposed by Barnes for DSCS III.
- Earth image distortion and focus are not modeled. Excluding radiance, the earth image is assumed to be a perfect circle on the focal surface.
- The detector output approximation using $1^{o} \times 1^{o}$ squares causes very little error near null (normal operation) and up to 0.15^{o} maximum detector error at extreme attitudes (during acquisition). The extent of the errors near null and the sensor output errors during acquisition has not been analyzed. The approximation errors off null are on the order the errors due to earth radiance variation and earth image quality. Smaller squares may be used to improve accuracy but computer cost will go up.

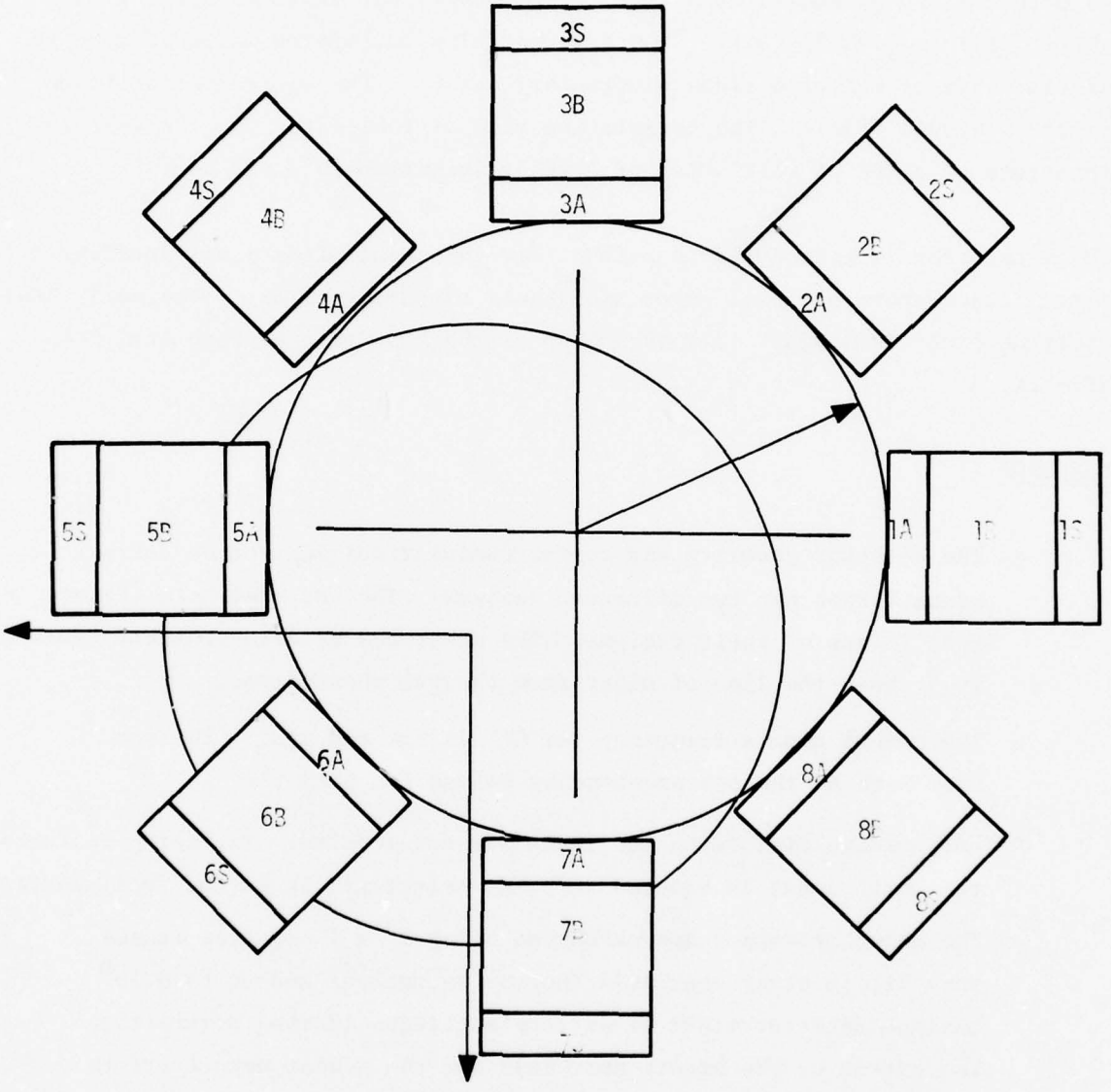

Figure M-5. Detector Geometry-- Axis Earth Sensor

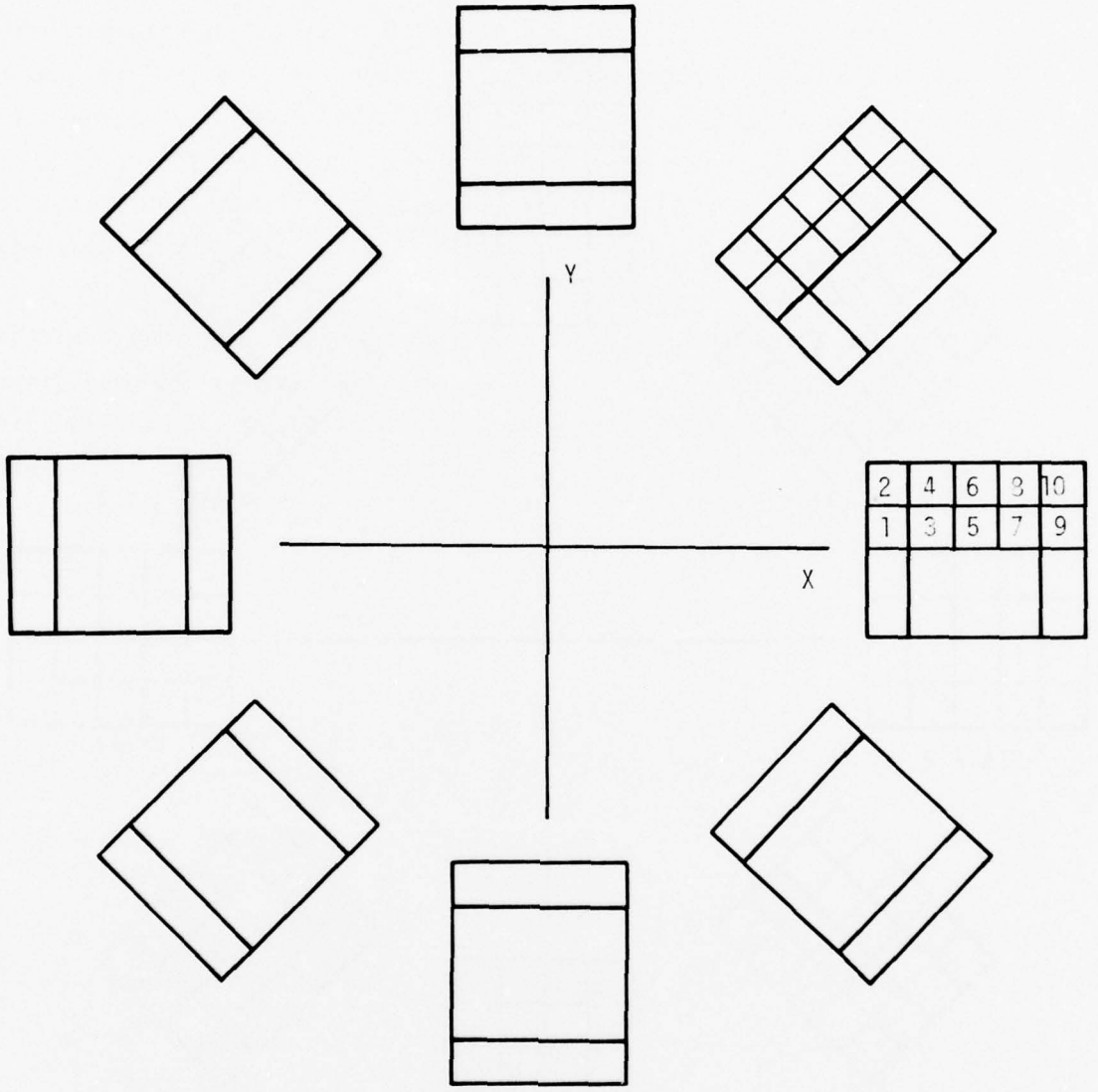

NUMBERING OF X-Y COORDINATES FOR POSITION OF 1^{o} x 1^{o} SQUARES. X-Y COORDINATES OF ALL 160 1^{o} x 1^{o} SQUARES ARE OBTAINED FROM THESE 20 STORED VALUES

Figure M-5. Detector Geometry--2-Axis Earth Sensor (continued)

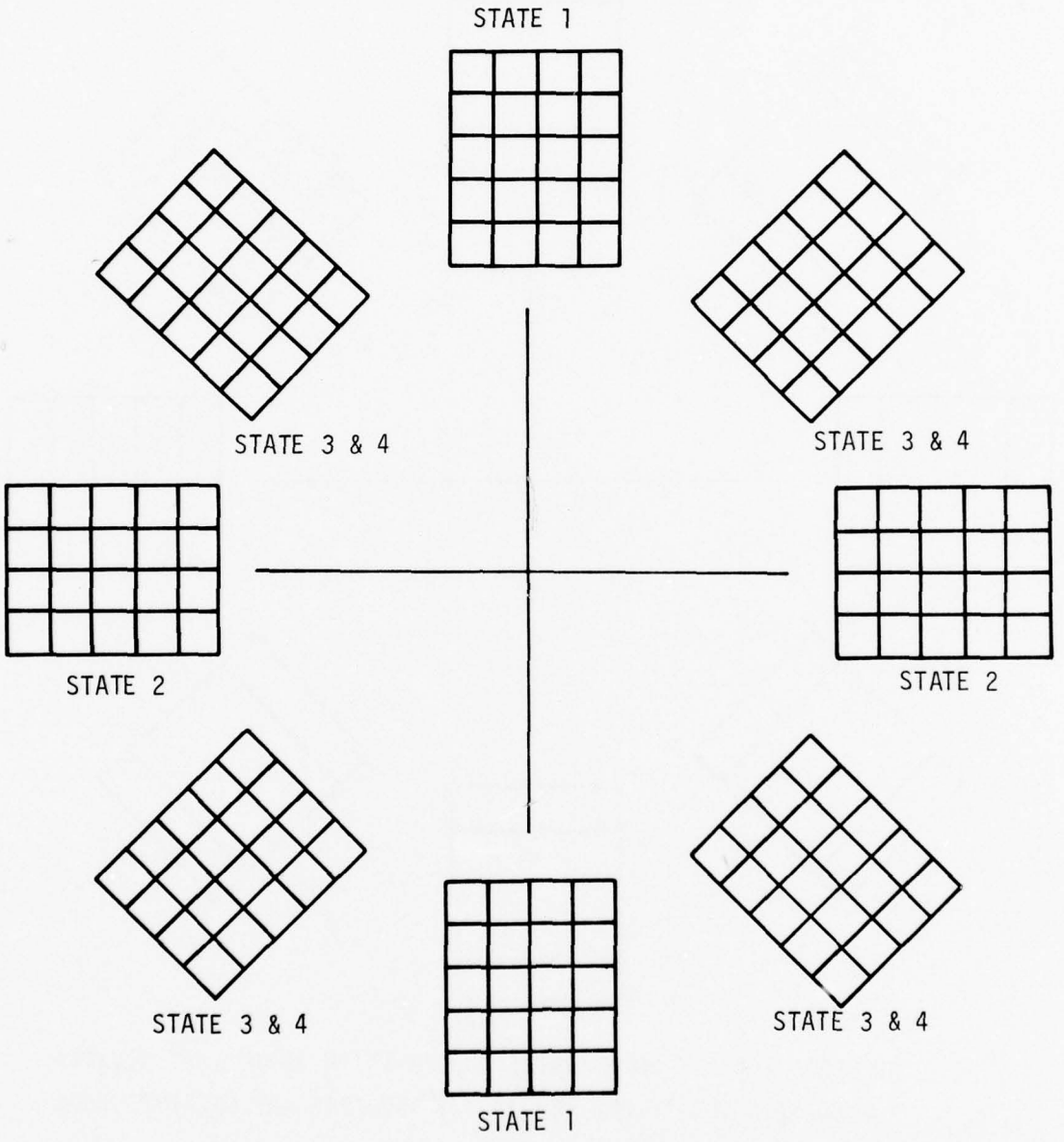

Figure M-5. Detector Geometry--2-Axis Earth Sensor (continued)

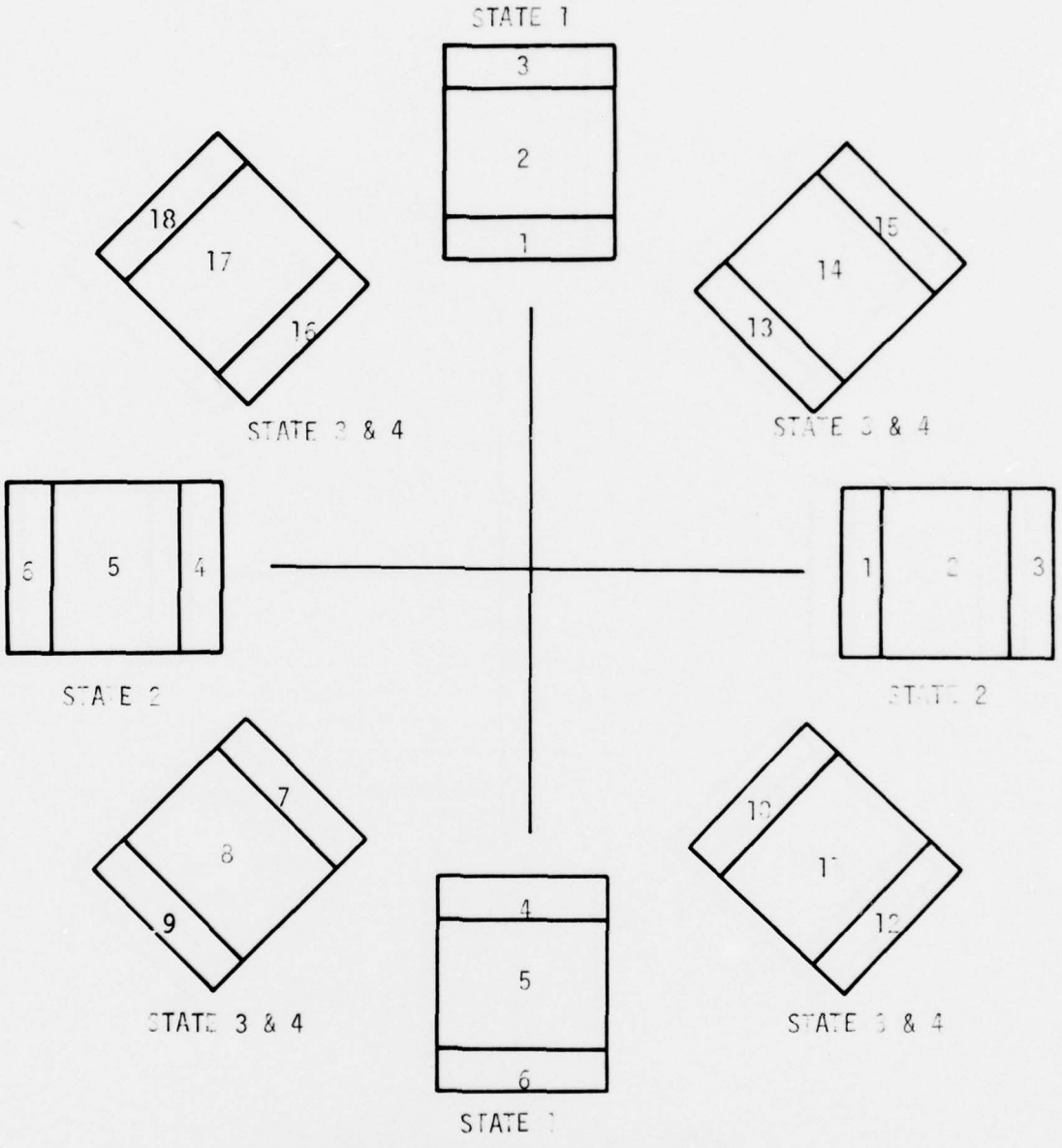

NUMBERING OF D ELEMENTS

Figure M-5. Detector Geometry--2-Axis Earth Sensor (continued)

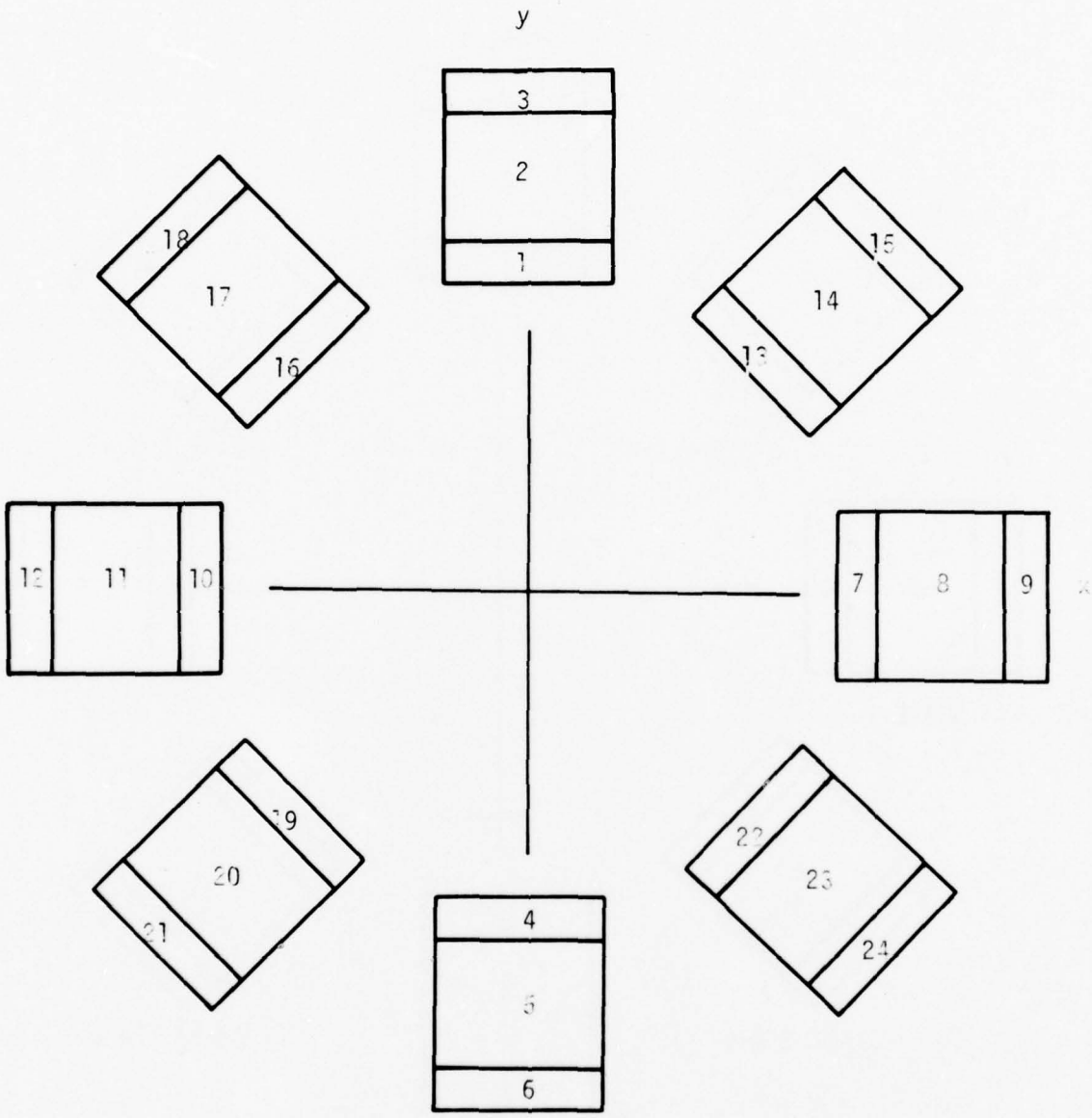

NUMBERING OF V AND DSAV ELEMENTS

Figure M-5. Detector Geometry--2-Axis Earth Sensor (concluded)

- Sun and moon interference are not included in this model description.

FLOW DIAGRAM

The combined earth sensor model flow diagram is shown in Figure M-6. The left arrow (←) within boxes indicates replacement, i.e., the expression on the right replaces the variable on the left. Mathematical subscripts are used. Symbols used in the flow diagram are defined in the sections below. Comments appear outside the boxes to describe the operations within the boxes.

INITIALIZATION DATA

Table M-2 lists the initialization parameters, nominal values, tolerance, and source of data. This data is to be input at the start of each run.

INPUT DATA

Table M-3 lists the input data the earth sensor model expects from the calling program each time the subroutine is executed in the normal mode.

OUTPUT DATA

Table M-4 lists the output data from the earth sensor model subroutine. Other subroutine variables may be outputs if the user desires.

INTERNAL VARIABLES

Internal variables used in the flow diagram are defined in Table M-5.

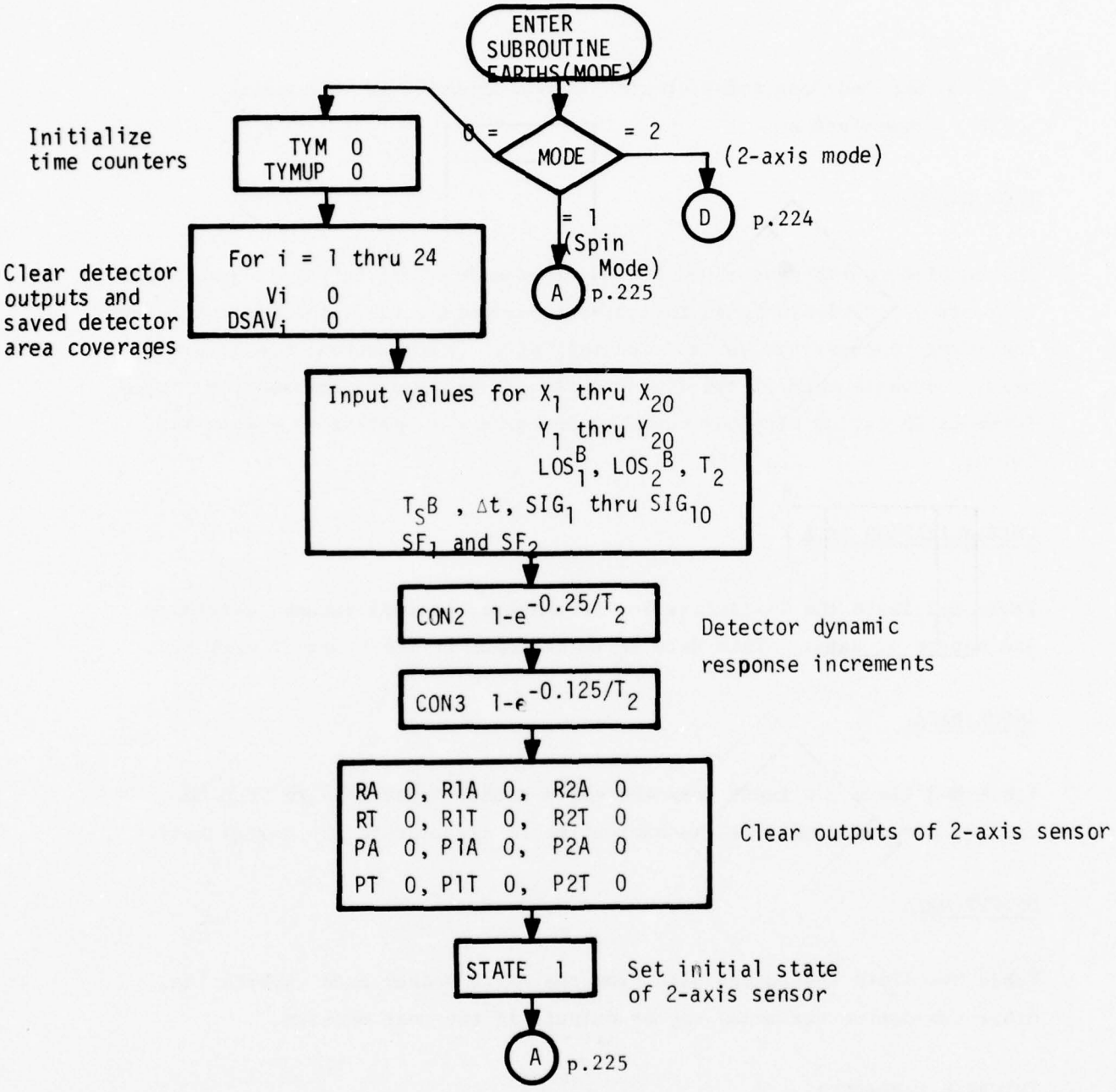

Figure M-6. Earth Sensor Flow Chart

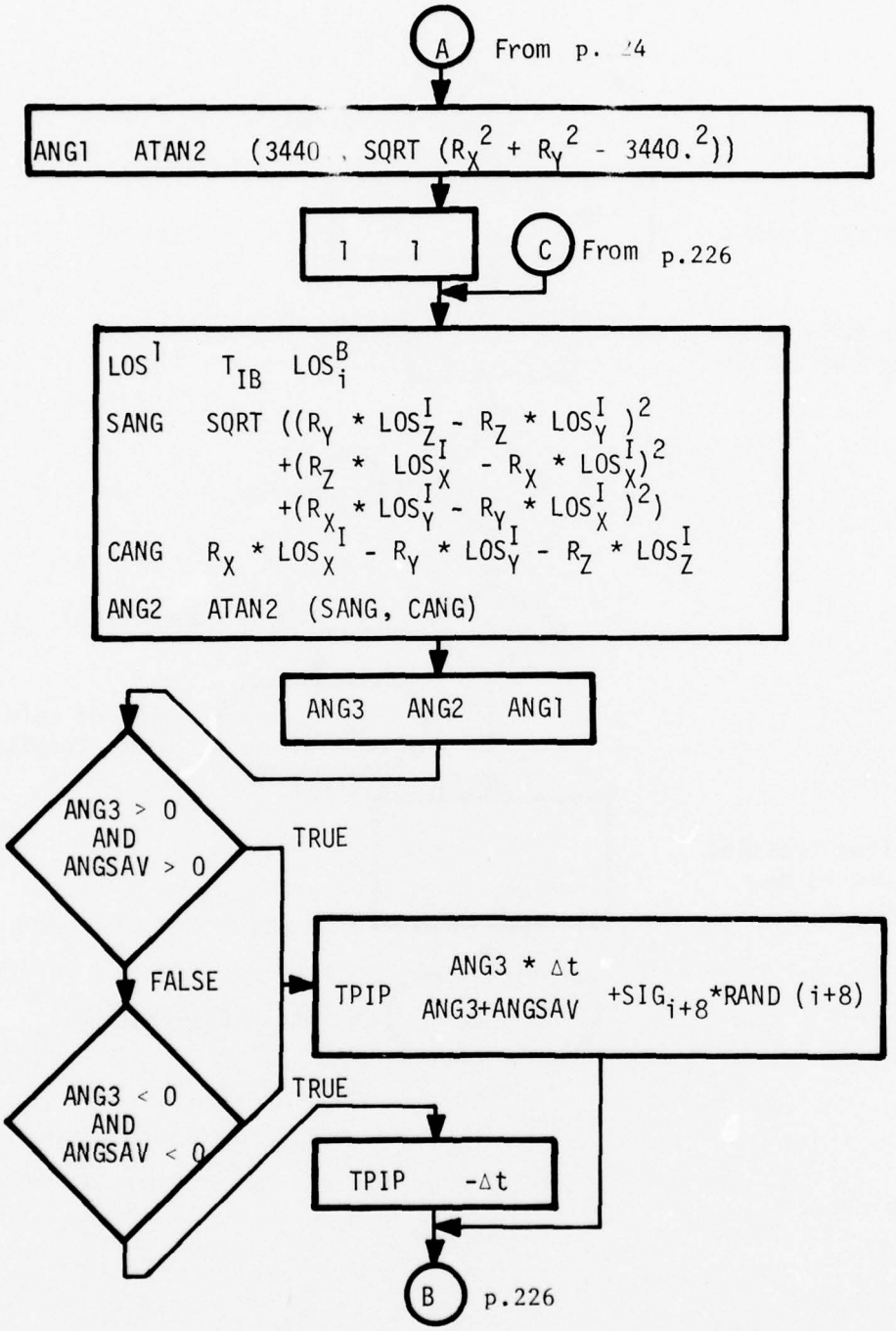

Figure M-6. Earth Sensor Flow Chart (continued)

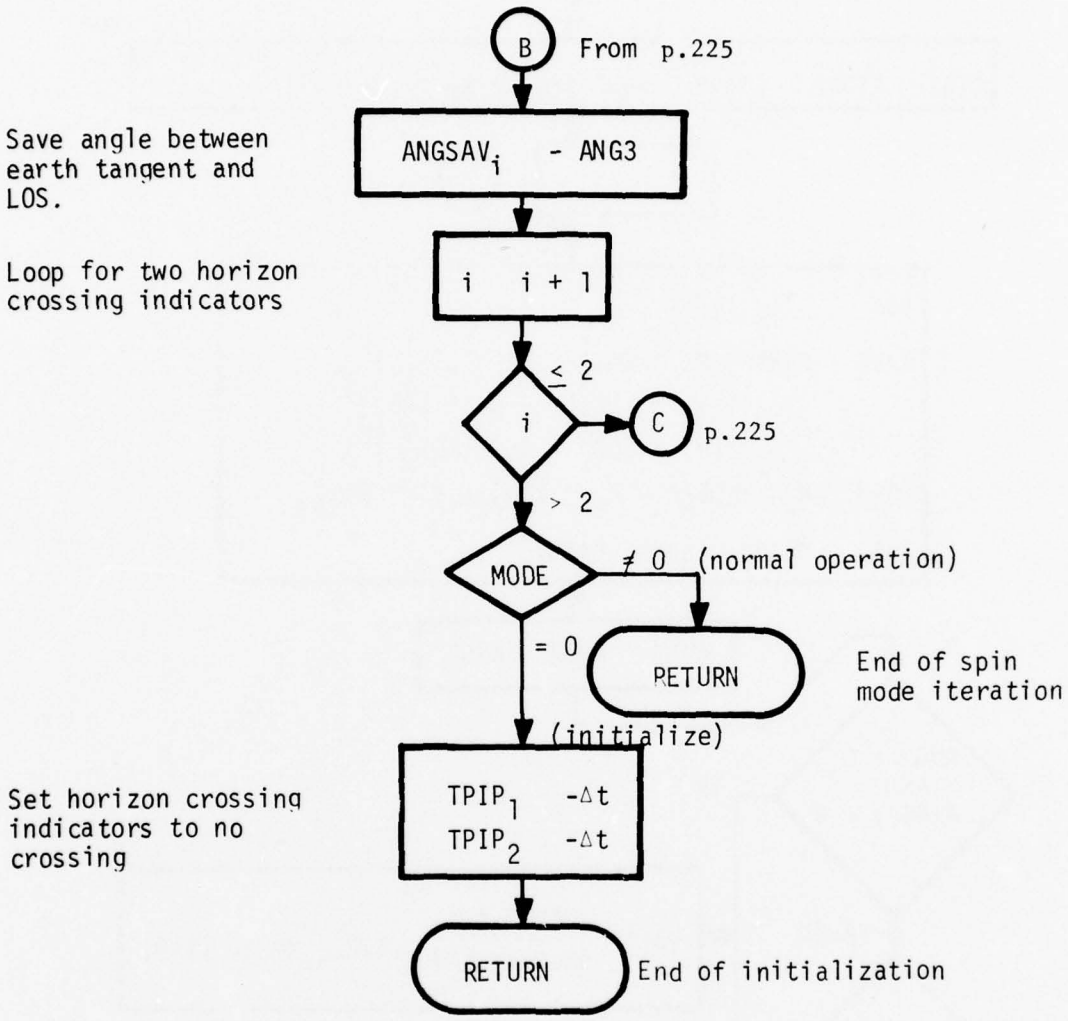

Figure M-6. Earth Sensor Flow Chart (continued)

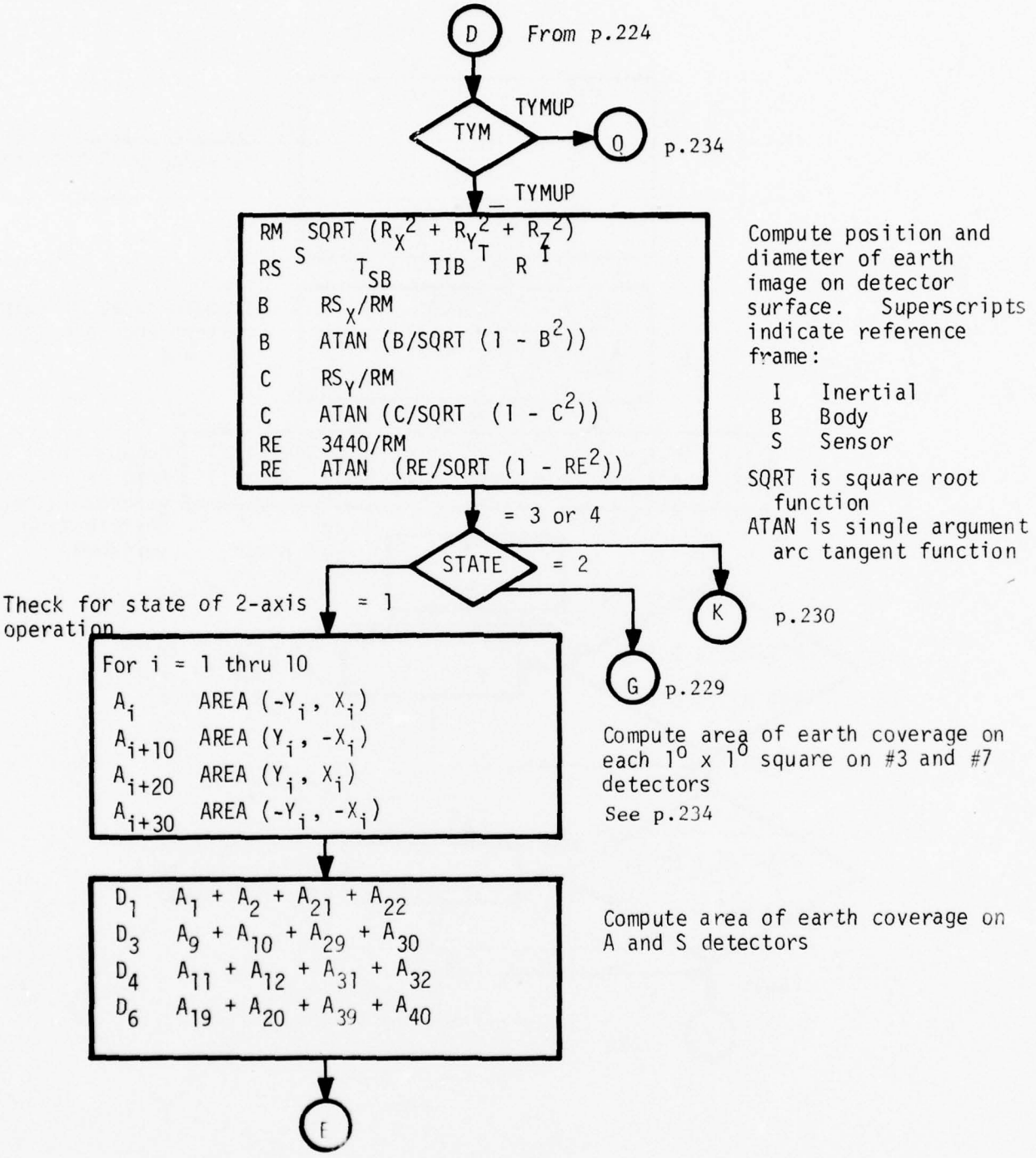

Figure M-6. Earth Sensor Flow Chart (continued)

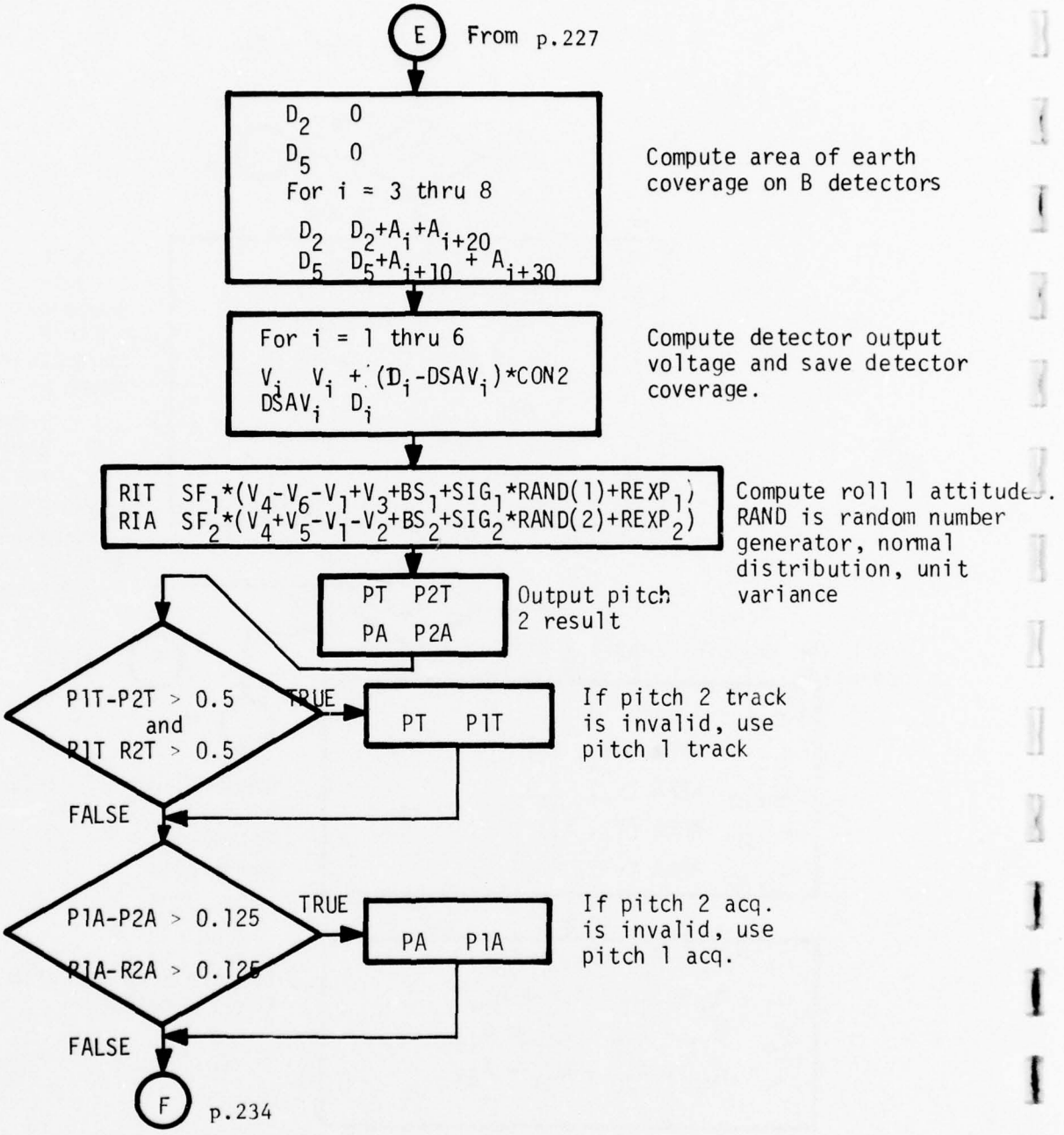

Figure M-6. Earth Sensor Flow Chart (continued)

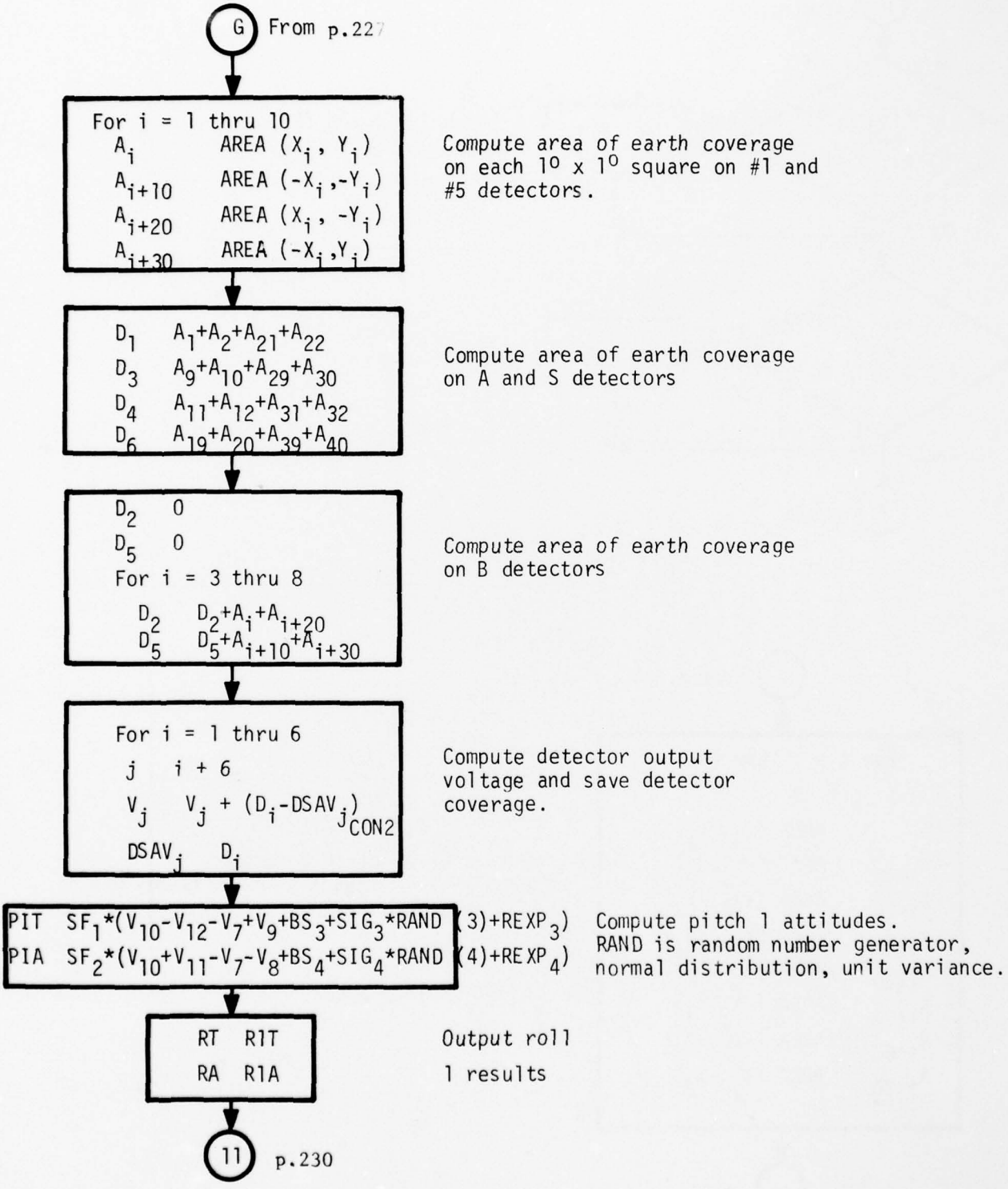

Figure M-6. Earth Sensor Flow Chart (continued)

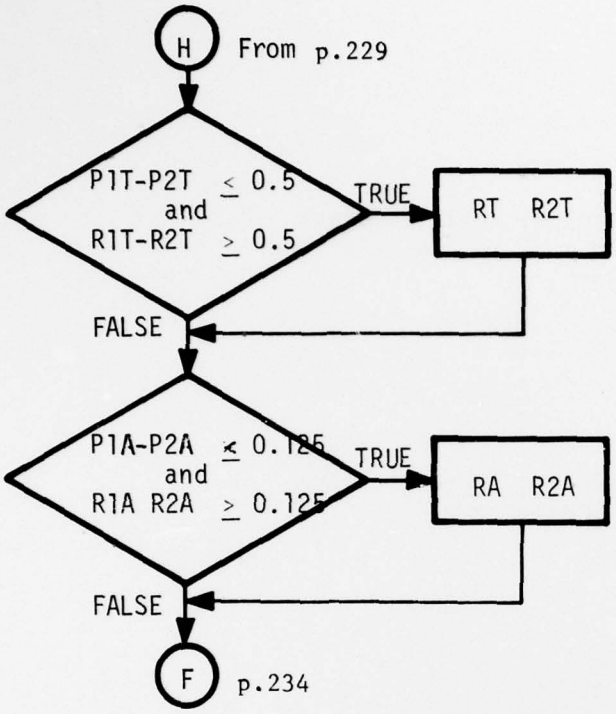

If roll 1 track is invalid, use roll 2 track

If roll 1 acq. is invalid, use roll 2 acq.

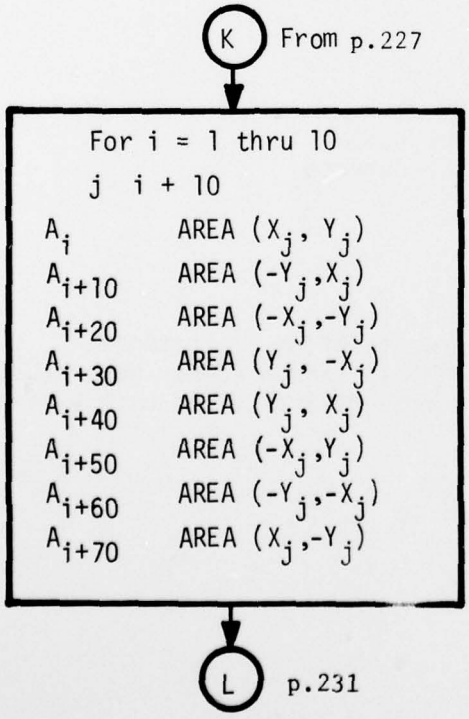

Compute area of earth coverage on each $1^o \times 1^o$ square on #2, #4, #6, and #8 detectors

See p.234

Figure M-6. Earth Sensor Flow Chart (continued)

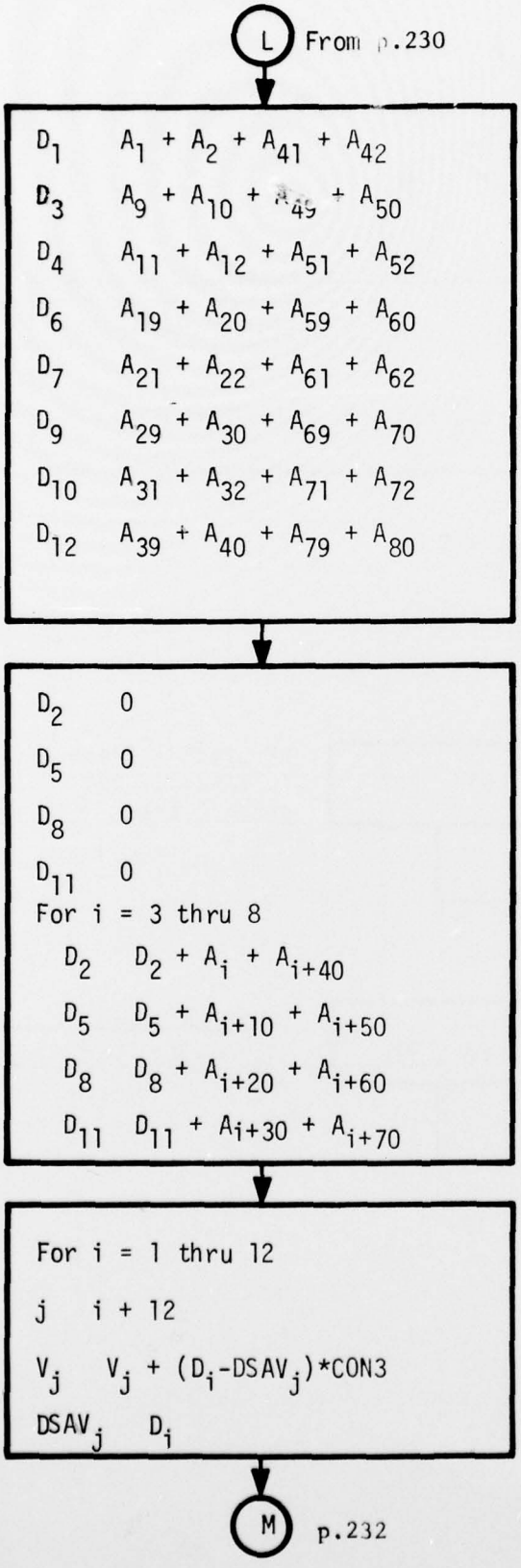

Compute area of earth coverage on A and S detectors

Compute area of earth coverage on B detectors

Compute detector output voltage and save detector coverage.

Figure M-6. Earth Sensor Flow Chart (continued)

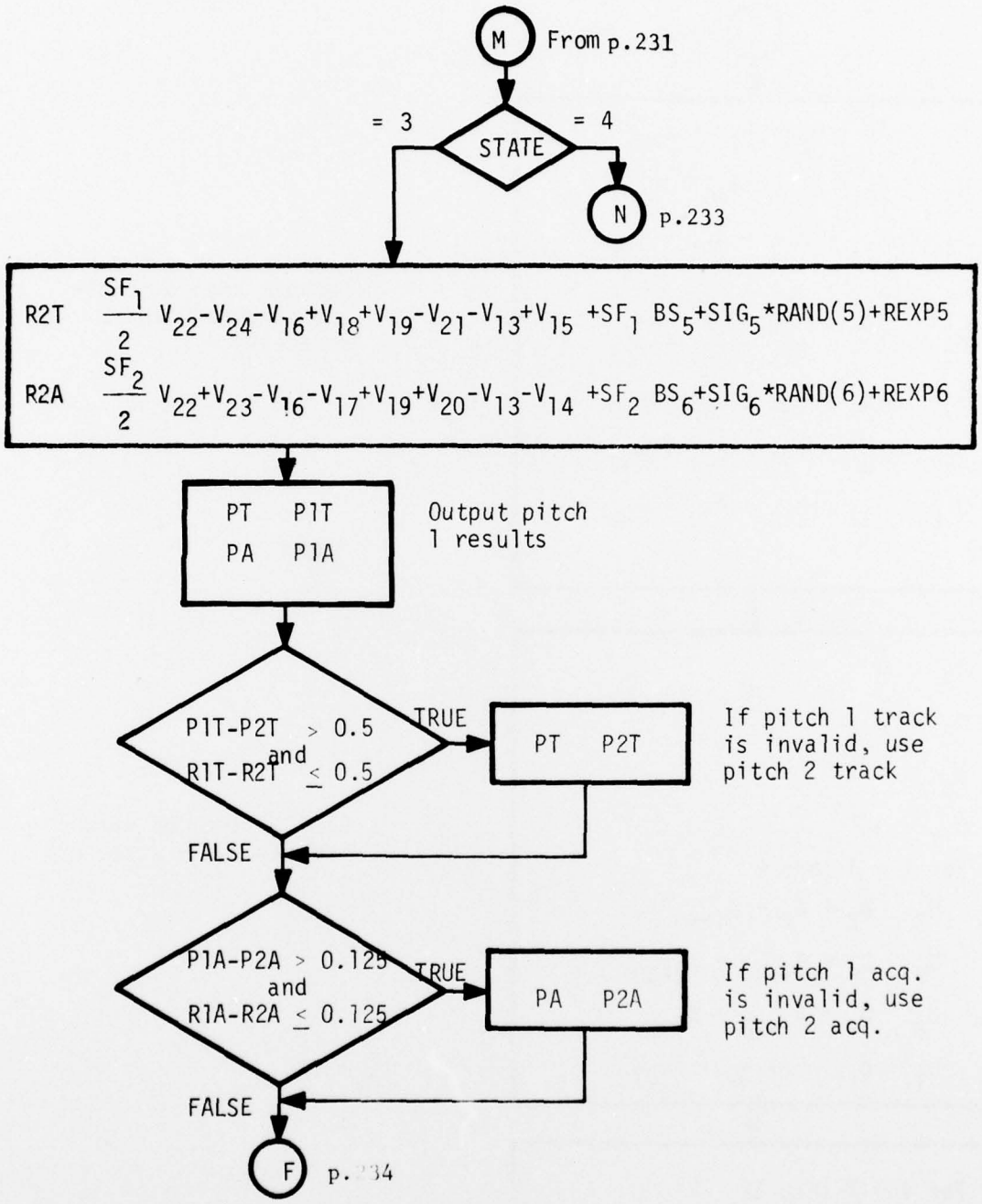

Figure M-6. Earth Sensor Flow Chart (continued)

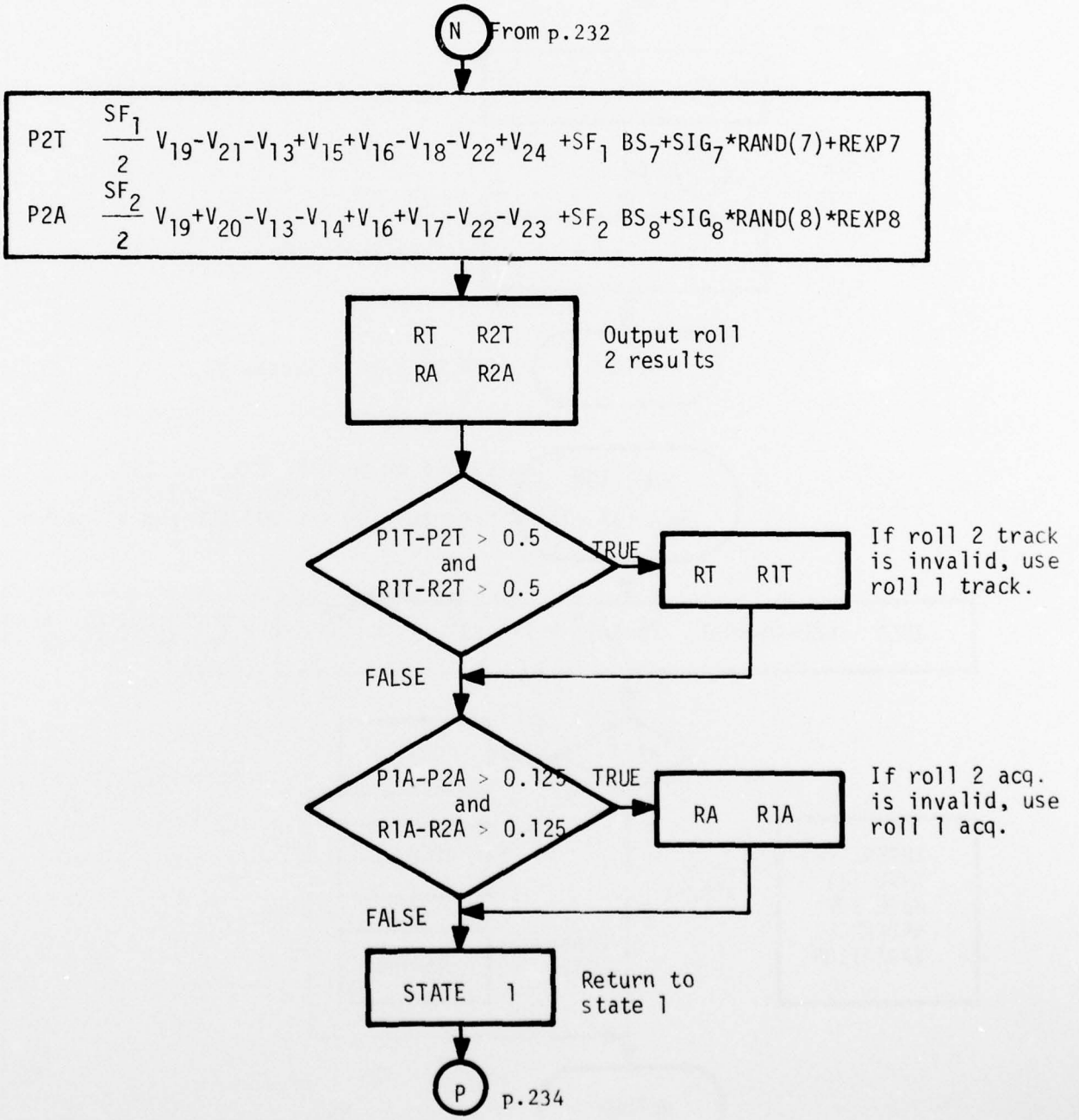

Figure M-6. Earth Sensor Flow Chart (continued)

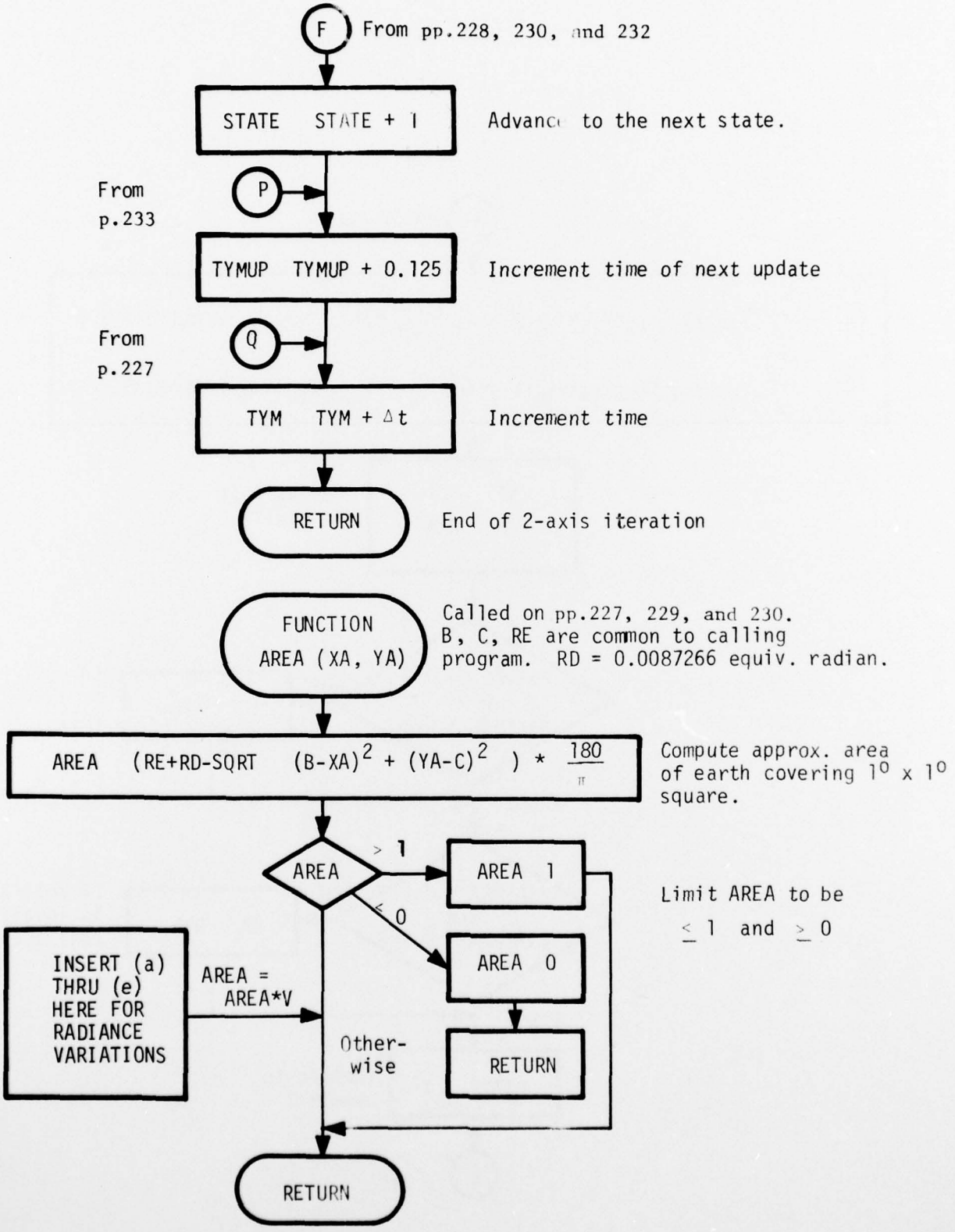

Figure M-6. Earth Sensor Flow Chart (concluded)

Where

SIG_I = 0.0020 (deg., 1σ) I = 1, ..., 8

BS_I = Bias error with worst case value 0.0285 (deg., 3σ) I = 1, ..., 8.

$REXP_I$ = Exponentially correlated noise with standard deviation 0.00283^{o} and correlation time 3.485 sec.

The function $REXP_I$ to be used to generate the exponentially correlated noise is given in the following:

```
FUNCTION REXPI
REXPIO = REXPI
BETA = 1./TMCNST
DREXP = -BETA*REXPIO
        +SQRT (2.*BETA)*RSIGI*RANDI
REXPI = REXPIO + DREXP
RETURN
END
```

Where

TMCNST = Correlation Time

RSIGI = Standard Deviation

RANDI = Random number generator with unit variance

REXPI to be assigned an initial value.

TABLE M-2. INITIALIZATION DATA FOR EARTH SENSOR MODEL

PARAMETER	SUBSCRIPT	UNIT	NOMINAL VALUE	SOURCE	TOLERANCE	SOURCE
Time constant of two axis earth sensor detectors, T_2		Seconds	1.4	Note 1	N/A	None
Line of sight of spin earth sensor field						
LOS^B, LOS_X	1	---	-0.9848	Note 2	N/A	Not specified
	2	---	-0.9848			
LOS_Y	1		0			
	2		0			
$LOS_{Z'}$	1		0.1736			
	2		-0.1736			
Transformation from body to sensor frame: (TSB)						
Row 1 Col. 1	1	---	1.0	Assumed	N/A	None
1 2	2		0	(nominal)		
1 3	3		0			
2 1	4		0			
2 2	5		1.0			
2 3	6		0			
3 1	7		0			
3 2	8		0			
3 3	9		1.0			
Calling time increment, Δt		Seconds	$\leq$0.00326	(spin mode)	See text	
			$\leq$0.125	(2 axis)	See text	
Center position of incremental detector area:						
X_I	1	Equiv.	0.2530727415	Note	N/A	None
	2	radian	0.2530727415	1 &		
	3		0.2705260341	Fig. 3		

TABLE M-2. INITIALIZATION DATA FOR EARTH SENSOR MODEL (continued)

PARAMETER	SUBSCRIPT	UNIT	NOMINAL VALUE	SOURCE	TOLERANCE	SOURCE
	4		0.2705260341			
	5		0.2879793266			
	6		0.2879793266			
	7		0.3054326191			
	8		0.3054326191			
	9		0.3228859116			
	10		0.3228859116			
	11		0.1727787808			
	12		0.1604374393			
	13		0.1851201222			
	14		0.1727787807			
	15		0.1974614637			
	16		0.1851201222			
	17		0.2098028052			
	18		0.1974614637			
	19		0.2221441467			
	20		0.2098028052			
Y_2	1	Equiv.	0.0087266463		N/A	None
	2	radian	0.0261799387			
	3		0.0087266463			
	4		0.0261799387			
	5		0.0087266463			
	6		0.0261799387			
	7		0.0087266463			
	8		0.0261799387			
	9		0.0087266463			
	10		0.0261799387			
	11		0.1851201222			
	12		0.1974614637			
	13		0.1974614637			
	14		0.2098028051			
	15		0.2098028051			
	16		0.2221441466			
	17		0.2221441466			
	18		0.2344854881			
	19		0.2344854881			
			0.2468268296			

TABLE M-2. INITIALI[illegible]ION DATA FOR EART[illegible]ENSOR MODEL (concluded)

PARAMETER		SUBSCRIPT	UNIT	NOMINAL VALUE	SOURCE	TOLERANCE	SOURCE
Noise Standard Deviation							
SIG on:	R1T	1	Volts	0.167	Note 4	N/A	
	R1A	2	Volts	0.0417			
	P1T	3	Volts	0.167			
	P1A	4	Volts	0.0417			
	R2T	5	Volts	0.167			
	R2A	6	Volts	0.0417			
	P2T	7	Volts	0.167			
	P2A	8	Volts	0.0417			
	$TP1P_1$	9	Sec.	0	Not Specified		Not Specified
	$TP1P_2$	10	Sec.	0	Not Specified		Not Specified
Two axis output scale factor							
Track, SF		1	Volt/sq. deg.	1.25	Note 3	0.0625	Note 3
Acq., SF		2	Volt/sq. deg.	0.3125		0.025	

NOTES TO TABLE M-2

1. Barnes presentation to Honeywell in St. Petersburg on 3-13-75.
2. Rockwell Spec MC 432-0214, Rev. B., 12-11-74.
3. Computed from data in Rockwell Spec MC432-0214, Rev. B, 12-11-74.

   Track scale factor

   1 degree attitude = 4 sq. deg. coverage = 5 ± 0.25V.

   $$\frac{5 \pm 0.25V}{4 \text{ sq. deg.}} = 1.25 \pm 0.0625 \text{ volt/sq. deg.}$$

   Acquisition scale factor

   4 degree attitude = 16 sq. deg. coverage

   $$\frac{1.25 \pm 0.1 \text{ V}}{4 \text{ sq. deg.}} = 0.3125 = 0.025 \text{ volt/sq. deg.}$$

4. Computed from data in Rockwell Spec MC 432-0214, Rev. B, 12-11-74

   Track mode

   $\pm 0.1^{\circ}$, 3 sigma

   0.1 x 5 volt/deg x 1/3 = 0.167 volt, 1 sigma

   Acquisition mode

   $\pm 0.1^{\circ}$, 3 sigma

   0.1 x 1.25 volt/deg x 1/3 = 0.0417 volt, 1 sigma

TABLE M-3. INPUT DATA FOR EARTH SENSOR MODEL

DEFINITION	FLOW DIAGRAM SYMBOL	DIMENSION	TYPE	UNITS
Mode control flag	MODE		Integer	0 = initialize 1 = spin operation 2 = 2 axis operation
Satellite position vector	R_x, R_y, R_z; R	3	Real	N Mi
Transformation from body to inertial frame	TIB	9	Real	

TABLE M-4. OUTPUT DATA FOR EARTH SENSOR MODEL

DEFINITION	FLOW DIAGRAM SYMBOL	DIMENSION	TYPE	UNITS
Spin earth sensor output	TPIP	2	Real	Seconds
Pitch attitude in track mode	PT		Real	Volts
Pitch attitude in acquisition mode	PA		Real	Volts
Roll attitude in track mode	RT		Real	Volts
Roll attitude in acquisition mode	RA		Real	Volts

TABLE M-5. INTERNAL VARIABLES FOR EARTH SENSOR MODEL

DEFINITION	FLOW DIAGRAM SYMBOL	DIMENSION	TYPE	UNITS
Two axis rise/decay increment for 0.25 sec.	CON2		Real	Volts per sq. deg.
Two axis rise/decay increment for 0.125 sec.	CON3		Real	Volts per sq. deg.
Area of incremental detector covered by earth	A	80	Real	Square degree
Time since start of run	TYM		Doub prec	Seconds
Time of next 2-axis update	TYMUP		Doub prec	Seconds
Satellite distance to earth center	RM		Real	N. Mi
Satellite position vector in sensor frame	RS_x, RS_y, RS_z; R	3	Real	N. Mi
Radius of earth image on focal surface	RE		Real	Equiv. radian
Position of earth image on focal surface, X component	B		Real	Equiv. radian
Position of earth image on focal surface, Y component	C		Real	Equiv. radian
State of sequential processing within sensor	STATE		Integer	
Area of detector covered by earth	D	12	Real	Square degree
Area of detector coverage from previous cycle	DSAV	24	Real	Square degree
Dynamic Detector output	V	24	Real	Square Degree

TABLE M-5. INTERNAL VARIABLES FOR EARTH SENSOR MODEL (concluded)

DEFINITION	FLOW DIAGRAM SYMBOL	DIMENSION	TYPE	UNITS
Pitch 1 track attitude	P1T		Real	Volts
Pitch 2 track attitude	P2T		Real	Volts
Roll 1 track attitude	R1T		Real	Volts
Roll 2 track attitude	R2T		Real	Volts
Pitch 1 acquisition attitude	P1A		Real	Volts
Pitch 2 acquisition attitude	P2A		Real	Volts
Roll 1 acquisition attitude	R1A		Real	Volts
Roll 2 acquisition attitude	R2A		Real V	Volts
Index	i		Integer	
Index	j		Integer	
Line of sight of spin sensor field in inertial frame	LOS^I	3	Real	
Normalized cross product magnitude of R and LOS	SANG		Real	
Normalized dot product of R and LOS	CANG		Real	
Angle between -R and tangent to earth	ANG1		Real	Radian
Angle between -R and LOS	ANG2		Real	Radian
Angle between LOS and earth tangent	ANG3		Real	Radian
Saved angle between earth tangent and LOS	ANGSAV	2	Real	Radian
Half dimension of $1^o \times 1^o$ square	RD		Real	Equiv radian. (a constant preset to 0.0087266)
Area of earth covering $1^o \times 1^o$ square	AREA		Real Function	Square Degree

REFERENCES

M-1. McArthur, W.G., "Horizon Sensor Navigation Errors Resulted from Statistical Variations in the CO_2 14-16 Micron Radiation Band," Ninth Symposium on Ballistic Missile and Space Technology, San Diego, California, August 1964.

M-2. "Performance Analysis of Static Sensor," Barnes Engineering Company, 4 August, 1975.